AGARD-AG-316

AGARD-AG-316

AGARD

ADVISORY GROUP FOR AEROSPACE RESEARCH & DEVELOPMENT

7 RUE ANCELLE 92200 NEUILLY SUR SEINE FRANCE

AGARDograph No.316

Hazard Studies for Solid Propellant Rocket Motors

(Etudes des Risque pour les Moteurs-Fusées à Propergols Solides)

NORTH ATLANTIC TREATY ORGANIZATION

AGARD-AG-316

NORTH ATLANTIC TREATY ORGANIZATION

ADVISORY GROUP FOR AEROSPACE RESEARCH AND DEVELOPMENT

(ORGANISATION DU TRAITE DE L'ATLANTIQUE NORD)

AGARDograph No.316

Hazard Studies for Solid Propellant Rocket Motors

(Etudes de Risque pour les Moteurs-Fusées à Propergols Solides)

Edited by

Thomas L.Boggs and Ronald L.Derr

This AGARDograph was prepared at the request of the Propulsion and Energetics Panel of AGARD.

The Mission of AGARD

According to its Charter, the mission of AGARD is to bring together the leading personalities of the NATO nations in the fields of science and technology relating to aerospace for the following purposes:

- Recommending effective ways for the member nations to use their research and development capabilities for the common benefit of the NATO community;
- Providing scientific and technical advice and assistance to the Military Committee in the field of aerospace research and development (with particular regard to its military application);
- Continuously stimulating advances in the aerospace sciences relevant to strengthening the common defence posture;
- Improving the co-operation among member nations in aerospace research and development;
- Exchange of scientific and technical information;
- Providing assistance to member nations for the purpose of increasing their scientific and technical potential;
- Rendering scientific and technical assistance, as requested, to other NATO bodies and to member nations in connection with research and development problems in the aerospace field.

The highest authority within AGARD is the National Delegates Board consisting of officially appointed senior representatives from each member nation. The mission of AGARD is carried out through the Panels which are composed of experts appointed by the National Delegates, the Consultant and Exchange Programme and the Aerospace Applications Studies Programme. The results of AGARD work are reported to the member nations and the NATO Authorities through the AGARD series of publications of which this is one.

Participation in AGARD activities is by invitation only and is normally limited to citizens of the NATO nations.

Published September 1990

ISBN 92-[illegible]-6

Printed by Specialised Printing Services Limited
40 Chigwell Lane, Loughton, Essex IG10 3TZ

Recent Publications of the Propulsion and Energetics Panel

CONFERENCE PROCEEDINGS (CP)

Problems in Bearings and Lubrication
AGARD CP 323, August 1982

Engine Handling
AGARD CP 324, February 1983

Viscous Effects in Turbomachines
AGARD CP 351, September 1983

Auxiliary Power Systems
AGARD CP 352, September 1983

Combustion Problems in Turbine Engines
AGARD CP 353, January 1984

Hazard Studies for Solid Propellant Rocket Motors
AGARD CP 367, September 1984

Engine Cyclic Durability by Analysis and Testing
AGARD CP 368, September 1984

Gears and Power Transmission Systems for Helicopters and Turboprops
AGARD CP 369, January 1985

Heat Transfer and Cooling in Gas Turbines
AGARD CP 390, September 1985

Smokeless Propellants
AGARD CP 391, January 1986

Interior Ballistics of Guns
AGARD CP 392, January 1986

Advanced Instrumentation for Aero Engine Components
AGARD CP 399, November 1986

Engine Response to Distorted Inflow Conditions
AGARD CP 400, March 1987

Transonic and Supersonic Phenomena in Turbomachines
AGARD CP 401, March 1987

Advanced Technology for Aero Engine Components
AGARD CP 421, September 1987

Combustion and Fuels in Gas Turbine Engines
AGARD CP 422, June 1988

Engine Condition Monitoring -- Technology and Experience
AGARD CP 448, October 1988

Application of Advanced Material for Turbomachinery and Rocket Propulsion
AGARD CP 449, March 1989

Combustion Instabilities in Liquid-Fueled Propulsion Systems
AGARD CP 450, April 1989

Aircraft Fire Safety
AGARD CP 467, October 1989

Unsteady Aerodynamic Phenomena in Turbomachines
AGARD CP 468, February 1990

Secondary Flows in Turbomachines
AGARD CP 469, February 1990

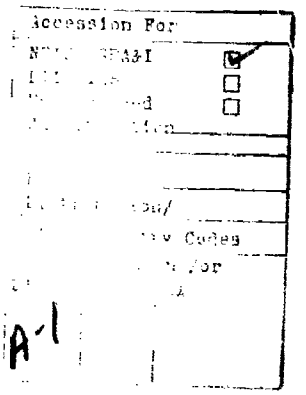

ADVISORY REPORTS (AR)

Through Flow Calculations in Axial Turbomachines *(Results of Working Group 12)*
AGARD AR 175, October 1981

Alternative Jet Engine Fuels *(Results of Working Group 13)*
AGARD AR 181, Vol.1 and Vol.2, July 1982

Suitable Averaging Techniques in Non-Uniform Internal Flows *(Results of Working Group 14)*
AGARD AR 182 (in English and French), June/August 1983

Producibility and Cost Studies of Aviation Kerosines *(Results of Working Group 16)*
AGARD AR 227, June 1985

Performance of Rocket Motors with Metallized Propellants *(Results of Working Group 17)*
AGARD AR 230, September 1986

Recommended Practices for Measurement of Gas Path Pressures and Temperatures for Performance Assessment of Aircraft Turbine Engines and Components *(Results of Working Group 19)*
AGARD AR 245, June 1990

The Uniform Engine Test Programme *(Results of Working Group 15)*
AGARD AR 248, February 1990

Test Cases for Computation of Internal Flows in Aero Engine Components *(Results of Working Group 1e)*
AGARD AR 275, July 1990

LECTURE SERIES (LS)

Operation and Performance Measurement of Engines in Sea Level Test Facilities
AGARD LS 132, April 1984

Ramjet and Ramrocket Propulsion Systems for Missiles
AGARD LS 136, September 1984

3-D Computation Techniques Applied to Internal Flows in Propulsion Systems
AGARD LS 140, June 1985

Engine Airframe Integration for Rotorcraft
AGARD LS 148, June 1986

Design Methods Used in Solid Rocket Motors
AGARD LS 150, April 1987
AGARD LS 150 (Revised), April 1988

Blading Design for Axial Turbomachines
AGARD LS 167, June 1989

Comparative Engine Performance Measurements
AGARD LS 169, May 1990

AGARDOGRAPHS (AG)

Rocket Altitude Test Facility Register
AGARD AG 297, March 1987

Manual for Aeroelasticity in Turbomachines
AGARD AG 298/1, March 1987
AGARD AG 298/2, June 1988

Measurement Uncertainty within the Uniform Engine Test Programme
AGARD AG 307, May 1989

REPORTS (R)

Application of Modified Loss and Deviation Correlations to Transonic Axial Compressors
AGARD R 745, November 1987

Rotorcraft Drivetrain Life Safety and Reliability
AGARD R 775, June 1990

Authors and Acknowledgements

This AGARDograph is dedicated to the memory of Dr John F.Kincaid (1912 to 1984), co-inventor of cast double base propellants — a gifted scientist who devoted his life to the future of mankind.

Acknowledgement is given to the many people who have contributed to this AGARDograph. Primary authors and contributors representing different countries and technical backgrounds are as follows:

G.Adomeit, Rheinisch-Westfälische Technische Hochschule (RWTH), Aachen, Germany

A.I.Atwood, Naval Weapons Center, China Lake, California, United States

K.N.Bascombe, Royal Armament Research and Development Establishment — Waltham Abbey, United Kingdom

T.L.Boggs, Naval Weapons Center, China Lake, California, United States, Editor

G.Bromberger, Royal Armament Research and Development Establishment — Waltham Abbey, United Kingdom

J.Brunet, SNPE-Groupe Technique Sécurité (GTS), France

J.Covino, Naval Weapons Center, China Lake, California, United States

R.L.Derr, Naval Weapons Center, China Lake, California, United States, Chairman

J.Goliger, SNPE-Groupe Technique Sécurité (GTS), France

A.H.Heemskerk, TNO, Prins Maurits Laboratorium, Rijswijk, The Netherlands

M.Held, Messerschmitt-Bölkow-Blohm GmbH (MBB), Schrobenhausen, Germany

R.Kent, SNPE-Groupe Technique Sécurité (GTS), France

C.O.Leiber, Bundesinstitut für chemisch-technische Untersuchungen beim Bundesamt für Wehrtechnik und Beschaffung (BICT), Swisttal-Heimerzheim, Germany

H.J.Pasman, TNO, Prins Maurits Laboratorium, Rijswijk, The Netherlands

R.Reed, Naval Weapons Center, China Lake, California, United States

A.J.Th.Rooyers, TNO, Prins Maurits Laboratorium, Rijswijk, The Netherlands

F.Trimborn, Bundesinstitut für chemisch-technische Untersuchungen beim Bundesamt für Wehrtechnik und Beschaffung (BICT), Swisttal-Heimerzheim, Germany

N.H.A.Van Ham, TNO, Prins Maurits Laboratorium, Rijswijk, The Netherlands

Acknowledgement is also given to the reviewers of the AGARDograph. These contributors are as follows:

Dr B.Zeller, Société Nationale des Poudres et Explosifs, Paris, France

Drs R.Weiss and C.Merill, Air Force Astronautics Laboratory (AFAL), Edwards Air Force Base, California, United States

Members of the staff of the Pilot NATO Insensitive Munitions Information Center (NIMIC), Columbia, Maryland, United States

Preface

This AGARDograph addresses potential hazards associated with present and future solid propellants and their use in rocket motors. The subject was recently introduced into the Propulsion and Energetics Panel through an AGARD Technical Specialists' Meeting "Hazard Studies on Solid Propellant Rocket Motors" held in Lisse, Netherlands, in May 1984. Following this meeting, representatives from NATO nations joined together to provide this written report summarizing those areas that are critical for the safety and suitability for present and future solid propellant rocket motors.

This AGARDograph is written for munition users, designers, and scientists and engineers involved in research and development associated with energetic munitions. The munition users will derive an appreciation for the complexities of designing safe and suitable munitions and the necessity for making tradeoffs between safety and performance. The designer will find rational approaches for assessing potential hazards and improved design tools based on recent results from studies of energetic material behavior. The research engineer studying reaction phenomena associated with energetic materials will recognize deficiencies in the fundamental understanding of energetic material behavior and new areas for research studies.

Final answers for resolving this problem of hazards associated with solid propellant rocket motors will not be found in this AGARDograph. Indeed, in some areas, considerable work is still needed to allow rational design approaches. As new energetic materials are introduced into solid propellant formulations to achieve improved rocket motor characteristics, existing design approaches should be challenged and new research needs to be placed on the scientist and engineer. When these new challenges arise, this AGARDograph should provide the basis for new and meaningful research and development studies. In this light, results reported in this AGARDograph represent the state of technology as of January 1989.

Préface

Cette AGARDographie étudie les risques potentiels associés aux propergols solides actuels et futurs et à leur mise en oeuvre dans les moteurs-fusées. Le sujet a été présenté au Panel AGARD de Propulsion et d'Energétique lors d'une réunion de spécialistes de l'AGARD sur "Les études de risque pour les moteurs-fusée à propergol solide" tenue à Lisse, aux Pays-Bas en mai 1984. Suite à cette réunion, des representants des pays membres de l'OTAN se sont associés pour rédiger ce rapport, qui met en relief les domaines d'intérêt qui sont critiques pour la sécurité et l'adéquation des moteurs-fusées à propergols solides actuels et futurs.

Cette AGARDographie est destinée aux concepteurs et aux utilisateurs de munitions, ainsi qu'aux scientifiques et aux ingénieurs impliqués dans la recherche et le développement des munitions énergétiques. L'utilisateur tirera une appréciation des complexités de la conception de munitions sûres et adéquates ainsi que de la nécessité de trouver le juste équilibre entre les performances et la sécurité. Le concepteur y trouvera des méthodes cohérentes pour l'évaluation des risques potentiels, ainsi que de nouvelles aides à la conception issues de certaines études récentes sur le comportement des matériaux énergétiques. L'ingénieur-chercheur qui étudie les phénomènes de réaction associés aux matériaux énergétiques relévera des lacunes dans les connaissances de base du comportement des matériaux énergétiques qui lui permettront d'identifier de nouveaux domaines de recherche

Cette AGARDographie ne prétend pas fournir les solutions définitives au problème des risques associés aux moteurs-fusées à propergols solides. En effet, dans certains domaines, des efforts considérables restent à fournir pour permettre le développement de méthodes logiques de conception. Les méthodes de conception existantes doivent être confrontées aux nouveaux matériaux énergétiques rentrant dans les formules des propergols solides afin d'améliorer les caractéristiques des moteurs-fusées et de nouveaux projets de recherche doivent être confiés aux scientifiques et aux ingénieurs. Cette AGARDographie devrait fournir les éléments de base pour le lancement de nouvelles études significatives de recherche et développement en tir et à mesure de l'évolution de ces nouveaux défis.

Contents

CHAPTER 1. INTRODUCTION

The subject of munition safety is one of continuing importance because of the potential damage capable of any device highly loaded with energetic materials and the impossible task of precluding their inadvertent initiation. The subject of this report is a subset of munition safety: rocket motors containing solid propellants. This topic is not new. In the past, AGARD addressed double-base solid propellants in AGARDograph No. 141-70, "High Energy Propellants." The material in this past report is still relevant; however, solid propellants have continued to evolve because of new performance requirements. It is significant that some solid propellant formulations in use today are almost identical to the formulations used in accepted high energy explosives. Accordingly, past incidents concerning high energy explosives are relevant to present and future incidents that could occur with modern solid propellants.

As this report was being planned and written, NATO nations have directed increasing attention to munition safety. Indeed, the NATO Conference for National Armament Directors (CNAD) has noted that the design and acceptance of safe munitions is one of the greatest impediments to weapon interoperability. In this context, nations have placed increased concern for the survivability of weapon platforms in a combat environment and the desire for "Insensitive Munitions."

The report addresses several needs associated with hazards and the design of solid propellant rocket motors. The needs include:

1) Methods to assess the potential hazards associated with current rocket motors. As solid propellants have become more energetic, the hazard potential has also increased. Many of the hazard tests that were used 20 years ago to discriminate between propellants for hazard potential are no longer adequate.

2) Design methods for providing safety while still maintaining operational effectiveness. Solid propellants became more energetic in the quest for increased range, velocity, and payload. Performance was, and continues to be, a major consideration. Safety, while always a consideration, has increased in importance to the point where performance/hazard trade-off considerations are being more frequently made. The propellant and rocket motor designers increasingly need experimental and analytical methods that allow them to assess the performance and hazard characteristics early in the design cycle.

3) Interoperability within NATO. As each country within NATO makes these performance hazard assessments and trade-offs, there needs to be some commonality within NATO to ensure interoperability. The NATO group AC/310 on Safety and Suitability of Munitions is addressing this need as will be discussed in Chapter 7.

4) Methods of assessing, and increased insurance of a launch platforms survivability. As weapons become more powerful and more sophisticated, it becomes imperative that the launch platform, whether it be a ship or an aircraft or a tank, be able to survive not only threats due to the enemy but also self-induced threats.

5) Response to the "Insensitive Munitions" major programs in several countries. While is it easy to declare the desire for "Insensitive Munitions," it is much more difficult to design such items, and involves consideration of the needs mentioned above.

To illustrate and highlight a portion of these needs one only has to consider energetic materials and the devastation that they can cause. The energetic materials in modern munitions are sensitive to heat and shock. Inadvertent stimuli of sufficient levels to initiate reactions in the energetic materials can result in violent reactions which pose extreme hazards to personnel and material.

March 12, 1907, Aboard ship Iena in drydock, France. Accidental ignition of gun propellants in the ammunition magazine. Fire, explosions, 117 killed, 33 injured.

September 25, 1911, Aboard ship Liberte in Toulon Bay, France. Accidental ignition of gun propellants in the ammunition magazine. Fire, explosions, Liberte is lost, 226 killed, 160 injured.

December 12, 1917, Halifax, Nova Scotia, Canada. A collision between a Belgian boat and a French cargo ship loaded with ammunition, at the entrance of the harbor, caused the rupture of gasoline drums which caught fire. While the crew was fighting the fire, another boat approached the area. Seeing that the fire was getting out of control, the crew left the boat. 17 minutes later a dreadful explosion occurred that razed the town of Richmond killing 5,000 people and injuring 10,000. Even some Indians who were 6 miles away were killed (Biassutti, 1985).

July 10, 1926, Naval Ammunition Depot, Lake Denmark, New Jersey, United States. Lightning struck a magazine containing 670,000 pounds (303,912 kg) of explosives. Reactions spread. A total

of 3.2 million pounds (1.45 million kg) detonated. Twenty one individuals died and 52 were injured. Loss of life would have been worse except that the workday had ended at noon. The Navy and adjacent Army facility suffered an approximate $75 million loss, as well as significant mobilization potential (Roylance, 1981).

July 17, 1944, Port Chicago, California, United States. Three explosions of approximately 10,000 tons of munitions resulted in 320 dead and 390 injured, and caused major damage within a 1 mile radius and minor damage as far as 25 miles away.

November 24, 1944, USS Princeton. The carrier received a single Japanese 250 kg bomb. Fire, explosions, destroyed the ship.

January 4, 1947, United States. A bomb was dropped during handling in the magazine. The explosion was transmitted to the 70 tons of bombs in the magazine. 10 killed. The igloo-shaped magazine was destroyed.

July 15, 1949, Prüm, Eifel. Burning, on top of a hill (Kalvarienberg), by unknown reasons, of a storage containing about 500 t of TNT-filled ammunition transited to a disastrous explosion after 1-1/2 hours. Shortly thereafter it was followed by a second explosion. The top of the hill (about 250,000 m^3) was blown away, down to the city of Prüm, covering it with debris and trees. Due to prior evacuation only 12 were killed and 60 injured. 76 houses were totally damaged and 161 seriously (Local report, 1949).

1950, Royal Naval Ammunition Depot, U.K. Explosion - 36000 kg equivalent of HE -- Stores destroyed.

May 22, 1957, New Mexico, United States. Accidental dropping of a nuclear weapon from a plane. The chemical explosive detonated on impact (International Herald Tribune 1986).

March 4, 1960, Cuba. Explosion of ship containing 76 tons of weapons ammunitions, probably due to the dropping of case of grenades. More than 100 killed.

June 2, 1966, Muiden, Netherlands. 2400 kg of TNT exploded in a melting shop at Muiden (Dutch explosives factory KNSF). Substantial material damage. No serious personal injuries. Overheating of the melting vessel by steam and impurities in the TNT turned out to be the cause of this explosion (Groothuizen et al, 1970.

October 1966, USS Oriskany. Fire - 44 killed, 156 injured, 3 aircraft destroyed. $15.6 M estimated cost.

June 12, 1967, Utrecht, Netherlands. Explosion of a ship loaded with 1.,000 kg of ammunition, great damage to surrounding industrial area. 2 people killed, 200 people wounded. The ammunition was obsolete and prepared for dumping. During the handling of pyrotechnic ammunition one of the items must have activated. As the ship was loaded with all types of ammunition, deflagration from the pyrotechnic munition grew to a detonation of the high explosive munition also present (Prins Maurits Laboratory, 1967).

29 July 1967, USS Forrestal. Accidental explosion of rocket which sets fire to the fuel tank. The fire propagates to the aircraft ammunitions. 134 killed, 162 injured, 21 aircraft destroyed, 43 aircraft damaged. $172 M estimated cost.

January 14, 1969, USS Enterprise. Fire - 28 killed, 343 injured, 15 aircraft destroyed, 17 aircraft damaged. $57 M estimated cost.

April 1969, Danang, Viet Nam. Fire, explosions with propagation to ammunitions magazine.

June 22, 1969, Hannover, Linden, Federal Republic of Germany. Blocked brakes on a running railroad car wheel produced a temperature increase up to more than 750°C. Showers of sparks caused smouldering of the railroad car. As the train stopped for fire fighting, 175-mm-grenades filled with Composition B, but without detonator exploded probably in low order. 8 firemen and 4 railroad employees killed and 40 people had been injured. Indications of a LVD are bent and deformed axles and wheels and unusually large debris of the grenades (Public Attorney's report).

May 24, 1973, Roseville, California, United States. Explosion over a 32 hour period of an ammunition train, 18 freight cars of which were carrying Mk 82 bombs, each loaded with 500 lbs of high explosives. The initial cause of ignition was ignition of a wooden floor impregnated with sodium nitrate. The train was destroyed and also 140 meters of train tracks were lost.

May 28, 1975, Belgium. Explosion of a bomb during loading of a wagon. The fire propagates to a wagon filled with TNT located 40 meters away. 13 injured. Many wagons are destroyed.

August 7, 1978, Herlong, California, United States. Detonation of a bomb loaded with a high explosive is transmitted to 8 others. These bombs were stored between the igloo shaped magazines of the storage area. A nearby igloo was crushed, and its munitions were damaged without reaction.

May 26, 1981, USS Nimitz. A crash during landing of an aircraft was followed by explosions. (Note: One of the explosions was a delayed detonation of a Sparrow warhead.) Fire - 14 killed, 48 injured, 3 aircraft destroyed, 9 aircraft damaged. $150 M estimated cost.

August 18, 1981, Zimbawbe. Explosion of an ammunition magazine. Probably due to the explosion of a gas bottle. Destruction of hundreds of tons of ammunition.

May 13, 1984, USSR. Series of fires and explosions at Severomorsk Naval Base. The fire lasted several days.

January 11, 1985, Waldheide, Heilbronn, Federal Republic of Germany. While lifting a Pershing II motor from its shipping container, in January 1985, electrostatic discharge caused inadvertent ignition of the motor. The cold dry day contributed to this event. 3 people were killed and 9 injured. The accident may have been due to the high sensitivity to electrostatic discharge of the cold propellants.

August 4, 1985, United States. During a road transportation of 10 bombs loaded with 500 kg of TNT, collision occurred, fire, detonation, very large craters. Temporary evacuation of 6000 people.

December 27, 1987, Brigham City, Utah, United States. While pulling the casting mandrel from an MX (solid propellant rocket motor), the propellant ignited killing 5 people and destroying the facility. The accident was attributed to electrostatic discharge and friction.

May 4, 1988, Henderson, Nevada, United States. More than 8 million pounds of ammonium perchlorate (AP, a key ingredient in modern solid propellants) burned and detonated killing two people and injuring more than 350 local residents, and causing damage estimated to exceed $73 million (C&EN, 1988).

In addition to such incidents, many of which occurred during normal peacetime operations, threats to munitions are even greater in battle conditions where enemy fire threatens them with thermal and shock stimuli of fire and bullets and the blast and fragment products of detonations. The loss of ships, tanks, and aircrafts in battle is often due to the secondary reactions of their own munitions following initiation by enemy fire.

While the reader can appreciate the needs listed earlier, each will view them from a slightly different perspective. The needs and perspectives vary depending on whether one is a user, a buyer, a developer of munitions, or a technical specialist. The user and buyer discuss the safety of a whole round such as bombs, rockets, guns, etc. over the entire life cycle. The system designer amongst other design considerations must worry about the hazard technical areas such as sympathetic detonation, cook-off, bullet and fragment impact, response to shaped charge jets, and response to electrostatic discharge as derived from the safety requirements. The scientist/technologist tends to think along lines of mechanistic understanding of shock-to-detonation transition (SDT), deflagration-to-detonation transition (DDT), terminal ballistics, penetration mechanics, ignition and combustion, breakdown voltages, etc. Obviously all of these people have a piece of the puzzle, with linkages between these pieces. This has been illustrated in Fig. 1 as a three-dimensional matrix. Shown are some of the items mentioned above. The various boxes within the matrix involve the concerns of the munition user/buyer, the munition designer, and the scientist/technologist. For example, the munition user wants a missile having a motor, warhead, etc., and he wants it to be insensitive to sympathetic detonation, fragment/bullet impact, etc. The designer, because he will be queried by the buyer/user, is concerned how his components and subcomponents will respond. For example he may be concerned with how the motor case, liner, and propellant will react to various fragments and bullets, and may turn to the scientist/technologist for help. As will be shown later in this book, the scientist/technologist will translate this concern for response of the motor to fragments/bullets into concerns such as the response of the propellant to mechanical shock and whether shock to detonation transition occurs, and the penetration mechanics of the fragment on the case/propellant and whether ignition and subsequent explosion can occur.

The purpose of this AGARDograph is to address the various parts of the matrix shown in Fig. 1. That is, it addresses the general response of solid propellant rocket motors to sympathetic detonation, cook-off, bullet impact, etc.; translates these system concerns into technical/scientific areas such as impact leading to shock to detonation transition; considers each technical/scientific area in terms of

mechanisms, data requirements, and data usage; and describes mitigating the hazards based on understanding the causal mechanisms. This can be described as the following steps:

For a given system (existing or proposed):

- what can happen
- why does it happen
- how can it be prevented or lessened

The result would be a better system.

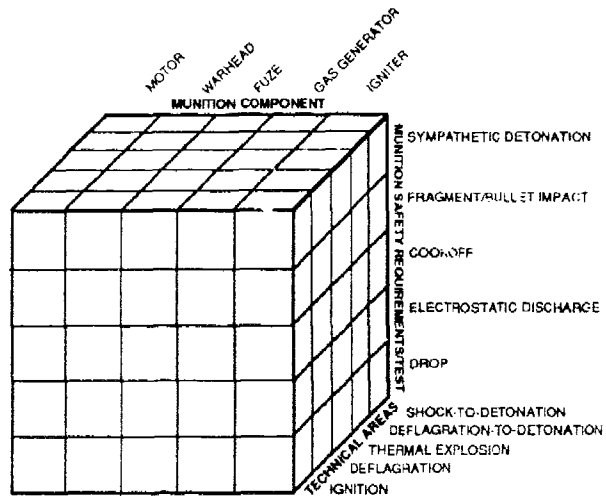

Fig. 1. Propulsion Hazards or "Insensitive Munitions" Programs Concern the Munition's Components, Hazard Threats, and Technical Areas.

The chapters that follow reflect this organization are as follows:

Chapter 2 - Description of Solid Propellant Rocket Motors
Chapter 3 - Overview of Solid Propellant Rocket Motor Hazards and Hazard Testing
Chapter 4 - Solid Propellant Rocket Motor Response to Threats
Chapter 5 - Hazard Response Technical Areas
Chapter 6 - Mitigation of Responses
Chapter 7 - NATO Standardization Activities to Promote Munition Safety
Chapter 8 - Future Needs

CHAPTER 2. DESCRIPTION OF SOLID PROPELLANT ROCKET MOTORS

2.1. MISSILE PROPULSION

For the most part, projectiles require some form of propulsion to accelerate them to the required velocity and to overcome air resistance and gravity. In this context, the term "missile" is limited to self-propelled weapons and restricted to those which traverse the air. For missiles, the propulsive thrust is based on Newton's Law of Action and Reaction, the reaction being provided by a mass of material which is accelerated backwards from the missile. In practice this material is produced by chemical reaction, either between a fuel carried with the missile motor and surrounding air (jet propulsion) or of matter which has entirely been carried within the missile (rocket propulsion). Jet propulsion is necessarily limited to travel in the atmosphere and therefore missiles that travel at high altitudes are necessarily rocket-propelled. The term "rocket motor" is applied to such a propulsion unit. A missile may contain one or more rocket motor stages as well as warheads, guidance systems, and sensor systems.

Rocket motors may be of four distinct types:

(1) Liquid monopropellant motors in which the liquid is injected into a combustion chamber where it reacts.

(2) Liquid propellant motors in which the two reacting liquids are injected separately into the combustion chamber and react there. Such systems can in general provide higher performance than monopropellant motors.

(3) Solid propellant motors where the propellant burns in situ within the motor (used in most missile applications).

(4) Hybrid propellant motors in which a solid fuel is combined with a liquid oxidizer.

(5) Ducted rocket motors that use a fuel-rich propellant and ducted air for a source of oxidizer

In all five types, the reaction produces hot gases which are expelled from the motor to produce the thrust.

This AGARDograph is concerned only with solid propellant rocket motors and the energetic materials used in this type of motor. These motors are designed to provide high performance [high-thrust-time for a given mass of propellant consumed, high specific impulse (I_{sp}), and associated desired pressure-time characteristics] along with other considerations such as:

- Burning stability - Absence of pressure, thrust fluctuations
- Low observables - Low signature from:
  - Primary smoke - Primarily metal oxide particles or other solid/liquid particles in the exhaust plume
  - Secondary smoke - Contrail formation due to water condensation (particularly aggravated by hydrogen halide nuclei, e.g., HCl, HF)
  - Afterburning - Combustion of fuel rich exhaust plume with the ambient air
  - Visible radiation
  - Infrared radiation
  - Radar cross-section
- Hazard/safety - This is the major concern and the reason for the AGARDograph.
- Producibility/affordability - The motor and any hazard mitigation must be capable of being produced at an affordable cost.
- Reliability - Similarly the motor and any hazard mitigation systems must work reliably when needed.

2.2. BRIEF DESCRIPTION OF SOLID PROPELLANT ROCKET MOTOR OPERATION

The terms underlined in the following paragraphs are shown in Fig. 2 and included in the English/French/German glossary (see Table 1, Section 2.4, p. 14).

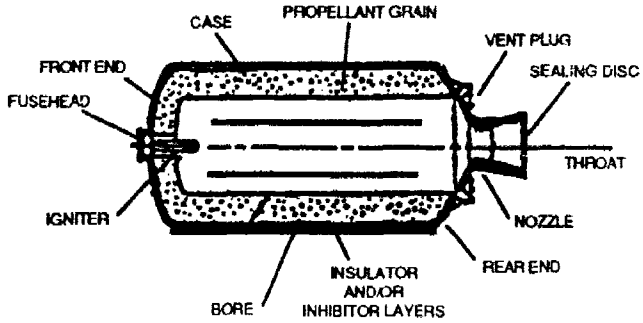

Fig. 2. Typical Solid Propellant Rocket Motor (Case Bonded).

The action of the motor depends on the combustion of the propellant producing hot gases which are expelled through the rear end of the motor to produce the thrust. The propellant grain is carefully designed in combination with the nozzle to provide the required thrust over the required period of operation for the application required. Many rocket motors are single-stage and ideally should provide a steady thrust throughout the burning process, maintaining a steady pressure and temperature within the port and local sonic flow through the throat of the nozzle; this throat area must be less than the port cross-sectional area at all times. Ignition of the propellant is by means of a fusehead which is itself initiated electrically and forms part of an igniter system. The pressures and temperature within the port are both high and the case must be sufficiently robust to eliminate the possibility of failure.

The propellant grain can be cartridge loaded or bonded to the case. For the cartridge loaded grain, where the grain is manufactured separate from the motor case, the interface between the propellant grain and the case is critical. It is vital that the outer surface of the propellant grain is not ignited as the hot gases resulting would lead to case damage and rapid failure. To prevent this a layer of inhibitor material may be wrapped around and bonded to the outside of the propellant grain before it is inserted into the case. In the later stages of combustion, as the propellant burning surface approaches the case, this may become heated by conduction through the diminishing thickness of the propellant web. If the insulating power of the inhibitor is not sufficient, a separate layer of insulator may be required and this will be attached to the case itself. In modern case bonded designs of rocket motors where the grain is manufactured within the motor case, the functions of inhibitor and insulator can be performed by a single layer of material or two separate interbonded layers. This case bond system must provide bonding on all interfaces between the case and propellant charge. The case bond system must be rubbery in character to withstand the stresses and deformations resulting from ignition pressure surge and acceleration of the motor on firing.

The purpose of the sealing disc is to prevent the ingress of dust and moisture into the motor. This disc is very thin so that it does not present an obstacle on ignition. If the propellant is a nitric-ester based composition, which slowly produces gas on storage, a vent plug may be required as shown in Fig. 2, especially with large motors.

For some applications an initial brief vigorous boost of the payload is required, to be followed by a longer term sustainer action to overcome the effects of air resistance, etc. These requirements can be met by separate boost and sustainer motors, or by (1) different grain configurations with large surface area in the beginning (star, wagon wheel, etc.), (2) two different propellants in one motor, or (3) an integrated boost and sustain motor.

2.3. DESCRIPTION OF COMPONENTS

2.3.1. Case. The main function of the motor case is to contain the hot expanding gases resulting from combustion of the propellant. The hoop stress on the case is in practice the critical factor and, for this reason, all modern rocket motors are essentially cylindrical in shape.

2.3.1.1. Metal

Traditionally rocket motor cases have been made of metal. Seamless steel and aluminum tubing have been most commonly used. The wall thickness is determined by the internal pressure developed in the conduit.

Aluminum alloy has, in comparison with steel, a much lower density which compensates for the extra case thickness required by the lesser tensile strength, but the much lower softening temperature

may constitute a problem. Useful applications of aluminum alloy cases (with no ove wrap material) have occurred only where adequate insulation protection (usually heavier than for steel cases) has been provided for motor wall protection.

2.3.1.2. Composite

The desire to reduce the mass of cases has led to the use of composite case materials, on account of ease and comparative cheapness of manufacture as well as reduced mass. The composite case offers advantages when exposed to fuel fire and in some bullet impact situations because the case comes apart, allowing the propellant to burn rather than react in an explosive manner due to its confinement.

Carbon-fiber reinforced plastic (CFRP), glass-reinforced plastics (GRP), and Kevlar, are composite materials being used extensively in development and production rocket motors.

2.3.1.3. Hybrid

Two specialized types of "hybrid" case materials have recently been developed.

Cases consisting of multiple laminated steel strips wound concentrically (in some cases helically) and joined by means of a suitable resinous adhesive have given encouraging results in reducing the violence of response of rocket motors in fuel fires. The resin used begins to weaken at about 200°C so that when the propellant (protected by a layer of insulator/inhibitor) is cooked off, the case is so weak that it simply delaminates, although pieces may be thrown a few meters. Similar reductions in violence of response have been claimed for fragment/bullet attack though the effect here would not be expected to be so dramatic; if time permits, delamination should develop around the entry hole(s) of the projectile(s) and also the exit hole(s) if any. In other respects however, the case behaves similarly to a normal steel one; there is no significant difference in mass.

Prospects for reducing significantly the mass of the case while retaining the full temperature range and internal pressure capability appear at present to rest on the use of a two-layer case, consisting of a metal "inner tube" for adequate longitudinal integrity and outer layers of overwound tensioned high strength fiber such as Kevlar to provide the necessary extra hoop strength. The tube may be of steel or aluminum alloy; the saving in mass may be limited by the minimum practical thickness of the metal case due to manufacturing considerations. This system is confidently expected to show reduced vulnerability to fragment and bullet attack in comparison with a single metal tube, since the projectile cuts the fiber coating, locally destroying its contribution to the hoop strength of the tube, and causing ready venting around the area of attack, which is also the region where ignition of the propellant will begin. Violence of response to the fuel fire may also be reduced, by a thermite or other pyrotechnic "tab" or a thermally activated line charge can be incorporated into the overwrap to cut the fibre wrapping and lead to venting once the propellant is ignited.

Additional data concerning mitigation of hazards by a case design is found in Chapter 6 of this report.

2.3.2. Nozzle

The nozzle converts the thermal energy of the reacted gases into propulsive thrust. Rocket motors in general employ the De Laval or convergent-divergent type of nozzle (as in Fig. 2) through which the high-pressure gases from the combustion chamber are expanded to create a high-velocity jet in which the exhaust velocity is substantially greater than the sonic value attained at the nozzle throat. This augmentation of velocity, which is essential to maximize the thrust produced, is responsible for the addition of the divergent section of the nozzle.

The design of the nozzle is highly critical and the material chosen has to be highly resistant to erosion by the hot high-pressure propellant gases, and the longer the burn time, the more resistance is required. Graphite, various steels, and molybdenum have all been employed, while vapor-deposited tungsten on a graphite substrate and pyrolytic graphite deposited as a shell on a graphite substrate have been proposed for high-performance motors.

2.3.3. Propellant

Solid propellant rocket motor compositions may be grouped into three major classes: (1) those based on an intimate mixture of nitroglycerine (NG) and nitrocellulose (NC) (double-base propellants); (2) those based on a two-phase system of fuel/oxidizer, usually ammonium perchlorate (AP) and (usually) a hydrocarbon-based polymeric fuel and often a metallic fuel (e.g., aluminum) (composite propellants); (3) hybrid compositions containing (e.g.) AP and a binder (often with metallic fuel) as well as NG and NC (composite-modified double-base propellants). These propellant classes may each be subdivided into several types as described in the following subsections.

2.3.3.1. Nitroglycerine/Nitrocellulose Based Propellants

(1) Double-base

This is the oldest type of rocket propellant (apart from black powder) and was originally developed from gun propellant compositions (cordites), giving extruded double-base (EDB) propellants. NC, which is a fibrous and bulky material is gelatinized by dissolving it in NG, and the resulting colloidal mix is extruded through a die. However, the solubility of NC in NG is reduced by increase in the nitrogen content of the NC, and in addition the colloid may be too hard for extrusion. This requires the addition of plasticizers such as high-molecular weight esters (solventless cordite) or of a volatile solvent which softens the cordite and has to be removed after extrusion (solvent cordite). A mixture of NG and NC alone is too energetic and also probably too sensitive for practical use. The plasticizer may also serve as a coolant, or separate coolants may be used. In addition, nitric esters such as nitroglycerine are essentially unstable and their decomposition is autocatalytic, so that a stabilizer has to be incorporated - examples are carbamite, and 2-nitrodiphenylamine. Since the stabilizer is used up in carrying out its function, the life of propellants containing nitric esters is finite and diminishes with temperature rise. In addition, if the gases resulting from the propellant/stabilizer reactions are not sufficiently soluble in the propellant, cracks may develop in the charge, with potentially disastrous results on firing.

In general, the burning rates (r) of propellants increase consistently with pressure (p) and temperature as shown in Figs. 3 and 4. A formula of the type

$$r = ap^n \qquad (2.1)$$

where a is a constant and n is an index of value less than unity, may be applicable over limited pressure ranges, although the relationship must be determined experimentally over the temperature and pressure range of the intended application. Certain lead salts added to the composition act as ballistic modifiers, enhancing the burning rate at low pressures while not affecting it at high pressures; the result is that the rate of burning/pressure curve may have in the intermediate region a pressure range where the rate does not alter significantly (a plateau) (Fig. 3), or even a regression (mesa) (Fig. 4). This generally occurs at pressures around 5-10 MPa. Consequently many double-base rocket motors are designed to operate in this pressure region.

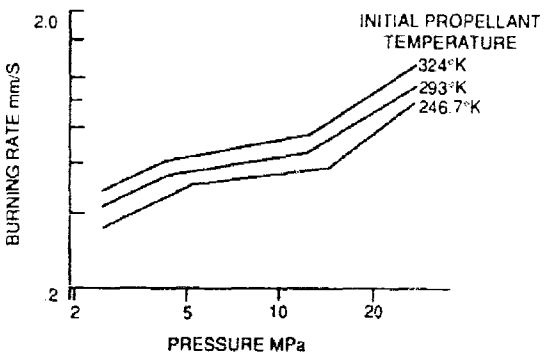

Fig. 3. Example of Burning Rates for Platonized CDB Propellant.

Many EDB compositions have been developed and used, but the size of propellant charges that can be made by the solventless process is limited by the practicalities of extrusion. Although large diameter presses may be used, it is difficult to produce satisfactory propellants having a cross-sectional area greater than about 40% of that of the press cylinders, even using heated equipment to reduce the viscosity. Diameters of about 300 mm are reported in the literature. On the other hand if solvent is employed, a drying time of weeks or months may be required. These difficulties led to the development of cast double-base (CDB) propellants. A mold (which may be the rocket motor case itself, with any necessary lining) is filled with granular casting powder and flooded with casting liquid - desensitized and stabilized NG. The casting powder is basically NC, but also includes all of the other ingredients as mentioned above; for more energetic compositions, some stabilized NG is also used in the casting powder. The NC causes the powder to swell up and absorb the liquid over a period of a few days at a "curing" temperature of about 60°C. Complete homogeneity is not however obtained in a finite time and sections through CDB charges present a characteristic mottled appearance. This method is much more suitable for making charges of complicated cross-section (as required when a high mass burning rate and hence a large burning surface is called for) than processes based on extrusion.

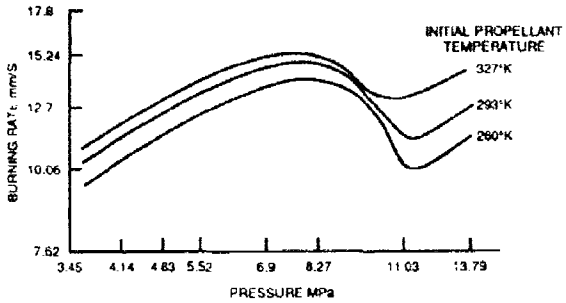

Fig. 4. Example of Burning Rates for Mesa Propellant.

2.3.3.2. Composite Propellants

Composite propellants contain solids, generally in the form of powders, which are uniformly suspended in a rubber binder. They are widely used because they can be loaded into motors ranging from small guided missiles to large space boosters. Moreover, such characteristics as wide temperature range mechanical properties, thermal stability and aging characteristics are generally superior to other classes of solid propellants.

1. Asphalt

The first slurry cast composite propellants were made in the mid-1940's from a molten asphalt-oil binder, and an oxidizer. A propellant containing 75% potassium perchlorate was used in jet assisted take-off units (JATO).

2. Polysulfide Rubber

A liquid curable polysulfide rubber soon replaced the relatively weak asphalt. These prepolymers were terminated in mercapto (SH) groups. Mild oxidizing agents were used to convert these groups to -S-S links, a process which yields a rubbery polysulfide. Polysulfide propellants were processed under conditions similar to those used for current composite propellants. These propellants were widely used in the 1950's and 1960's, in tactical rockets, as well as in sounding rockets and aircraft seat ejectors.

The energy of these formulations suffered from the presence of sulfur, which decreases both working fluid and enthalpy release.

3. Polybutadiene

The next major advance in composite propellants came with the introduction of liquid curable polybutadiene acrylic acid copolymers and terpolymers containing acrylonitrile. These binders enhanced processibility and mechanical properties of propellants. Energy was also enhanced since higher solids could be realized with a binder that contributed to a high yield of working fluid and enthalpy release. These binders were soon exploited in the Minute Man, 260-inch boosters, and other large rockets.

These binders contained random carboxyl groups and were, therefore, not capable of giving propellants with adequate elongation at the lower operational temperatures. Binders having terminal carboxyl and higher molecular weight were then developed which gave propellants with improved mechanical properties.

However, even these binders were not free from deficiencies, such as relatively high viscosities, high curing temperatures, and a tendency to undergo a gradual hardening (post curing) as the propellant aged. The curing involves the reaction of the terminal carboxyl of the binder with the epoxy curative to produce a chain extended hydroxy ester. This reaction is slow and incomplete, requires an excess of epoxy, and long cure times are needed (14 days at 145°F).

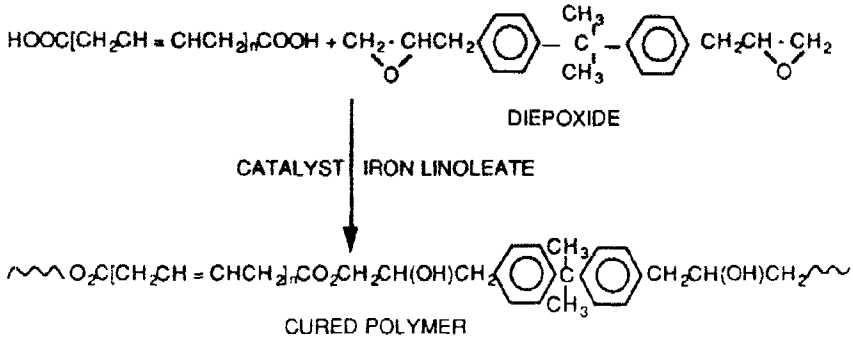

Some improvement in the curing was attained by replacement of the epoxy curatives with their nitrogen equivalents, aziridines. The curing reaction involves formation of the amido ester,

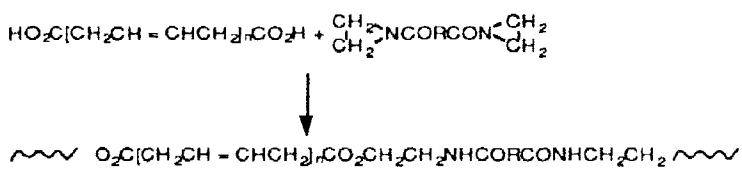

Aziridines, however, suffer from homopolymerization and oxazoline formation which require them to be used in excess as well.

Many of these problems were eliminated by the arrival of hydroxyl terminated polybutadienes (HTPB) in the mid-1960's. HTPB propellants tended to display processing, curing, and mechanical properties which were superior to CTPB's. Since HTPB was made from butadiene and hydrogen peroxide, it was less costly than CTPB's. These and other properties have caused it to become the "workhorse" binder for solid propellants. HTPB propellants can be mixed and cured at comparatively low temperatures because of the efficiency of the curing reaction, the formation of polyurethane links. The reaction with a common curative (isophorone diisocyanate IPDI)

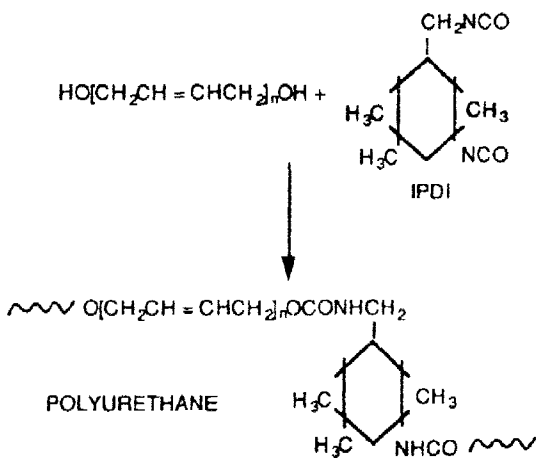

No catalyst is required unless plasticizers are present.

While the problems associated with HTPB propellants are much less formidable than with their CTPB analogues, the matter of lot-to-lot variation in the HTPB (R-45M) mechanical properties is still of concern. Lithium initiated HTPB polymers are very likely purer and are more reproducible; they

are also available in higher molecular weights, which can result in propellants having improved low-temperature elongation. These polymers are, however, more costly than R-45M.

While polysulfide and polybutadiene propellants were being produced, work was being done to develop more energetic propellants containing polyesters, nitrate ester plasticizers, AP, and Al. These gradually evolved into the modern cross linked double base propellants which contained hydroxyl terminated polyethers and polyester binders, nitrate esters, and HMX in addition to AP and Al. Double base was used at low levels to enhance tensile stress and modulus in these highly plasticized propellants. Nitrate ester plasticized polyether compositions, NEPE, propellants were developed from a higher molecular weight polyether (Peg E-4500). NEPE propellants have relatively high elongations (> 200%). Gradually, cellulose acetate butyrate has replaced the NC as a cross which has less tendency to degrade elongation. Recently propellants containing tri and tetra functional polyethers high molecular weight (≥ 21,000 daltons) have been found to exhibit stress values over 160 psi and elongations over 800%. These tough propellants containing no NC or CAB to degrade elongation may be useful in "Insensitive Munitions."

2.3.3.3. Hybrid Compositions

This term is applied here to compositions sharing some of the characteristics of both double-base and composite propellants. Composite-modified cast double-base (CMCDB) compositions have been manufactured using the CDB process. They contain a substantial proportion of aluminum and ammonium perchlorate in addition to the normal CDB ingredients. These additional ingredients are added to the casting powder. For these compositions carbamite and 2-nitrodiphenylamine are not effective stabilizers and resorcinol is used instead. Unlike the CDB compositions these are not platonized or mesonized, nor are they smokeless. CDB compositions containing nitramine are mentioned above. At least one cast composition containing AP, aluminum and nitramine as well as CDB ingredients is in service use. Composite modified double base propellant are made by a composite propellant process.

Elastomer-modified cast double base (EMCDB) propellants have been developed in the UK to reduce propellant frangibility. These materials can incorporate a reduced NC/NG ratio which leads in turn to a reduction of observables in the plume. These compositions like the CDBs, may be modified by the addition of nitramines.

2.3.4. Igniter

The type of igniter most commonly used with solid propellant motors having a bore configuration is a pyrotechnic device, the main charge consisting generally of a heterogeneous mixture of powdered metal (e.g., aluminum or magnesium) and an oxygen-rich inorganic salt (e.g., a metal perchlorate). It may be in the form of pellets or powder; if the former, then some powder is still required to convey the ignition to the pellets from the initiation system - a fusehead (squib) electrically initiated. The container may be a paper carton (for small motors) or a perforated metal container with the holes sealed with thin metal foil. The action is to convey the heat of reaction of the igniter composition partly by convection of hot gases, partly by impact of hot particles of solid or liquid metal oxide and partly by radiation, to the propellant surface. The igniter is normally located at, or extending down the conduit from the head end of the motor (Fig. 1) so the efflux of gas from propellant ignited near that end will help to spread the ignition along the motor.

Although much research has been done in this field, the ability of such an igniter to perform satisfactorily (igniting the whole exposed propellant surface in say 15 to 20 ms) can in practice only be assessed empirically; in addition, the igniter composition reaction products are smoky. With the development of larger motors the trial and error approach became too costly and this has led to the development of the pyrogen igniter, which consists essentially of a propellant charge with nozzles, i.e., in effect a small rocket motor used to ignite the larger motor. The replacement of the pyrotechnic composition, whose burning mechanism is not well understood, whose heat transfer mechanism involves two phases, and whose products of combustion are smoky, by a propellant composition whose mass burning rate can be controlled, whose combustion products may be gaseous only, and also effectively smokeless (if a double-base or ammonium nitrate based propellant is used) obviously improves the prospects of placing igniter design on a more scientific basis. In the meantime pyrogens have been incorporated in a range of large rocket motors and the viability of the concept has also been demonstrated for smaller motors.

2.3.5. Discussion

The development of rocket motors follows the general pattern that (other things being equal) the greater the performance sought, the greater the hazard presented, but as with all such generalizations, this cannot represent the whole picture, since the "other things" in practice are not "equal." There are in fact several points to be taken into account.

The oldest type of rocket propellant, EDB, had adequate performance and relatively (although not completely) smokeless exhaust, but suffered from a high temperature coefficient of burning rate which can result in a considerable increase in chamber pressure between the upper and lower ends of the service temperature range. This led to penalties since not only is the chamber required to withstand the maximum pressure at the highest operating temperature (and is therefore unnecessarily strong and massive at lower temperatures), but in addition the thrust/time characteristics would vary. From the point of view of hazard, EDB propellants are very brittle under fragment and bullet attack conditions over the whole service temperature range and this can lead to very violent deflagrations. At low temperatures brittle characteristics will be exhibited at lower stresses and shrinkage cracks may develop. At high temperatures the life of the motor is limited by the stabilization of the propellant, and the possibility of gas-cracking as a result of the rate of generation of gas from decomposition of the propellant and stabilizer outstripping the rate of diffusion to the outer surface of the charge and exceeding solubility in the propellant - this latter being expected to diminish as the temperature rises. In addition the inhibitor may soften if nitroglycerine and/or gas diffuse into it, especially at high temperature.

CDB propellants share many of the defects of EDB propellants, but owing to the different method of manufacture, they are less brittle and show lower vulnerability to projectile attack at room temperature and above, though still exhibiting brittle fracture at temperatures below 0°C. Aluminum can be incorporated into the casting powder which increases the performance at the expense of greater opacity of the exhaust. Compared to EDB propellants, CDB propellants are more likely to exhibit exudation of NG (more or less diluted) on to the surface of the propellant; this is encouraged by low temperatures when the NG can crystallize out. Although larger motors can be manufactured using CDB than with EDB it has to be remembered that gas cracking will be a more serious problem with these larger grains and consequently service life at high temperatures may be reduced.

CMCDB propellants exhibit higher performance than CDB but exhibit the various problems associated with the CDB and EDB classes; in addition, the addition of AP destroys the platonization which has been one of the advantageous properties of the other classes of propellant.

To increase the efficiency of rocket motors it is desirable if possible to increase the chamber pressure and since the pressure range for platonization in double-base propellants varies very little between different compositions, there is now an increasing tendency to use composite propellants.

These consist of mixtures of fuels and oxidants as separate molecules, now usually bound together in a polymeric rubbery matrix. Their main advantages over double base propellants lie in their increased overall energy, density, burning rate, and specific impulse, their improved mechanical properties and storage life and their reliable stable combustion in the presence of metallic fuels such as aluminum. The main disadvantage of composite propellants is undoubtedly their smoky exhaust plumes. Many missile designers are looking for high energy smokeless propellants with minimum signature and attenuation. The smoke they produce can conveniently be classified into two types, viz. primary smoke, produced from the combustion of aluminum to Al_2O_3 which gives the characteristic white plume, and secondary smoke, derived from the condensation of HCl in humid conditions. Primary smoke can obviously be eliminated by formulating nonaluminized compositions, but this usually results in energy reduction. Nitramines have been used as alternative oxidizers but these also have disadvantages such as slower burning rates, higher pressure exponents, and increased vulnerability of the system.

In addition, when the metal content in composite propellants is reduced considerably or eliminated altogether there follows the distinct possibility of combustion instability, which has been found to depend also on the size distribution of the oxidant present. This problem can sometimes be overcome by redesigning the motor and grain geometry, but often more effectively by small changes in composition involving addition of refractory materials such as ZrC, Al_2O_3, or TiO_2 in carefully monitored particle sizes.

Composite propellants can undergo surface oxidation under storage at high temperatures, particularly in the presence of certain burning-rate modifiers. This process results in extra cross-linking and formation of a hard skin, which in turn may sensitize the propellant charge to mechanical stimuli.

The propellant-to-case weight ratios for traditional metal-cased rocket motors may be improved by the substitution of part of the metal by means of structural fiber, and further improved by the use of aluminum rather than steel for the remaining thickness. However if the external layer is of insulating fiber (e.g. Kevlar) and adhesive, this in combination with the metal layer below will (unless the metal is earthed/grounded) introduce a capacitive effect, leading to the capability to store and discharge electrostatic energy. Handling the motor, especially under low humidity conditions, may produce large electrostatic charges on the insulating outer layer, and the electrically isolated propellant grain will then acquire a substantial electrical charge by induction. Any break in the continuity of the conductive surface (e.g., the nozzle end of the motor) may then lead to a discharge to the propellant,

and to internal ignition. Experimental work suggests that cracking of the propellant always precedes such ignition, and the extra burning surface so produced may lead to a very violent event.

This hazard is not necessarily revealed by laboratory-scale tests on finely divided propellant, and increasing the size of the sample may lead to a reduction in the electrostatic spark energy necessary to ignite the material and hence to an apparent increasing sensitiveness. The development of the event appears to be related to the conductivity of the propellant under high voltage conditions, which may lead to breakdown of matrix insulation between adjacent metallic particles.

Future trends in rocket motor development appear to extend in two principal directions which give the impression of leading opposite ways. The first is in response to a demand for increasingly energetic and faster-burning compositions. Increase in energy is a matter of thermochemistry; most propellants in service are fuel-rich in terms of stoichiometry to the most favorable product system, viz carbon dioxide and water, and development of energetic binders for composite propellants, to replace the older types discussed earlier, should improve the energy output. Stability problems, however, may complicate matters. The use of nitramines in nitroglycerine/nitrocellulose based systems is expected to be further developed. Increase in burning rates may be achieved by the use of "ultra-fine (US) or "micronized" (UK) ammonium perchlorate in composite propellants. Both these types of development are expected to increase potential hazards and to run counter to the second trend: the development of "insensitive" or more precisely "low-vulnerability" munitions. Any type of composition may be manufactured to include thin wires to improve the conduction of heat from the reaction zone into the unburnt propellant. The result is effectively to increase the burning surface area

To meet performance requirements in addition to the demand for reduced vulnerability has called for re-examination of the motor case material as well as the propellant composition(s). The frangibility of the latter is of prime importance in determining vulnerability to projectile attack since even a local increase in burning surface following crack propagation can lead to motor explosion. This has led to an increasing interest in the use of elastomeric binder compositions to decrease frangibility in all classes of propellant. The problem is expected to be most severe at low temperatures where dramatic increases in vulnerability to projectile attack are experienced at temperatures below the strain-rate-adjusted glass transition temperature. The use of polymer-fiber-overwrapped case materials (in addition to reducing the case/propellant mass ratio, leading to increased motor performance) decreases motor vulnerability to projectile attack; cutting the fibers leads to substantial reduction of case strength and consequent easier venting.

Cook-off presents a different problem, unless the case strength itself can be reduced by degradation of the case material before the propellant ignites, as with steel strip-laminate cases. Here interest is being shown in the use of linear charges of pyrotechnic composition ("thermite tabs") or line-cutting charges to weaken the case and provide venting before the propellant ignites and the motor becomes propulsive or explodes.

The application of unexpected mechanical stresses, e.g., if the motor is dropped, can also result in damage leading to disaster on subsequent ignition; in general any motor which has been dropped is considered unsuitable for use.

With very large rocket motors extra problems arise. The motor case or beaker (tape wrapping around the propellant grain with compatible adhesive) provides support to the charge, but the larger the charge the greater are the distortions produced by the strains experienced on motor acceleration ("g" stresses). Depending on the propellant rheology these deformations may become unacceptable, e.g., if they lead to even partial blocking of the conduit or nozzle, producing internal pressure rise and motor failure. Case bonding is always a potential source of weakness and the position is more critical with large motors; debonding, loss of support to and consequent disruption of the grain can be expected to have catastrophic results. With such motors the balance between performance, standards of manufacture and maintenance, and hazard is even more critical than with normal motors, especially in view of the greater potential consequences of failure.

2.4. TERMINOLOGY

The equivalent terms for the various parts of the motor are given in Table 1.

Table 1. Equivalent Terms in Rocket Motor Technology.

UK, USA	Germany	France
Motor	Motor (Triebwerk)	Propulseur
Head end	Kopfseite	Fond avant
Rear end	Düsenseite	Fond arriére
Case	(Brenn)Kammer	Structure
Propellant (or Propellent)	Treibstoff	Propergol
Grain (or Charge)	Treibsatz	Bloc
Solid	Fest	Solide
Port/perforation	Gasströmungskanal	Canal
Nozzle	Düse	Tuyére
Throat	Düsenhals	Col de Tuyére
Closing disc	Abdichtmembran	Opercule
Web	(Wand or Web)stärke	Epaisseur
Vent plug	Entlüftungsstopfen	Bouchon évent
Inhibitor	Inhibitor	Inhibiteur
Insulator	Isolation	Protection Thermique
Liner	Liner	Liner
Pressure relief	Druckentlastung	Dispositif d'arret de poussée
Igniter system	Anzündsystem	Systéme d'allumage
	Anzündpille	Inflammateur
Igniter	Anzünder	Allumeur
Fusehead/squib	Anzündsystem	Inflammateur
Thrust	Schub	Poussée
Single-stage motor	Einstufen-Motor	Moteur á un étage
Two-stage motor	Zweistufen-Motor	Moteur á deux étages
Rocket	Rakete	Roquette
Casting powder	Giebgranulat	Poudre á mouler
Casting liquid	Giebflüssigkeit	Solvant de moulage
Missile	Flugkörper	Missile
Boost Motor	Start Motor	Moteur d'accelération
Boost Propellant	Start Treibsatz	Propergol d'accelération
Sustainer Motor	Marsch-Motor	Moteur de croisière
Sustainer Propellant	Marsch-Treibsatz	Propergol de croisière
Case binded Propellants		
Blast Tube		
Port		

CHAPTER 3. OVERVIEW OF SOLID PROPELLANT ROCKET MOTOR HAZARDS AND HAZARD TESTING

This Chapter introduces terms and concepts in order to lay a proper foundation for discussions in subsequent discussions in this report. Following definition of selected terms, the concept of flow charting is introduced. Flow charting is used to show the process associated with an initial event leading to the response of a rocket motor. This is important in the concept of hazard protocols which is introduced in Chapter 4. Finally, important aspects associated with hazard testing are presented.

3.1. DEFINITIONS

HAZARD - The ever present potential or threat of causing damage or loss, independent of any specific unsafe situation or stimulus. Hazard is an inherent property of each ordnance item, especially of the active parts. The hazards can appear within the context of:

- Safety: chance events
- Vulnerability: effects of deliberately hostile stimuli
- Normal functioning or functional hazards: hazards when a solid propellant charge is consumed functionally. These could result, for example, from the nozzle exhaust plume - thermal effects, hot gases, small particles of alumina, and excessive noise.

In this AGARDograph, functional hazards are not considered.

The problems of hazard are compounded by the desire to always want the highest performance that can be achieved. Unfortunately, as the energy density of the propellant is increased, the hazard sensitivity and output of unwanted reactions are usually increased also. Thus the problem is to provide the maximum performance consistent with acceptable hazard. This involves performance/hazard trade-offs.

DANGER is a property of a certain defined unsafe situation, characterized by the hazards of the danger source, the vulnerability of the endangered object, and environmental conditions.

SAFETY is the antonym to DANGER; a high safety level corresponds to a low danger level and vice versa. The concept of SAFETY is linked with accidents. ACCIDENTS are unintended events that produce effects that may lead to damage. 100% SAFETY or ABSOLUTE SAFETY means the absence of any hazard in the regarded danger situation. For activities involving active parts of ammunition, such as rocket motors, absolute safety is not possible. Therefore they are said "safe," if the danger emanating from them is limited to an acceptable level compared to other risks to which we are exposed.

SAFETY and DANGER are linked to an activity such as loading, transporting, storing, testing, or operational use of a rocket motor; it is not a property of the motor itself. For example we do not refer to the safety of a motor, but to the safety of machining propellant or transporting the motor.
RISK is a measure of danger and involves consideration of probability and potential damage level.

RISK PRESENTED BY AN ACTIVITY contains the probability of the undesired event(s), the output level of that event(s), and the extent of the possible damage or consequences. There is no internationally agreed generally "acceptable risk" level. The degree of acceptability obviously changes with situations. In war time much higher risks are accepted than in peace time. Similarly if an ordnance item is "critical" more risk will be accepted than if the item were "normal."

The task of RISK ANALYSIS is to identify hazards and the causal chain for specific danger. The possible causal chains are of central importance because they serve as a pattern for developing preventive measures and as a basis for estimating the rate of occurrence of the undesired event.

MITIGATION is an action to reduce the reactivity of the ordnance to a given stimulus.

INITIAL EVENT is the trigger event that leads to a stimulus(i) being applied to a rocket motor and the subsequent RESPONSE of the propellant, producing EFFECTS or OUTPUT that result in DAMAGE to personnel or materiel in the surroundings. The following sections discuss these subjects.

3.2. INITIAL EVENTS

Initial events are associated with some activity with the rocket motor. These activities include:

- manufacture
- shipping and handling

- storage (includes placement in and removal from)
- active storage or staging (e.g., "bomb farms" on aircraft carrier decks)
- integration on platform (aircraft, tank, ship) in a semi-ready state
- arming (semi-ready to ready, armed state)
- operation (both test and actual use)
- destruction, demilitarization

The initial event can be due, as shown in Fig. 5, to:

- the rocket motor alone
- the rocket motor as an integral part of the missile
- the environment (everything outside the motor or missile)

The initial event can lead to an undesired event through the four paths shown in Fig. 5.

In path one, the initial event is generated by the motor itself. For example, stabilizer depletion in the solid propellant could lead to an autocatalytic reaction and ejection of part of the propellant grain through the nozzle causing a rapid pressure increase in the motor.

In path two, the environment affects the motor. For example, external heating such as fire or exhaust impingement; vibration during shipping, handling, captive carriage; abnormal stimuli from accidents such as truck crash, aircraft crash; lightning or electrostatic discharge; and deliberate hostile acts such as bullet or shaped charge jet attack.

In path three, the environment causes reaction of a missile component or subcomponent other than the motor, which in turn results in a reaction of the motor. For example, a fragment impact detonates the warhead which in turn causes an undesired reaction in the motor.

Path four is similar to path three, but instead of an outside stimulus setting off a missile component, the component sets itself off and causes an undesired reaction in the motor.

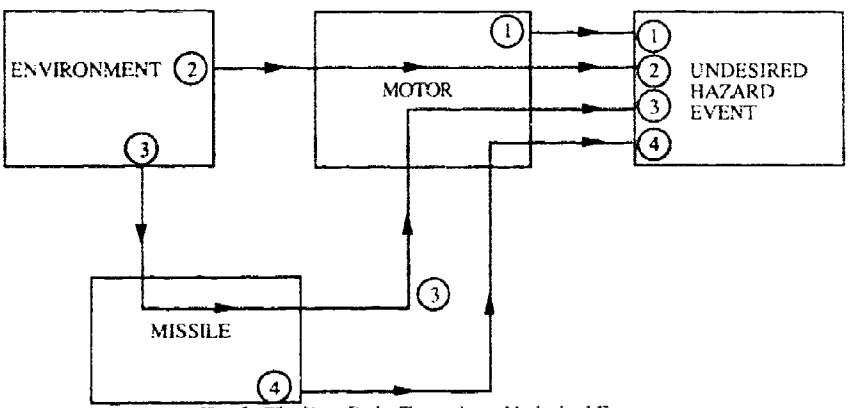

Fig. 5. The Four Paths Towards an Undesired Event.

3.3. RESPONSE OF MOTOR TO INITIAL EVENT

Fig. 6 presents the various responses of the motor to the initial event. The initial event induces response of the motor into either:

1. No chemical reaction with or without motor degradation (mechanical damage). When degradation occurs and is undetected, then a hazardous operating situation may be encountered.

2. Chemical reaction which could be:

- local decomposition or burning
- burning
- thermal explosion
- partial detonation (detonation of a portion of the propellant grain)
- detonation

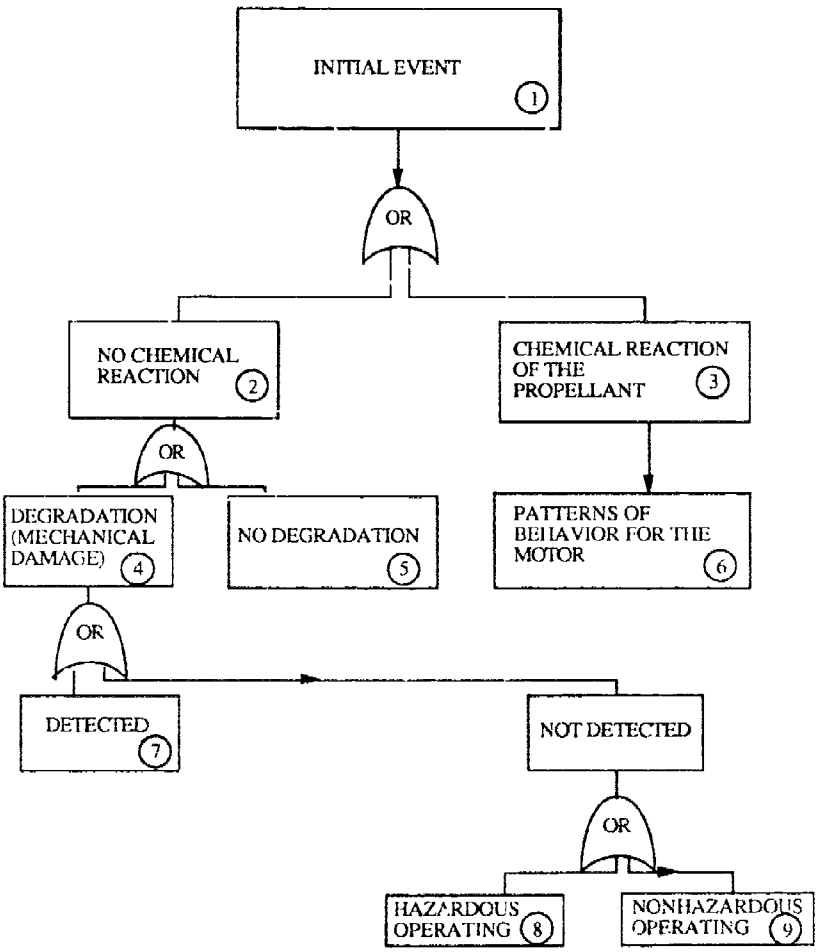

Fig. 6. The Nature of the Response of a Motor to an Initial Event.

These chemical reactions could lead to any of the following motor actions:

- no significant external output
- burning with or without limited projection of debris
- self-propulsion
- mechanical burst/pressure burst
- deflagration with propulsion
- partial detonation
- detonation

3.4. OUTPUT/EFFECTS

The response of the propellant to an initial event may produce primary and secondary effects that include:

- Thermal flux, flames
- Projection of motor fragments and live and inert propellant debris
- Self-propulsion of the motor
- Blast and shock waves
- Smoke

The projection of propellant is of concern because these fragments can possibly explode or detonate at their point of impact, causing an indirect hazard, that greatly spreads the area that must be considered.

The energy release rate of the propellant will determine the intensity of these effects. Data relevant to establishing a propellants' energy release in terms of TNT-equivalency and debris distribution, thermal radiation levels, and fireball diameter can be found in Baker et al, 1983.

3.5. HAZARD RESULT/DAMAGE CONSEQUENCES

Hazard output causes damage to personnel and materiel. As previously mentioned, the main damage mechanisms are thermal (fire, heat), blast overpressure and hazardous fragments. The damage caused will depend on the environment in which it occurs. For example, levels of blast that are catastrophic in the confined space of a tank or ship's holds, or near an aircraft, may be relatively benign in the open. Similarly the damage potential of thermal and fragment output from reacting munitions is dangerous in proportion to proximity of personnel, other munitions, or susceptible material. For review of probabilities of injury or death of personnel, damage to structures or equipment as a function of output intensity, publications by Zaher, 1975l; Mosely, 1986; and Boisseau, 1986, a recommended:

The damage done to other motors is also of importance. As will be shown in later chapters, the composition and the condition of the propellant is an extremely important consideration: less than 1% voids dramatically changes the response to mechanical shock. Damage cannot only come from primary sources described above but can be caused by:

- handling (dropped, rough handling)
- storage (temperature and humidity)
- multiple captive carriage
- age
- debonded from the case

This subject is treated more fully in NATO AC/258 and U.N. Recommendations for the Transport of Dangerous Goods.

3.6. TESTING IN GENERAL

Testing of energetic materials is concerned with whether or not a sample responds to a given stimulus and the type and level of response for a given stimulus in a given environment. Realistic description of sample, stimulus, and environment is important, as will be seen later. For example, the same material may respond differently to the same stimulus depending on environmental effects such as confinement; lack of confinement may make the difference between a detonation response and a mild reaction. Similarly, the state of the sample may determine whether initiation occurs; for example, a slighdy damaged propellant may detonate when subjected to a given shock level while its undamaged counterpart will not detonate.

Statistical probability is one of the problems associated with inadvertent initiation of munitions or articles containing energetic materials. In cases where hazard risk is expressed in probabilities of one response in tens, hundreds, or thousands of trials, statistically meaningful testing is so costly and time-consuming as to be impossible. In reality, the issue is usually completely avoided by performing inexact tests that demonstrate "safety" with two no-go responses to a "standard" stimulus. Quite obviously, when this is done, we are often so far from conditions that will initiate hazardous reaction that almost nothing relevant is learned from the tests.

3.6.1. Types of Tests

The stimuli the motor is likely to see and its frequency of occurrence must be defined in the context of the environment. This definition of environment and stimuli is the threat assessment, telling the munitions designer what threats he must design for. Just as the designer is told what vibration

levels, g-loadings, and temperatures the design must accommodate, he also should be told what hazard situations must be considered.

The hazard phenomena and the methods of assessing the hazard may differ between countries, but all hazard assessments include testing and analysis. Chapter 5 discusses the testing and analytical methods for each of the technical areas. Before those discussions, it would be good to review testing in general, before discussing specific testing.

Development of motors require tests at both ends of the design spectrum: (1) tests, usually small-scale laboratory or test cell tests, that yield data necessary early in the design cycle for the actual design work, (2) intermediate, and (3) large-scale, all up component or munition tests obviously occurring at the end of the design cycle that tell the program office whether the design goal was achieved and by what margin. The large-scale tests are the "proof of the pudding"--no matter how good your small-scale test results and predictive methods are, you will still have to do some large, all-up tests. However, large-scale testing has some drawbacks.

1. Large scale tests are costly and we don't do many. The total cost includes the test itself and the cost of the test article--a rocket motor or a warhead section. Both are expensive.

2. Poor instrumentation. Because of the potential violence of a hazard reaction, most large-scale tests are done in a remote location. With few exceptions the level of instrumentation on these field tests is much less extensive than on laboratory or test cell tests. In many cases there is no instrumentation other than slow speed video cameras, and the test results are either "go" or "no-go".

3. Emphasis on "pass". Often it is the program office who is paying for the large-scale test. Understandably, their emphasis is on passing the test; hazard testing is just one more milestone that must be successfully accomplished. If two passes are achieved, who wants to press their luck?

As a result of the above considerations, large-scale testing usually yields few, very "relevant", but poorly instrumented pass/fail results. There is no real measure of margin of safety, and the data do not provide much of a statistical base (especially when many of our hazards are 1 in 100 to 1 in 1,000,000 probability).

You may question why one should worry about hazards whose probability of occurrence are so low. But concern must be given if (1) the consequences of reaction is extremely severe, e.g., detonation of a ballistic missile, or (2) if the number of "trials" is high, e.g., launching and retrieving aircraft on an aircraft carrier. These are ends of the spectrum; we must be able to make assessments that consider probability of occurrence and severity of output. Unfortunately a few large-scale tests may not provide us with the information necessary to make the assessments.

Consider a series of N tests with x tests resulting in explosions. The probability of an explosion occurring on any one test is P, independently of what happens on any other test. Then the probability that no explosion will occur on any of the N tests is $(1 - P)^N$; hence, the probability P_X of at least one explosion occurring in N tests is

$$P_N = 1 - (1 - P)^N. \tag{3.1}$$

This equation can be used to calculate P_N if we are given P and N. Or, we can solve this equation for N to get

$$N = \frac{\ln(1 - P_N)}{\ln(1 - P)}, \tag{3.2}$$

which can be used to calculate N if we are given P and P_N.

For example, suppose P = 0.01, and we perform N = 50 tests. Then by Equation (3.1), the probability of seeing at least one explosion is

$$P_N = 1 - (1 - 0.01)^{50} = 0.395\ldots$$

Thus, there would be only a 40% probability of seeing at least one explosion in 50 tests. To find out how many tests we would need to increase P_N from 40% to 95%, we invoke Equation (3.2) to get

$$N = \frac{\ln(1 - 0.95)}{\ln(1 - 0.01)} = 298$$

Similarly, if there is only a one-in-a-thousand chance of an explosion occurring on any one test, then to be 95% certain of seeing at least one explosion, the number of tests needed would be

$$N = \frac{\ln(1 - 0.95)}{\ln(1 - 0.001)} = 2{,}994$$

In many hazard testing programs, especially those involving large scale tests, only two trials are run at a given condition. Equation 3.1 can be solved for this case of N = 2 tests to see what is the probability of getting an explosion in the two tests, given the probability P of an explosion occurring on any one test. Results of such a calculation are given below.

Table 2. Dependence of Probability of Explosion on Number of Tests.

P, probability of explosion in one test	P_N, probability of explosion in N = 2 tests
.001	.2%
.01	2.0%
.05	10.0%
.10	19.0%
.20	36.0%
.30	51.0%
.40	64.0%
.50	75.0%

As mentioned earlier, many hazards, one in a thousand, one in a hundred, or one in ten occurrences (actually, one in ten hazard or higher occurrences) are often said to be too hazardous and we try to avoid those situations altogether, yet when only two tests are conducted, we have a low probability (.2%, 2%, and 19% for the 1 in 1000, 1 in 100, and 1 in 10 cases) of detecting the hazard.

In addition to low statistical basis for even a given test with prescribed stimulus and environment, a few tests cannot cover the range of stimuli and environmental conditions the munition is likely to encounter. As will be discussed later, a 20 mm bullet fired at service velocity is but one point in bullet mass - velocity plane. As will be shown, passing the 20 mm bullet test does not necessarily mean that other bullet tests will be passed; smaller, slower bullets, or the 20 mm bullet at lower velocity, may cause explosion of motors that passed the standard 20 mm bullet test. See the hazard mapping of Chapter 4.

Margin of safety, a desired design consideration (tells the designer whether he's on the ragged edge between passing or failing, or whether he has much flexibility before approaching the edge) cannot adequately be assessed by a few pass/fail tests.

Small-scale laboratory or test cell tests, on the other hand, inexpensively provide (usually) much data with reasonable control of the variables within the range of experience. However small scale tests only give order of magnitude comparison with data from experience (or in comparison to a well known reference test material), therefore the relevance of the small scale data to the large scale situation may be questioned. We must select the correct way to predict scaling effects. This latter consideration may require predictive analytical models; unfortunately, in many of the hazard areas the models are not sufficient to do this extrapolation. Thus, from the small-scale tests we may get much data in controlled situations, but we must ask ourselves how we are going to use these data.

3.6.2. Testing to Failure

If a "pass" response is achieved, continued testing (more tests or altering the stimulus or environment) should occur until failure responses are achieved. We usually learn more from a "failure" than a "pass" - (initiating stimuli, violence of output, margin of safety, etc.). But perhaps more importantly, lack of failure can be deceiving as just discussed with respect to the 20 mm bullet test. One of the most common deceptions resulting from lack of failure surrounds the card gap test (this test is discussed later). Many people publicize propellants "having zero card gap" as being nondetonable. This is not the case. A zero card gap simply means that the critical diameter (the smallest diameter which can sustain a steady state detonation) of the propellant is larger than the 1.44 inch diameter of the card gap test. It doesn't tell you if the critical diameter is 5 inches or 40. If it were 5 inches and you loaded that propellant into a 13 inch end burning motor, you would have a detonable motor. Again, lack of results can be deceiving.

3.6.3. Test Categorization

The major types of stimuli are

- Heat
- Mechanical deformation
- Shockwave
- Electrical discharge

Within each of these types of stimuli one can distinguish different levels of intensity of the stimulus.

Heat stimuli range from slow (bulk) heating to fast heating associated with unpacked munitions in a fuel fire.

Mechanical deformation can be caused by a drop of unpacked munition of several meters, or by bullet/fragment impact.

Shockwaves can be generated by high velocity impact of projectiles and shaped-charge jets, as well as the adjacent detonation of high explosives.

Sparks can be generated as a result of static electricity by humans or machines, faults in electrical equipment and even lightning.

Electromagnetic radiation can lead to a reaction in ammunition by its action on the Electro Explosive Device (EED).

These types and degrees of stimuli usually are discussed under labels of fast cook-off, slow cook-off, or thermal explosion, sympathetic detonation (fragments and/or blast are stimuli), bullet or fragment impact, and electrostatic discharge.

Tests are usually called out for these phenomena. For example, the U.S. in its Joint Service "Insensitive Munitions" Policy addresses these hazard threat areas, and has pass/fail criterion for each test. These are given in Table 3.

Table 3. Insensitive Munition Requirements Source: NAVSEAINST 8010.5 (See also proposed MILSTD 2105A).

Hazard Threats	Record	Criteria
Slow Cook-Off	• Internal Temp at Energetic Mat'l/ Inert Interface at Reaction • Blast Over Pressure	No Reaction More Severe than Burning
Fast Cook-Off	• Fire Temp • Blast Over Pressure • Location of Debris	No Reaction More Severe than Burning
Fragment Impact		• Assessment and Credible Event Analysis • No Reaction More Violent than Burning
Bullet Impact	• Blast Over Pressure • Location of Debris • Camera Coverage	No Reaction More Severe than Burning
Sympathetic Detonation (Ship Stowage, Magazine or Launcher)		• Assessment and Credible Event Analysis • No Sympathetic Detonation in Stowage Configuration

3.6.4. Sample Selection

The sample itself must be adequately identified and described. Is the item(s) to be considered a rocket motor?, the missile?, several missiles in a shipping container? In the instance of the rocket motor by itself or as a subcomponent of a larger consideration, what is the propellant (ingredients, amounts, particle sizes, grain configuration, etc.) and is the propellant:

- freshly manufactured, freshly loaded
- aged (perhaps with stabilizer depletion, particle size change, etc.)
- damaged

3.7. EVENT PROBABILITIES

For peacetime conditions it is useful to apply the methods of risk analysis and safety assessment to assess the hazards in a given situation in a quantified way. The methods used for such a safety assessment are briefly described in Annex I. A more complete description will be found in "Compilation of Damage Models," 1989.

CHAPTER 4. SOLID PROPELLANT ROCKET MOTOR RESPONSE TO THREATS

A new hazard analysis approach for solid propellant rocket motors is introduced in this chapter. This analysis approach, termed Hazard Analysis Protocol, involves assessment of a given threat and the identification of tests and analysis necessary to yield the necessary data for the design and fabrication of solid propellant rocket motors. This is a pivotal chapter in this report in that it relates the subject of system threat to that of the technical areas associated with hazards.

4.1. THE CONCEPT OF HAZARD ANALYSIS PROTOCOL

Hazard threats are not simple and should be considered early in the design of a solid rocket motor. Consider the hazard threats listed in Table 2. These are mixtures of stimuli and response. It can be seen that bullet impact and fragment impact are stimuli, sympathetic detonation is a response, cookoff is an incomplete combination of stimulus (heat) and response (the response is either no reaction, burning, deflagration, explosion, or detonation). To move from these hazards areas and identify the tests that would provide data necessary for rocket motor design (rather than pass/fail criteria), the hazard areas must be further divided and refined.

The Hazard Analysis Protocol concept can be divided into the following four phases:

Phase 1, Protocol Process (Flow Charting)
Phase 2, Hazard Mapping
Phase 3, Application of Hazard Technology, and
Phase 4, Identification of Methodology Deficiencies

In the following sections, the Hazard Analysis Protocol Concept is defined in terms of these phases.

4.1.1. Phase 1, Establish Hazard Process Protocol

The term protocol is meant to be the order or procedure for consideration of a subject (here taken to be the hazard area). While the term protocol may be a bit unfamiliar the process is not: we use the approach many times a day -- every time we must make a multi-step decision. For example when we awaken in the morning, we make a decision whether to get out of bed. The time of day, day of week, plan for the day, and other factors influence whether we get up or not. The following logic is an example of a protocol. The first question we might ask if we awakened without the alarm clock might be "what time is it?" "Is it before or after the normal awakening time." If it is before the time to get up you might ask if you want to get up. If yes, get up. If no, is it a "special day" that requires an earlier rising. If not you can go back to sleep and start the process again later. If on the other hand, the time is the normal rising time or later, you might ask yourself if today is a work day or not. If it is, then you'd better get up. If it is the weekend or holiday, you can decide whether to get up or sleep in. The decision will partly be made by your planned activities. This then is a very simple protocol, with most of the questions amenable to a simple yes or no answer. It can be sketched in flowchart form as shown in Fig. 7. The hazard analysis protocols presented later are more complicated than this simple example but utilize the same pattern of logic. In the hazard analysis protocols presented later, because they are more complicated, each box may represent several considerations that are grouped into one topic box for ease in presentation. In formulating the various protocols, we attempt to determine what information is needed. The result of this protocol phase is a flow chart (or series of flow charts), and a list of what information is required. The list tells what information is needed; the flow chart tells when the information is needed. In many cases a piece or type of information is not needed because we are in a different part of the flowchart.

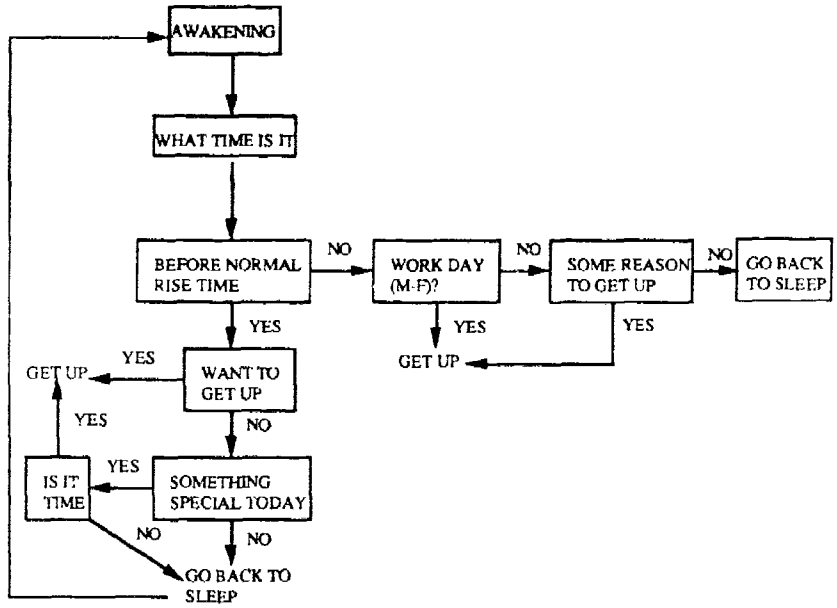

Fig. 7. Example of Hazard Analysis Protocol.

4.1.2. Phase 2. Determine Hazard Mapping

The hazard maps transform a list of information to curves on plots, and shows the location of the various curves relative to each other. The purpose of this phase is to show how you are going to use the information the flowchart said was needed. We use the plots with their information: (a) to understand phenomena, (b) to compare the hazard response with anticipated threat to determine vulnerability, (c) to aid in design predictions, (d) to help select and predict the response of large-scale tests, and (e) to indicate what further data are needed.

This chapter will present the hazard analysis protocols and a hazard mapping for for the fragment impact example. Chapter 5 will continue the process by assessing existing test methods and analyses for all hazard threat areas.

4.1.3. Phase 3. Assess Existing Techniques (Experiments and Analyses)

The listing of the phases of the process are in priority order: note that assessment of existing tests comes after you have determined what information you want, why you want it, and how and when you are going to use it. In evaluating proposals for "Insensitive Munitions" work, all too often, we see people essentially start with their existing experimental tests and analyses and try to bend them to the "Insensitive Munitions" effort. Unfortunately in many cases, the efforts are irrelevant; we cannot use the data. But having done the hazard protocol and plots phase, we know what information we need and how we're going to use it. Then we seek how we're going to obtain the data. Our assessment of existing experimental test methods includes, for each test:

- What is the test - The description would include a brief description of the test.
- What does the test measure?
- How does the test measure the desired phenomena?
- What are the advantages of the technique? How well does it measure the hazard?
- What are the limitations of the technique?

Similar consideration is given to the various analyses within each area.

4.1.4. Phase 4. Identify Deficiencies

Identify deficiencies. The above phase identified deficiencies of the individual test techniques and analyses. This phase identifies deficiencies in the application of the techniques of Phase 3 as well as other deficiencies of the program:

- Do we lack needed data?
- Do we lack needed tests and analyses? Phase 3 may have indicated that we have no viable technique for assessment.
- Do we lack instrumentation?
- Do we lack consistency between investigators and establishments?
- Where we cannot reach consensus, can we at least identify and make recommendations as to how the issues may be resolved?

Given the above process, the various hazard situations described in Chapter 3 will be examined. It will be noted that the hazard - Fragment Impact - has the most complete analysis according to the Hazard Analysis Protocol. Other hazard threats were in a preliminary stage at the time this report was written.

4.2. COOK-OFF/THERMAL THREAT

Originally the term cook-off was reserved for the situation of a cartridge within a gun not being initiated by the bolt but igniting after heating by the hot barrel. With the increasing energy content of energetic materials the meaning of the term cook-off has broadened and now is concerned with how munitions react to thermal stimuli ranging from exhaust impingement or fuel fires (fast cook-off) to bulk heating or self heating (slow cook-off). The thermal gradients dT/dx and heating rate dT/dt are the prime differentiations between fast and slow cook-off (other than heat source). Slow cook-off reactions are bulk heating (very low dT/dx) and slow heating rate (3.3°C/hr in U.S. "standard" slow cook-off test heating rate). Fast cook-off is concerned with high gradients (several hundred °C/m) and high rates (hundreds of °C/m).

A preliminary hazard analysis protocol for cook-off has been developed as a tool to recognize and evaluate the hazard. By answering the questions in the first flow chart, Fig. 8, with a yes or no answer, one ends up with a number (1-4) or a letter (A-D). If the result is a letter, one proceeds to a second flow chart, Fig. 8. Then, in the same way one finds a combination of a letter and a number. The effect and response time is estimated by reference to Table 4.

The questions of Fig. 8 are:

- Is the heat source direct-fuel fire (or bon-fire), or exhaust impingement?
- Is the ordnance item packed in its shipping container/storage container?
- If it is packed, is there thermal protection by flame retardant (direct heating) or heat shielding (indirect heating)?
- If not packed does the motor case provide thermal protection (e.g., intumescent paint or insulating liner) (direct heating) or a missile heat shield (indirect heating).

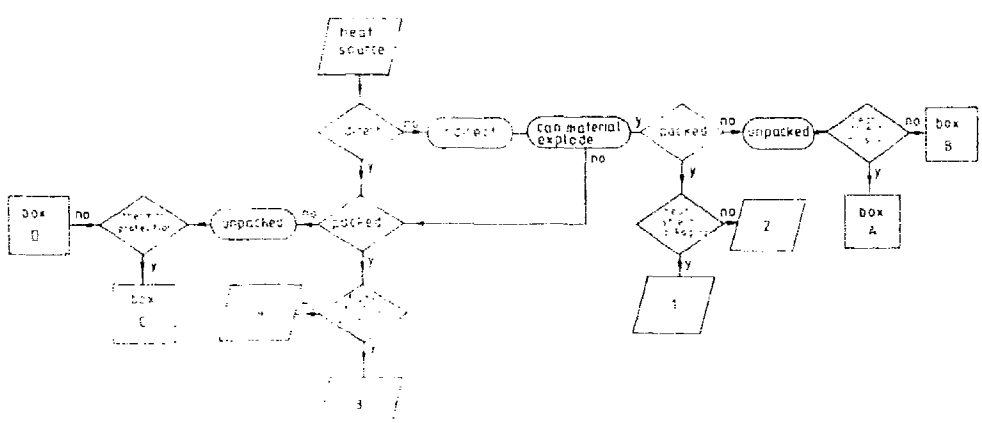

Fig. 8. Preliminary Hazard Analysis Protocol for Cook-Off.

The answers to these questions give 1-4 or A-D results. If the result is A, B, C, or D then the questions of Fig. 9 must be answered. The questions include:

- Is the missile assembled, or are we dealing with components?
- What is the casing material?
- Are there pressure vents designed in the casing?

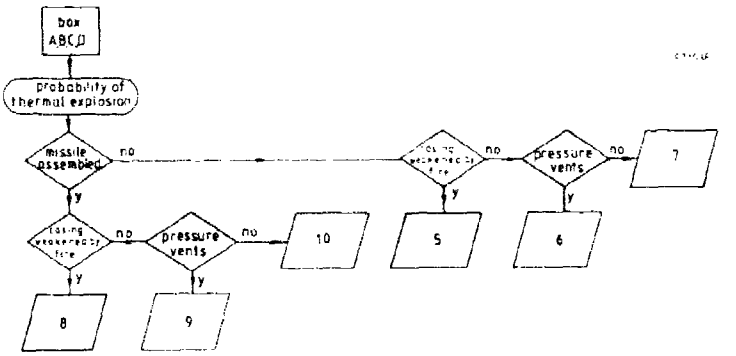

Fig. 9. Continuation of Preliminary Hazard Analysis Protocol from Fig. 8 for Responses A, B, C, or D.

Table 4 is then consulted to get output and response time. The protocol is illustrated by the following example.

Table 4. Probable Cook-Off Reactions for the Instances Determined in Figs. 8 and 9.

Source	Indirect											Direct										
Packed	Yes		No										No									
Missile or package with thermal protection	Yes	No	Yes					No				Yes	No	Yes					No			
	1	2	A					B				3	4	C					D			
Missile unassembled			5	6	7			5	6	7				5	6	7			5	6	7	
Missile assembled						8	9	10			8	9	10				8	9	10			8	9	10
Expected response time	>> ..... hours ..... <											= 1/2 hr		= 1 - 2 mins								
Expected effect	No reaction or violent pressure development if long enough time				Partial detonation			Mild pressure development			Partial detonation	Mild to violent pressure development		Mild burning	Mild pressure development	Violent pressure development		Partial detonation	Mild burning	Mild pressure development	Violent pressure development		Partial detonation

EXAMPLE

A fire is reported in a relatively isolated store house. In the store house rocket motors are stacked in standard transport packaging. The contents of a 587 liter drum of a highly volatile cleaning fluid have been spread out over the floor and are burning. Because an inspection team recently checked the rocket motors in the store house, one of the motors is still out of its packaging.

Based on these facts one has to answer the question, if it is advisable to send in a fire fighting team and, if so, what precautions one should take.

Following the flow chart one has to decide if the heat source is working directly or indirectly. Since in the example a flame engulfment is present, one has a direct heating source. Furthermore the presence of one unpackaged rocket motor leads to box C or D. Because consultation of the first chart led to a box with a letter, one has to continue with the second flow chart.

Since no warhead has been fixed on the motor and the motor has a full metal casing without pressure vents, the result is either C6 or D6.

By applying the results to the table one finds that the possible maximum affect is a violent pressure development which will occur within 1-2 minutes after the flames have reached the unpackaged rocket motor. If only packaged rocket motors were present, it would take about half an hour for a violent response to occur.

4.3. FRAGMENT IMPACT THREAT

Figure 10 presents in cartoon form the fragment impact situation to be considered. The first frame shows the fragment (here taken as a blunt nosed, 5 gm fragment traveling at 1500 m/s) just impacting a .318 cm thick steel case backed by propellant. Within microseconds of the moment of impact a shock wave races through the case and into the propellant as shown in the second frame. During the time between the second and third frame, the propellant will most likely react to the shock transitioning to a detonation, or not. If the propellant does not transit to a detonation (no shock to detonation transition), we still must consider the effects of damage and the penetration mechanics of the fragment into the case, as shown in the third frame. Here the fragment breaches the wall, pushing debris ahead and compressing the propellant, with damage to the propellant. The fourth frame shows the hot projectile and debris at rest in the propellant. This is obviously one possibility, but the fragment also could have exited the motor, that is, gone in one side, through the propellant, and out the other side.

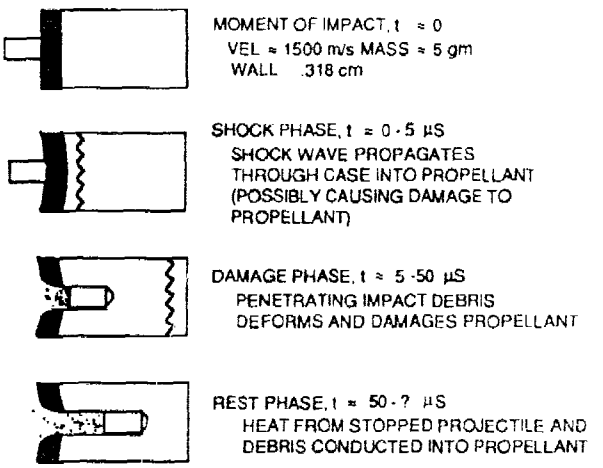

Fig. 10. Fragment Impact Phases Relating to Cased Propellant.

4.3.1. Phase 1, Fragment Impact Hazard Analysis Protocol

These various phenomena are addressed in the protocol depicted in Fig. 11.

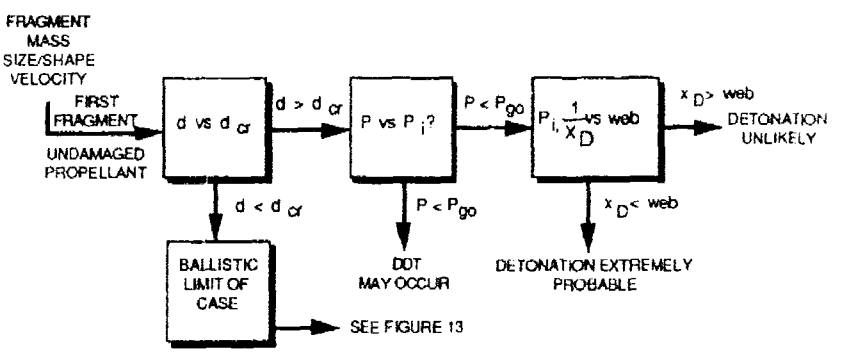

Fig. 11. Hazard Analysis Flowchart for Fragment Impact, Prompt Shock to Detonation Transition.

Starting with a fragment (we do consider multiple fragments below) of specific mass, size and shape, and velocity impacting the ordnance item (this is the first fragment and the ordnance item contains undamaged energetic material), the first consideration is the characteristic size of the fragment (d) compared with the critical diameter (d_{cr}) of the energetic material.

Critical diameter is the smallest diameter of a cylindrical bare charge that will sustain a steady-state detonation. This consideration tells you whether you can shock a sufficient area to cause and sustain detonation. While this is usually not a design consideration for high explosives since most high explosives have small critical diameter, it is an important design consideration for solid propellant rocket motors. This is especially true for high performance minimum smoke propellants and high performance high burn rate propellants. Not only do high explosives usually have smaller critical diameters for the bare charge they are usually heavily confined in bombs or warheads. The effect of confinement is to reduce the effective critical diameter. In contrast, the confinement offered by motor cases is much less, but must also be considered.

Many propellants have critical diameters of several tens of centimeters, and are loaded in motors of 13-, 20-, and 33-centimeters diameter. The likelihood of being able to shock enough area to cause detonation of these propellants is very remote. While they may react violently, they will not detonate. In recent years, in order to achieve higher performance or reduced plume signature, increased amounts of nitramines and energetic binder have been considered for propellants. Smaller critical diameters (less than 2 cm in some cases) result from the use of nitramines and energetic binders, and now comparison of the fragment size to the critical diameter must be made. If the fragment is as large as or larger than the critical diameter, then other issues need to be considered. Two- and three-dimensional effects are obviously important and must be considered. For the sake of simplicity in providing an example of the protocol, these important considerations are not discussed here.

The critical diameter, while a convenient way to discuss detonability of cylindrical charges, has limitations when trying to determine the detonability of propellant grains, especially when they have a center perforation. When a solid cylindrical charge of less than critical diameter is overboosted, the detonation "dies out" after some length (although for some ammonium perchlorate based propellants it may take lengths of several diameters for the detonation to die out). However, when the same test is performed with a similar cylinder having an axial perforation, the entire sample may detonate. A discussion of possible causes is contained in Annex II.

These effects, and others, are more fully discussed in Section 5.5.

We next consider what pressure is imparted to the energetic material as a result of the impact and transmission through the case, liner, and insulator (p). This pressure and its associated time must be compared to the minimum pressure-time required to detonate the energetic material (p_i). If the stimulus pressure is over this threshold pressure (labeled as P_{go}, pressure required to produce a "go" in undamaged material), then detonation is obviously possible and one more consideration is required. If the pressure is not sufficient to cause prompt detonation, the propellant grain may be significantly damaged and ignited and a deflagration to detonation (DDT) reaction may occur (see Section 5.5.2).

For the given stimulus pressure, the run distance to detonation (X_D) needs to be known and compared to the energetic material dimensions (for example propellant web thickness). If the run distance is less than the dimension of the energetic material, then a detonation is very likely.

Often in the past the response of undamaged energetic material to a given shock input that roughly corresponded to some threat was the extent of consideration; however, work with damaged energetic materials indicates that the above considerations are not adequate. Work with pressed explosive charges indicates that the more porous the explosive, the more sensitive it is (Fig. 12).

Recent work on the effects of damage on shock sensitivity of propellants showed that damage of 1 to 4% voids can have a very significant effect on sensitivity, in some cases decreasing the critical initiating pressure by 40% and decreasing the critical diameter by a factor of 25. The strain levels and strain rates required to produce this damage were modest, in some cases being the strain level and strain rate that the propellant would experience on motor pressurization during ignition. Storage and/o rough handling can also produce voids in the propellant, also increasing its sensitivity (see also A-III).

Because of the critical effect of damage and/or porosity on the initiating pressure required, and since in a sympathetic detonation scenario multiple fragment impacts (both simultaneous and sequential) are highly probable, the flow chart of Fig. 11 must also be considered in terms of damaged energetic materials. Shock-to-detonation transition (SDT) with decreased critical initiating pressure and decreased critical diameter may result from shocking damaged propellant. (For example, a propellant when tested in the NOL card gap test in the undamaged state gave 70 U.S. cards (equivalent to 17.8 mm) or less, while the propellant with 1% voids gave greater than 70 cards, in the card gap test. Another propellant in its undamaged state had a critical diameter estimated to be over 1 m. Yet with about 1-4% damage, it "went" in the card gap test, indicating a critical diameter for the damaged

material to be less than 38 mm.) The above considerations are all part of the shock-to-detonation transition (SDT) technical area (discussed in Chapter 5).

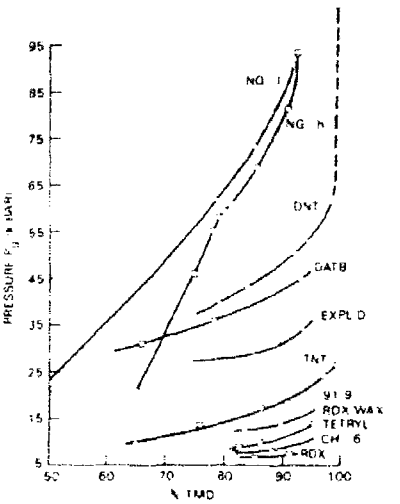

Fig. 12. Large-Scale Gap Test Gap Pressure for Pressed Charges of Organic Explosives (Naval Surface Weapons Center MP-81-399, 1981).

Another possibility leading to detonation involving highly damaged propellant would be that the subsequent fragment ignited the damaged energetic material and a deflagration-to-detonation transition (DDT) ensued. Yet another possibility is that ignition of the damaged energetic propellant may result in a pressure burst of the case that hurls chunks of energetic material into bulk heads or other structures and results in a delayed shock-to-detonation transition (XDT) (thought to be the cause in at least two incidents involving propellant detonation during testing of propulsion systems). Because of the increased sensitivity and increased opportunities for detonation, testing of damaged energetic materials must be done, as well as testing of the undamaged materials.

The type and extent of damage (Chapter 5.4.13), and its effect on SDT, is an important consideration.

In another path (in Fig. 11, the path indicated starting with "ballistik limit of case") leading to extremely violent reaction (and to detonation in some cases), the size of the fragments is less than the critical diameter of the energetic material so that prompt shock-to-detonation transition of the impacted round is unlikely. Penetration mechanics, ignition, and venting must be considered to estimate whether an explosion might occur. If the mass and velocity of the fragment exceeds the ballistic limit of the case, the next question is, by how much? The ballistic limit of the case is the velocity of a given fragment that will result in penetration of the case.

If the velocity greatly exceeds the ballistic limit of the case, the fragment may completely pass through the ordnance item and not deposit enough energy to cause reaction. Whether or not ignition occurs for those instances where the fragment passes entirely through the motor depends largely (though not entirely) on the propellant. Many ammonium perchlorate based propellants will ignite while many of the nitramine based propellants will not. However, if the fragment does not exit the ordnance device, the fragment may have (1) lodged in the energetic material, or (2) barely exceeded the ballistic limit, contacting the energetic material but blocking the hole (no vent). In any instance, the critical consideration is whether or not the energetic material ignites. If the material ignites, the next question is whether the gaseous reaction products vent fast enough to avoid an explosion. This involves consideration of the burning rate, r, burning area, A_b, and resulting pressurization rate, p, coupled with considerations of the confinement. If not vented fast enough, explosion of the round will probably result. This explosion could, in turn, accelerate large pieces of case that might be of sufficient size and velocity to cause detonation in adjacent rounds, or accelerating pieces of propellant that upon impacting result in XDT. The various questions in this path are shown in Fig. 13. [NOTE: If in a test there is no apparent ignition, investigators need to wait a while before running out to examine the hardware. Violent explosions have occurred in tens of minutes of apparently no reaction after impact.]

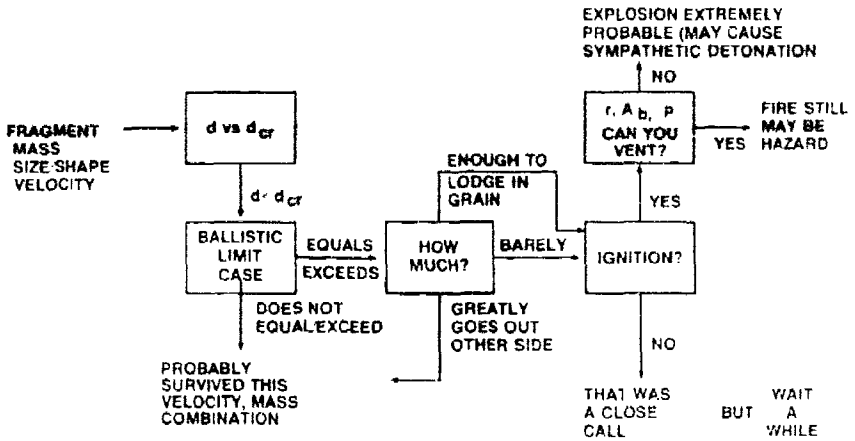

Fig. 13. Hazard Analysis Flowchart for Fragment Impact, Violent Explosion.

From the above (very cursory and simplified) discussion, a list of parameters that need to be known can be assembled. These include:

- critical diameter of energetic material
- critical initiating pressure of energetic materials
- pressure, run distance, time relationships

} for damaged and undamaged samples

- ballistic limit of case
- mechanical response of case, and confinement offered by case
- ignitability of propellant
- burn rate characteristics of propellant
- high strain rate mechanical behavior of propellant as it determines:
  - damage
  - area available for burning
- thermochemistry and energetics as they determine pressure rise rate in DDT and explosion (includes equations of state)

It must be noted that the above is a simplified presentation. Each of the boxes in the flow chart embodies many separate research programs. Space precludes a detailed listing.

4.3.2. Phase 2, Fragment Impact - Hazard Map

Figure 14, a plot of fragment mass and fragment velocity (these parameters along with size/shape were the input to the Hazard Analysis Flowchart of Figs. 11, 13), presents several lines representing information identified as necessary in the test protocol. This plot is a generalized depiction. The subsequent chapter describes how the exact location of the lines are determined. In order of time sequence, the first consideration of the fragment hitting the motor was the formation of a shock wave, and whether the shock wave has sufficient strength, area, and duration to cause a detonation. This is depicted by the area on the upper right hand of the map. Combinations of mass and velocity to the right of the line, result in detonation. The extent of this region is ameliorated by critical diameter considerations.

If the shock wave does not cause detonation, the next consideration is the penetration of the fragment into the motor. Obviously there are some low value combinations of fragment mass and velocity, where nothing happens. The fragment does not penetrate the case and causes no reaction. For some combinations of mass and velocity there is sufficient energy to penetrate the case. This ballistic limit is shown on the plot as the "B.L." curve.

Another line on the plot is the ignition line. There are several possibilities. The simplest is that the fragment pierces the case and comes to rest in the propellant. In the map, there may be separation between the ballistic limit line and ignition line reflecting that a projectile may get through the case but not have sufficient thermal energy to cause ignition (this may occur with composite motor cases and/or hard to ignite propellants and/or at low temperatures). In some rare instances, investigators (Sewell, 1982) have found the ignition line to the left of the ballistic limit line. In these cases, the fragment did not pierce the case, but did enough work in deforming the case or producing spall that the energetic

material ignited. This has been observed with steel cover plate bonded to a CDB propellant. This seems to be more of an issue with heavy wall cases, such as in a warhead or bomb.

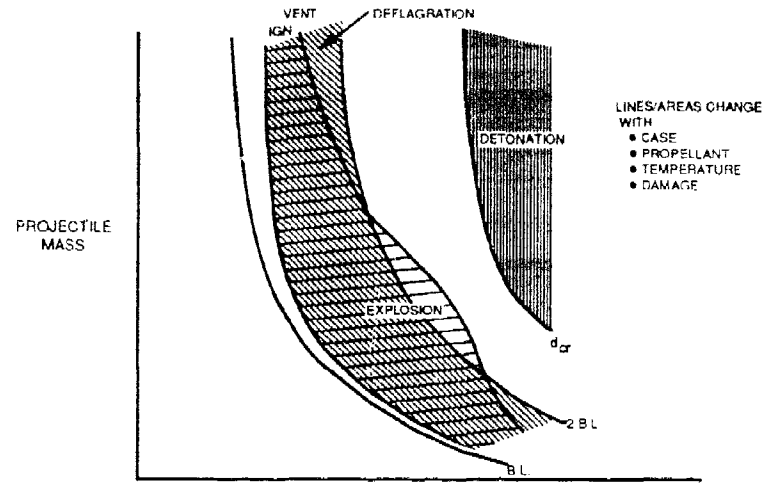

Fig. 14. Generalized Hazard Maps for Fragment Impact.

Once the propellant is ignited, if the gases produced by burning cannot be vented fast enough (by nozzle, entry hole, vent, or pressure burst), an explosion is very likely. This is the shaded area of the plot. If the vent area is large enough - to the right of the "vent" line, then the propellant will burn but not cause an explosion. In many instances, especially with hard to ignite propellants, the fragment passes completely through the motor and no reaction or a mild burn occurs. Thus, to the right of the vent line and/or the line marked "2 B.L.", a region of no reaction or mild reaction may be encountered. [Note: A burn and/or propulsion reaction is acceptable according to U.S. "Insensitive Munitions" goals since it is milder than explosion or detonation.]

The location of these lines, and their position relative to other lines is a function of the motor case, the propellant, the temperature, degree of damage of the propellant and many other factors.

The next chapter will more fully discuss how these parameters are obtained.

4.4. BULLET IMPACT

Bullet impact is very similar to fragment impact in both the hazard protocol and hazard map, although some investigators believe that the primary bullet impact hazard response is explosion - the bullet ignites the propellant but does not provide sufficient vent or burning - not detonation. Increased number of investigators have results where detonation resulted from impact of a bullet (kinetic energy only not a bullet having an explosive charge). In the case of bullets having an explosive charge - e.g., 23 mm HEI - a detonation can be obtained. Obviously the shape of a bullet must also be considered: it is easier for a bullet to penetrate the motor case (and perhaps translate through the propellant and out the other side) than a "chunky" fragment of equal mass and equal velocity.

Variation of response can be caused by deviation in path from the straight path. Response may be worst for fragments over bullet for equivalent mass and velocity.

4.5. SYMPATHETIC DETONATION

Much of what has been presented so far leads to consideration of mass reaction or sympathetic detonation of munitions. Up to this point this AGARDograph has presented various possible reactions and output levels of a single motor or munition responding to stimuli. However severe the detonation of one munition, it is not the major concern. Our major concern is whether that detonation can cause propagation of detonation to adjacent stores. Those adjacent stores can be on the launch platform (tank, ship, aircraft), in some transportation configuration (rail cars, trucks), in storage magazines or in the manufacturing areas.

Unfortunately, while massed reaction (with sympathetic detonation as the most severe mass reaction) is what we try to prevent or mitigate, we have little understanding of the area. Some calculations and experiments have been made for propagation of detonation from one base charge to another as a function of distance between the charges, and collocated, heavily confined explosive charges with charge separation, case thickness, and various barrier materials (Howe et al, 1981). These calculations help us understand propagation, but it is hard to extrapolate these results to multiple pallet loads of munitions, or to a magazine full of a mixture of munitions (see for example Howe, 1987; Swisdak et al, 1987; Dyer et al, 1985; Parsons et al, 1988; Lucht and Hantel, 1988; and Moore, 1988).

The reason that we don't have encompassing and comprehensive treatment of sympathetic detonation is that the area is very complex with complicated geometric and time considerations. The initial donor event can result from shock to detonation transition, deflagration to detonation transition, XDT, cook-off, or explosion, as presented in the earlier sections. Each of these areas is complicated in itself. Thus we must be concerned with the propagation into a complex situation from an event that is complicated. This can be seen in the following example.

Example. A fire starts in one area of a munition storage area. The fire can cause several reactions (e.g. inadvertent ignition of a motor, cook-off of a motor, cook-off of a warhead, etc.). Each of these possible reactions can cause other subsequent reactions. In this example, let us consider the ignition and propulsion aspect. If the motor ignites and the munition goes propulsive, again several possibilities can occur (e.g. it hits nothing, it hits other munitions, it hits a bulkhead or some other obstruction and perhaps undergoes an SDT or XDT reaction, etc.). Again, each of these possibilities can cause other subsequent reactions. In this example, let us consider that the missile hits other missiles. Again several possibilities arise (e.g. the impact causes prompt initiation of detonation of the impacted munition, the impact does not cause detonation but breaks up and/or ignites the energetic fill in the munition, the impact does not cause detonation but ignites the propellant causing this impacted missile to go propulsive, etc.). Again each of these possibilities can cause other subsequent reactions. Let us take the case where the impact did not cause prompt detonation but broke up the propellant or explosive and ignited it with several possibilities (burn, explosion, deflagration-to-detonation transition). As before, each of these reactions can have several subsequent reactions and the process can continue in several paths, many that can lead to sympathetic detonation.

The above was just one situation with a multiplicity of possible paths and reactions. Many other initial situations exist (e.g. rather than a fire, the initial situation may have been detonation of enemy warhead, explosion of one of your own warheads, electrostatic discharge causing inadvertent ignition, etc.), and for each of these situations many possible paths and reactions also exist.

The many initial starting situations, and vast multitudes of subsequent paths and reactions make any consideration of sympathetic detonation very complicated. The complexity is further compounded because of the individual probabilities associated with branching of the paths, and with each reaction. In part because of this complexity of myriad paths, reactions, and probabilities, consideration of sympathetic detonation often centers on defining the maximum credible event and then applying quantity-distance considerations.

For any given scenario in which an explosive event might occur, it is important to know what the worst possible event could be so that proper protection, preventive measures, and precautions can be involved to either prevent the occurrence or lessen the magnitude of its effects. The term used to express this worst case is Maximum Credible Event (MCE). The U.S. Department of Defense Explosives Safety Board defines MCE by "In hazards evaluation, the MCE from a hypothesized accidental explosion, fire or agent release is the worst single event that is likely to occur from a given quantity and disposition of ammunition and explosives. The event must be realistic with a reasonable probability of occurrence considering the explosion propagation, burning rate characteristics, and physical protection given the items involved. The MCE evaluated on these bases may then be used as basis for effects calculations and casualty predictions."

Within the U.S. the various military services have concerns regarding sympathetic detonations of munitions and consequently each has performed large scale tests to determine the MCE of various storage arrangements of various munitions. When the explosion effects exceed the tolerable limits for a service's operational or logistic scenario, tests have been conducted on techniques to reduce the MCE to an event, the explosive effects of which are tolerable. A more thorough discussion of MCE is presented in Swisdak et al, NATO AC/310 CP-001, March 1987.

The definition of MCE talks of "quantity and disposition." Disposition considerations include both arrangement of items in the immediate locale (e.g. a number of munitions on a pallet, or on several contiguous pallets) and the separation between such locations. The number of items and their explosive weights in each locale are the quantity and the separation between such locations, such that a detonation will not propagate between locations, is the "distance" in "quantity-distance" considerations.

Probably the first systematic experimentation on determining quantity-distance relationships was carried out by Burlot (1930). Jarrett (1968) presented an excellent discussion of the extension of Burlot's work and the derivation of the British explosives safety distances, while in the same publication Roylance (1968) presented the quantity-distance protection considerations for the U.S. (as well as presenting some historical background). Since those articles were written, progress has obviously been made but these articles still provide well written backgrounds as well as empirical relationships (albeit, somewhat dated).

In order to standardize considerations and to use the vast amount of data on which the older quantity-distance tables are based, the explosive weight is often reduced to a "TNT equivalence." The TNT equivalency of a particular energetic material is the weight of TNT (usually expressed as a percent of the total energetic material weight) required to produce a shock wave of equal magnitude to that produced by a unit weight of the energetic material. [NOTE: There are several TNT equivalents for a given material depending on whether the equivalency is based on peak overpressure, positive impulse, time of arrival, etc. The equivalency also varies as a function of the distance from the charge. These considerations are beyond the scope of this volume.]

As an example of TNT equivalence consider a magazine containing 20 missiles, with each missile having a 20 kilograms warhead with 120% TNT equivalence and a 100 kilogram motor with 40% TNT equivalence. If a simultaneous detonation should occur the net explosive quantity (NEQ) is

20 warheads	x	20 kg	x	1.20	=	480 kg
20 motors	x	100 kg	x	.40	=	800 kg
NEQ				= 1280 kg TNT		

With this explosive quantity the estimates of damage, vulnerability, and quantity/distance ratios can be determined.

The above discussion is obviously very simplified but a full discussion of this complicated sympathetic detonation event is beyond the scope of this AGARDograph. More detailed discussions can be found in the minutes of the various Explosive Safety Seminars sponsored by the U.S. Department of Defense Explosive Safety Board (Chick and Bussell, 1987).

4.6. ELECTROSTATIC DISCHARGE (ESD)

The ESD hazard analysis flowchart (Fig. 15) provides a framework of questions and criteria which can be used to assess the response of a weapon system to Electrostatic discharge. Basically, the protocol is divided into three parts: (1) charge generation and accumulation; (2) propellant knowledge; and (3) mechanism of energy dissipation or discharge. The assessment proceeds through a series of logical questions and where appropriate, limiting conditions are defined. The statements marked (*) indicate the need for quantitative data. The basic premise is the comparison of the maximum available parameters, for any conditions, with the minimum ignition of the most sensitive or vulnerable system component. Thus, there is a need to give consideration and to make measurements over the range of parameters and conditions that will be relevant during the service life of the weapon.

In Fig. 15, the first question one asks to assess the ESD hazard of a rocket motor is: what is the case material. If the outer case is conductive, no further action is required. However, if these conditions are not satisfied then it is necessary to proceed further through the protocol.

Energy can be generated directly on the surface of a weapon system, or on other sources, such as personnel or packaging material that are anticipated to be in the vicinity of the system. The volume resistivity of the case material should not exceed 10^8 Ω-m, under all conditions of temperature and humidity that may be encountered; similar criteria apply to other, adjacent articles. If this condition is not fulfilled then it is necessary to measure the rate of energy accumulation, which implicitly involves the relative permittivity, and finally to determine the levels of maximum energy (ME) and maximum voltage (V_{MAX}), again under service conditions. Specific values of the maximum energy and maximum voltage that a propellant can hold is a function of propellant composition and is experimentally determined.

The second part of the protocol is concerned with the electrical and ignition properties of energetic materials and components in the weapon system. There is sufficient evidence to conclude that solid propellants which contain any metal particles, aluminum and magnesium, and powerful oxidizing agents such as ammonium perchlorate and teflon (PTFE) are particularly sensitive to ignition by electrical energy, and any system that contains any such materials must be regarded with suspicion. Energy deposition in the bulk of an energetic material, and consequent mechanical damage or thermochemical effects leading to ignition are the result of either high initial electrical current flow or dielectric breakdown followed by current flow.

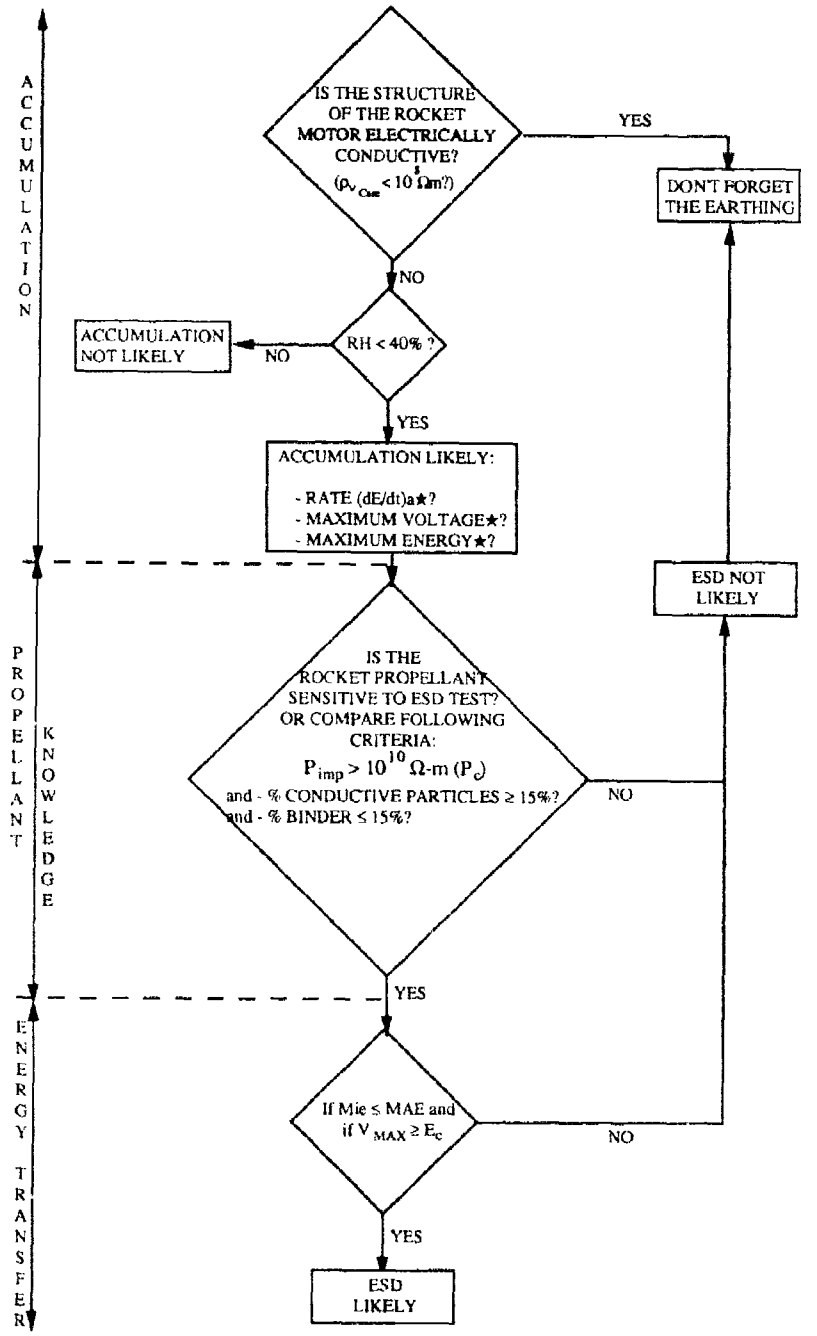

Fig. 15. ESD Hazard Analysis Protocol, with $\rho_{V_{case}}$ = case volume resistivity, P = percolation coefficient, RH = relative humidity, P_c = critical percolation coefficient, and $(dE/dt)_a$ = rate of energy accumulation.

Measured values of the resistivity of the energetic material provide an indication of charge mobility through it, and calculation, from composition parameters, of the Percolation coefficient provides an estimate of the ease of breakdown and current flow. The percolation coefficient is defined as follows:

$$P_{imp} = \left(\frac{\rho_n}{\rho_c}\right) \cdot \left(\frac{wt\%C}{wt\%nf}\right)\left(\frac{d_{nf}}{d_{cf}}\right)\left[\frac{\rho_b}{wt\%b}\left(\frac{wt\%C}{\rho_c} + \frac{wt\%n}{\rho_n}\right) + 1\right] \qquad \rho_{vb} = \left(\frac{vol\%C}{vol\%nf}\right)\left(\frac{d_{nf}}{d_{cf}}\right)^3 \left(\frac{1}{vol\%b}\right)\rho_{vb}$$

where

ρ_n	=	density of nonconducting particles
ρ_c	=	density of conducting particles
wt%C	=	weight percent of conducting particles
wt%nf	=	weight percent of finest fraction of nonconducting particles
d_{nf}	=	diameter of finest fraction of nonconducting particles
d_{cf}	=	diameter of finest fraction of conducting particles
ρ_b	=	density of binder
wt%b	=	weight percent of binder
wt%n	=	weight percent of all nonconducting particles
vol%C	=	volume percent of conducting particles
vol%nf	=	volume percent of finest fraction of nonconducting particles
vol%b	=	volume percent of binder
ρ_{vb}	=	volume resistivity of the binder in Ω-m

It was found by experiment that if P_{imp} was greater than 10^{10}Ω-m (ρ_c), the propellant was considered potentially hazardous to ESD. In the final part, to supplement these data, measurement of dielectric breakdown strength (E_c) can provide an assessment of the significance of the measured maximum voltage (V_{MAX}), or potential difference across the material. It should be noted that the critical electric field strength for breakdown, and duration of the field, which may be intensified by the presence of points or sharp edges, appear to have an inverse relationship.

Measured values of minimum spark ignition energy for the energetic material content of a system can be an important indicator of the response of the weapon. Most compositions exhibit an enhancement of sensitiveness with changes in a variety of parameters; temperature, sample size, prior exposure to electric field, pressure, duration of discharge, humidity and repeated discharge are all known to significantly reduce the quantity of energy necessary for ignition, and these effects require assessment as part of any characterization exercise.

Finally, if the Minimum Ignition Energy (MIE) for a component material is less than the Maximum Available Energy (MAE), and if maximum voltage levels (V_{MAX}) will cause the breakdown field strength (E_c) to be exceeded, then the hazard of an ignition exists. In addition, although the need for appropriate precautions is well understood, the hazard from ESD to firing circuits must not be overlooked.

To conclude, for any component or system that contains energetic material, primary and secondary explosive, pyrotechnics and propellants, there is a potential ignition risk from electrostatic energy. The above scheme is intended to provide a logical basis for the assessment of this risk, to allow adequate safety measures to be adopted.

4.7. SHAPED CHARGE JET IMPACT

Shaped charge jets represent a formidable threat to munitions due to the very high velocity, high density focused jets impacting the munitions. It is important to understand and be able to predict the response of an energetic filling to a shaped charge jet with a view to controlling the event. Hazard analysis flowcharts have been developed by M. Chick, R. Frey, H. James and other for the situations of shaped charge jets impacting (1) bare or thinly covered energetic materials and (2) thick covered energetic materials. These hazard analysis flowcharts are presented in Figs. 16 and 17 respectively.

4.7.1. Bare or Thinly Covered Energetic Material

This area is concerned with responses associated with shock from the jet impact directly upon the surface of the energetic material or upon a thinly covered energetic material. Cover thicknesses are limited to a few jet diameters due to rarefactions rapidly eroding the small diameter, very high pressure shock. Generally the critical jet velocities are on the order of 50% lower than the covered energetic material category. Under some situations where the jet diameter is much smaller than the critical detonation diameter of the energetic materials this mechanism can fail to produce detonation "on contact," but jet penetration into the explosive can subsequently produce detonation by the processes described by the covered energetic material category. If there is confinement in this category it is generally light.

The hazard analysis flowchart for this category of shaped charge jet attack is shown in Fig. 16. Given a jet of given velocity, diameter, and density, the first comparison is the diameter of the sample D versus the critical detonation diameter, d_{cr} (see Section 5.7). If the sample diameter is less than the critical diameter, a deflagration or minor reaction is likely to ensue. However, if the sample diameter is larger than the critical diameter a detonation may ensue and other considerations must be made.

The next comparison is the critical diameter versus the jet diameter. If the critical diameter is very much larger than the jet diameter then again deflagration or minor reaction are the most likely possibilities. If the critical diameter is larger than the jet diameter, detonation does not occur immediately, but may result with jet penetration as mentioned above and is treated using the heavily covered flow analysis of Fig. 17.

If the critical diameter is less than the jet diameter, or if the critical diameter is only moderately larger than the jet diameter then prompt detonation may ensue and the comparison of pressure imparted by the jet must be made with the critical pressure pulse required for initiation. If the pressure is sufficient a detonation will probably result. If the pressure is insufficient the effect of the thin confinement (if present), may determine whether the reaction is relatively minor, or if a deflagration to detonation transition might occur.

The hazard analysis protocol present in Fig. 16 for shaped charge jet attack on bare or thinly covered energetic material is very similar in considerations as that presented earlier for fragment impact (see Section 4.6). Thus, the parameters measured to determine the likelihood of detonation reaction to fragment impact may also be used to predict detonation due to shaped charge impingement.

4.7.2. Heavily Covered Energetic Material

This classification deals with the initiation and failure processes associated with the jet penetration through the cover material, air gap (if present) and into the energetic material. Generally jet velocities for the detonation threshold in this area are much higher than those required for the bare/thinly covered energetic material category. Two mechanisms appear to be involved: initiation from the bow wave shock from supersonic jet penetration of the energetic material and subsonic penetration for larger diameter jets. Critical run to detonation distances can be several centimeters or greater. This system has significant confinement which can effect both the critical jet velocity for detonation and the degree of violence of the nondetonative reaction.

The hazard analysis flowchart for this category is presented in Fig. 17. The first consideration is identical to that of Fig. 16 and is concerned with the diameter of the sample and its corresponding critical diameter. If the sample is larger than its critical diameter then a detonation may ensue.

The next consideration is whether or not an air gap is present between the heavy cover material and the energetic material. If a gap is present then the problem can be treated similarly to the bare or thinly covered energetic material and the flowchart of Fig. 16 used.

If an air gap is not present then the result of the jet penetration bow wave must be made. The first consideration is the pressure produced from the bow wave compared to the critical pressure pulse required for detonation.

If the pressure is less than that required for detonation, the effect of confinement must be considered, and a confinement modified critical pressure pulse p' considered. If the pressure from the jet is not greater than this confinement modified threshold pressure then deflagration will result with either low order or deflagration to detonation reactions following.

If the confinement modified threshold is less than the pressure from the bow wave then detonation may ensue, as it might if the pressure had been higher than the critical pressure pulse (the $P > P_i (d_j, p_j)$ path). The next consideration is to compare the sample diameter versus the run distance to detonation (D vs x). If the sample diameter is less than the run distance, then deflagration is likely. If the sample is larger than the run distance then detonation is very likely.

The previous discussion is for the consideration of bow wave produced by supersonic jets. We earlier mentioned the subsonic penetration of large diameter jets. Going back to the P vs $P_i (d_j, p_j)$ block, and the large d_j path coming from that block, the next consideration is the comparison of the jet penetration velocity with the bulk sound speed. If the jet penetration velocity is greater than the critical velocity then detonation is likely, if less then deflagration is likely.

From the hazard analysis flowchart of Fig. 17 several considerations must be made to determine whether the response is low order, deflagration to detonation, or prompt detonation. Chapter 5.7 discusses the methods used to obtain the data required in these considerations.

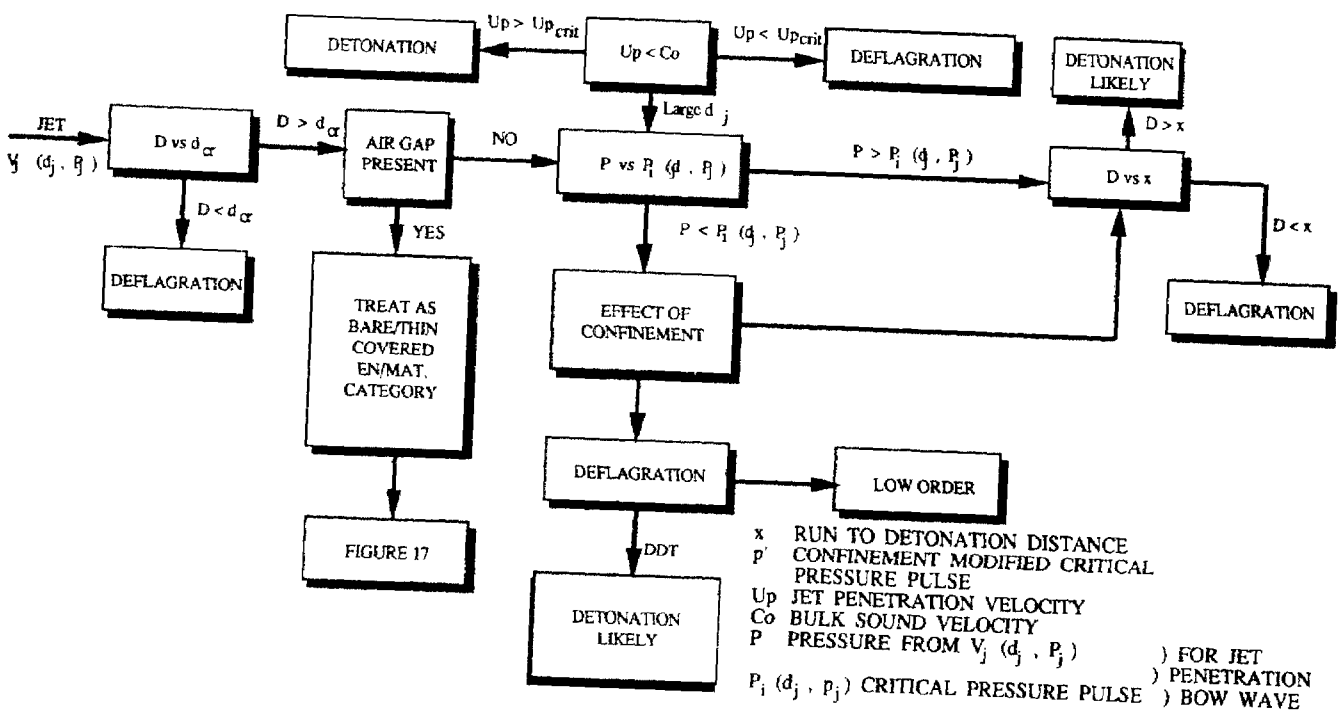

Fig. 16. Hazard Assessment Flow Chart for Category "Cover Energetic Material" Systems.

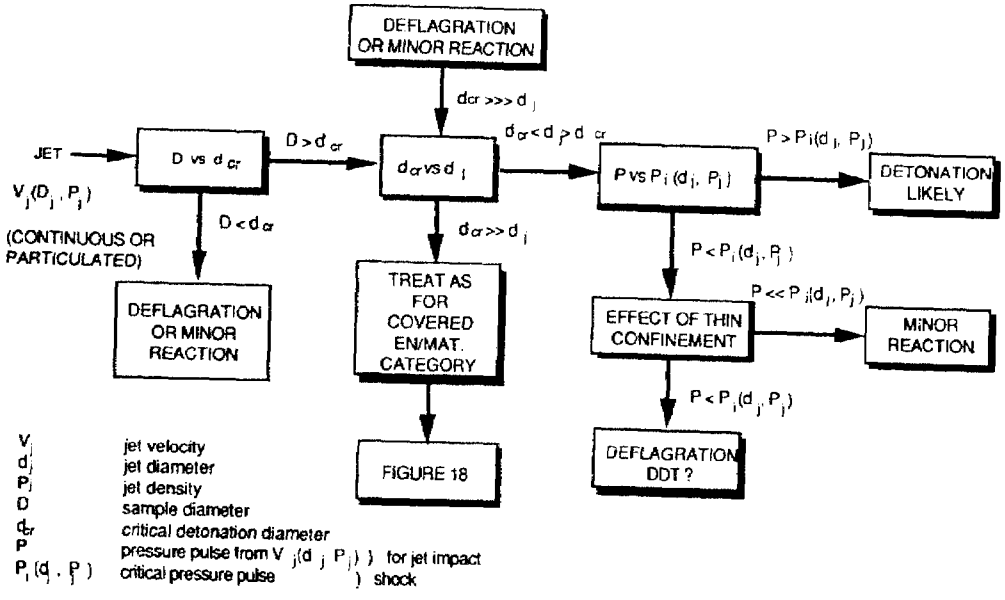

Fig. 17. Hazard Assessment Flow Chart for Category "Bare/Thin Covered Energetic Material" Systems.

CHAPTER 5. HAZARD RESPONSE TECHNICAL AREAS

Chapter 4 presented the system hazards, what types of technical data are required to address the hazards (the various hazard analysis protocols), and how these data are used in the hazard assessment. This chapter presents a more technical view of the experimental techniques used to obtain these data, and what analytical methods are required to use the data. This chapter does not contain a complete description of all methods, rather illustrative examples are given. A more detailed discussion can be found in NATO Allied Ordnance Publication 7 (1982). This chapter covers thermal explosion, slow cook-off, fast cook-off, ignition and deflagration, detonations (including shock to detonation (SDT), deflagration to detonation (DDT), delayed detonation (XDT), and low velocity detonation) as well as the role of damage, penetration mechanics and ballistic limits, and electrostatic discharge.

5.1. THERMAL EXPLOSION

The contributions of the Soviets to the thermal explosion theory are most important. An excellent review is given by two Soviet scientists, A. G. Merzhanov and V. G. Abramov (1981). We shall follow this review closely.

The simplest model of thermal explosion assumes that:

- radiation can be neglected;
- a single temperature-dependent reaction proceeds in the reactant, its rate being independent of the reactant concentration (a zero-order reaction);
- the temperature is uniform throughout the reactant;
- all the parameters of the process (ambient temperature, shape and size of the specimen, heat exchange with surroundings, etc.) remain constant till the explosion occurs.

The heat balance under these conditions is described by the equation:

$$c\,\rho\,\frac{dT}{dt} = Q\,\rho\,k_0 e^{-E/RT} - \frac{\alpha S}{V}(T - T_0) \qquad (5.1)$$

where T is the reactant temperature; t is time; c, r are heat capacity and density of the reactant; Q, k_0 and E denote heat of reaction, pre-exponential factor and activation energy of the reaction, respectively; a is the heat transfer coefficient; S is the heat transfer surface; V is the reactant volume; T_0 is ambient temperature.

The left-hand side of Eq. (5.1) gives the rate of the heat accumulation in the reactant; the first member of the right-hand side is the rate of heat generation due to reaction, the last member is the rate of heat loss to the surroundings. The principal feature of Eq. (5.1) which determines the characteristic properties of the phenomena is the very strong exponential dependence of the heat generation rate on temperature.

Semenov (1928) was the first to mathematically analyze the heat balance equation and to lay the foundation of the thermal explosion theory. He compared the dependences of heat generation and heat loss rates on temperature in the "$\dot{q}$-T" diagram (with $\dot{q} = dq/dt$ and t = time) (see Fig. 18) which is often called the Semenov diagram and showed the regimes of the reaction that were thermally possible:

- the heat generation curve $\dot{q}_{rel} = Q \cdot \rho \cdot k_0 e^{-E/RT}$ intersects the heat loss straight line $\dot{q}_{rem} = \alpha S/V(T - T_0)$ in the region of low temperatures (curve 1, Fig. 18) at these conditions. The reactant will always be maintained at the temperature which corresponds to the lower point of intersection (T_1 in Fig. 18). This temperature is close to the ambient temperature T_0. To realize a similar regime, the difference of the initial reactant temperature from T_0 should not be great (the initial temperature must not be higher than T_2 corresponding to the second intersection point);
- the heat generation curve does not intersect the straight line of heat loss in the low temperature region (straight line 3). The superiority of heat generation rate over that of heat loss results in progressive self-heating of the reactant to very high temperatures, and thermal explosion occurs.

The critical condition for thermal explosion is the tangency between the heat generation curve and the heat loss straight line (straight line 2). The rates $\dot{q}_{rel}$ and $\dot{q}_{rem}$ and their derivatives are equal in the tangency point T_*. Hence it follows that

$$\frac{Q\rho V}{\alpha S} \cdot k_0 e^{-E/RT_*} = (T_* - T_0) \tag{5.1a}$$

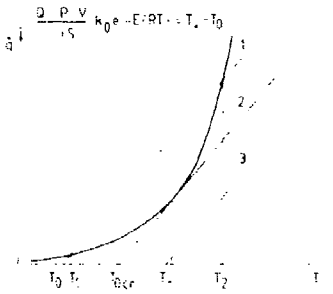

Fig. 18. $\dot{q}$-T Diagram of Semenov, 1928.

From the equations of both heat rates and the derivatives of the heat rates at temperature T_* it follows that

$$T_* - T_0 = \frac{RT_*^2}{E}$$

The group RT_* for explosives and propellants is usually much less than the activation energy E. Hence

$$T_* \approx T_0 + \frac{RT_0^2}{E} \tag{5.2}$$

$$\frac{Q \cdot \rho \cdot V}{\alpha S} \cdot \frac{E}{RT_0^2} \cdot k_0 e^{-E/RT_0} = \frac{1}{e} \tag{5.3}$$

Expression (5.2) gives the reactants maximum temperature in the nonexplosive regime. The expression shows that it differs from the ambient temperature by

$$\Delta T_* \approx \frac{RT_0^2}{E} \tag{5.4}$$

which is the maximum pre-explosive (or characteristic) temperature rise. The temperature rise for explosives and propellants is usually of the order of 10-20°C.

5.1.1. Induction Period of Thermal Explosion

The temperature-time history of the reactant as is seen from Eq. (5.1), is associated with the difference between heat generation and heat loss rates. The smaller the amount of heat transferred to the surroundings the faster is the rise of the reactant temperature and the shorter is the time to explosion. Consider the case where heat losses are negligibly small in comparison with heat generation (adiabatic regime). This is the case when either heat loss is inhibited, e.g., by a large size of the body or by insulation, or temperatures are high and the heat loss rate with linear dependence on temperature becomes small as compared to the exponentially growing rate of heat generation.

Eq. (5.1) under adiabatic conditions is of the form:

$$c\frac{dT}{dt} = Q \cdot k_0 e^{-E/RT}$$

The reactant temperature at the beginning of the induction period is not necessarily equal to the ambient temperature. The initial condition for this equation can be written as:

$$t = 0,\ T = T_i$$

Todes (1933) was the first to derive a solution for this equation as an exponential integral function. Frank-Kamenetsky (1955) utilized the exponential transformation:

$$e^{-E/RT} = e^{E/RT_0} \cdot e^{E/RT_0^2 T - T_0} \tag{5.5}$$

where T_0 is the temperature in the vicinity of which the transformation is effected, and obtained an approximated expression for this solution:

$$T \approx T_i + \frac{RT_i^2}{E} \cdot \ln \frac{1}{1 - \frac{Q}{c} \cdot \frac{E}{RT_i^2} k_0 (e^{-E/RT_i}) t}$$

The exponential transformation here is performed in the vicinity of the initial temperature T_i. As is seen from this expression, a temperature rise to very high values under adiabatic conditions proceeds during the approximated finite time:

$$t_{ad} \approx \frac{c}{Q} \cdot \frac{RT_i^2}{Ek_0} e^{E/RT_i} \tag{5.6}$$

This time is actually the induction period of thermal explosion under the adiabatic conditions, or the adiabatic induction.

5.1.2. Thermal Explosion and Heat Transfer

Semenov's uniform spatial temperature distribution and Newtonian heat transfer to the surroundings are realized when heat transfer throughout the reactant is considerably facilitated as compared to the heat loss to the surroundings. Similar conditions of heat transfer can be ensured by a small size of the specimen, good thermal conductivity of the reactant, its mixing and poor contact with the heat transfer surface. Under other conditions, the heating is nonuniform and temperature gradients appear. Thermal explosion with temperature gradients within the reactant was first treated by Frank-Kamenetsky (1939).

To describe the process in this case, the equation of heat conduction with continuously distributed heat sources due to chemical reaction is chosen instead of the heat balance equation:

$$c \cdot r \cdot \frac{\partial T}{\partial t} = Q \cdot r \cdot k_0 e^{-E/RT} \phi(\eta) + \operatorname{div} \lambda \operatorname{grad} T \tag{5.7}$$

where λ is thermal conductivity. Frank-Kamenetsky, following Semenov, considered the case of a zero-order model reaction with $\phi(\eta) = 1$. All the principal parameters are brought into a complex designated Fk:

$$Fk = \frac{Q \cdot r}{4\lambda} \cdot \frac{E}{RT_0^2} \cdot d^2 \cdot k_0 e^{-E/RT_i} \tag{5.8}$$

where d is a characteristic dimension of the sample: thickness of the slub or diameter of a cylinder or a sphere. Surface temperature was assumed constant (boundary conditions of the first type) (Lykov, 1967).

Analysis of Eq. (5.8) reveals that if Fk is less than a certain critical Fk_{cr}, a steady temperature profile with a maximum in the center sets in the reactant; thermal explosion occurs at $Fk > Fk_{cr}$. Hence, the critical condition for thermal explosion takes the form:

$$\frac{Q \cdot r}{4\lambda} \cdot \frac{E}{RT_0^2} \cdot d_{cr}^2 \cdot k_0 e^{-E/RT_0} = Fk_{cr} \tag{5.9}$$

Fk_{cr} and maximum pre-explosive temperature rise are related to the sample's geometry. They are analytically found for infinite slabs and cylinders using exponential transformation Eq. (5.5). In the case of a sphere the problem reduces to tabulated functions (Frank-Kamenetsky, 1955). The values of Fk_{cr} and ΔT_* for these geometries are listed in Table 5.

Table 5. Effect of Sample Geometry on Critical Conditions.

Geometry	Fk_{cr}	$\Delta T_* \cdot E/RT_0^2$
Slab	0.88	1.2
Cylinder	2.00	1.37
Sphere	3.32	1.6

5.1.3. Effect of the Initial Reactant Temperature. Transition to Ignition. Hot Spot Thermal Explosion

In case of cook-off in, e.g., a fire, the ambient temperature T_0 is higher than the initial temperature of the explosive material T_i. At $T_i < T_0$, the process can be divided into two stages: that of the reactant heating to T_0 and that above T_0. With limited external heat transfer, the entire sample is heated uniformly and necessarily passes over the state when its temperature is equal to that of the surroundings. This circumstance enables the induction period reading from this moment; T_{ind} then becomes independent of the initial temperature. The time in which T_0 is attained is called the time of preheating. It depends on both T_0 and T_i. The overall time of explosion delay is found by adding the time of preheating and the induction period. The study of temporal characteristics of the process with uniform distribution of temperature is reported in Merzhanov and Grigoryev (1967).

Thermal explosion with limited internal heat transfer and the stage of heating were first treated in Zinn and Mader (1960). The sample heating in this case is non-uniform. Due to an exothermic reaction, the temperature rise maxima are generated close to the surface. They increase with time and travel towards the center (Merzhanov and others, 1963). The temperature maximum in a nonexplosive regime is eventually established in the sample's center. In the case of explosion, two possibilities arise:

- the temperature maximum goes to the sample center where ignition starts. The preheating stage in this case does not essentially affect the process behavior. The induction period of thermal explosion is read from the moment the sample's center is heated and is in good agreement with the induction period in the case $T_i = T_0$;
- the temperature maximum does not reach the center and ignition starts at the periphery. Of course the overall time of ignition delay cannot then be divided into the time of preheating and the induction period.

In the first case a thermal explosion occurs, while in the second a transient regime between thermal explosion and ignition is realized. Hence, in both cases explosive behavior only occurs for a number of combinations of parameters describing internal and external heat transfer.

Results of calculations of temperature distributions depending on external heat to internal heat transfer (Biot number: $Bi = \alpha \cdot d/\lambda$) and for certain values of Fk are shown in Figs. 19 through 21.

If only a part of the reactant is heated to a high temperature, a hot spot thermal explosion is said to occur. The critical size of the hot spot of heating, following Merzhanov and others (1963) and Merzhanov (1966) is written as:

$$d_{cr} = a\sqrt{\frac{4\lambda}{Qr}\frac{RT_i^2}{E}\frac{1}{k_0}e^{E/RT_i}}\left[\ln\left(\frac{E}{RT_i^2}(T_i - T_0)\right)\right]^b \qquad (5.10)$$

Coefficients of a and b for various shapes of hot spot are given in Table 6.

Table 6. Effect of Sample Geometry on Critical Conditions.

Shape	a	b
Slab	1.63	0.65
Cylinder	2.72	0.42
Sphere	3.48	0.30

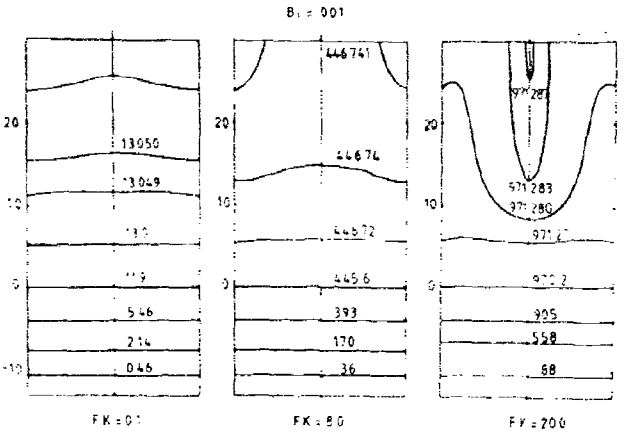

Fig. 19. Non-Steady Temperature Profiles at Bi = 0.01; for Several Values of Dimensionless Time t/t_{ad}.

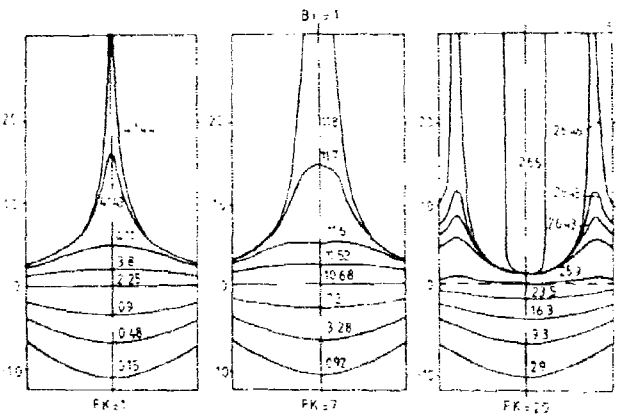

Fig. 20. Non-Steady Temperature Profiles at Bi = 1; for Several Values of Dimensionless Time t/T_{ad}.

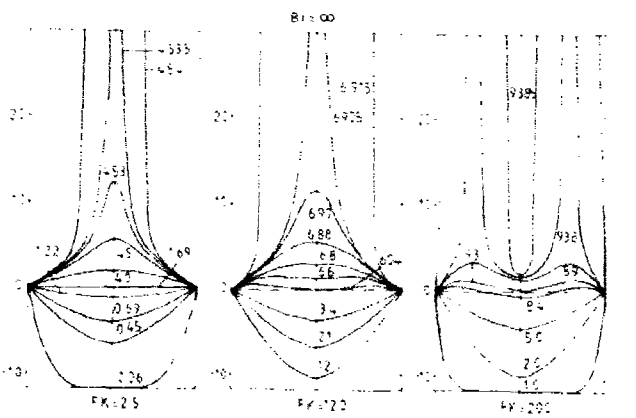

Fig. 21. Non-Steady Temperature Profiles at Bi = ∞; for Several Values of Dimensionless Time t/t_{ad}.

The size of the sample in case of a hot spot explosion as well as in case of ignition is not essential. The induction period does not differ from that measured under adiabatic conditions by more than a factor of two (Merzhanov and others, 1963) even in the immediate vicinity of a critical condition.

The hot spot thermal explosion is treated as a possible mechanism of explosion in the theory of reactant sensitivity to mechanical action (Rideal and Robertson, 1948 and Bowden and Yoffe, 1952).

5.1.4. The "Safe" Diameter and the "Safe" Lifetime

As mentioned in the previous paragraph the safe diameter of an infinitely long cylindrical propellant charge is defined as the smallest diameter at which self-ignition takes place. According to the theory of Frank-Kamenetsky (1939), the following equation is valid for the safe diameter D_{T_a}:

$$D_{T_a} = \sqrt{\frac{4\delta_c \lambda R T_a^2}{\rho_b E q_{T_a}}} \qquad (5.11)$$

where the rate of heat generation q is a function of temperature according to

$$q = F(Q) \exp(-E/RT) \qquad (5.12)$$

δ = dimensionless parameter, Frank-Kamenetsky (see pg. 344, Frank-Kamenetsky, 1969)

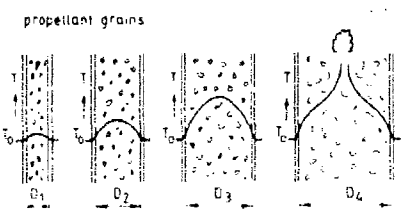

Fig. 22. Schematic Temperature Distributions on Self-Heating of Propellant in Vessels With Increasing Diameter, But at the Same Ambient Temperature.

A period of safe life can be assigned if the minimum safe diameter can be predicted for a storage period at ambient temperature. In order to establish the stability of a propellant for a storage period up to 10 years, it is required to simulate experimentally the temperature profile which may occur during such a period. In accordance with the requirement that ammunition has to withstand temperatures up to 71°C the following temperature-time program for 10 years' storage period can be drafted for the investigation of the self-ignition hazard:

10 years at 30°C (303°K) including a fortnight storage with the following daily temperature profile
- 2 weeks storage with a daily temperature profile of
  - 9 hours at 35 C (308 K)
  - 5 hours at 50 C (323 K)
  - 5 hours at 60 C (333 K)
  - 5 hours at 71 C (344 K)

In order to reduce the period of time for the experimental simulation to an acceptable standard test period, during which sufficiently strong heat generation signals are measured, isothermal heat generation tests are performed at 85°C. It has been established by heat generation tests (Mey and Heemskerk, 1984), by determination of stabilizer content ('t Lam and Heemskerk, 1985) and by chemiluminescence measurements (Mey and Heemskerk, 1985) that the degradation at this temperature agrees well with the degradation effects (for longer periods) at ambient temperatures. When conducting an isothermal heat generation test at 85°C it can be calculated from Eq. (5.12) that after an aging period of 1 week at 85°C the propellant reaches an aging stage corresponding to a 10 years' storage including the assumed 2 weeks temperature-time profile (Van Geel, 1971).

Since for practical reasons the heat generation is measured at a higher temperature (T_m) than the expected storage temperature, the critical diameter at the storage temperature, T_a, can be calculated using Eqs. (5.11) and (5.12). From these it follows that:

$$D_{T_a} = \sqrt{\frac{4\delta_c \lambda R T_a^2}{\rho_b E q_{T_a}}} \exp\left\{\frac{E}{R}\left(\frac{1}{T_a} - \frac{1}{T_m}\right)\right\} \qquad (5.13)$$

The heat generation, q_{T_m}, is not constant, but depends on various conditions including the degree of decomposition. Therefore, the maximum heat generation observed in the isothermal heat generation test (IST) (see Section 5.1.5) during the experimental simulation period of 1 week at 85°C is applied in the calculation of the safe diameter. This is the maximum diameter permitted during the storage of the propellant for a period of 10 years at ambient temperature.

So:

$$D_{safe} = K\sqrt{\frac{\delta_c \lambda}{\rho_b (q_{T_a})_{max}}} \qquad (5.14)$$

where:

$$K = \sqrt{\frac{4RT_a^2}{E} \exp\left\{\frac{E}{R}\left(\frac{1}{T_a} - \frac{1}{T_m}\right)\right\}} \qquad (5.15)$$

As already mentioned before T_m = 358 K (85°C). The temperature T_a corresponds to the list of storage temperatures. If the value of the activation energy E is known, the value of K can be calculated. As shown in Fig. 23, however, the value of K does not vary much for values of E between 40 and 200 kJ/mole and the minimum of K will be 12.1. The use of this value implies that the activation energy of the propellant need not be known and the safe diameter of the propellant will be:

$$D_{safe} = 12.1\sqrt{\frac{\delta_c \lambda}{\rho_b (q_{85})_{max}}} \qquad (5.16)$$

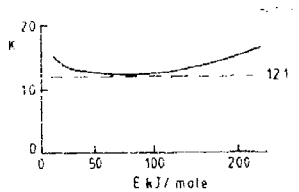

Fig. 23. K-Value as a Function of the Activation Energy for T_a = 344 K and T_m = 358 K.

Results With Cellulose Nitrate Propellant

The heat generation as a function of time of 10 different propellants (their chemical composition is listed in Table 7) is given in Fig. 24.

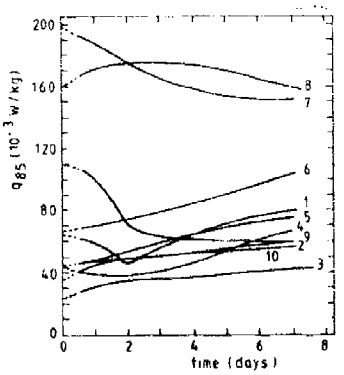

Fig. 24. Heat Generated by 10 Different Propellants at 85°C Over a Period of 7 Days.

Table 7. Chemical and Physical Properties of the Nitrocellulose Propellants Included the Investigations. (The chemical composition is given in percentages).

Propellant No.	1	2	3	4	5	6	7	8	9	10
Cellulose nitrate	83.8	96.2	91.0	90.4	49.5	55.4	57.48	79.15	21.0	19.8
Glycerol trinitrate					47.0	49.7	41.33	16.0	20.9	20.0
Nitroguanidine									54.8	56.0
Dinitrotoluene	9.5	0.7	6.2	5.3						
Sodium cryolite									0.35	0.3
Dibutylphthalate	2.6	0.3		2.3		0.2		6.9		6.9
Diphenylamine	0.9	0.4	0.6	1.0			0.44	0.4		
Nitrodiphenylamine								0.5		
Ethyl centralite	0.1	0.4		1.0	3.5				2.95	3.6
Methyl centralite						1.8				
Vaseline						0.4	0.44			
Potassium cryolite										0.3
Potassium nitrate						0.8		0.9		
Potassium sulphate	0.7		0.5							
Graphite		0.35	0.05			0.2	0.38	0.35		
Calcium carbonate					0.15			0.3		0.1
Tin Oxide								0.75		
Moisture	1.3	1.25	1.2			0.5	0.33	0.55		0.2
Solvent	1.1	0.2	0.45					0.15		
N% cn.	13.14	13.23	13.20	13.15	12.2	12.99	12.1	13.28		
Cal, value (kJ/kg)	1090	3986	3747	3662	4920	5024	5037	3525	3643	3705
Bulk density (kg/m^3)	799	553	963	855	1000	740	883	949	1000	899
Heat Conductivity (W/m C)	0.12	0.08	0.09	0.12	0.13	0.08	0.09	0.10	0.11	0.10
Year of production	1969	1962	1963	1966	1942	1955	1915	1966	1965	1955

From these measurements the safe diameter (D_{safe}) and the decreases in calorimetric value at 20°C and 30°C have been calculated, and the results are given in Table 8.

Table 8. Safe Diameter and Decrease in Calorimetric Value of the Tested Gun Propellants. Referenced to storage schedule shown in Fig. 24.

Propellant	D_{safe} (m)	$(\Delta Q_{ex})_{20}$ (%)	$(\Delta Q_{ex})_{30}$ (%)
1	0.60	0.24	1.0
2 single base	0.50	0.34	1.0
3	0.70	0.70	0.5
4	0.65	0.15	0.7
5	0.60	0.12	0.6
6 double base	0.50	0.17	0.8
7	0.30	0.48	1.7
8	0.35	0.61	2.5
9	0.60	0.16	0.7
10 triple base	0.65	0.14	0.7

The calculated decrease in calorimetric value differs markedly from pro[illegible] propellant.

How far a decrease in calorimetric value is permissible depends on the future [illegible] the propellant.

Heat Generation Test in Relation to Other Stability and Compatibility Tests

In the past a large number of stability and compatibility tests have been developed. These tests generally involve an accelerated aging of the propellant at temperatures between 333 K (50°C) and 413 K (140°C) and the examination of distinct degradation phenomena such as:

- the rate of gas evolution
- the rate of stabilizer depletion
- the loss in weight under standard test conditions
- the lapse of time until the appearance of nitrogen oxide gases (NO_x)

Table 9 shows the outcome of a comparative investigation that has been performed concerning the relation between the Isothermal Storage Test (IST) (Van Geel, 1971) and five more conventional tests: the 95°C test (the propellant is placed in a closed container, 0.33 g of propellant/ml, at 95°C for 8 hours/day; red fumes within 20 days indicate an unstable propellant), the Dutch weighing test (Bofors and Kruit, 1960), the Abel heat test (Bofors and Kruit, 1960), the 65.5 C test (Stanag 4117, 1968), and the methyl violet test (MV test, Bofors and Kruit, 1960). These tests are described below.

Abel Heat Test

Application: Determination of the momentary stability of propellants at 80°C using the detection of the NO_x generation by its reaction with a potassium iodide starch paper.

Equipment: The equipment consists of a thermostat bath with a constant temperature of 80°C. An amount of 1.6 g propellant is weighed into standard glass tubes with a length of 140 mm, an external diameter of 16.5 and an internal diameter of 14.5 mm. The tube is provided with a cork carrying the potassium iodide starch indicator paper suspended on a platinum wire. The indicator paper is wetted in the center (maximum wetted diameter 5 mm) by a glycerine-water mixture. The NO_x gases react with indicator paper resulting in a darkening yellowish-brown circle at the dividing line between the moistened and unmoistened paper parts. The period of time which has elapsed between the start of the experiment and the occurrence of a dark brown line, is a measure of the stability. The results of the test may be affected by decomposition of materials other than the propellant itself.

Typical results: Propellant: Double base. Test at 80°C with 1.6 g.: 24 minutes.

Dutch Weighing Test

AOP-7 Registry No: Netherlands/Explosives/202.01.004

Type of Test: Safety/Thermal

Brief Description: The loss in weight caused by the decomposition of the propellant is determined as a measure of the stability. The test is performed at a temperature of 378 K for a double- and a triple-base propellant and at 383 K for a single-base propellant. The sample is heated under standardized conditions for 8 hours to determine the content of volatiles. After this, the sample is heated for another 64 hours to determine the weight loss.

Typical Results:

Small caliber single-base propellant	(383 K) 0.6% weight loss
Single-base cannon ammunition	(383 K) 0.9% weight loss
Double base propellant (with high nitration nitrocellulose)	(383 K) 1.1% weight loss

The Vacuum Stability Test

AOP-7 Registry No: Netherlands/Explosives/202.01.005

Type of Test: Decomposition by heat

Brief Description: The volume of gas evolved, when a mixture of equal parts of explosive or propellant and the material under test is heated at a constant temperature of 100°C (90°C in some cases) for 40 hours in an initial vacuum, is compared with the volumes evolved from the explosive or propellant and the test material when heated separately under otherwise identical conditions. Compatibility of the components of the mixture is judged by means of the volume of additional gas produced because of the contact between these components.

Typical Results: The Vacuum Stability Test for one combination:

Material: 10 g high explosive or propellant (grain size, 0.2-2 mm)
10 g test material (grain size 0.2-2 mm)
Duration of a test: 4 days

Methyl-Violet Test

AOP-7 Registry No: Netherlands/Explosives/202.01.002

Type of Test: Safety/Thermal

Brief Description: The appearance of brown fumes of nitrogen oxides is determined as a measure of the stability of the propellants. The appearance of the brown fumes is detected with the help of methyl-violet paper. The sample is kept under standardized conditions at a temperature of 408 K for a single-base propellant and at 393 K for a double-base propellant. Nitrogen oxides must not appear and explosions must not occur within specified times.

Bergmann and Junk Test

AOP-7 Registry No: Netherlands/Explosives/202.01.003

Type of Test: Safety/Thermal

Brief Description: In the Bergmann and Junk Test the sample is heated to 405 K (±0.5 K) for a single-base propellant and at least 393 K (±0.5 K) for a double-base propellant. The sample must be heated under standardized conditions for a prescribed period. At the end of this period the nitrogen oxide evolved is quantitatively determined as a measure of the stability of the propellant under investigation.

Typical Results: Nitrocellulose (405 K) 1.7 ml NO per 10^{-3} kg, small caliber ammunition single-base (405 K) 7.8 ml NO 5.10^{-3} kg, cannon ammunition single-base (405 K) 8.3 ml NO per 5.10^{-3} kg, double-base propellant (393 K) 5.8 ml NO per 5.10^{-3} kg.

The tests are done with samples after accelerated aging at 65.5°C for periods between 60 and 240 days. The chemical composition of the propellants before aging is given in Table 9.

Table 9. Chemical Composition of the Cellulose-Nitrate Propellants Used for Comparative Tests.

Propellant No.	11	12	13	14
Cellulose nitrate	57.05%	75.9%	82.6%	84.0%
Glyceroltrinitrate	40.1	19.8		
Diphenylamine			0.8	0.95
Ethylcentralite	0.8	0.8		
Dinitrotoluene			10.3	9.6
Dibutylphthalate			5.2	3.6
Potassium sulphate	1.7	1.0		0.65
Barium nitrate		1.4		
Graphite	0.15	0.25		
Moisture	0.2	0.35	0.8	0.8
Solvents (about)	traces	0.5	0.3	0.4

Table 10. Comparison of the Isothermal Storage Test With Other Stability Tests. (Underlined values do not meet the requirements.)

Propellant No.		11	11	12	13	14
Duration of the aging at 65.5°C before the test	(days)	60	120	69	240	240
IST D_{safe}	(m)	0.7	0.01	0.9	0.7	0.6
95°C-test	(days)	9	7	26	76	76
Dutch weighing test	(%)	0.6	3.3	12.0	0.8	0.88
Abel heat test	(min)	6	3	6	13	8
65.5°C-test	(%)	0.38	0.18	0.55	0.15	0.24
MV test - Salmon coloration	(min)	65	55	95	40	30
- Red fumes	(hours)	6.0	7.5	8.0	5.5	5.5

From Table 10 it can be seen that there is hardly any correlation between the tests performed. This is to be expected because of the fact that the different tests make use of different criteria to judge self-ignition hazard. Only the IST which is based on a direct measurement of the heat generated by the stored propellant gives a reliable figure for the risk of self heating and consequent ignition.

The Course of the Heat Generation Process

a. Initial Heat Effect

During the experimental program, it was observed that the heat generation of some lots of propellant was relatively high during the first days of the measurement. This initial effect was not observed in triple base propellants.

When investigating this effect it was found that the initial heat generation was much less when the propellant was not pulverized and that the generation was reduced when replacing the surrounding air was replaced by nitrogen (Mey and Heemskerk, 1985). The effect of moisture was investigated as well. A definite effect on the rate determining reaction step could be observed although the overall effect remained relatively small.

In this connection it is advisable to carry out the heat generation test with unpulverized propellant grains in air since this is as close to the storage conditions as possible. In case of large units of propellant (rocket propellants) relatively large pieces of the propellant can be chipped from the propellant.

b. Autocatalysis

After a proionged measurement in the heat generation meter, the rate of heat generation increases sharply by autocatalysis. This effect is caused by the depletion of stabilizer. In Fig. 25 the heat

generation is given of two single base propellants. The difference between the two propellants was the type of stabilizer, but the stabilizer content was the same.

From Fig. 25 it follows that diphenylamine has a better stabilizing effect than the same amount of ethyl centralite for this type of propellant.

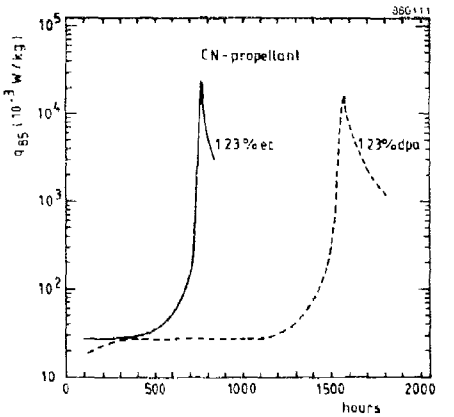

Fig. 25. Heat Generation at 85°C of Two Samples of Single Base Propellant With Different Stabilizers.

As has been discussed before, the heat generation of most propellants is less than 100 mW/kg during the first week at 85 C. This means that the safe diameter is at least 0.5 m at ambient temperatures. However, when the period of autocatalysis is reached, the safe diameter will decrease sharply. Because of this effect, the question rose whether an inhomogeneous stabilizer distribution could give rise to self-ignition. To investigate this problem tests were done with a mixture of the single base propellant with 1.23% diphenylamine from Fig. 23 and the same propellant, but without stabilizer (weight ratio 99:1 respectively).

The results are given in Fig. 26 in which curve 1 represents the heat generation of the nonstabilized propellant, curve 2 the heat generation of the mixture, and curve 3 the same as 2 but with pulverized propellant.

From Fig. 26 it follows that there is a stabilizing effect from the surrounding grains and that this effect becomes stronger with decreasing grain size.

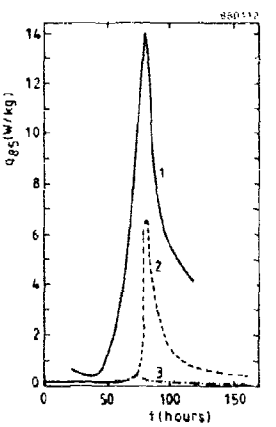

Fig. 26. Heat Generation at 85°C of a Nonstabilized Single Base Propellant.

(1) The pure unstabilized propellant.
(2) A mixture of the propellant and the stabilized propellant
(3) A mixture of the propellant and pulverized stabilized propellant.

Further Investigations

For a more precise prediction of the decomposition phenomena for different storage conditions much more knowledge is necessary about the kinetics of the propellant decomposition, in particular at lower temperatures (30°C). Low temperature measurements have been performed with stabilizer reactivity and chemiluminescence ('t Lam and Heemskerk, 1985, and Mey and Heemskerk, 1985). In this connection, further investigations will have to be conducted with respect to the influence of the gas atmosphere and the gas-tightness of the propellant container on the course of the decomposition phenomena.

More information is necessary on the distribution of stabilizer in the propellant and the effect of possible inhomogenities on both the self-ignition hazard and the ballistic stability.

It should be stressed that the stability requirements the propellant has to meet, can only be drafted in detail if the above mentioned information is obtained. A reliable judgment of the stability control will be the result.

Finally, it should be investigated how heat losses in a stack of propellant containers relate to the loss of a single unit. This will provide the ultimate information about the allowable safe diameter.

5.1.5. Fundamental Thermal Stability Tests

Differential Scanning Calorimeter (DSC)

Differential scanning calorimetry (DSC) is a technique in which the heat generation of a sample is measured as a function of the temperature. The same temperature rise is applied to a reference material and a sample material. The difference in energy supply is proportional to the heat generation in the sample.

During this temperature program endothermic and exothermic changes in enthalpy may appear which may be caused by, for instance, phase transitions or chemical reactions.

The apparatus comprises two identical measuring cells made of a platinum alloy. Each cell has a temperature sensor and a heating element. The cells are mounted in an aluminum block which is kept at a constant temperature. The measuring cells can be used in the temperature range between 130 and 870 K with heating rates between 10^{-3} K/s and 3 K/s.

The measurements can be performed with open or with closed sample vessels with a volume of 45×10^{-9} m^3 and a maximum overpressure of 15 MPa. The atmosphere surrounding the sample vessel can be flushed with noncorrosive gases. The minimum heat generation that can be measured, amounts to approximately 5 W/kg with a sample mass of 10 mg.

An example of a DSC curve is shown in Fig. 27. The sample under investigation was composed of several organic peroxides. The DSC curve shows two degradation peaks with a measured onset temperature at about 300 K and a total reaction enthalpy of -1510 kJ/kg.

In view of the low onset temperature and the high reaction enthalpy, the sample must be regarded as a potentially hazardous material.

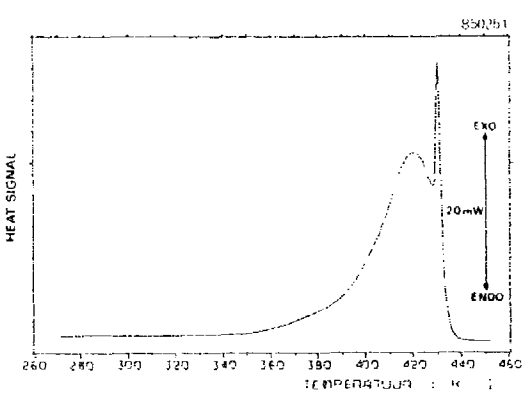

Fig. 27. DSC Curve of a Sample Composed of Several Organic Peroxides.

Isothermal Storage Test (IST)

In the Isothermal Storage Test (IST) the heat generated at constant temperature due to reaction of decomposing substances is measured as a function of time. Performance of these measurements at a series of temperatures leads to a quantitative understanding of the relation between the temperature and the heat generation of the substance under investigation. The IST is applicable to solids, liquids, pastes, and dispersions.

The IST in Fig. 28 consists of a large heat sink (an aluminum block) which is kept at a constant temperature. In the block are two holes with a heat flow meter (e.g., a Peltier element) at the bottom of each hole. Identical holders are placed on both heat flow meters. One holder contains the sample, the other an inert substance.

The heat generated by the sample results in a voltage signal from the heat flow meter which is proportional to the heat flow. Random fluctuations in the heat flow are avoided by monitoring the voltage difference between both heat flow meters.

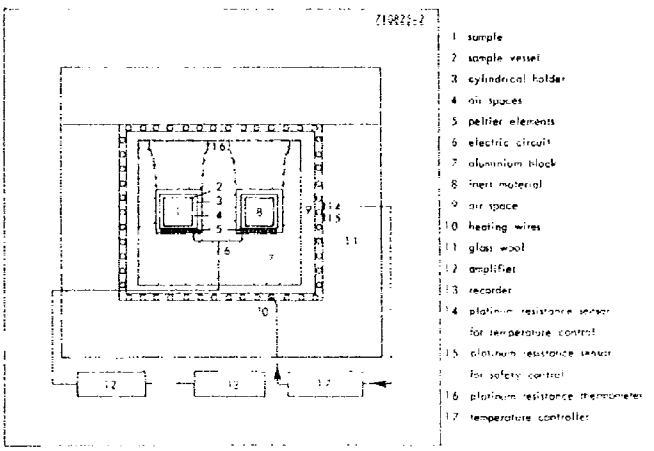

Fig. 28. Cross-Section of the Isothermal Storage Test.

The stainless steel sample holder has a volume of 70 cm^3. The sample mass amounts to about 20 g. Measurements can be performed in the temperature range from 250 K to 420 K. Heat generations can be measured between the lower limit of 5 mW/kg and the upper limit of 5 W/kg with an accuracy of at least 30% in the lower range to 5% in the higher range.

In Fig. 29 three IST curves measured with a single base propellant at different temperatures are shown. With these heat generation curves an activation energy for the degradation process of 125 kJ/mol has been calculated. By applying the thermal explosion model of Frank-Kamenetsky and introducing appropriate physical properties of the propellant, the safe storage diameter at the ambient storage temperature of 300 K is found to be 0.6 m. Integration of the heat generation curves results in a decrease of the calorimetric value, which can be extrapolated to the required storage temperature and time of storage.

Adiabatic Storage Test (AST)

In the Adiabatic Storage Test (AST) the heat generated at nearly adiabatic conditions by reacting or decomposing substances is determined as a function of time. The AST is applicable to solids, liquids, pastes, and dispersions.

The AST shown in Fig. 30 consists of a 1.5×10^{-3} m^3 Dewar vessel sealed with a stainless steel lid. This lid is provided with insulating material on the inside. The Dewar vessel is placed in an oven. The temperature of the oven is kept equal to the temperature of the sample in the Dewar vessel. In this way the heat loss is kept at a minimum and a nearly adiabatic situation is created.

An internal electric heating coil is used to heat the sample to the desired initial temperature. The heating coil is also used to determine the specific heat of the sample.

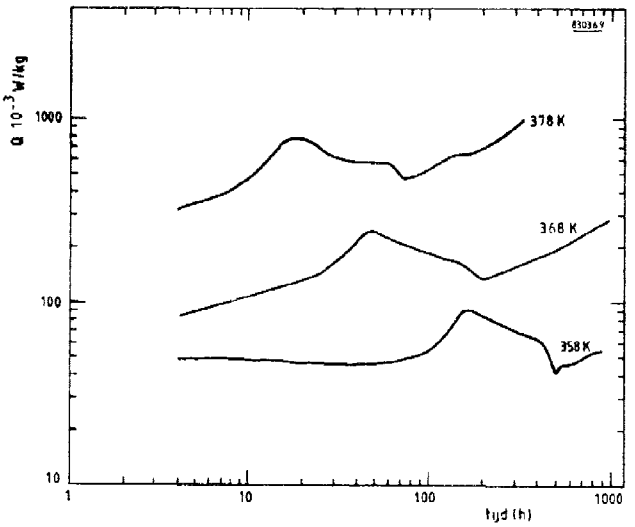

Fig. 29. IST Curves of a Smokeless Propellant.

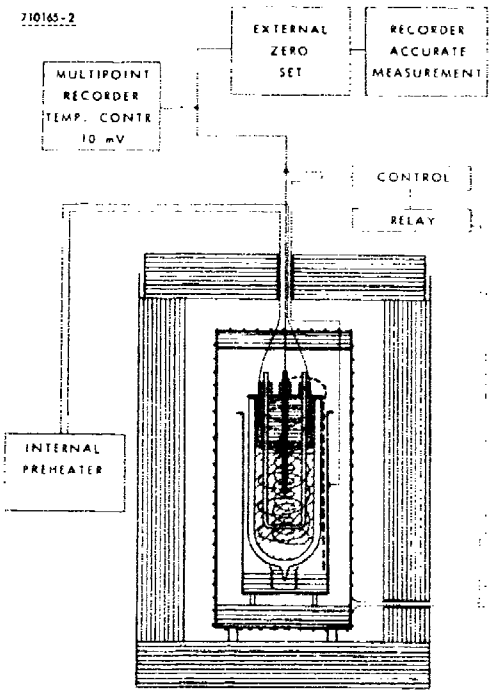

Fig. 30. Arrangement of the Adiabatic Storage Test (AST).

A gas can be led through the Dewar vessel by means of tubes passing through the lid of the vessel. From the inlet tube the gas is spread over the bottom of the Dewar vessel. The gas outlet is at the top of the Dewar vessel. Thus the entire sample is brought into contact with the gas. Before being supplied to the Dewar vessel the gas is carefully thermostated at a temperature equal to that of the sample. Because of the nearly adiabatic conditions (the maximum heat loss is 10 mW), the heat generated by the sample is almost completely converted into an increase in temperature of the sample.

Therefore, the temperature of the sample is recorded continuously as a function of time. From the increase in temperature in relation to the specific heat and the mass of the sample the heat generated by the sample can be determined.

An experiment is discontinued when the heating rate is too fast. In this case the system is cooled down with the aid of a cooling coil. Measurements can be performed in the temperature range from 250 K to 470 K.

Even at relatively low temperatures small heat generation can be determined. The smallest temperature increase that can be determined corresponds to a heat generation of 15 mW/kg. The upper limit is determined by the capacity of the cooling coil. If water is applied as coolant, a maximum heat generation of 500 W is allowed. The accuracy of the measurements is at least 30% at 15 mW/kg and 10% from 100 mW/kg to 10 W/kg.

An example of a result of an AST experiment is shown in Fig. 31. The first part of the curve, up to about 300 hours, has been measured in the AST. The second part has been extrapolated by using the last part of the measured temperature-time curve. The maximum temperature of 526 K is the auto-ignition temperature of the sample under investigation.

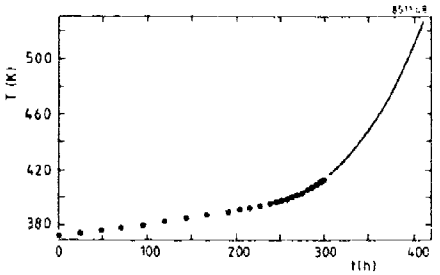

Fig. 31. Example of an AST Curve.
••• measured values.
___ extrapolated values.

Thus, with the AST experiment the induction period is observed in which the sample is self-heated up to the auto-ignition temperature under adiabatic conditions, starting from an arbitrary initial temperature.

Thermal Step Test (TST)

With the Thermal Step Test (TST), kinetic studies of the decomposition of energetic materials are performed. The activation energy can be obtained over a wide temperature range (300 - 1400 K). Furthermore the influence of catalysts and additives can be assessed.

The experiments are performed by confining some energetic material in a capillary stainless steel tube with a fixed internal diameter of 1 mm and a variable outer diameter from 1 - 2 mm and with a length of 70 mm.

After inserting the tube in an electric circuit and by discharging a capacitor through the tube, the temperature of the tube is raised in about 30 microseconds. Temperatures up to 1000 K can be maintained for a prolonged period (up to several hours). The induction time, the time needed to rupture the tube, as a function of tube temperature is measured.

In Fig. 32 results of five different AP based composite propellants are shown (Schrader and others, 1984 [AGARD]). The compositions are given in Table 11. It turned out that composite propellants start to decompose at a lower temperature than the pure ammonium perchlorate. This behavior is believed to be caused by the binder, because the binder is able to generate radical like species at a relatively low temperature which could enhance the decomposition.

A wide variety of energetic materials has been investigated with the TST. In the temperature domain, relevant for the cook-off phenomena, all investigated explosives (Schrader and others, 1983, and Schrader and others, 1984 [Ninth Int. Pyr. Sem.]) and propellants show a pseudo first order Arrhenius type of decomposition.

Table 11. Compositions of the Propellants (% w/w).

Compound	H1	H2	H3	P1	P2
AP	67.9	69.4	80.0	67.0	65.0
Aluminum	16.7	18.0		17.0	
HTPB based PU	11.1	7.5	15.0		
PPG based PU				11.6	15.1
IDP*	3.6	4.2	5.0	4.0	4.8
NGu					15.0
Fe_2O_3	0.6	0.6			
$Cu_2O \cdot Cr_2O_3$				0.3	
Rest	0.1	0.3		0.1	0.1

* IDP = isodecylpelargonate (plasticizer)

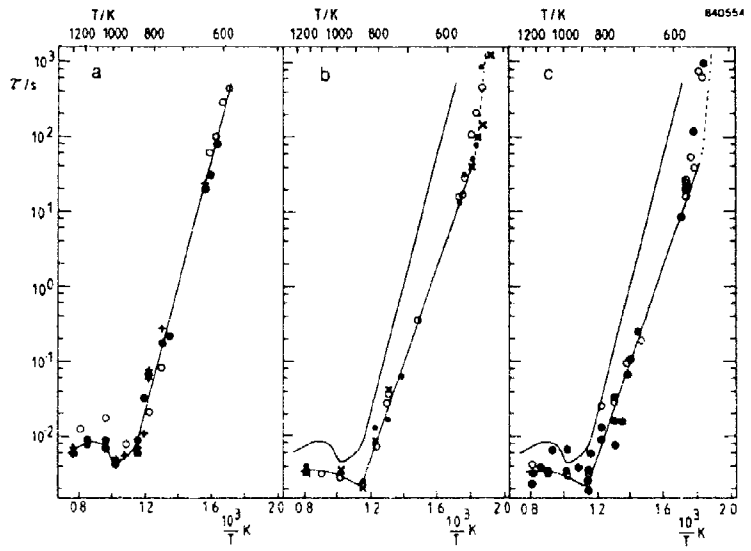

Fig. 32. Induction Time as a Function of Temperature of: (a) • AP, + AP-Al, and o AP-NGu, (b) x H1, • H2, and o H3, and (c) o P1, • P2. The solid curve from a is also drawn in b and c, the solid/dotted curve from b is also drawn in c.

One Dimensional Time to Explosion Test (ODTX).

The ODTX (McGuire and Tarver, 1981, Catalano and others, 1976, and Tarver and others, 1978) test has been developed at Lawrence Livermore National Laboratory as a well controlled environment in which to measure times to explosion at confinement pressures up to 150 MPa. The diameter of the hemispheres containing the energetic materials is 12.7 mm. The hemispheres are heated and the time to explosion is recorded. The spherical geometry has been chosen, since it is well suited for computer modeling.

The ODTX test has only been used to study high energy explosives like TATB, TNT, and plastic bonded explosives containing RDX and HMX, (cf. Fig. 33). Typical temperatures used range from 420 up to 620 K. The times to explosion range from a few seconds up to about 1 day. Chemical kinetics, more complicated than the simple type Arrhenius equation, are employed to fit the experimental results within a theoretical frame work.

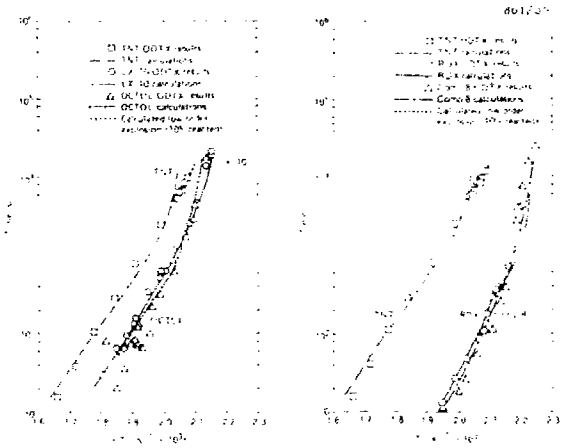

Fig. 33. Experimental and Calculated Times to Explosion for 12.7 mm Diameter Spheres of TNT, LX-10, and OCTOL (A); and of TNT, RDX, and Comp. B (B).

5.1.6. Computational Methods

As stated earlier in the introduction a heat balance can be made

$$c\,\rho\,\frac{dT}{dt} = Q\,\rho\,K_{0e}^{-E/RT} - \frac{\alpha S}{V}\,(T - T_0)$$

Unfortunately, many of the properties are temperature dependent and this equation cannot be solved analytically without making approximations.

The advent of the computer made it feasible to employ numerical methods to solve the differential equation. In the early sixties Zinn and Mader (1960) and Zinn and Rogers (1962) were the first to calculate temperature profiles and times to explosion which were in good agreement with experimental results. Since then many have used numerical methods to describe cook-off phenomena with success.

The most widely used method to numerically solve the above equation is the so-called finite differences method (Richtmeyer and Morton, 1967). Since a thorough treatise of this subject is beyond the scope of this chapter; only a brief outline will be presented.

First, the continuous time and space coordinates are changed into discrete variables, the finite differences Dr and Dt, the grid size, and the time step, respectively. Now, the key of the finite differences method is to approximate the equation by substituting the differentials by the differences, i.e., dr/dt = r/Dt. The resulting differences equation can be easily solved by either an explicit or an implicit method.

An explicit method is characterized by the fact that to calculate the temperature at a certain place at a certain time only the temperatures of the previous time step are needed. Explicit methods are easy to use, but they do have one distinct disadvantage; the solution is not always stable. This means, that if the time step is too great as compared with the grid size no meaningful results are obtained. So if one has to calculate long times to explosion, implicit methods are to be favored because they are always stable.

With an implicit method, the temperatures of all grid points at a certain time are described by means of a set of coupled equations. Thus at every time step this set has to be solved by means of an iterative process or by means of a matrix inversion technique.

To finish this section we cite a number of examples illustrating the possibilities of numerical methods.

At Lawrence Livermore, finite difference methods have been used to model the times to explosion of several high explosives simulating numerically the ODTX (cf. preceding section). In this

calculation, besides Arrhenius type of chemical kinetics, more complicated kinetics have been employed as well. The outcome of the modeling showed that good agreement with experimental data can be obtained.

In France, numerical methods have been applied to investigate and understand the thermal decomposition of propellants. Basis for the calculations was the model of Zinn and Rogers. Again a satisfactory agreement between theory and experiment can be obtained.

In the Netherlands, numerical methods have been used to model the decomposition of unstable compounds in electroexplosive devices (Prinse and Leeuw, 1986). In that case one has not only to deal with energy release due to chemical processes, but also the energy input due to the electrical power must be considered.

In Fig. 34 the temperature rise in the wire of an electroexplosive device is shown. The dotted line denotes the experimental data points and the solid line is the theoretical result. As can be seen, there is good agreement between theory and experiment.

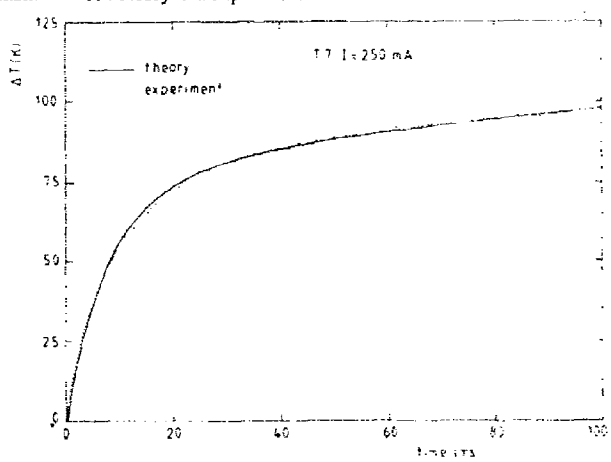

Fig. 34. Temperature Rise of EED Bridge Wire Vs. Time at a Fixed Current.

So one can conclude that theoretical simulation based on numerical methods can be a very powerful means to get a feeling for the behavior of thermally unstable compounds. It is to be expected that in the light of the rapid developments - both in hardware and in software - numerical methods will prove to be even more successful in the near future.

5.1.7. Slow Cook-Off Test

Slow cook-off tests are characterized by very low heating rates (a few degrees per hour to a few degrees per minute). Tests range from small scale requiring several grams of energetic materials to large scale tests involving the full sized weapon system. These tests are to provide data that might be used to predict the response of ordnance slowly heated primarily in storage or handling mishaps. (For example, munitions in a rail car heated by the burning of adjacent rail cars, or munitions in a storehouse adjacent to a burning storehouse, or weapons in the hold of a ship with fire in adjacent compartments.)

The small scale slow cook-off tests are described as follows.

SNPE Test (France)

This test set-up (Kent and Rat, 1982, and Rat and Kent, 1981) (Fig. 35) consists of a steel cylindrical combustion chamber with an internal diameter of 80 mm and a depth of 600 mm, which can be heated electrically to 680 K (see Fig. 35). At a certain time a cylindrical piece of propellant, diameter 50 mm, variable height, fitted with a thermocouple, is introduced in the preheated combustion chamber. The time to ignition and the temperature history of the propellant are recorded. Quantities up to 200 grams can be measured this way. The combustion chamber cannot be closed gastight so total confinement is not obtained.

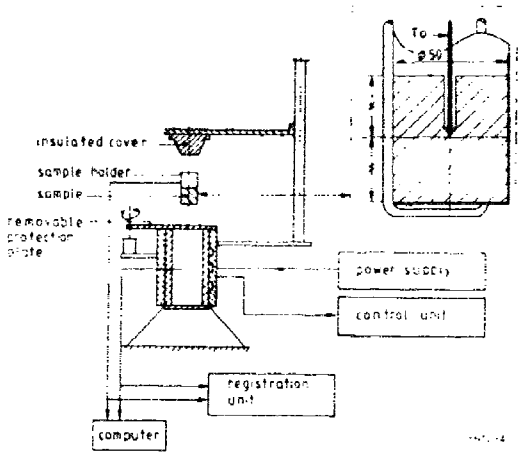

Fig. 35. Experimental Set-Up of the SNPE Test.

Some results of this test applied to propellants are shown in Fig. 36. Typically, the critical temperature is around 450 K and the induction times can be as long as 18 hours. In Casenave and Racimor (1984), the experimental data are used as input for theoretical calculations based on the work of Zinn and Mader (1960) to predict induction times and critical temperatures for other geometries as well, (cf. dashed lines in Fig. 36.)

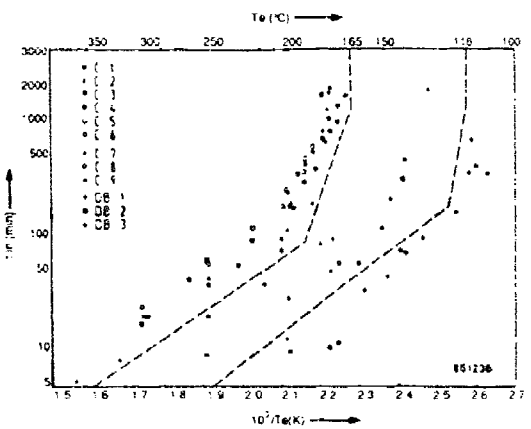

Fig. 36. Induction Time as Function of $1/T_e$. C = Composite propellant. DB = Double base propellant.

The Belgian E(cole) R(oyale) M(ilitaire) (Erneux and others, 1983) test is similar to the French SNPE test. The main differences are that less material is used (0.2 to 2 gr), and that cook-off can be studied under confinement as well. Comparison with theoretical calculations showed a good fit, for these small quantities (< 2 gr).

SNPE also performs slow cook-off tests using the model motor presented in Fig. 37. This model motor is placed within an oven instrumented with thermocouples as indicated in Fig. 38. The temperature within the oven is increased at 3.33°C/hour. The temperature at which reaction occurs and the severity of reaction is determined.

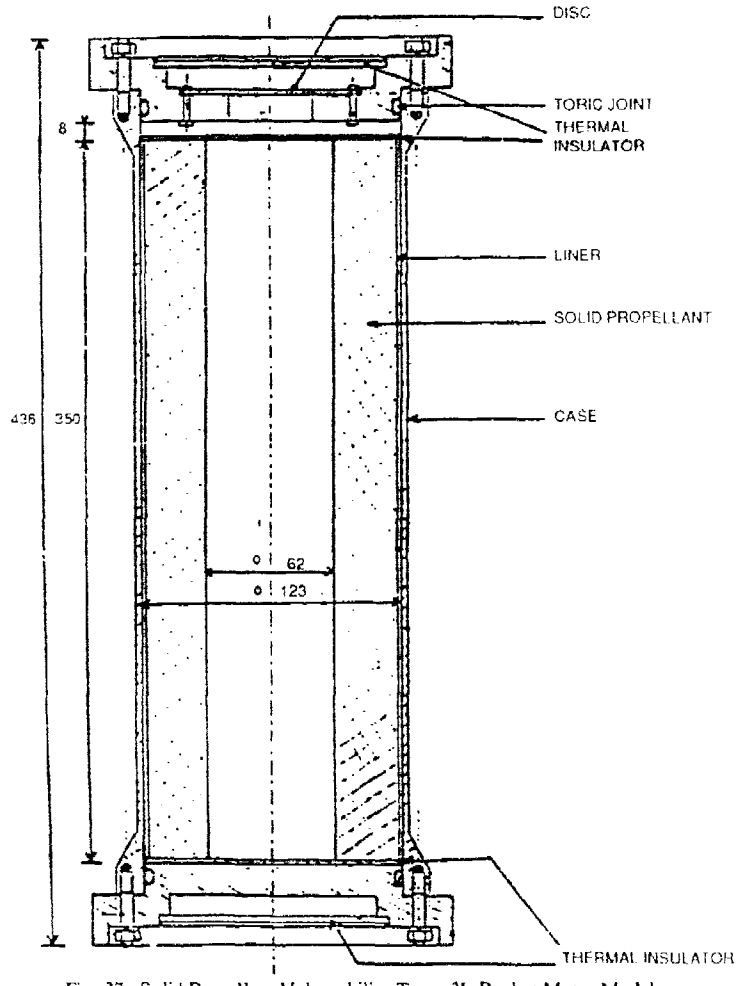

Fig. 37. Solid Propellant Vulnerability Tests, 3L Rocket Motor Model.

UK Slow Cook-Off Test

In this test, which can be used for all types of explosive stores, the item under trial is placed in a disposable metal jacket, which is cylindrical in shape and constructed in halves which are bolted together after the store is put in. Ample space is left for air circulation all around the store. The ends of the jacket are attached to flexible hoses for circulation of air; the air circulation is closed, and the whole air-duct construction is heavily insulated in order to conserve energy. The air heater and pump are separated from the jacketed store by a reinforced concrete wall. The air temperature inside the jacket half-way along the length of the store is monitored by a thermocouple which controls the heat flux from the heater to the circulating air to maintain the rate of temperature increase in accord with a preset program [heating rate 3.3°C/hr (6°F/hr)]. Up to five other thermocouples may be installed within or on the surface of the store. A demolition charge on a remotely-controlled trolley is provided nearby, for use should the trial be aborted for any reason, or the maximum temperature programmed be reached without event.

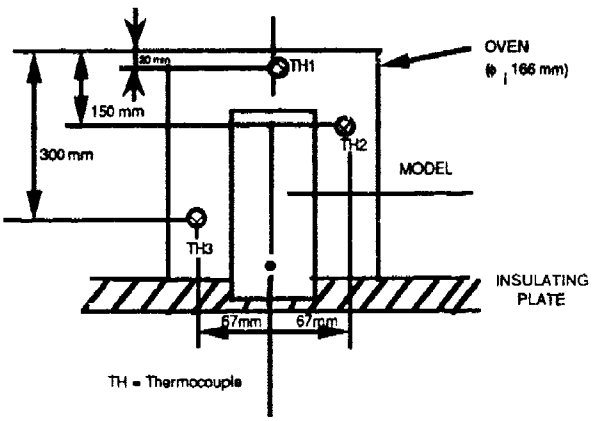

Fig. 38 Solid Propellant Vulnerability Tests, Slow Cook-Off Test. Temperature Increase Rate: 3.33°C/h.

RARDE Large Scaled Vessel Test (U.K.)

This test is nominated for propellants in the AOP-7 test manual (1982). In the Large Scaled Vessel (LSV) Test (heated type) the material under test is sealed in a standard vessel made of seamless steel tubing (76 mm ID, 95.2 mm OD) with welded end-plugs 450 mm apart. The volume of the vessel is approximately 2 liters. Nickel-chrome heating wire is wound around the tube and current is applied to heat it at 5°C per minute, monitored by means of a thermocouple inside the vessel and in thermal contact with its inner face through its housing. In due course a runaway reaction begins and failure of the vessel ensues. The violence of the response is assessed by means of the degree of fragmentation of the vessel. A variant of this test, using internal ignition is used in the U.K. for hazard division assessment of propellants.

RARDE Temperature of Ignition Test (U.K.)

This test is nominated for the AOP-7 tests manual (Allied Ordnance Publication, 1988). It is used for all types of explosive material. A standard glass test-tube (100 mm long, 12,13 mm OD) containing 0.20 g of prepared sample powder, cut-out discs or pellets as appropriate) is inserted into a metal block which is externally insulated and heated at 5°C per minute. The temperature of ignition and information concerning the nature of the event are recorded. The heating rate can be varied if desired.

NWC Super Small Scale Cook-Off Bomb (SSCB)
(U.S., Pakulak and Cragin, 1983)

In this method, the test fixture, a super-small scale cook-off bomb (SSCB), consists of a steel tube 2.8 cm OD/2.3 cm ID x 7.6 cm long (~1.1-inch OD/0.9-inch ID x 3-inches long) spot welded (4 points) to a witness plate 6 cm diameter x 1 cm thick (3-inch diameter x 3/8-inch thick). A similar top plate is used and bolted to the tube-witness plate for explosive confinement. An internal aluminum sleeve 2.3 cm OD/2.0 cm ID x 7.6 cm long (~0.9-inch OD/0.8-inch ID x 3-inches long) is used to spread input heat evenly and temperature measurement is made with a thermocouple. The explosive material is cast, pressed, or cured in steel tubes 2 cm OD/1.5 cm ID x 3.2 cm long (0.8-inch OD/0.6-inch ID x 1.25-inches long). Each tube contains about 10 grams of explosive and two steel tubes are used per test. This allows a 1.3 cm (1/2-inch) void area for thermal expansion. The outer steel tube is heated with two, 125 watt bard heaters. With 220 VAC applied, the heating rate is ~1°C/sec and is ~0.2°C/sec with 110 VAC. The higher heating rate is similar to a heavy steel wall 1.3 cm (~0.5-inch) munition in a fuel fire; the lower heating rate is similar to an area that is not in a direct heat path from the fuel fire; i.e., fuze cup, thermally protected case, etc.

This test method is used for determining the cook-off temperature and reaction of an explosive under confined conditions. The time-temperature plot is used to determine the cook-off temperature at a given heating rate. The body fragments and witness plate are used to assess the severity of the reaction. This test satisfies the mandatory requirements for qualification testing of booster and main charge explosives. The cook-off temperature is dependent on heating rate and can be used to predict

cook-off time and temperature in a fuel fire. The severity of the cook-off reaction is assessed in the following manner and is listed below:

Observed Results		
Outer Tube	Witness Plate	Cook-Off Reaction
Intact/Split	Dent ≤ 1.3 cm (0.5")	Burning
1-4 Pieces	Dent ≤ 1.3 cm (0.5")	Deflagration
Many Pieces	Dent ≤ 1.3 cm (0.5")	Explosion
Many Pieces	Nearly Punched	Partial Detonation
Small Pieces	Punched Hole	Detonation

The severity of the cook-off reaction is dependent on the heating rate.

NWC Small Scale Cook-Off Bomb (SCB) (U.S.)

The SCB is adopted in the United Nations recommendations (Recommendations on the transport of dangerous goods, 1986) and simulates transport and storage situations involving slow external heating of substances. In the test a sample of the substance to be tested is contained in a 400 cc steel vessel with walls 3 mm thick. The vessel is electrically heated and is equipped with thermocouples. After insertion of the test material the temperature is raised from 300°C at a rate of 3°C a minute. The test is considered positive when the test material has deformed the vessel or the witness plate which forms the bottom of the vessel.

Table 12. Some Typical Results for the Small Scale Cook-Off Bomb Test (SCB).

Substance		Cook-Off Temp. (K)	Cook-Off Time (min)	Cook-Off Reaction
Guanidine nitrate	Technical grade	640	14.0	+
Propellant (cannon)	M-6 (USA)	473	14.2	+
Nitroguanidine	powder	553	4.0*	+
Tetryl	NSWC, Crane, IN	487	14.5	+

* Data taken at a higher heating rate of 1°C/s.

NWC Toaster Oven Slow Cook-Off Technique (U.S.)

The SCV test was initially implemented because it became apparent that very little was known regarding the changes that occur within propellants as a function of temperature during a slow cookoff. Speculations abounded that a particular propellant may swell or foam, and possibly even partially liquefy beyond some temperature, but very little data existed. Even less was understood about how variations in propellant formulation affect elevated temperature behavior. Therefore, a simple test was designed and implemented to provide insight and empirical data regarding propellant behavior as a function of temperature.

Early SCV tests were conducted with cylindrical propellant samples contained in Pyrex graduated cylinders that were heated at 25°F/hr in modified household toaster ovens while physical changes as a function of temperature were observed with a video camera. These early "toaster oven" SCV test efforts revealed the value of this type of test, and subsequent needs stimulated the evolution of the current SCV test.

The current SCV test is designed to provide the following data:

1. The bulk volume change of the propellant as a function of temperature.

2. Visible physical state changes that occur as a function of temperature. Most propellants undergo visually observable physical changes as a function of temperature. Some propellants soften, swell, and/or foam a great deal, while others show only small changes. Other propellants partially liquefy due to binder depolymerization and/or "melting" of one or more ingredients. Sometimes the liquid or semi-liquid phase foams and/or "boils" prior to autoignition. Significant color changes often occur as a function of temperature as well.

3. The radial thermal profile through the propellant sample as a function of temperature and time. Internal exothermic activities as well as endothermic decompositions and/or phase changes can be observed via thermocouple probes placed in a three-dimensional spatial arrangement throughout the sample.

4. The oven air temperature and the temperatures and thermal profile within the propellant sample at the time of autoignition.

5. Sometimes the location of autoignition can be observed. Autoignition can occur in the gas phase above the propellant sample, on a propellant surface exposed to air, or near the centroid of the propellant sample.

6. The composition and volume of gases given off by the heated propellant as a function of temperature and time. Up to the present time, this has not been done at the Naval Weapons Center.

This type of data is useful for predicting whether sufficient propellant physical property degradation and/or expansion will occur in a full-scale motor to cause propellant grain collapse and/or exudation of propellant through the nozzle. In addition, knowledge of the physical state of the propellant and the degree of propellant confinement at the time of autoignition provides important clues about how violently the propellant will react in a rocket motor. Data provided by the SCV test can also be used to estimate the time-to-reaction and cookoff temperature of full-scale motors. As a propellant formulation research tool, the SCV test can provide clues and insights regarding what is occurring within a propellant as a function of temperature. Knowledge of how propellant formulation changes affect propellant behavior during slow cookoff can be obtained by conducting a matrix of tests in which one ingredient change is made at a time.

SCV Test Hardware Description

Figure 39 shows an assembly of the basic apparatus used for the SCV test. A similar but less refined apparatus was used for the earlier "toaster oven" SCV tests.

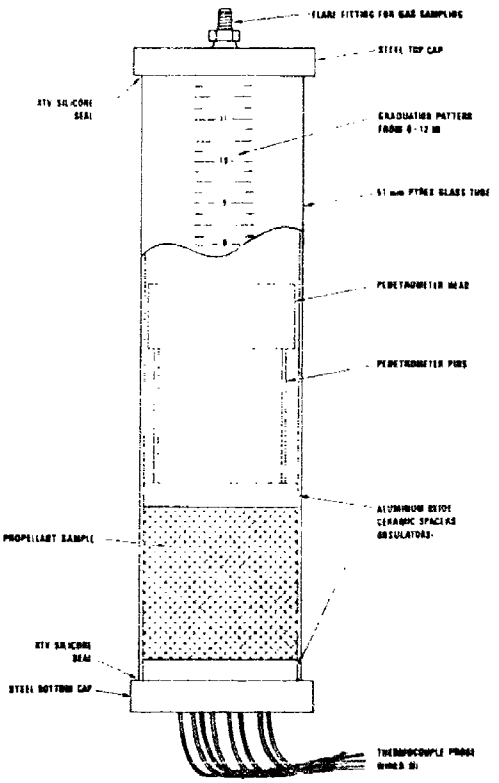

Fig. 39. SCV Test Apparatus Assembly.

The most recent version of the SCV test is conducted with a propellant sample cast or machined to form a cylinder 1.80 inches in diameter and 2.00 inches long. The propellant sample fits with a small clearance in a custom-designed 12-inch-tall Pyrex graduated cylinder. The Pyrex graduated cylinder has parallel red and white markings spaced 0.125 inch apart so that they can be easily observed with a video camera against a light or dark colored background. Eight thermocouple probes are integrated into the base of the graduated cylinder and extend into the propellant sample. Two thermocouples are placed at the outside radius, three at the half-radius, and three adjacent to the vertical centerline of the propellant sample. The thermocouples at the outside radius are 180 degrees apart and lie on the horizontal centerplane of the propellant sample. The three thermocouples at the half-radius and the three thermocouples at the center are spaced 120 degrees apart at three heights (1/4h,1/2h, and 3/4h) to form a three-dimensional spatial arrangement.

All of the SCV tests presented in this paper were instrumented with bare, 0.125-inch-diameter, stainless steel thermocouple probes. In the future, 0.0625-inch-diameter, glass or ceramic-coated stainless steel thermocouple probes will be used. The smaller probes displace less propellant, conduct less heat into or out of the sample, and can be more accurately positioned within the propellant sample. In addition, there is some speculation that propellant decomposition can be catalyzed by allowing the heated propellant to be in direct contact with metals containing iron, chromium, nickel, copper, etc., and it is felt that such contact should be avoided.

The 1/2-inch-thick white aluminum oxide ceramic fiberboard spacers shown in Fig. 39 insulate the ends of the propellant sample to reduce nonradial heat conduction. A penetrometer consisting of two 0.0625-inch-diameter, 2.75-inch-long pins loaded by a 255-gram head is shown in the glass tube on top of the propellant sample, with the tips of the weighted pins resting on the propellant surface. The penetrometer places point loads of approximately 92 psi upon the surface of the propellant sample and provides visual evidence of when the propellant has softened sufficiently to allow the penetrometer pins to penetrate the propellant. The pin spacing was chosen so that penetrometer pin location did not coincide with the location of thermocouple probes and so that heat transfer through the pins would have a minimal effect upon the thermal events occurring in the center region of the propellant sample.

Figure 40 shows a schematic of the SCV heating chamber. The SCV oven in current use is a heavily insulated chamber that has 0.25-inch-thick steel interior walls. The oven has an internal volume of approximately 27 ft^3 and is heated with an array of five 3000-watt electrical heaters that are isolated from the main oven cavity. Air is continuously circulated through the isolated heater bank and oven chamber volume with a fan to eliminate significant temperature gradients within the oven and to ensure even heating. Chamber temperature as a function of time is controlled with a Honeywell programmable temperature controller. The test apparatus is indirectly illuminated with six 40-watt appliance light bulbs so that a good video image can be obtained. The sample is viewed with a video camera through a pair of Pyrex windows mounted in the side of the chamber. The internal chamber cavity is instrumented with a flush-mounted high-temperature piezoelectric blast pressure gage and four air-temperature thermocouples. Two of the air-temperature thermocouples are adjacent to the propellant sample.

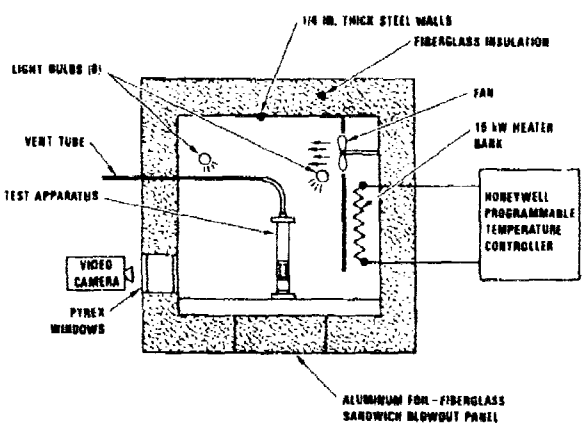

Fig. 40. SCV Heating Chamber.

SCV Test Description

The SCV test is conducted so that the heating cycle can be completed in one working day. During the first hour, the chamber is heated at a linear rate to a predetermined preheat temperature. Then the

chamber temperature is ramped at 25°F/hr until autoignition of the sample occurs. The preheat temperature is selected so that the total duration of the test will be between 7 and 9 hours. The 25°F/hr heating rate was chosen for two reasons: (1) to expedite the test and (2) to scale the heating rate to the sample size.

The subscale propellant samples are heated at 25°F/hr in an attempt to approximate thermal profile similitude with the bulk propellant in a typical full-scale rocket motor heated at 6°F/hr. Arguments can be made for maintaining temperature differential similitude versus temperature gradient similitude or some condition in between the two conditions. The 25°F/hr heating rate was empirically chosen to represent a reasonable intermediate condition of thermal similitude. While the 25°F/hr heating rate is a compromise, and true similitude (if "true" similitude can be defined) is probably seldom achieved since each rocket motor and propellant is different, the heating rate has yielded meaningful data, and no changes to the adopted heating profile scheme seem necessary at this time.

Test instrumentation consists of 12 thermocouples with the placements described earlier, blast overpressure within the chamber volume, and full-time video coverage. Gas collection, sampling, and analysis is an option that could be implemented to meet specific needs. After the entire test has been recorded on 3/4-inch video tape, the full duration of the test prior to autoignition is time-lapsed in the video laboratory so that a period of 5 minutes is compressed into 1 second. The video then gives an animated account of changes that occurred in the propellant sample as a function of time and temperature.

Selected "Toaster Oven" and SCV Test Results

At the present time, "toaster oven" and/or SCV tests have been conducted with 17 propellant formulations. While excellent duplication of results was obtained when the same propellant formulations were retested under identical conditions, virtually each of the 17 propellants exhibited dramatically different behaviors. This was a surprise, since it was felt that propellants within the same general class (HTPB/AP propellants, for example) would all behave in a more or less similar fashion. On the contrary, seemingly minor formulation changes, such as the substitution of yellow iron oxide for red iron oxide, were found to have a large impact on how the propellant behaved in slow cookoff. The type of binder, curing agent, burn rate catalyst, choice of plasticizer, and presence or absence of other ingredients were often found to dramatically affect the behavior of a propellant at elevated temperatures.

The data obtained from the early "toaster oven" tests are summarized in Table 12. Table 13 provides propellant formulation data for the propellants listed in Table 12. The data obtained from the more current and more refined SCV test are summarized in Table 14. Table 15 provides the propellant formulation data for the propellants tested in the SCV chamber.

The "toaster oven" tests were conducted in a manner fundamentally similar to the way the SCV tests were conducted. The primary differences between the "toaster oven" test and the SCV test, such as sample size and penetrometer point loading, are documented in Tables 12 and 14; it is important to note these differences when comparing the data listed in Tables 12 and 14. It is also important to point out that oven thermal gradients and poor thermocouple instrumentation technique yielded unreliable maximum propellant sample internal temperature values for the tests conducted in the toaster ovens.

Space does not allow a thorough discussion or analysis of the data presented in Tables 12 through 15. However, several interesting observations are briefly summarized:

1. Large differences in propellant slow cookoff behavior were observed, even between propellants in the same basic family. The cookoff behavior of nine R-45M/AP, three B-2000/AP, and three CTPB/AP propellants is summarized in Tables 12 and 14. Of these propellants, only Propellants D, E, and L (all members of the R-45M/AP family) exhibited closely similar behaviors.

2. Propellants A and B are the same basic propellant formulation and differ only in RDX content. Propellant A is a clone of a Fleet propellant and contains 4% RDX while Propellant B does not contain any RDX. The data in Table 12 reveal that the presence of RDX lowered the autoignition air temperature by 55°F, reduced the temperature of initial propellant expansion by 26°F, and increased the volumetric expansion of the propellant by a factor of 2.5.

3. Propellants E and F are also the same basic propellant formulation; they differ primarily in the type of burn rate catalyst used in the formulation. Propellant E is a clone of a Navy Fleet propellant and is formulated with red iron oxide as the burn rate catalyst, while Propellant F is formulated with yellow iron oxide. The seemingly insignificant change of substituting yellow iron oxide for red iron oxide reduced the temperature of initial propellant expansion by 49°F, lowered the autoignition air temperature 24°F, and increased the volumetric expansion by a factor of 2.3. Subsequent DSC/DTA/TGA studies with the yellow iron oxide revealed that weight loss, probably due to dehydration, began to occur at about 320°F very near the temperature of initial propellant expansion.

4. The B-2000/AP/copper chromite propellants (Propellants C and I) reacted many orders of magnitude more violently under the minimum confinement present in the SCV test than any of the other AP-based propellants. In addition, these two propellants have very similar formulations, yet they exhibited a large difference in volumetric expansion.

5. The formulation of Propellant N is similar to the formulations of Propellants D and L. The primary difference is the burn rate modifier. Propellant N was the only one tested that contained FeF3. The data listed in Tables 12 through 15 provide evidence that the FeF3 substantially lowered the autoignition temperature of Propellant N.

Table 12. Toaster Oven Test Data Summary.

Sample size = 1.375 inches in diameter by 2.750 inches long
Penetrometer point load = 77 psi.
All tests were conducted in modified toaster ovens

Propellant	Temperature of initial expansion, air/internal[a], °F	Temperature at which expansion stopped, air/internal[a], °F	Penetrometer movement, air/internal[a], °F			Volumetric expansion, %	Autoignition temperature, air/internal[a], °F	Relative reaction violence[b]
			Begin	End	Length, inches			
A	334/314	362/340	327/308	342/322	0.75	96	381/386	2.5
B	360/349	413/409[c]	None	---	---	38	436/458	3.8
C	No expansion	---	383/360	414/398	2.0	None observed	445/472[d]	9.5
D	390/361	411/385	None	---	---	24	422/402[e]	1.5
E	378/363	401/392	None	---	---	28	413/411[e]	2.0
F	329/321	362/358	None	---	---	65	389/389	2.0
G	255/237	281/279[f]	153/106	229/211	g	>220[f]	281/279[d,f,h]	3.5/11
H	293/247	378/269	273/233	338/266	g	85	378/269[d,e,h]	1[k]
I	331/311;407/391[f]	354/331, 422/416	354/331	390/371	g	32/24/45	421/437[d,h,m]	9.2
J	315/303	388/391	318/308	343/339	g	93	391/427[d,e,h]	1
K	354/336	378/365	None	---	---	26	410/425[h]	2.0

[a]Internal temperature values are not fully reliable on these early tests due to poor thermocouple placement and fixturing techniques as well as thermal gradients in the ovens

[b]Comparative scale. 0 = no reaction, 1 = quiescent burn, 10 = detonation

[c]Small amount of expansion observed just prior to autoignition

[d]"Liquid" phase observed prior to autoignition

[e]Ignition occurred on top surface of sample

[f]Propellant boiled over and ignited upon contact with the oven heating elements

[g]Full penetrometer excursion observed

[h]Propellant darkened in color during heating

[i]Vapor phase explosion followed by a 61 second quiescent burn

[j]Sample size = 1.750 inches in diameter by 2.000 inches long. Penetrometer point load = 92 psi

[k]Surface ignition followed by a quiescent burn for 2 minutes, 53 seconds

[l]Expansion occurred in two separate stages, propellant sample collapse began to occur at 378/359°F and stopped at 404/389°F

[m]Smoke observed 13 minutes prior to autoignition

Table 13. Toaster Oven Test Data Summary; Propellant Formulations.

Propellant	Theoretical I_{sp}, 1000 → 14.7 psia, seconds	Theoretical combustion chamber temperature, °F	Ingredients (listed in decreasing order of abundance)
A	—	—	AP, R-45M, RDX, DOA, DDI, ZrC, HX-752, DITBHQ, PCHPDA
B	...	..	AP, R-45M, —, DOA, DDI, ZrC, HX-752, DITBHQ, PCHPDA
C	...	...	AP, poly(1,2-butylene)glycol, (B-2000), Al, IDP, copper chromite, TP-4040, HDI, C-1, sulfur, FeAA and HAA, polymethylsiloxane
D	...	...	AP, R-45M, DOA, Al_2O_3, IPDI, Fe_2O_3 (red), HX-752, Catechol
E	...	...	AP, Al, R-45M, IDP, Fe_2O_3 (red), IPDI, HX-752, Protech 3105, triphenyl bismuth
F	...	...	AP, Al, R-45M, IDP, Fe_2O_3 (yellow), IPDI, HX-87B, Protech 3105, ODI, triphenyl bismuth
G	...	...	Proprietary formulation: nitroglycerine, RDX, nitrocellulose, plasticizer, elastomer, additives
H	—	—	RDX, HMX, BTTN, TMETN, PEG, PCP, Pb_3O_4, Al_2O_3, Desmodur N-100, carbon, MNA, CAB, MA, triphenyl bismuth
I	...	...	AP, Al, poly(1,2-butylene)glycol; (B-2000)/HDI, IDP, TP-4040, copper chromite, C-1, sulfur, paraquinone, FeAA and HAA, polydimethylsiloxane
J	...	..	AP, nitroguanidine, poly(1,2-butylene)glycol, (B-2000)/HDI, IDP, TP-4040, NPGA, C-1, sulfur, cupric sulfate, FeAA and HAA
K	...	...	AP, CTPB, Al, DOA, Fe_2O_3 (red), di/tri-epoxy resin, polybutadiene, binder additives (phenyl-B-naphthylamine; N,N-bis(1,4-dimethyl pentyl) paraphenylenediamine; thiodiphenylamine), chromium octoate

Table 14. SCV Test Data Summary

Sample size = 1.750 inches in diameter by 2.000 inches long
Penetrometer point load = 92 psi
All tests were conducted in the SCV test chamber

Propellant	Temperature of initial expansion, air/internal, °F	Temperature at which expansion stopped, air/internal, °F	Penetrometer movement, air/internal, °F			Volumetric expansion, %	Autoignition temperature, air/internal, °F	Relative reaction violence[a]
			Begin	End	Length, inches			
I	370/359 426/419[b]	405/393 446/517	315/297	354/342	0.38	23/26	446/517[c]	1.0
A	327/314	374/437	293/248	340/331	[d]	112	378/470	2.5
M	349/338	376/373[e]	295/254	376/373	1.6	40	436/562[c]	2.0
N	326/322 367/392[b]	329/326 367/420	293/270	312/306	0.13	17/19	367/420	2.2
O	315/310	342/337	265/194	324/318	[d]	35	421/516	1.2
G[f]	246/236	278/347[g]	160/133	236/226	[d]	>170[h]	278/347[g,i]	9.8
P[f]	369/361	430/508	292/262	374/367	[d]	34	430/508	3.2
Q	333/322 395/391[b]	355/347 405/464	376/368	405/464	0.13	22/37	405/464[c,i]	2.0

[a] Comparative scale. 0 = no reaction, 1 = quiescent burn, 10 = detonation
[b] Expansion occurred in two stages
[c] Ignition occurred on top surface of sample
[d] Full penetrometer excursion observed
[e] Small amount of expansion observed just prior to autoignition
[f] Sample size = 1.375 inches in diameter by 2.750 inches long
[g] Propellant liquified and boiled prior to autoignition
[h] Expansion continued off scale
[i] Propellant darkened in color during heating

Table 15. SCV Test Data Summary; Propellant Formulations.

Propellant	Theoretical I_{sp}, 1000 → 14.7 psia, seconds	Theoretical combustion chamber temperature, °F	Ingredients (listed in decreasing order of abundance)
L	—	—	AP, R-45M/IPDI, Oxamide, DOA, Al_2O_3, HX-752, carbon
A	—	—	AP, R-45M, RDX, DOA, DDI, ZrC, HX-752, DiYBHQ, PCHPDA
M	—	—	AP, R-45M/IPDI/DOS/Agerite white/Araldite 6005/TET, ZrC, graphite
N	—	—	AP, R-45M/IPDI, DOA, graphite, FeF_3, ZrC, Al_2O_3, HX-752
O	—	—	AP, Al, CTPB, Oxamide, DOA, MoO_3, di/tri-epoxy resin, polybutadiene, binder additives (phenyl-B-naphthylamine; N,N-bis(1,4-dimethyl pentyl) paraphenylenediamine; thiodiphenylamine), chromium octoate
G	—	—	Proprietary formulation: nitroglycerine, RDX, nitrocellulose, plasticizer, elastomer, additives
P	—	—	AP, CTPB, Al, ballistic modifiers
Q	—	—	AP, Al, HMX, R-45M, DOA, IPDI, HX-878, ODI, triphenyl bismuth

NWC Large Scale Slow Cook-Off (U.S.)

A standard U.S. test is the slow cook-off test based on WR-50 and DOD-STD-2105 (Navy) (1982) and most recently described in DOD-STD-2105A (1989 draft) in which the air surrounding the test item is heated at a rate of 6°F (3.3°C) per hour until reaction occurs. To save time the test may begin with the test item preconditioned to a temperature 100°F (55.5°C) below the predicted reaction temperature.

The test equipment (oven) is required to be capable of providing a controlled thermal environment for the test item with temperature increasing at the required rate throughout the test. Its design must minimize hot spots and ensure (by circulation or other means) a uniform thermal environment to the item being tested. A means of avoiding gradual pressure buildup in the test equipment must be provided.

Numerous thermocouples are used to monitor temperature throughout the test. As a minimum thermocouples monitor air and case wall temperature. It is particularly valuable if thermocouples can monitor internal positions in the motor too. The test is normally performed with motor nozzle covers securely in place.

At the Naval Weapons Center one or more external video cameras are used to monitor the test and provide an estimate of the reaction violence. Recently an internal video camera (considered expendable) has been added to observe the nozzle end of the tested motor for exudate and the location of ignition. A steel witness plate positioned beneath the test item (and possibly outside the oven) helps assess the reaction violence. A blast overpressure measuring system is also used to assess the reaction. The reaction violence is determined by assessing the various measurements described above as well as the post test condition and position of recoverable test item material.

This large scale slow cook-off test is not an obvious analog of any particular operational scenario. The test conducted is identical to that originally specified in WR-50 for determining the temperature at the case-liner interface when reaction occurred. In WR-50 the requirement was that reaction not occur until the case-liner interface exceeded 300°F. The recently adopted U.S. "Insensitive Munitions" requirement for slow cook-off is that no reaction more violent than burning occur regardless of the temperature and time during the test.

Because rocket motor reactions in the slow cook-off test are usually considerably more violent than burning, the Naval Weapons Center recently studied the cook-off behavior of four different rocket motors at heating rates of both 6°F per hour and 75°F per hour. The higher heating rate was chosen because analyses have shown the possibility of thermal scenarios with such a heating rate. The four motors studied all appeared to detonate at the lower heating rate, but at the higher heating rate two of the motors had much less violent reactions (at least approaching burning) while the other two resulted in at least partial detonations. It is interesting to note that the two propellants (one HTPB/AP and one CTPB/AP/Al composite) that reacted more mildly at the higher heating rate expand in volume considerably at temperature slightly below their slow cook-off temperature so that the reaction finally occurs in a semi-rigid foam with a density between 50 and 70% that of the original propellant. The

two propellants (one PU/AP/Al composite and one HMX/RDX-TMETN/BTTN-PEG/PCP) that detonated at both heating rates liquify prior to reaction in the slow cook-off test. Further thermal studies of these behaviors are ongoing.

Explosion Temperature

A blasting cap containing the energetic material, is immersed to a fixed depth in a bath of molten Woods' metal (NAVORD OD 44811, 1972). The time of immersion required to cause flashing or explosion is noted. The temperature of the bath is varied and a number of tests are made in order to produce smoke, fume flashes, or explosion over a range of approximately 2 to 10 seconds. A temperature-time curve is constructed in order to finalize the temperature required to cause flashing or explosions in 5 seconds.

Another typical example of a large scale slow cook-off test is a test performed on a Penguin Warhead (Strømsøe and others, 1984). The warhead was placed in an oven, see Fig. 41, and the temperature of the air was raised about 3.3 K/hour to simulate the temperature rise in the interior of a store house adjacent to a burning store-house. From the results, it became clear that if the warhead case is not gas tight, a violent reaction cannot occur (cf. Fig. 42) Instead the contents of the shell (TNT/RDX/Wax) did melt and were found on the floor of the test stand.

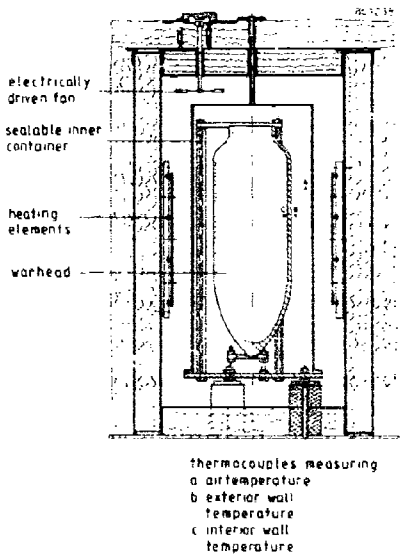

Fig. 41. Heating Facility for Slow Cook-Off Test.

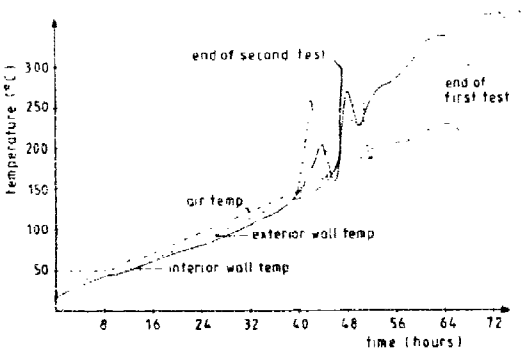

Fig. 42. Slow Cook-Off Test. Temperature measurements.

5.1.8. Fast Cook-Off Tests

In the fast cook-off tests the propellant, motor, or munition is subjected to rapid heating usually from direct flame impingement, as in a fuel fire test.

5.1.8.1. Koenen test

The sensitivity of solid and liquid substances to the effect of intense heat when under partial and defined confinement is tested by the Koenen test. The method yields quantitative results in the form of the limiting diameter of an orifice, as indicated below.

In summary the substance is tested as follows. A cylindrical steel tube (height 75 cm, inner diameter 24 mm) is filled with the substance to a depth of 60 mm. The top of the tube is closed by a steel orifice plate with an aperture which can be varied in diameter (1 to 24 mm). The tube is heated by four burners under standard conditions. As the tube is likely to be destroyed during the test, the heating is done in a protective steel box. The burners are located at three sides at the bottom of the box in a position, which optimizes heating of the tube. The decomposition gases may destroy the tube (bursting pressure several hundreds of bars) depending on the diameter of the aperture of the orifice plate. By testing the substance with series of aperture diameters the largest diameter for which the tube is destroyed in at least three fragments is determined. This diameter is called the limiting diameter. Its aperture area is a measure for the effect of the decomposition of a material under severe heating. Some typical results taken from Recommendations on the Transport of Dangerous Goods (1986) are shown in Table 16. This is an official test for UN classification for transportation of dangerous goods.

Table 16. Example of Results.

Substance		Limiting Diameter (mm)
2.4-dinitrotoluene	99%, cryst.	1
1,3-dinitrobenzene	cryst.	1
Ammonium nitrate	high dens. prills	1
Ammonium nitrate	low dens. prills	1
Nitroguanidine	cryst.	1
Guanidine nitrate	cryst.	1.5
Cellulose nitrate	dry	14
DB (NG/NC = 40/50)	full cylinder	< 1.5
	chips	20
Comp (AP/Al/binder = 65/16/18	full cylinder	12
	chips	18
RDX/NG/AP/binder - 50/25/10/15		12
		18
AP/picrite/binder = 75/10/15		14
		14
Cellulose nitrate	dry, 13.4% N	20

5.1.8.2. Thermal Detonability (Fast Cook-Off) NSWC (U.S.)

This fast cook-off test for explosive boosters and main charge explosives utilizes very simple cook-off test apparatus. It consists of a fire pan filled with standard JP-5 jet fuel and a cook-off bomb containing the explosive to be studied. The bomb itself consists of a standard 3.8 cm long 2.5 cm internal diameter (2.5 inch long x 1 inch diameter) pipe nipple enclosed with two pipe caps. A thermocouple is inserted through one pipe cap and attached to the inner surface of the bomb. The bomb contains the explosive cylindrical charge, 25 mm in diameter and 25 mm long. The fuel is ignited and the resultant temperature rise is recorded. The cook-off temperature and the effect of the cook-off on the bomb is recorded. The cook-off temperatures reported here are those of the bomb inner surface/explosive surface interface. Temperature increases at the bomb inner surface are usually between 40°C/minute and 50°C/minute. Temperature at cook-off vs. heating rate can be determined. Five levels of severity of reaction are observed in this test:

Level 1: Mild burning
Level 2: Mild pressure rupture
Level 3: Violent pressure rupture
Level 4: Partial detonation
Level 5: High order detonation

5.1.8.3. Fuel Fire Test

A standard U.S. test is the fuel fire (fast cook-off test) based on DOD-STD-2105 (Navy) (1982) and MIL-STD-1648(AS) (1982) (see also NATO AC/310 SG II STANAG 4240: Fuel Fire). The

most recent description of the test is described in MILSTD-2105A. In this test an item is suspended horizontally 3 feet (0.9 m) above the surface of a pit filled with JP-5, JP-4, JP-8, or JET A-1 jet fuel. The flame temperature is determined by measurements from four thermocouples (with time constants of 0.1 second or less) located 4 to 8 inches outside the ordnance skin (positioned on each end and side of the ordnance in a horizontal plane through the ordnance centerline). The test specification states that flame temperature shall reach 1000°F (538°C) within 30 seconds after ignition as measured by any two of the thermocouples. An average flame temperature of at least 1600°F (870°C) as measured on all valid thermocouples (without contribution of the burning ordnance) is considered a valid test. This temperature is determined by averaging the temperature from the time the flame reaches 1000°F until all ordnance reactions are completed. Reaction severity is determined from video coverage of the entire test (usually from several distances and perspectives) and by post test examination of the condition and positions of debris. Blast overpressure measurements are valuable if violent explosions or detonations occur.

The test site (fire pit) must be large enough to ensure complete engulfment of the test item by fire for the duration of the test. Generally complete engulfment can be provided if the pit dimensions are at least 10 feet larger in all directions than the dimensions of the munition. In addition, the burning area of the pit must be at least 400 square feet (36 square meters) to ensure a full intensity fire. The item is tested in the configuration appropriate to the logistic phase being duplicated by the test. Items with rocket motors should be restrained to avoid launching due to a propulsive reaction. However, the restraining and suspension methods should not interfere with heating of the item.

External conditions can have a major influence on the test results. For example even slight wind can affect the flame temperature due to effects on flame turbulence. Moderate wind or gusts can cause intermittent or irregular heating as the flame whips around and sometimes fails to engulf the test item. In cold weather the fuel is more difficult to ignite and growth to a full intensity fire may take several minutes.

From observation of a great many fast cook-off tests in the U.S. it is concluded that the motor case is the predominant factor in determining the violence of rocket motor responses to the test. Case materials, insulation, liner, attachments (including wings and fins), and design details all seem to be more influential than the specific propellant enclosed. It seems to be impossible to predict the fast cook-off response of a full-scale munition from subscale tests. Three-dimensional heat transfer analyses may be useful provided all details of the tested munition are modeled including all internal and external heat paths of the fully assembled unit.

Some motor case designs, specifically steel strip laminate and fiber/epoxy composite, have consistently yielded mild reactions because the heat of the fire causes the case to fail before ignition of the propellant. Monolithic cases, on the other hand, have shown inconsistent results. However the inconsistencies can be traced to differences in fire temperature or internal and external heat paths of the case.

Recently the Naval Weapons Center has added two refinements to the test that greatly increase the information obtained. One of these refinements is the use of a heavily insulated video camera positioned at the motor nozzle exit to observe the motor bore during the test. The other refinement involved the use of a 9 MEV x-ray system operating across the fire pit during the test. Both of these instruments have provided visual records of events occurring in rocket motors throughout the test.

In Evans and others (1984) a description is given of the fuel fire experiments performed with rocket motors produced by Royal Ordnance Summerfield consisting of a double base propellant directly bonded to a casing manufactured following the strip laminate technique. The four trials ended in motor burn out or mild pressure bursts. Also the results of some experiments with exposure of the rocket motor to a burning propane torch are described.

5.2. IGNITION TO DEFLAGRATION

5.2.1. Introduction

The transition of a combustible system from a nonreactive or very slowly reactive state to the state of self-sustained combustion can either be effected by an external source of ignition or may originate in the combustible system on its own, if the boundary conditions are in an appropriate range. This latter process is called autoignition or thermal explosion and has been dealt with in Section 5.1 of this AGARDograph. Ignition is the beginning of every combustion process. Hence it must be handled effectively when a controlled combustion process is to be initiated, and it must be prevented reliably if accidental fires and explosions are to be avoided. This process is also important in laboratory type investigations either to look into the ignition process itself, or else to classify the sensitivity of propellants with respect to planned or accidental ignition stimuli, to classify additives, or to assess the influence of external parameters. Concepts such as minimum ignition energy or ignition temperatures have been introduced in this manner, notions which have certain merits in spite of the fact that their

meaning is equivocal and that boundary conditions are important, which usually is ignored when applying the data to other situations.

Solid propellant ignition is both a process and the successful completion of that process. As a propellant sample is externally heated, there is an increase in the surface temperature and a build up of a thermal profile. When gasification of the sample begins, the gaseous products begin to react exothermically. This heat release increases the gas temperature, and thus, the reaction rates. With additional heating and accumulation of gas phase species the flame will "snap back" to the propellant surface. At this point, the flame provides sufficient energy for propellant pyrolysis, the external heat source is no longer necessary, and ignition is complete. These processes are graphically illustrated in the general log flux-log time, ignition plot shown in Fig. 43.

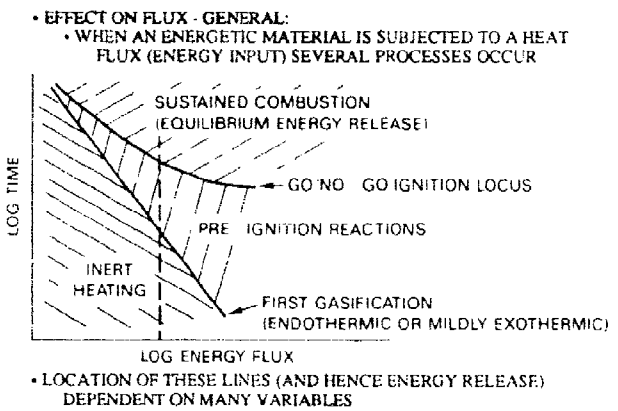

Fig. 43. General Depiction of Ignition Process.

For a given energy level (the dotted line in Fig. 43) a series of events are shown at various times over which the sample is subject to the flux. For some initial time, nothing appears to be happening. If the energy flux is terminated during this time and the sample examined, no significant decomposition of the exposed surface is seen. Figure 44 shows a sample of a high energy propellant containing nitramine which was subjected to 200 cal/cm^{2}sec for a time just prior to first gasification (evidenced by "first light" detected by a photodiode). No significant reaction has occurred but a thermal profile is being established within the solid. It is not until the "first gasification" time is achieved that the sample starts to significantly decompose. The flux has established and deepened the thermal profile in the solid until a surface temperature is reached that causes significant ablation/decomposition at the surface. For exposures slightly longer than the time necessary for this initial gasification, the sample continues to gasify but does not ignite in the classic sense of ignition. That is, if the external energy flux is removed, the sample will cease gasifying, the temperature profile in the solid will collapse, and the sample will not combust. Figure 44b is a sample subjected to 200 cal/cm^{2}sec at a time just after first gasification (as evidenced by "first light") and shows some decomposition of the surface, while Fig. 44c shows another sample at 200 cal/cm^{2}sec and a time just less than that required for "go/no-go" ignition. This sample shows significant decomposition. Ignition is not achieved until the conditions of flux-time associated with the line indicated as "go/no-go ignition" on Fig. 43 have been achieved. At this time, and for longer exposure times, the sample is ignited in the sense that if the external energy flux is removed, the sample will continue to burn by itself without the external stimulus (Boggs, et al, 1984). There is another region of "overdriven" combustion--higher fluxes and steeper thermal profiles, where removal of the flux will also cause the sample to extinguish (Ohlemiller, et al, 1972).

Exposing a solid propellant to high energy levels may not be sufficient to initiate combustion. The pre-ignition region is important in that it is in this region that the solid has gasified into reactive intermediate species (pyrolysis products), but these intermediate species have not reacted to final products; thus self-sustained combustion has not been attained. Unfortunately, many investigators view propellant ignition as simply a switch based on a critical temperature associated with the surface temperature of the solid. When satisfied, an instantaneous change is made from a non-reacting inert solid to burning at steady-state with fully reacted gases. While this criteria may be useful in some cases of ammonium perchlorate-rubber propellants where the samples ignite almost immediately upon vaporization, it does not match reality for all solid propellants and test conditions (Boggs, et al, 1986). In general, AP-based propellants tested at low flux levels and high ambient pressures show little or no detectable difference between go/no-go and first light/first gasification. Nitramine based propellants under similar conditions, display significant pre-ignition behavior (Boggs, et al, 1984). Pre-ignition behavior can be demonstrated in the AP-based propellants by increasing the flux level and decreasing the test pressure (Crump, et al, 1984).

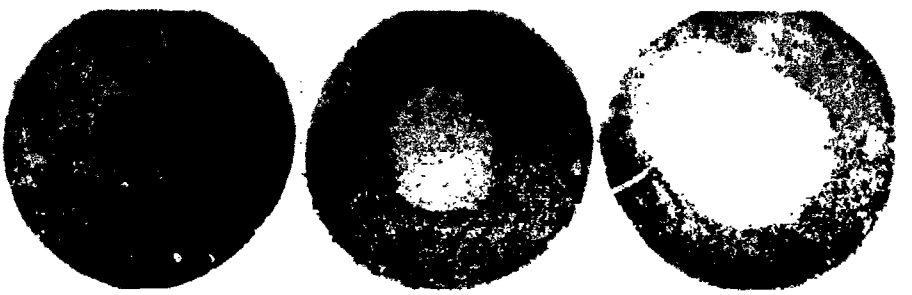

(a) (b) (c)

Fig. 44. Nitramine Containing Propellant Exposed to 200 cal/cm^{2}sec at (a) Prior to First Light/Gasification, (b) Just After First Light/Gasification, and (c) At a Time Preceding Go/No-Go or Complete Ignition.

Figure 43 is a generalized depiction of the ignition process. It defines three regions separated by two lines:

Inert heating region
First gasification line
Pre-ignition region
Go/no-go ignition curve
Self-sustained combustion region

The location of these lines and their relationship to the described regions is dependent on many variables. Propellant formulation, external energy level, and test pressure all contribute to the time relationship between the establishment of the thermal profile and self-sustained combustion.

The process of ignition and the ensuing combustion proceeds via a complex system of elementary reactions involving many radical species. A full theoretical description of the combustion process must describe the variation in space and time of all the molecular species involved. This may be done by formulating and solving the conservation equations of mass, momentum, energy and of all the species occurring for multicomponent, reactive flows, which in most practical cases are even turbulent. The theory of combustion phenomena, hence, is based upon chemical thermodynamics, chemical kinetics, transport processes, and fluid dynamics. The reader, who wants to familiarize himself with this field should consult the pertinent literature (e.g., Lewis and von Elbe, 1951; Mullins and Penner, 1959; Glassman, 1977; Williams, 1985; and Kuo, 1986). It is evident that even with the largest computing facilities available these problems become easily untractable, particularly if heterogeneous propellants are to be considered. Even if numerical solutions are used drastic simplifications are necessary and even more so when closed form solutions are desired.

Concerning the process of ignition the state of the art is such that valuable information may still be gathered if considerably simplified systems are investigated. One example being the replacement of the complex chemical kinetics by a one-step exothermic reaction with an Arrhenius approximation for the overall reaction rate. The ignition process is effectively considered then as a momentary imbalance between energy production over energy loss. Even in this case the ignition process remains complex since flow, transport, and reaction processes must be followed in the different phases (solid, liquid, and gas), and the space and time dependence of a considerable number of dependent variables (temperature, pressure, flow velocity, and concentrations of fuel, oxidizer and products) must be determined, taking into account the respective fluxes on the boundaries limiting the different phases. Of course, further simplifications may be introduced, e.g., limiting the reactions to the solid phase and neglecting fuel consumption. Valuable information has been gathered in this manner.

The progress has been surveyed in various review articles which have appeared at steady intervals and the interested reader is urged to have a look at these (Kuo, 1986; Merzhanov and Averson, 1971, Price, et al, 1966; Kulkarni, et al, 1984 and 1980; Hermance, 1984; and Williams, 1981). Also the respective chapters of the books by Williams (1985) and by Kuo (1986) give a good introduction into the problems encountered in dealing with ignition, the methods of solution available and the information obtained in this manner.

Price has introduced a classification according to whether the reactions proceed in the solid, or in the gas phase, or heterogeneously on the boundary between both phases (Price, et al, 1966). In his review paper, published recently, Hermance compares the results obtained in this manner, and he comes to the conclusion that gas phase reactions appear to be of major importance in the ignition of

accounted for by the more simple models, but e.g. the effect of pressure and composition of the gas phase can only be described correctly if gas phase reactions are taken into account. More recently investigations have been performed simultaneously taking into account all the above described features (Adomeit and Hocks, 1982; Bradley, 1975; Birk and Caveny, 1980 and 1983; Lengelle, 1975; and Kumar, et al, 1984).

The time as an independent variable may be eliminated if limiting conditions of ignition are considered. In this case, only the steady state equations need to be solved. In this manner it is found that under certain boundary conditions, i.e. for certain ranges of values of pressure, flow velocity, and flow temperature either a nonreacting state, or a state with fully ignited combustion, or both simultaneously may exist. The points of transition between these three regions denotes respectively the points of ignition and quenching of the system when the above listed variables are varied (Adomeit and Hocks, 1982). Another well known example is the process of autoignition. The dependence of critical dimensions upon temperature of the surroundings may be determined in this manner (Merzhanov and Averson, 1971).

If the time history of the ignition is to be followed the time dependent balance equations must be solved. An important quantity, which may be used to characterize the temporal ignition behavior of the system, is the ignition delay. It may be defined as the time interval required for the system to reach the state of self-sustained deflagration counted from the moment when the ignition stimulus is imposed. Though being conceptually clear the definition is usually of little use for experimental investigations as well as for theoretical ones. So in practice it is replaced by various other definitions which Kuo has classified (Kuo, 1986; and Kularni, et al, 1982 and 1980).

One concept which has been applied frequently, is that of thermal runaway. If a combustible substance is ignited, e.g. by contact with a hot body, the material is heated by heat transfer from the hot body. In the initial phase the temperature profile in the combustion material is essentially determined by the heat conduction process. Only when the gradient of the temperature profile close to the surface has become sufficiently small the exothermic reaction becomes important. if the temperature is registered at some location close to the surface as a function of time this behavior can be followed. Initially the rate of temperature increase, determined by heat conduction, slows down with time and only when the reaction becomes important it accelerates and thermal runaway sets in. If a precise definition of ignition delay is desired, this becomes difficult again. Only for the particular case of simplified analysis, where the reactant consumption is neglected and the Arrhenius law for the rate term has been expanded making use of the fact that the activation energy is large, the temperature of the system goes indeed to infinity. The amount where this occurs is clearly defined. For more detailed models the definition of ignition delay has to resort to other concepts (Kuo, 1986; and Kulkarni, et al, 1982 and 1980). Fortunately there are many systems, where this difficulty appears to be of minor importance, as is discussed, e.g. in Williams, 1985; Kuo, 1986; and Kulkarni, et al, 1982 and 1980).

The source of ignition of a propellant is generally a source of energy and the forms of energy may vary. They can be thermal, chemical, mechanical, electrostatic, electromagnetic. If thermal energy is supplied to the propellant, e.g. by heat transfer from a hot gas flowing along the surface, or by contact with a hot body, the energy is evenly distributed over all internal degrees of freedom of the substance. It is this case where the assumption of a one-step exothermic reaction with an Arrhenius approximation for the global reaction rate may well be appropriate. If the energy is supplied in a different form the situation becomes more complicated. Chemical energy may be supplied in the form of radicals or by hypergolic reactants, which react even at room temperatures with the fuel. To deal with this situation the balance equations must be formulated taking into account a sufficiently complete set of kinetic equations. The same holds when electrostatic or electromagnetic energy is introduced in form of electrons, ions, or radiation. It may, of course, happen that these forms of energy equilibrate rapidly over all internal degrees of freedom and become effective as a source of ignition only afterwards. This, for example, is quite generally assumed when the ignition of a combustible gas mixture by an electric spark is considered.

In practical ignition systems the thermal energy prevails. In those cases, where this does not hold, it frequently is assumed that the energy is dissipated into thermal energy which then induces ignition. To enumerate the most important systems, hot surfaces and particles, electrically heated wires and layers, hot gases flowing across the propellant surface, radiant energy, ignition flames, pyrotechnic igniters and electrical sparks and discharges should be mentioned. Laboratory systems also include shock tubes, lasers, arc image devices and impact testers. Hazard situations may arise due to ignition by external fire, penetrating objects or friction effects. This enumeration should make clear that the ignition process does not only depend upon the properties and the physical state of the propellant to be ignited and certain global quantities of the igniter, e.g. the amount of energy added in ignition, but that the initial and boundary conditions of the whole system considered and the type of ignition stimulus applied, i.e. the kind of energy added and its spatial and temporal distribution, play an important role. Of course, concepts like balance between heat loss and heat produced by the combustion reaction, thermal runaway, and minimum ignition energy have shown to be valuable tools in describing and

understanding ignition processes. But for a reasonably complex system usually little can be done falling short of solving a sufficiently complete set of balance equations taking due account of the boundary conditions of the system to be ignited and of the ignition stimulus considered. This is the reason why the following classification of ignition processes appears to be unavoidable.

To avoid some of the difficulties encountered in this manner, test facilities have been designed and are in use in various laboratories to assess ignition properties of propellants, their sensitivity to additives temperature, pressure, etc., and also the effectivity of certain ignition sources. The results obtained in this manner are certainly very interesting and of value by themselves. If they are to be applied, however, to situations differing considerably from those investigated it must be expected that unexpected deviations occur, which can only be assessed on closer scrutiny. The reader interested in these facilities should consult the respective sections of the AGARDograph.

The classification of ignition chosen in the following is based upon the mode of energy transfer and the type of energy added. This fact, of course, reflected itself in the pertinent types of experiment and the form of balance equations and boundary conditions needed to obtain the solution.

Since the systems differ considerably and the results cannot be lumped together in a simple fashion, certain illustrative examples are described more fully. In the review literature and the monographs on combustion various other examples have been discussed in detail. They should be consulted if further information is needed (Lewis and von Elbe, 1951; Mullins and Penner, 1959; Glassman, 1977; Williams, 1985; Kuo, 1986; Merzhanov and Averson, 1971; Price, et al, 1966; Kulkarni, et al, 1984 and 1980; Hermance, 1984; and Williams, 1981).

5.2.2. Ignition by Constant Energy Flux

This is a standard problem of ignition and it has served as a basis for developing approximate solutions to the transient ignition processes. Its basic version consists of a semi-infinite solid. A constant energy flux is absorbed at the surface and transported by heat conduction inside the body. An exothermic reaction, proceeding inside the body, may lead then to ignition. The energy flux is started at zero time and lasts for a given interval or up to infinity. This problem has been investigated theoretically in a detailed manner, comparing numerical solutions with asymptotic approximations of different complexity (Linan and Williams, 1971). The results have been published in various papers, but their essential features are also described in the above mentioned monographs and reviews (Williams, 1985; Kuo, 1986; Kulkarni, et al, 1984 and 1980; Hermance, 1984; and Williams, 1981).

The process of constant energy flux absorbed at a surface is not easily accomplished experimentally. The transfer of radiant energy by arc image or laser irradiation is the method which has been applied most frequently. This radiation is absorbed in a surface layer of the propellant, the thickness of which depends upon the constitution of the surface and of the propellant, and the frequency of the irradiation. The essential results have been compiled in the references mentioned above (Kuo, 1986; Kulkarni, et al, 1984 and 1980; and Hermance, 1984). More recently various complications of this process have been discussed. Strakovskii (1985) points out that propellants and explosives may be transparent to certain frequencies of electromagnetic radiation. In this case the absorption by inhomogenities and inclusions becomes important, leading to hot spots inside the body, and inducing ignition of the type described in Section 5.2.5 of this AGARDograph. For this reason arc image samples are usually coated with materials like ZrC to absorb the visible radiation at the surface rather than in depth. CO_2 lasers are often used because at 10.6 mm wavelength most propellants are opaque. Recent findings indicate that gas phase reactions must also be included if all observed trends are to be explained (Kumar, 1983).

A radiant energy source is used for ignition testing because of the ease of controlling and reproducing the energy flux and the exposure time and because a majority of the energy is absorbed at the propellant surface or at a coating on the propellant surface.

A schematic of a xenon arc image furnace ignition system is shown in Fig. 45. A xenon arc lamp is focused via mirrors to a primary and secondary focus. The propellant sample is mounted in the combustion chamber with its surface located very close to the secondary focus. The xenon light enters the combustion chamber through a 3-inch diameter quartz window. Normally-open and normally-closed iris leaf shutters are located at the primary focus. The shutters (open/close) are controlled with an event sequencer. The length of sample exposure is determined by a photodiode located near the combustion chamber on the system axis, viewing the shutter assembly. A light sensing photodiode, located so that the optical axis is aligned parallel with and approximately 1/16-inch above the sample surface and looks across the center of the sample, is used to detect first gasification/first light (Hightower, 1967). Maximum working radiant energy level achieved on this instrument is 100 cal/cm^{2}sec.

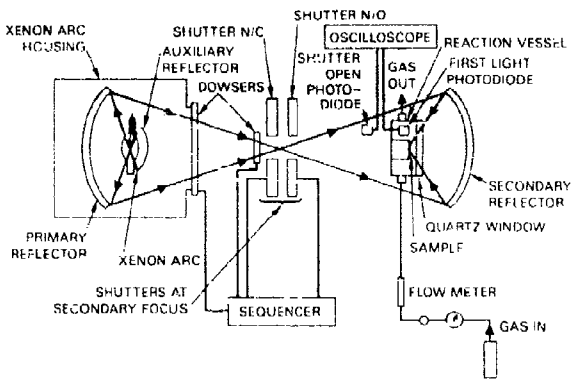

Fig. 45. Schematic of Xenon Arc Image Ignition System.

Further examination of Fig. 45 reveals a highly divergent incidence angle for the radiant energy delivered to the sample surface. To accommodate this highly divergent beam, a large diameter (3-inch) quartz window is needed in the combustion vessel. This large, unsupported diameter limits the working pressure of the vessel to 250 psia. As the propellant sample surface regresses due to pyrolysis, the amount of energy delivered to the surface of the propellant being tested changes.

A schematic drawing of a CO_2 laser ignition system is seen in Fig. 46. This system is composed of the energy source, external electronics, and ignition apparatus. The energy source consists of a Photon Sources Model 300 CO_2 laser. The laser is average rated at 450 watts. The wavelength of the laser is 10.6 μm. The external electronics provide pulse control and record test data. The ignition apparatus contains the combustion chamber with sample holder, lens system, and chopper wheel. Laser light passes through a long focal length lens system to decrease overall beam diameter. The chopper, located at the focal point of the lens system, provides a square energy pulse. The laser beam enters the combustion chamber through a ZnSe window and strikes the propellant surface. First light/gasification is determined as described for the xenon arc image furnace. Output from the oscilloscope includes length of laser pulse, first light photodiode, and calorimeter output. Electronically gated pulsing coupled with the external chopper wheel rotation, control sample exposure time. The minimum working radiant energy currently being used on this system is 50 cal/cm^{2}sec. Currently the laser will not operate in a stable mode at lower energy levels. The maximum energy currently being used on the laser system is 200 cal/cm^{2}sec--well below the maximum energy output of the laser system.

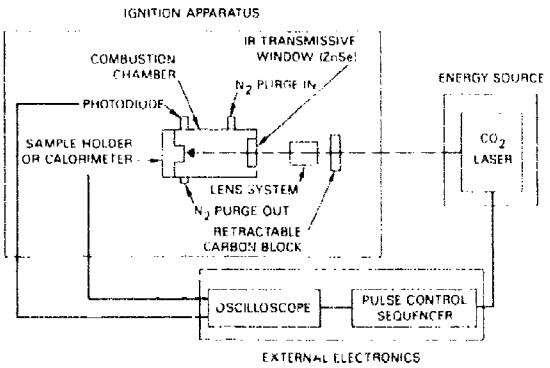

Fig. 46 Laser Ignition Schematic.

While efforts have been made to keep the CO_2 laser and xenon arc systems as similar as possible, two fundamental differences remain that should be noted: (1) the wavelengths of the incident radiation and (2) rise time of the radiation impinging the sample.

The spectral distribution of energy radiated from the arc is broad band. Most of the energy lies between 0.3 and 1.1 μm with several peaks in the near infrared between 0.8 and 1.0 μm (Hightower,

1967). Radiant energy from the CO_2 laser is monochromatic with the energy being randomly polarized at 10.6 μm.

Ideally, the radiant sample exposure time should be an instantaneous step function; practically, this cannot be achieved. Arc image sample exposure time is mechanically controlled by two iris leaf shutters. The arc image shutter "opening" function currently averages about 3.5 msec and is being mathematically described by a sine function.

The timing mechanism on the laser system also experiences, albeit shorter, a measurable rise time for the incident radiation to reach the propellant surface. A rotating chopper system was installed in the laser system to remove non-uniformities in the leading edge of the laser pulse. A two-tine 90% transmission aluminum wheel rotates and chops the laser beam at the focal point of the lens system. A photo transistor monitors the wheel position, triggers the laser on and starts a timer when the wheel eclipses the laser beam. The timer turns the laser off after a controllable interval, and the width of the laser pulse is equal to the delay between the wheel in eclipsing the beam and the timer shutting off the laser (Zurn and Atwood, 1981). A chopper wheel delay of 3.2 msec was used for these tests. The rise time of the laser system currently averages 130 msec and can be mathematically described by a versine function. As the chopper blade exposes the laser beam, the energy quickly builds to a maximum.

The radiant energy level for both systems is calibrated with an asymptotic calorimeter located in the propellant sample position in the combustion chamber. An effective flux level can be determined to account for the "opening" function of either instrument.

A series of ignition tests is run at each energy level and pressure. Once the general ignition region has been established, a go/no-go scheme is run using equally spaced exposure times in an up-and-down procedure of testing. Fifteen to 17 individual tests are usually run at each energy level to establish each go/no-go point. first light, or the point of detectable first gasification is an average of the measured photodiode output of each ignitability test.

Arc image propellant samples are coated with ZrC powder to provide a more uniform absorptivity for arc image propellant ignition test samples (Fleming and Derr, 1975). Variations in absorptivity are introduced by the nature of the ingredients in a given formulation. Sample coatings of ZrC are employed in the laser system as well, to maintain sample uniformity between the instruments. It has been found that the presence of the ZrC coating enhances the first light/gasification signal.

Typical Results

The effects of flux, depicted earlier in a general fashion, and of pressure are shown in Fig. 47 for a predominantly ammonium perchlorate-HTPB binder propellant. The effect of flux is clearly seen for the first gasification line and the various go/no-go lines. The region of pre-ignition reactions discussed earlier (the difference between first gasification and go/no-go lines) is clearly evident for the 50 psia case, as is the diminishment of the pre-ignition region with pressure increase to 100 and 200 psia.

Similar behavior, but with even more pronounced pre-ignition behavior, is shown in Fig. 48, the ignition map for a cast modified double base.

Similar ignition plots for an ammonium perchlorate-aluminum-HTPB propellant is shown in Fig. 49. Note in the figure that the low pressure go/no-go curve is for 1 atm (not 50 psia as in the previous plots). The reduced pre-ignition region for metallized ammonium perchlorate based systems is further illustrated in Fig. 50; the ignition map for a propellant with a high percentage of solid ingredients ammonium perchlorate-aluminum-HTPB system. The effect of composition is further illustrated in Fig. 51 where the ignition maps for a modified cast double base propellant and an ammonium perchlorate-aluminum propellant ignited at 100 psia are plotted. The pre-ignition region is much less for the AP based propellant.

The implications of the pre-ignition region on deflagration to detonation transition and other transient combustion related hazards has been discussed in Boggs, et al (1982), Price and Boggs (1983), and Isler (1988).

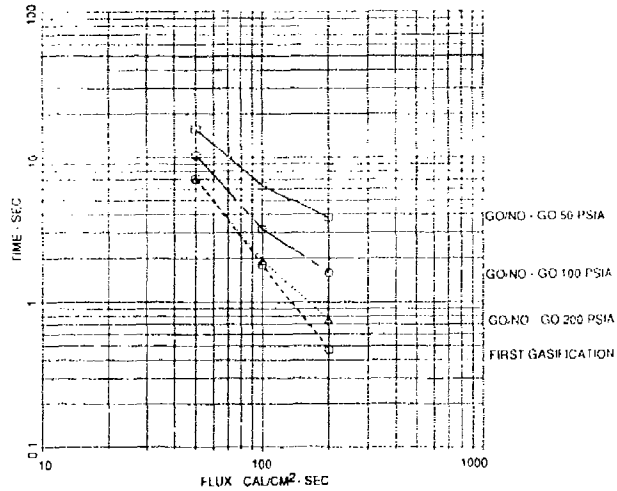

Fig. 47. Effect of Flux and Pressure on Ignition of Ammonium Perchlorate-HTPB Propellant.

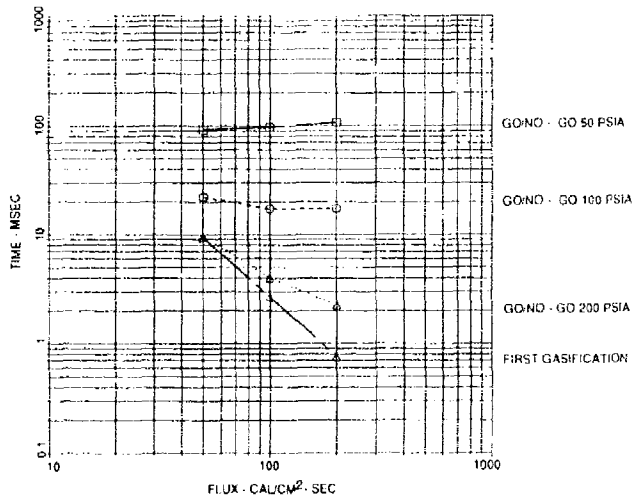

Fig. 48. Effect of Flux and Pressure on Ignition of Cast Double Base Propellant.

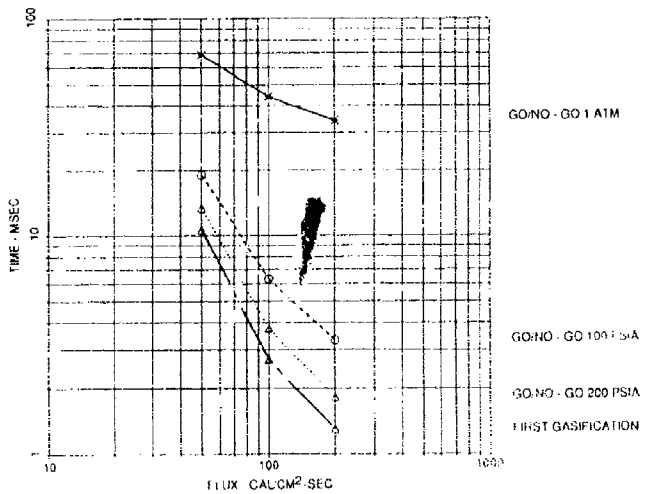

Fig. 49. Effect of Flux and Pressure on Ignition of Ammonium Perchlorate-Aluminum-HTPB Propellant.

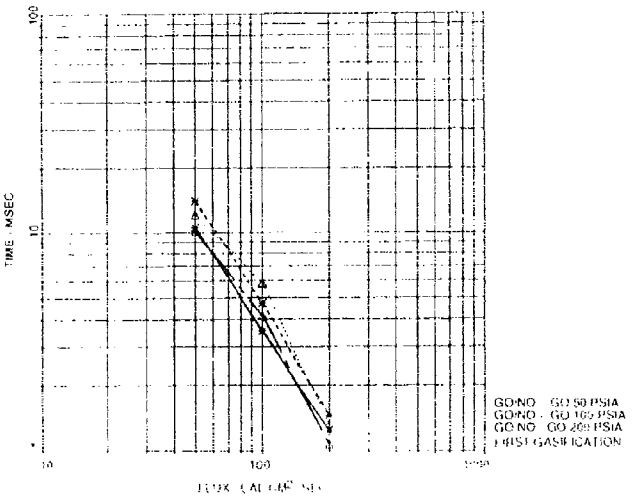

Fig. 50. Ignition map of Highly Loaded AP-Al-HTPB Propellant at 1 atm(*) and 100 psi (Δ). The bottom line of each pair is the first gasification; the upper curve is the go/no-go ignition locus.

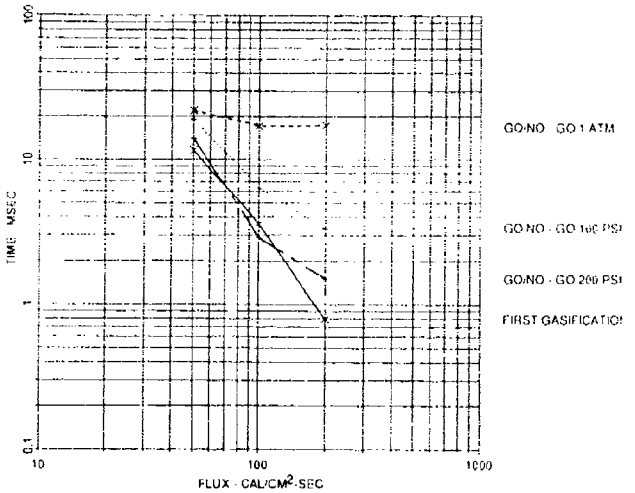

Fig. 51. Comparison of Ignition of Cast Double Base (x) with AP Composite Propellant (+) at 100 psi. The bottom line of each pair is the first gasification; the upper curve is the go/no-go ignition locus.

5.2.3. Ignition by Convective Heat Transfer

If a propellant surface is subjected to the cross flow of hot gases, it is heated and may ignite. This process is of considerable practical relevance and is realized in many ignition systems, e.g. ignition by a pyrotechnical igniter, by a pilot flame, by the hot gases of an accidental fire or in the laboratory by the flow across a propellant surface induced inside a shock tube. Since this process is also of basic importance, it will be discussed in some detail. The most simple case is that of a stagnation point flow of a hot inert gas impinging upon a propellant surface. Figure 52 gives a schematic representation of the system considered. The flow of the hot gases impinges perpendicular to the propellant surfaces located at y = 0 and is directed in Fig. 52 opposite to the y-axis. The propellant is heated by heat transfer and decomposes according to the reaction

$$\text{solid} \rightarrow A_1 + A_2 \tag{5.17}$$

with a rate law

$$\dot{m} = \rho_s B_s T_w^{\,m} \exp(-E_s/RT_w) \tag{5.18}$$

The initial products A_1 and A_2 are further heated by mixing (diffusing) with each other convectively with the approach flow and react exothermically according to the rate law

$$r = B\left(\frac{\rho\, YA_1}{M_1}\right)\left(\frac{\rho\, YA_2}{M_2}\right)T^n \exp(-E/RT) \tag{5.19}$$

to form the product species B_1 and B_2

$$A_1 + A_2 \rightarrow B_1 + B_2. \tag{5.20}$$

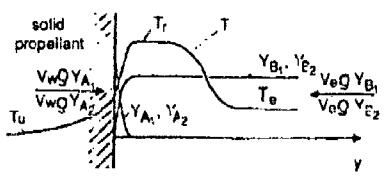

Fig. 52 Stagnation Point Region of Monopropellant Surface Burning in Inert Gas Crossflow.

The transport processes occurring are described by the heat conduction equation inside the solid and by the boundary layer balance equations in the stagnation point flow field. they take the following form (Adomeit and Hocks, 1982) for

mass

$$\frac{dV}{d\eta} + f\eta = 0, \tag{5.21}$$

momentum

$$2Vf_{\eta\eta} - (1f_{\eta\eta})_\eta - (\rho_e/\rho - f_\eta^2) = 0, \tag{5.22}$$

energy

$$2V\theta_\eta - \frac{1}{c_p}\left(\frac{c_p\rho}{Pr}\theta_\eta\right)_\eta + \sum_{i=1}^{N} W_i h_i/c_p T_r = 0 \tag{5.23}$$

species i

$$2VY_{i\eta} + J_{i\eta} - W_i = 0. \tag{5.24}$$

Here V denotes the velocity perpendicular to the surface, η is the dimensionless boundary layer coordinate perpendicular to the surface, f is the stream function, ($f_\eta = df/d_\eta = u$ is the velocity parallel to the surface), θ is the dimensionless temperature, Y_i the relative mass fraction of species i. The terms in the energy equation represent, in the order as listed, the convective transport, the heat conduction, the energy transport by diffusion of the different species and the thermal energy liberated by the gas phase reaction.

These steady state equations have been solved in closed form for the limiting cases of infinitely fast and frozen gas phase reactions, and numerically for the general case of finite reaction rate (Adomeit and Hocks, 1982). Taking the kinetic and caloric data of ammonium perchlorate the results shown in Fig. 53 have been obtained. In this figure the dependence of the combustion rate $\dot{m}$ upon the free flow velocity (here represented by the velocity gradient a) is shown for a free flow temperature of T_e = 805 K. The curve displayed in the center refers to the general case of finite gas phase reaction, which is of interest here. It possesses the shape of an "S", which is characteristic of systems which may be ignited. One sees that at low free flow velocities (at this elevated free flow temperature of T_e = 805 K) a solution with a high value of burning rate $\dot{m}$ is established. Increasing the flow velocity, i.e. increasing a, the solution shifts to the right passing through the points A_1 and A_2, and in Q the solution jumps from the upper branch to the lower one with a considerably reduced rate of mass ablation rate $\dot{m}$. In the point Q, hence, the combustion process is quenched. If now the velocity is decreased the solution moves initially along the lower branch with a low rate of $\dot{m}$. In the point I it jumps again to the upper branch with high combustion rate $\dot{m}$, the system ignites.

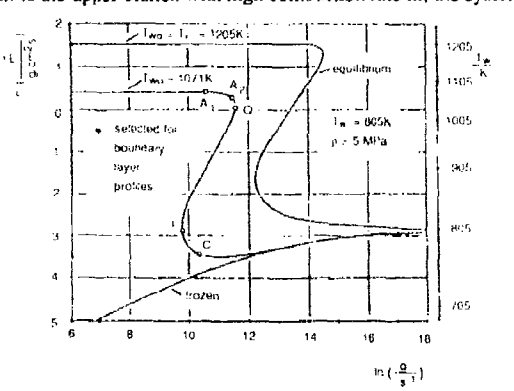

Fig. 53. Dependence of Burning Rate Upon Velocity Gradient: Closed-Form Limiting Solutions, Numerical Solution for ρ = 5 MPa.

That in the points I and Q indeed the homogeneous gas phase reaction is ignited respectively quenched becomes clear if one looks at the temperature and reaction rate profiles inside the gas phase boundary layer shown in Fig. 54 and Fig. 55 for the different states of the system denoted by A_1, A_2, Q, I and C in Fig. 53. Various features are noteworthy. Comparison of curves I and C shows that at the point of ignition the temperature distribution differs only slightly from the convection controlled profile C and the rate of homogeneous reaction at the point of ignition is still at a very low level.

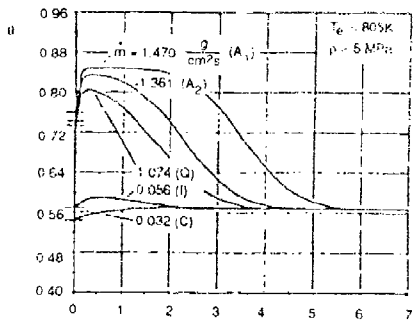

Fig.54. Boundary-Layer Profile of Temperature.

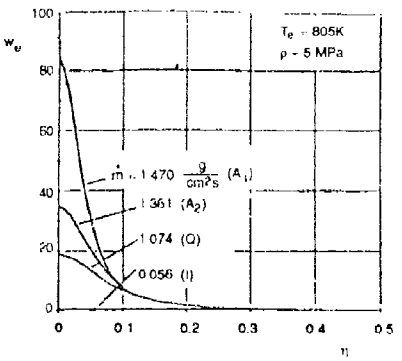

Fig.55. Boundary-Layer Profile of Rate of Gas-Phase Reaction.

Curves A_1 and A_2 denote fully ignited states, where the premixed flame is stabilized in front of the body. The temperature θ reaches its maximum value at a location of η of about $\eta = 0.3$. In the point of quenching (curves Q) the temperature has decreased but not that much as might have been supposed. The size of the gap between the limiting states I and Q is quite considerable. It depends upon the free flow temperature Te and becomes smaller with increasing values of T_e, as may be gathered from Fig. 56, where the burning rate $\dot{m}$ is plotted versus the velocity gradient a for various values of the free flow temperature T_e. The quench and ignition limits are shown as dotted curves. Eliminating $\dot{m}$ from the lower dotted line the critical condition of ignition $T_{e,i} = T_{e,i}(a)$ is obtained, which gives the free flow temperature Te needed for ignition in dependence upon the velocity gradient a, i.e. as function of the velocity of the free flow v_e.

It is also interesting to note that for higher values of T_e the combustion rate curves $\dot{m} = \dot{m}(a)$ lose their "S" shape character, the transition between low and high values of $\dot{m}$ becomes continuous and points of ignition and quenching can no longer be defined. This fact is noteworthy in particular with respect to the discussion given above concerning the definition of the ignition delay, since in this region no "thermal runaway" will occur.

These results give a clear picture of the interaction between the flow with its characteristic parameters a, T_e and p, the exothermic combustion reaction proceeding in the gas phase, and the decomposition of the propellant at the surface. That the gas phase processes are indeed responsible for the ignition of propellants by convective heat transfer has also been established experimentally by ignition experiments performed in shock tubes (Birk and Caveny, 1980).

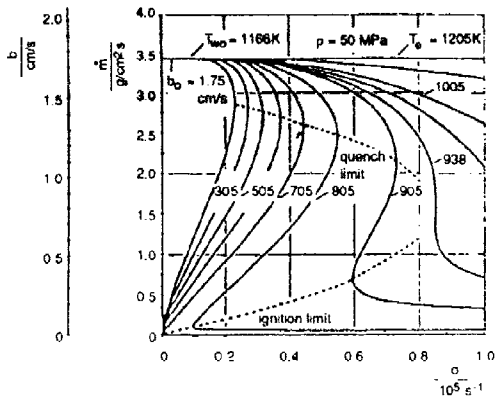

Fig. 56. Burning Rate Dependence Upon Velocity Gradient.

5.2.4. Ignition by Hot Surfaces, Layers and Particles

This is an important group of ignition stimuli present in many practical systems. Hot particles form part of the multiphase flow issuing from a pyrotechnic igniter and appear to contribute significantly to the ignition of solid rocket fuels and gun propellants. They may act as single particles, but also the formation of a layer is conceivable when their number is large or when condensation occurs at the propellant surface.

Also in hazard situations hot surfaces in contact with propellants may act as sources of ignition, the primary energy being provided thermally or also by friction. Furthermore ignition devices have been designed consisting of wires or metallic films, which are heated by electric discharge and serve as sources of ignition. Also the "Thermal Step-Test" belongs to this group (see Section 5.1.5). This latter has been used to determine the ignition characteristics of propellants (Schrader, et al, 1984). In this test a small steel tube filled with the explosive is heated in a very short time interval by a capacitor discharge. The induction time which is the time lapse between the heating pulse and the moment when the tube is ruptured, is measured as a function of tube temperature. Induction times as short as 50 ms have been measured at temperatures up to 1400 K.

A theoretical treatment of the related problem of ignition of a reactive solid exposed to a step in the surface temperature has been given by Linan and Williams (1979). The results obtained make use of an asymptotic expansion and agree with numerical results if the activation energy is sufficiently large. The model considered assumes heat conduction and an exothermic reaction inside the solid. Gas phase reactions are neglected.

To overcome the ensuing limitations, Adomeit and coworkers have investigated the case of a hot solid layer of thickness d brought into contact with a propellant surface. The propellant is heated by conduction and pyrolizes according to Equations (5.17) and (5.18) given above. The gases evolved form a gas layer between the propellant surface and the heating solid, reducing the heat flux to the propellant. At the time the temperature of the hot solid layer decreases due to heat conduction. Inside the gaseous gap the exothermic gas phase reaction described by Equations (5.18) and (5.19) may induce ignition, which occurs as soon as the gap width reaches a sufficient size under the condition that the temperature of the heating solid is still high enough. This problem has been investigated by solving the pertinent nonsteady state balance equations numerically, neglecting fuel consumption, which is justified in many cases up to the moment of ignition. Some of the results are represented in Figs. 57 through 59. Figure 57 shows the ignition delay t_i in dependence upon the initial temperature T_O of the hot solid layer. Parameters are the thickness of the solid layer d and the pressure imposed. Kinetic data of a typical mono-propellant have been used. The igniting layer was assumed to consist of B_2O_3. The solid curves give the dependence of ignition delay $t_i = t_i(T_O,P)$ for infinite thickness of the layer. As expected, with increasing temperature T_O, the ignition delay decreases rapidly. For finite thickness d the dashed curves are obtained which below a certain temperature deviate from the ignition delay obtained for infinite thickness. It is also interesting to note that these curves, obtained for finite thickness, terminate at certain values of temperature and ignition delay. Below this temperature ignition cannot be effected anymore.

The minimum ignition temperatures $T_{i,min}$ belonging to these terminal points have been plotted in their dependence upon the thickness of the solid layer d in Fig. 58 for copper and boron oxide as the heating materials. It is seen that the temperature just leading to ignition may be lower for copper. The

energy contained under these conditions in this layer, which is a kind of a "minimum ignition energy," is plotted in Fig. 59 again versus the layer thickness d. Whereas the minimum temperature required for ignition decreases with the layer thickness, the energy stored in the layer increases. Qualitatively similar results have been obtained for hot spherical particles (Adomeit et al 1987).

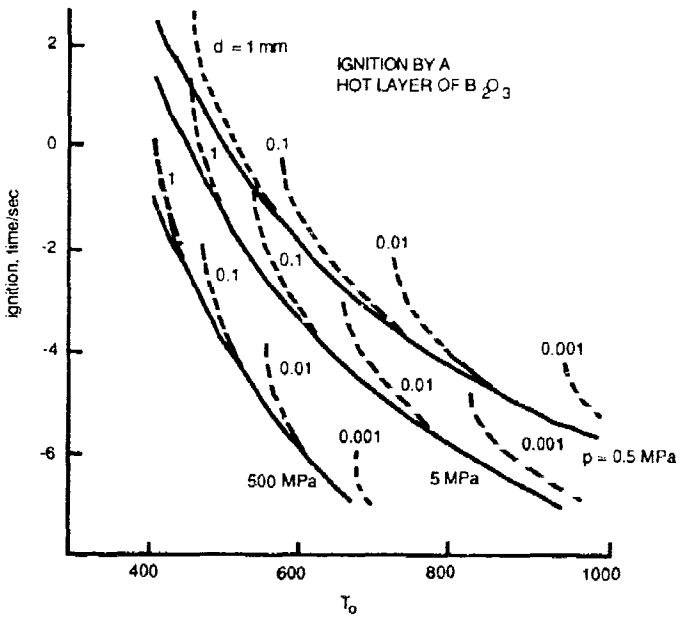

Fig. 57. Ignition Delay t_i of Propellant vs Initial Temperature T_0 of Layer of B_2O_3. d is the Layer Thickness.

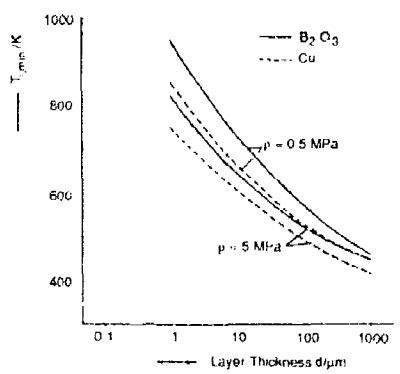

Fig. 58. Minimum Value of Initial Layer Temperature Needed for Ignition in Dependence Upon d. Layer Material: Copper and B_2O_3.

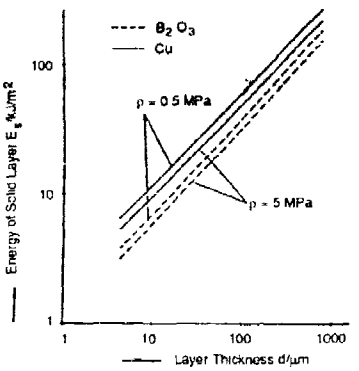

Fig. 59. Energies Contained in the Solid Layer Per Unit Area Under the Conditions Given in Fig. 60.

5.2.5. Ignition by Impact, Friction, and Fracture

The ignition by impact and friction is certainly an important mode of ignition under hazard conditions. The processes involved are complex and since the relevance of these concerning regular ignition is limited, only partial progress has been made in the understanding in these processes. In the following, recently performed investigations are described which should be consulted if detailed information on the topics considered is needed.

Impact

Although some researchers point out that tribochemical or molecular fracture mechanisms may be responsible under certain conditions for an ignition by impact it appears to be generally accepted that in most cases the initiation is thermal in origin. The compression and adiabatic heating of gas bubbles has been put forward as a possible source of ignition by various workers, whereas it was rejected by others. Other mechanisms proposed are heating by viscous flow between impacting surfaces or between grains, friction between surfaces or grains of the material in relative motion, or localized adiabatic deformation in regions of mechanical failure.

Swallow and Field (1982) impacted samples of explosives with a falling weight-investigating the effect of added particles to the explosive samples. Whereas Bowdon and Gurton (1949) have shown that for hard, high-melting point particles the "hot-spot" temperature is usually controlled by the melting point of particles, Swallow and Field (1982) have found that also relatively soft, low-melting-point polymers can sensitize samples of explosives. Polymers that sensitize appear to be those that fail catastrophically either by fracture or localized adiabatic shear bands and that possess low values of specific heat, of latent heat and of thermal conductivity. As has been shown by infrared radiation measurements the temperature of the hot spots produced during rapid deformation can greatly exceed the polymer's softening point (Swallow and Field, 1982). The authors have also shown that it is possible to successfully predict whether or not a polymer will sensitize an explosive by examining its mechanical and thermal properties. In a series of experiments Andersen and coworkers (Anderson and Louie, 1979; Anderson, et al, 1979; and Anderson and Stillman, 1983) investigated the ignition of propellants by projectile impact varying the impact velocity, the mass and the dimensions of the projectiles and the composition and structure of the propellants. It was found that above a certain ignition threshold deflagration is initiated. If the impact velocity is increased further, detonation is initiated. For small projectile diameters these two threshold curves merge, such that with projectiles of smaller diameter a deflagration cannot be established. For single, double and triple base propellants the same type of behavior was found (Bowden and Gurton, 1949).

An investigation of the effect of particle size and porosity for the same propellant, used in the work of Anderson and Louie (1979 is described in a third paper (Anderson and Stillman, 1983). The porosity sensitized the propellant to both deflagration and detonation at large projectile diameters, but the effect was relatively small. At small diameters the effect was negligible. The increase of particle size of HMX by a factor of 22 when it is imbedded in the polymethane binder has a very pronounced effect on sensitizing the propellant at all projectile diameters.

In another, theoretical paper Anderson (1980) postulates a model based on the formation of hot spots to explain some of the described experimental results. A more detailed theoretical investigation is performed by Dubovik and Lisanov (1985), who calculate the heat production rate inside shear

bands assumed to occur in impulsively loaded explosives and formulate in a global manner an ignition criterion, which appears to agree with experimental results.

Friction

As mentioned above friction is considered to be one of the possible causes of ignition by impact. This process has recently been investigated by Amosov, et al (1979), who consider a rough solid surface gliding over the surface of a propellant. If the pressure is not too high, the local area of the points of contact is only a small fraction of the nominal contact area. In this case the process of friction leads to a considerable rise of temperature at the actual points of contact while the temperature of the rest of the surface remains low. Amosov considers a strip of width d sliding under a pressure p and with a given velocity v over a propellant surface. The reaction leading to ignition is assumed to proceed initially only inside the solid propellant. The resulting boundary value problem is solved numerically giving the temperature distribution inside the propellant, with d, v, and p as parameters. An ignition criterion is derived taking into account the essential parameters of the problem, as velocity v, pressure p, activation energy E, thermal diffusivity a, and others.

These results were applied to the ignition of various types of propellants. Taking into account the hardness of these substances it turns out, that ignition would be achieved only for pressures where the contact surface becomes continuous and equal to the nominal area. Hence the considered mechanism of friction and ignition will not prevail for the usual soft propellant. The authors, however, maintain that an explosive with high melting point and high hardness, such as lead azide, may be ignited as described at isolated points of contact.

Gomez and Wake (1985) consider the case of a propellant sliding with friction across an inert surface assuming the heat produced to be a given constant. Taking into account a global exothermal reaction inside the solid they derive ignition criteria for different propellant slab configurations.

Fracture

In fracture, the initial chemical processes causing ignition take place in the solid phase. In substances consisting of one chemical component, crack propagation can rupture the molecular or intermolecular bonds (depending on the crystallite size). This rupture results in strong thermal effects on the tip of the crack and negligible electric and surface effects on the crack boundaries. For the interesting substances, exact data are not available. The energy liberated by a crack may be of the order of 1 kJ, the electric effects on the boundaries may be of the order of 1 MeV (10^{-12} J). Both data are given only to indicate the order of magnitude, not to discuss the values themselves or to the parameters on which they depend. The result of fracture effects was studied investigating single and multicrystals of high explosives. PETN, for example, shows local chemical decomposition, but no initiation of explosive reactions. Neat explosives are unsuitable as solid propellants; no direct observations of fracture effects concerning solid propellants have been reported, so it can not be said, how important are the discussed effects for solid propellants. In composite substances crack propagation normally divides the components. Neat substances including large crystallites or defined limited regions of material can be divided by a crack along the internal borderlines. In this case triboelectric effects on the boundaries may become important. Fracture can also induce gaseous electrical breakdown in the crack.

This electrical breakdown induced by mechanical fracture can be regarded as the inverse effects to the "electrically induced fracture". The current in the breakdown is of the order 1 mA, the energy may be of the order of 1 J. This energy is in a range, in which ignition by electric sparks can occur. Probably it is this effect which causes the ignition of composite propellants during fracture in the modified spigot-test described below.

In a sequence of publications Kumar, Kuo, et al (1980 and 1982) have investigated experimentally and theoretically a gas dynamic ignition phenomenon occurring in cracks and holes inside propellants. These researchers noticed that under rapid pressurization rates of about 10^4 MPa/s anomalous ignition occurred near the crack tip region. High-speed photography showed clearly that the tip of the crack ignites before the convective ignition front propagates from the crack entrance to the tip. Hence under this condition two flame fronts are observed, one propagating from the crack entrance and the other from the crack tip.

Further diagnostic experiments revealed that the initial luminous zone near the crack tip is caused by combustion of unreacted species from the igniter system. Thin film thermocouple measurements showed that high heat flux values occur, which are due to heating by the compression wave reflected at the closed end, due to the heat release when the unreacted igniter species burn near the tip behind the reflected compressive wave, and due to enhanced heat transfer by recirculating gases in the tip region. The combined effect of these processes ignites the propellant at the crack tip.

It is conceivable that in the combustion of a fractured or perforated propellant, numerous ignition regions can be generated in this manner, giving rise to further rapid pressurization which in turn leads to new ignition kernels, ending finally in catastrophic failure of the system. In Kumar, et al (1982), they have presented a convincing experimental investigation of this process and solved a detailed theoretical model by numerical methods leading to good agreement between measured and predicted ignition delays in cracks. It is noteworthy that the phenomena described display a strong similarity to the processes observed under knocking conditions in gasoline piston engines.

German Spigot-Test

For investigation of fracture in solid propellants, its effects and its governing parameters, a modified "Spigot-Test" is used in Germany (see also Watkins work at Imperial College, London). The scheme shown in Fig. 60 illustrates the test.

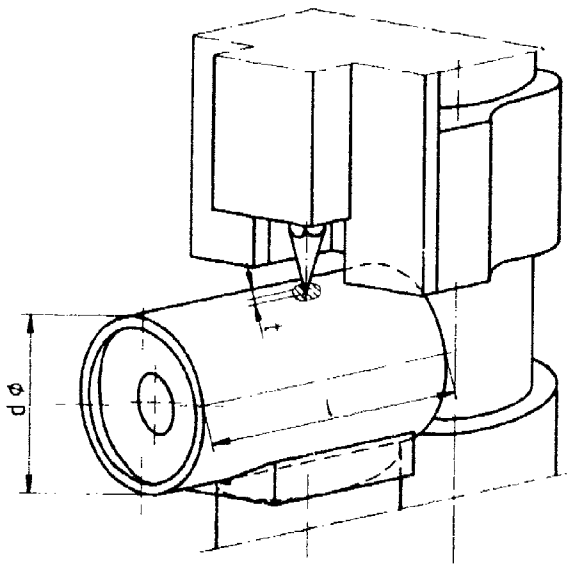

Fig. 60. Schematic Illustration of the Spigot Test.

A section of a true rocket motor or of a model is placed on an anvil. The bottom side of a metal block is equipped with one of the three "spigots": slender cone, small edge or rounded plug. The metal block falls from a determined height and the spigot meets the rocket motor section. The result is observed visually. Most successful in causing fracture is the cone, when even penetrating into the grain of the propellant. An ignition by cracks depends on a series of parameters. The most important are:

Type of propellant - the propellant must contain at least two different phases. Ignition occurs, easily in highly-filled composite propellants AN/AL/HTPB.

Shape, confinement, liner - Ignition is favored by inner boreholes in the propellant grain, strong but elastic confinement, and a good connection between grain and confinement.

Thermal and mechanical history, internal stresses - Reversal of load and temperature create internal stresses in the propellant.

Sample temperature, brittleness, test temperature - The cooler the sample, the more brittle the propellant. In a brittle material cracks arise easier and in a greater number. This and a great difference between the temperature of the sample and the test set-up favor ignition. Other parameters, e.g. the exact chemical composition or the energy of the penetrating spigot are of smaller importance for the ignition process.

The ignition itself is a complex process. A typical development of an ignition in a section with an inner hole is as follows: During the penetration a flash lights up on the place of penetration, spreads along the liner and extinguishes. After some tenth of a second smoke and/or flames appear at another place and disappear. This phenomenon repeats at further places. After a relative long time (in the

magnitude of seconds) if there is no extinguishing, the propellant grain burns self-sustained. At each of the intermediate stages, the process can extinguish without any further reaction.

A very similar response was observed in projectile-impact trials, in which the delay time was 1 or 2 s between impact and ignition. There are two different possibilities to explain this behavior. In the projectile impact trials only unconfined solid grains of propellant and shaped grains in metal confinement have been tested. In the first ones the described ignition phenomenon was not observed, but in the second ones it was. Consequently it may be attributed to spallation of the metal confinement and thermal ignition by spalled particles.

In the German Spigot-Test, the same phenomenon occurs with metal or non-metal confinements but strongly depending on the shape of the grain and the temperature. Therefore the explanation of the phenomenon in terms of fracture effects seems to be applicable. Final ignition is a consequence of relaxation and cumulation effects in the formation of cracks and ignition centers. The discussed ignition behavior is of great importance in hazard research. A tip of a heavy object or a projectile can penetrate into a rocket motor, without external visible consequences. Seconds later, the motor burns up.

RARDE Spigot Drop Test (UK)

This test is used for assessing the hazard associated with dropping a rocket motor on to a steel spike or rail. The standard version of the test uses a mild steel tube with a 1.5 mm steel cover plate welded over one end. The spigot, loaded with a 45 kg weight, falls onto and pierces the cover plate, cutting a disc out and pushing it into the propellant charge contained in the tube (Fig. 61). This test also is used in a standard form for qualification of rocket propellants; in general ignition occurs if the propellant is penetrated. For experimental purposes the case material and dimensions can be varied and liners can be employed.

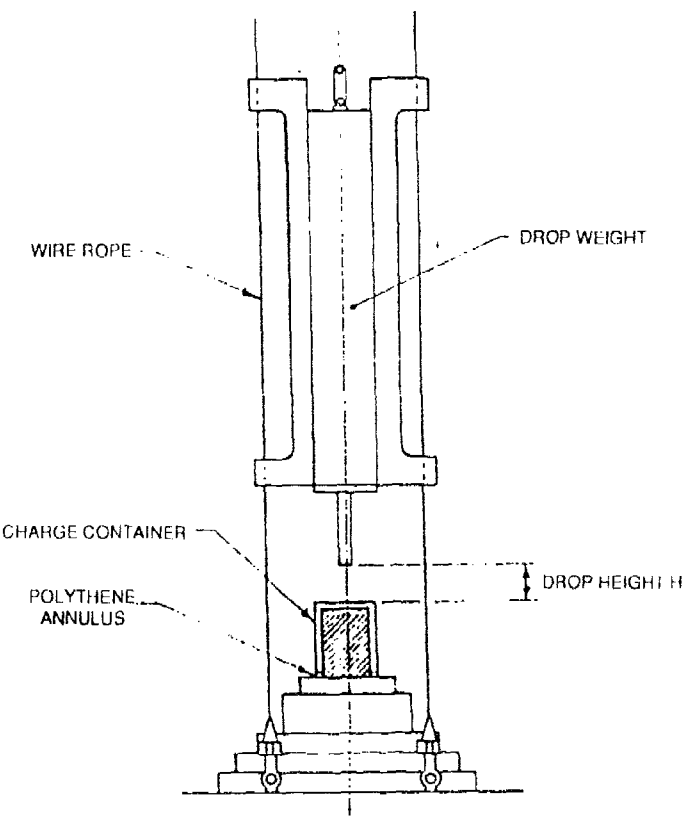

Fig. 61. RARDE Spigot Drop Test Assembly.

5.3. BURN RATES OF ENERGETIC MATERIALS

The rate at which a solid is converted to gas, commonly called the burning rate, has been measured using various devices. These devices and the data that they produce have been reviewed (Boggs and others, 1976). As discussed by Boggs and others, (1976), there are basically two types of combustion bombs: low loading density (less than 0.01 gram of sample per cubic centimeter of bomb volume) combustion bombs (LLDCB), such as strand burners or window bombs, and high-loading density (greater than 0.01 gram per cubic centimeter) combustion bombs (HLDCB), such as the closed bomb. The LLDCB are essentially constant-pressure, constant-volume devices which give the burn rate at a given pressure. To get a burn rate versus pressure curve, multiple runs have to be made.

The HLDCB is essentially a constant-volume device. As the sample burns, the pressure within the closed vessel increases. By measuring the pressure-time record of the process and applying suitable thermochemistry, the mass burning rate-time (or burning rate-pressure) can be calculated. By assuming a form function (a burn area-surface regression relationship), the surface regression rate (burn rate)-pressure relationship can be calculated. Thus in one run, a burn rate-pressure curve can be calculated.

The burn rate as a function of pressure and initial sample temperature is also often determined. These data are useful in determining the kinetics and energetics of the deflagration reactions as discussed by Price and Boggs (1985).

The Effect of Strain on the Burning Rates of High Energy Solid Propellants

High energy propellants usually have a high solids loading (the portion of solid ingredients such as ammonium perchlorate (AP), cyclotetramethylenetetranitramine (HMX), aluminum and other ingredients such as solid catalysts) as compared to the polymeric binder. An obvious condition accompanying high solids loading is that there is less polymeric binder "glue" to hold the solid particles together to form propellants having acceptable mechanical properties. Given these highly loaded propellants, one would like to know such things as how far can a propellant be strained before ballistic anomalies (such as burn rate augmentation) become significant.

The burning rate of a high energy propellant as a function of strain is presented in Fig.62a. The data show that no significant augmentation of burning rate occurs for pressure below 500 psi regardless of strain (the samples fail at approximately 25% strain). At higher pressures ($p \geq 750$ psi) burn rate augmentation appears for strains above approximately 8%. At 1500 psi and strains above approximately 12%, the sample burns in a vigorous and nonplanar fashion precluding meaningful measurement of a linear surface regression.

Data for several types of propellants show burn rate increase at pressures and strains greater than some threshold values. (The magnitude of the threshold values depends on the propellant.) It should be emphasized that both threshold values have to be exceeded, exceeding just one is not sufficient. For example high strain but low pressure will not cause augmentation nor will high pressure but low strain.

The mechanical response of the propellants to strain was studied using a binocular microscope. These studies showed, using the propellant of Fig. 62a as an example, that at 4% strain, debonds (separation, on a micro-scale, of the solid particle from the polymeric binder) between ingredients occurs. Between 9-11% strain, these debonds are often fully developed cracks, with the walls of the crack in close proximity. At approximately 16% these cracks are open voids; that is, the walls of the crack are no longer in contact with one another. At approximately 24% the sample is often riddled with large cracks and the sample fails.

The above, coupled with our knowledge of flame stand-off distance decrease with pressure increase, provides a mechanistic understanding for the burn rate augmentation due to strain and pressure. The mechanism is shown in Fig. 62b. At low strain values the propellant is not significantly damaged and so regardless of the flame stand-off (Fig. 62b (top)) augmentation will not occur. When the propellant is highly strained and fissured, augmentation occurs if the flames can penetrate into these fissures. At low pressures the flame stands too far from the surface to allow penetration, but at high pressures the flame is close enough to the surface to penetrate the fissures and cause burn rate augmentation.

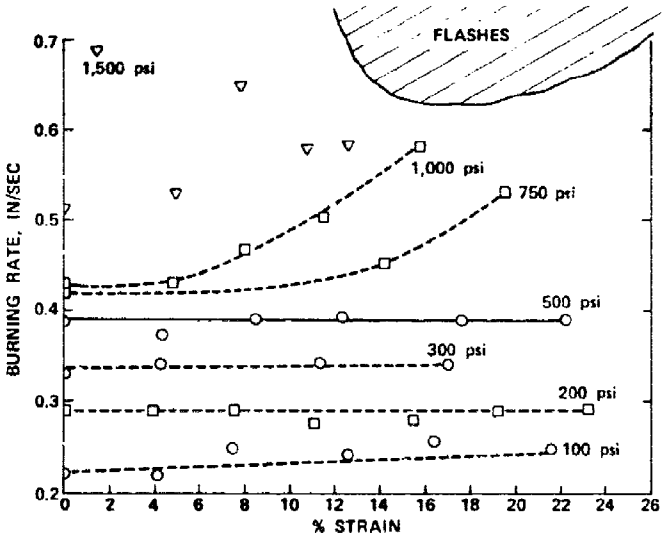

Fig. 62a. Burning Rate of a High Energy Propellant as a Function of Pressure and Strain.

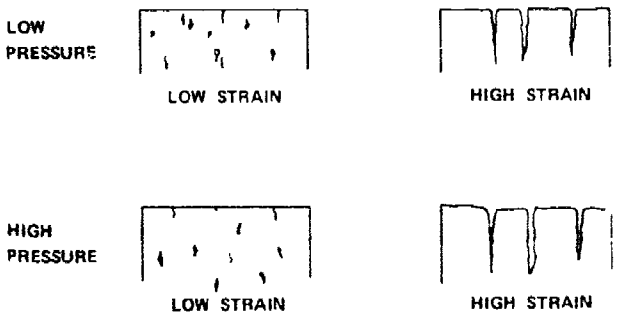

Fig. 62b. A Mechanism for the Augmentation of Burning Rate Due to Pressure and Strain.

Since flame penetration into the defects seems to be required for burn rate enhancement a study was done using propellants that had been strained almost to failure and then the tension removed. The voids closed and when these samples with the closed voids were burned, the burn rate was identical to the undamaged propellant burned at that pressure.

These data indicate that strain can cause damage, and if that damage is sufficient and open, and if the pressure is high enough to allow flame penetration into the defects, then burn rate enhancement can occur.

5.4 DETONATION

Chapter 4 presents solid propellant rocket motor hazard response to various threats in general stimulus-output terms. Slow cook-off, fast cook-off, fragment and bullet impact, sympathetic detonation, and response to electromagnetic radiation are the hazard areas and no-reaction, burning, burning with propulsion, deflagration, explosion, and detonation are output responses. Detonation is the most severe of these output responses.

There are several major paths to detonation. The detonation may be the result of a shock stimulus - (shock-to-detonation transition, SDT), or the result of transition from burning (deflagration-to-detonation transition, DDT), or a combination, or delayed detonation (often called XDT). Within each of these areas, SDT, DDT, XDT, there are several alternate routes that can result in a detonation.

The purpose of this chapter is to transform the general hazard threats discussed in the previous chapter to the various technical concerns. This section will primarily be devoted to the SDT, DDT, and XDT technologies that provide the basic information necessary to assess the sympathetic detonation, bullet and fragment impact areas. Specifically to be discussed are:

- **Mechanistic understanding of the phenomena - includes** consideration of sample, stimuli, and environment.
- What information is required to characterize the hazard situation and predict the response?
- What tests are required to provide this information?
- What analytical modeling is used to provide this information?

Detonation

Ideally, the detonation is a discontinuity or shock wave moving through the unreacted energetic material at supersonic speed and driven by the exothermic chemical reactions of energetic material reacting to final products. In this ideal picture, this discontinuity moves into the energetic material of initial density and temperature. On the other side of this discontinuity are reaction products at high pressure, high temperature, high density.

The above description assumes infinitely fast chemical reactions which of course is physically not possible. There is a finite reaction time associated with the conversion of energetic materials to final products, thus there has to be a reaction zone separating the unreacted energetic material and its final reaction products. This is shown in Fig. 63.

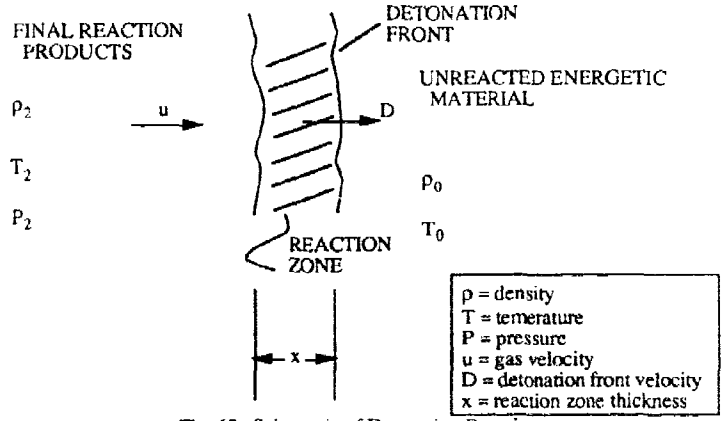

Fig. 63. Schematic of Detonation Reaction.

Typical values for parameters are given in Table 17.

Table 17.

	ρ_0 g/cc	ρ_2 g/cc	P_2 Kbars	u mm/μsec	D mm/μsec	x mm
RDX	1.77	2.38	338	2.21	8.64	0.8
TNT	1.64	2.15	189	1.66	6.94	0.3
HMX	1.89		390		9.1	
AP	1.95		187 (cal)			

The pressures and times necessary to initiate detonation typically are in tens of kilobars applied for a few microseconds. This is even for the case of DDT where even though the process may take hundreds of microseconds, most of the process is the build-up of reactions to produce these pressures. Once the high pressures are obtained, it only takes a few microseconds for the detonation

to occur. The response of the energetic material is dependent on the time and shape of the pressure pulse. In response to square pulse shock, the detonation pressure-time often obeys a relationship of $p^n t$ = constant. The value of n = 2 is often used (Walker and Wasley, 1969).

5.4.1. Shock to Detonation Transition (SDT)

SDT is the development of detonation through a pressure (shock wave) imparted to an energetic material. For a rocket motor, this pressure could be the result of an impact (e.g. bullet, fragment, or shaped charge jet) to the motor case with transmission of a pressure pulse of mechanical shock through the case, liner and insulator, and into the propellant. As discussed in the fragment impact protocol, critical diameter, initiation pressure, run-distance, and time are critical considerations. These are discussed below.

5.4.1.1. Critical Diameter/Critical Dimension, d_{cr}

There are basically three ways to measure critical diameter. The first is to have many different-sized cylinders of various diameters and sufficient length, and test until a clear demarcation is found. Cylinders of diameter larger than the critical size will detonate, while samples with smaller diameter will not. This can be a rather lengthy process. Other methods consist of either a conical or stepped charge initiated at the large end (Fig. 64). The detonation is followed until it fails. Both of the latter two methods may suffer from the overboosting of the detonation wave. The consequences of this can be minimized. For the cone situation, a cone of large taper angle is usually used to get an approximate value; then a cone of diameter near this value and with a very narrow cone angle is tested in order to minimize the overdrive. Another approach is to vary the cone angle and extrapolate to zero angle.

In the stepped cylinder case, care must be taken to have the length-to-diameter ratio (l/d) of each cylinder sufficient to achieve a steady-state detonation. In some cases this may require l/d of 8 to 12. This seems to be the case for ammonium perchlorate propellants and it brings up an interesting point. If it takes 10 diameters for the detonation to "die" (50 inches for a 5 inch diameter) and our motor length is less than this length needed for "die-out", do we care - the entire motor may detonate.

Other investigators measure a critical height or critical dimension. One method is to have a wedge of propellant placed on a witness plate, as shown in Fig. 65. The witness plate is "read" to see where the detonation failed. Another method of determining the critical dimension is shown in Fig. 66.

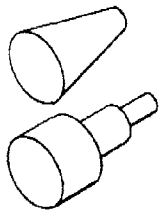

Fig. 64. Critical Diameter Test Specimens.

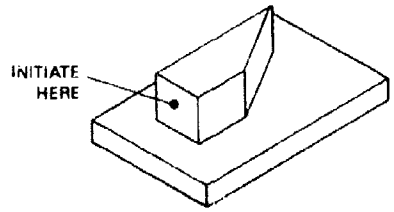

Fig. 65. Wedge Used for Critical Dimension Test.

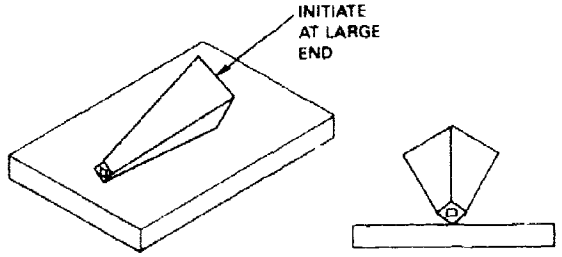

Fig. 66. Critical Dimension Test.

In this test the witness plate is "read" to determine when the detonation died out. This test is often run with crush-up coaxial velocity probes on the side of the sample, so that the detonation velocity is measured, as well as the point where the detonation failed.

Unfortunately, the data produced from critical diameter experiments do not always agree or correlate with data from critical dimension experiments. Additional work needs to be done in this area.

Critical diameter data for propellants unfortunately often are not available. The lack of data has forced some investigators to make an analogy to Project SOPHY data (Elwell and others, 1967) which presented critical diameter of different propellants incorporating various amounts of RDX. Unfortunately the comparison may no longer be valid. The critical diameter may significantly be greater or less than predicted using the SOPHY data. This seems to be most prevalent in modern high solids loading and/or highly catalyzed and/or nitramine containing propellants (Brunet and Salvetat, 1988).

The concept of a critical, or failure, diameter is more complex when applied to propellants than to high explosives. In a given configuration such as shown in Figs. 64 through 66, the detonation runs until the critical dimension is reached and then promptly dies out (although there may be some overdrive). Recent work with modern ammonium perchlorate based propellants having high solids loadings (and with some explosives incorporating significant amounts of ammonium perchlorate), this prompt cessation of detonation at the critical dimension does not necessarily occur. Three instances are described below.

(1) Several investigators have reported that when ammonium perchlorate based materials were boosted to detonation, the material continued to detonate much further down the tapered sample than expected from the critical dimension determined in other experiments. Although the velocity was decaying, it took lengths equal to several times the supposed critical diameter before the wave became subsonic. This seems to be consistent with the observations quoted above on the stepped cylinder experiments; the detonating propellant forming the donor charge for the material downstream.

(2) A high solids loading ammonium perchlorate based metallized propellant was recently tested in the apparatus of Fig. 66. This propellant tested zero-cards in the NOL card gap test. That is, no detonation was produced even when the donor was placed right on top of the acceptor. Three different length samples were tested - one 36 inches long (≈91 cm), one 24 inches long (≈61 cm), and one 16 inches long (≈41 cm). The samples had coaxial crush velocity probes along all four sides of the sample. The results of the tests are shown in Fig. 67. The top of the figure presents a schematic showing that for comparison purposes, the apex of the cone is considered the zero distance reference.

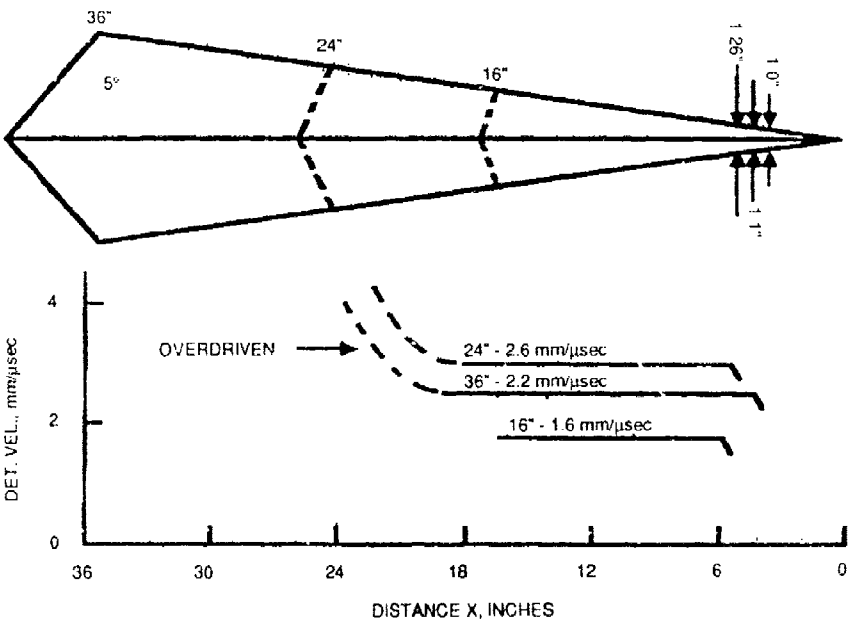

Fig. 67. Typical Wedge Test Results.

Thus the plot shows that

(1) the 36 inch long sample was detonated with the detonation wave, which was traveling at approximately 8 mm/μsec, diminishing to 2.2 mm/μsec at approximately the 18 inch (≈46 cm) distance. From the 18 inch to 4 inch (≈10 cm) distance the wave traveled at a constant velocity of 2.2 mm/μsec. At approximately the 4 inch (≈10 cm) distance the probe crush ceased. This corresponded to a 1.0 inch (≈2.5 cm) critical dimension.

(2) The 24 inch test resulted in a detonation wave of decreasing velocity to the 18 inch (≈46 cm) mark. From the 18 inch to approximately the 5 inch (≈12.7 cm) distance, the wave proceeded at 2.6 mm/μsec. At approximately 5 inches it died out, corresponding to a 1.1 inch (≈2.8 cm) critical dimension. The 16 inch long test did not show the long region of high velocity wave as seen in the 24 and 36 inch tests. Instead this test showed a constant velocity of approximately 1.6 mm/msec from onset to approximately 6 inch (≈15 cm) distance, corresponding to a critical dimension of 1.26 inches (≈3.2 cm).

The sound speed was also measured for these propellants and was found to be 2.05 mm/μsec.

While detonation physicists may argue whether these reactions traveling at approximately 2 mm/μsec were "true" or "robust" detonations, the violence of the reaction should be considered.

(a) It had sufficient impulse to crush the coaxial velocity probe. An explosion or deflagration does not.

(b) The brass witness plate showed removal and flow of metal. Again, explosions and deflagrations do not.

(c) The reactions were traveling at approximately sonic velocity. The point to be made is that this intermediate reaction, which took place over a long run distance is more closely akin to a detonation rather than an explosion in terms of violence of output.

(3) Work on propellant samples has shown that a center perforation can make the sample more sensitive (same outside diameter). This is in contrast to reports from the SOPHY program that claimed that in their work center perforations decreased the sensitivity. In these more recent tests, 10 inch (≈25 cm) and 8 inch (≈20 cm) diameter by 10 inch long samples detonated when initiated by a plane wave booster. (The length of the sample was limited by charge weight safety limitations for the given firing arena.) Six inch (≈15 cm) diameter samples detonated but appeared to be failing at the end of the charge. Five inch (≈12.7 cm) diameter samples showed a detonation only at the center 2 inches (≈5 cm) at the end of the charge. When a sample having a 1 inch (≈2.5 cm) cylindrical center perforation was tested, the entire sample was consumed in a detonation of more than usual brisance as related by occupants of laboratory buildings some distance away.

These are preliminary results but are of concern to propulsion personnel since many of our motors have a center perforation or conduit.

A more detailed description of detonation phenomena in charges with an axial hole is found in Annex II.

The effect of center perforation also seems to have more of an effect (increased sensitivity) than reported in SOPHY.

5.4.1.2. Initiating Pressure, p_i

There are many tests available to measure initiating pressure. These include various gap tests (including aquarium tests), booster tests, wedge tests, projectile impact tests, and a relatively new test--the flying foil test--designed to test very small amounts of propellants and explosives.

Gap Test. Probably the most widely used tests are the various gap tests. Of these, the NOL large-scale gap test (Fig. 68) is the most widely used. It consists of an explosive donor, an attenuating material, and acceptor energetic material. The attenuator, usually polymethyl-methacrylate (PMMA), is adjusted in thickness to change the shock level to the acceptor. The donor is two pentolite pellets (50% TNT, 50% PETN). The acceptor, 1.44-inches (≈3.66 cm) in diameter, is confined in a steel sleeve. A mild steel witness plate, approximately 3/8-inch (≈1 cm) thick and standing 1/16-inch (≈1.60 mm) from the acceptor, is used to determine whether or not a detonation (a clean hole punched through the witness plate) occurred.

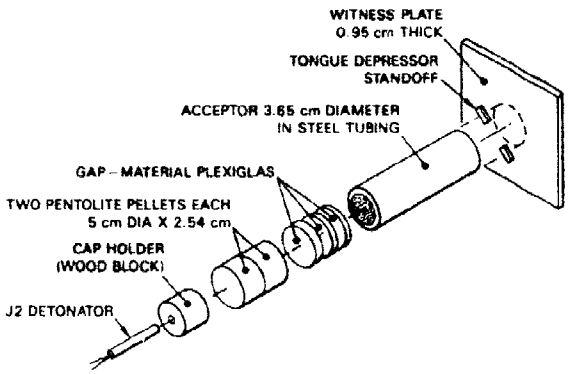

Fig. 68. Standard NOL Gap Test.

In the U.S., the NOL gap test has been used as the principal device to classify energetic materials as to their hazard. If the acceptor detonates when the gap is 70 cards (0.7-inch (=1.78 cm)) or greater, then the energetic material is given a 1.1 hazard classification; otherwise, the material is classed 1.3. While this test works well for testing most high explosives (except perhaps for highly porous materials, weak explosives, or explosives having a critical diameter larger than 3.8 cm), it has several drawbacks for propellant testing. In order for the test to have meaning, the acceptor sample critical diameter must be less than the approximately 1 1/2-inch diameter. Obviously most explosives fulfill this requirement while many propellants have larger critical diameters and hence are not amenable to testing using the NOL gap test.

Part of this reservation may be overcome through use of the 8-inch (≈20.3 cm) gap test; however, the size of the booster and acceptor with their considerable output makes this test too large for some installations.

Another problem associated with using the traditional NOL gap test with propellants is the lower output of many propellants as compared with more robust high explosives. Some compositions do not have enough output to punch a clean hole through the witness plate even though the reaction was a detonation . In some instances investigators (e.g. D. Price) have had to resort to using an energetic material as the witness plate: a detonation of the sample causes detonation of the energetic material "witness plate" while a nondetonation of the sample does not.

Aquarium Test. Aquarium tests are a type of gap test for which water is the gap and confining material. Water has advantages because its properties are very well characterized. In addition, the phenomena can be photographed showing initiation of donor, shock wave in water, shock wave into acceptor, and reaction of sample. Work at the Naval Weapons Center, modeled after the work of Liddiard (1965) with modifications suggested by S. Jacobs and D. Price, has utilized aquarium testing to study the shock sensitivity of undamaged and damaged propellant. Data from these tests compared favorably with wedge test data obtained by Los Alamos National Laboratory on the same propellants.

Wedge Test. Wedge tests offer significant advantages and can provide relationships between initiating pressure, run length, and delay time. In these tests, schematically shown in Fig. 69, a plane shock wave enters the test wedge. As the wave traverses the wedge, the position is seen as a moving line (moving toward the apex) on the aluminized mylar film attached to the wedge (shown at two times in schematic, Fig. 69).

With the angle known and the line position measured, the run distance can easily be determined. Since the measurements are time resolved, the run time is also easily determined. By varying the plane wave booster or the attenuator in the tests, the input shock pressure to the sample can be varied so that shock input pressure-run distance-time relationships can be made.

The run distance (X_d) initiating pressure (p_i) data are often plotted in what is referred to as "Pop" plots in terms of log run distance as a function of log input pressure. Data plotted in this fashion form a straight line with negative slope (Fig. 70).

These data are often used in the Forest Fire analysis of shock initiation (Forest, 1981).

While wedge tests provide much data--run distance and run time as a function of initiating pressure--there are some drawbacks. One is cost. The test uses samples whose dimensions must be carefully controlled, but more importantly it uses a plane wave booster for each shot. From a

technical standpoint, run length and delay time are not sufficient characteristics, especially for damaged materials; both run length and delay time vary with porosity, and the critical initiating pressure increases with porosity decrease (Price and Jacobs, 1981). Thus, more porous charges are easier to initiate (lower p) but require slightly longer run distance and run time. This can be confusing since one material may be more sensitive than another material at low pressure, but less sensitive at high pressure.

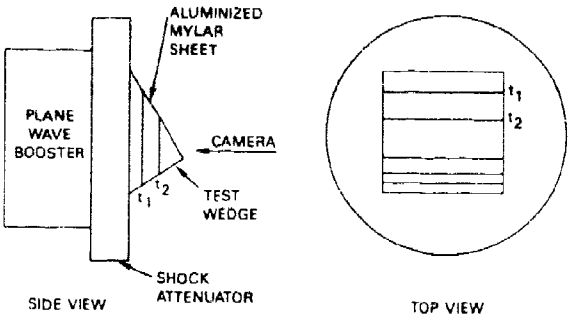

Fig. 69. Wedge Test Schematic.

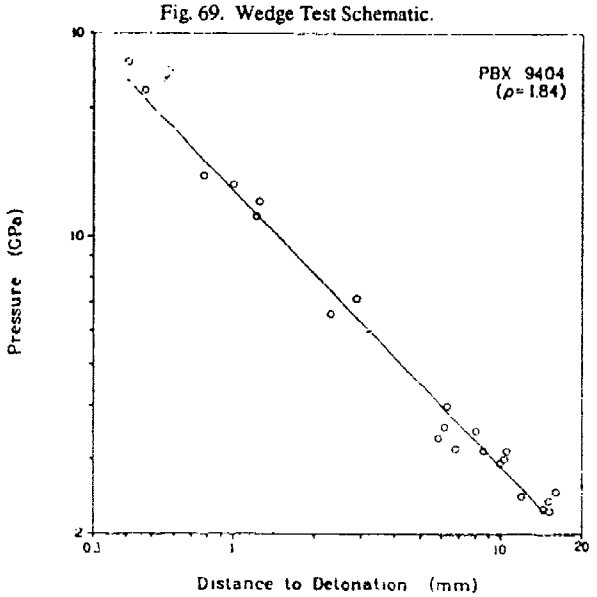

Fig. 70. "Pop" Plot for PBX 9404 at $\rho = 1.84$ gm/cm^3.

Minimum Priming Charge Test. In this test a cylinder of energetic material (usually 2-inches (=5 cm) in diameter and 2-inches (≈5 cm) high, or 1 1/2- (≈3.8 cm) by 1 1/2-inches) has a hemispherical cavity milled into one end. This cavity is then filled with Extex explosive (80% PETN/20% Sylgard) initiated by a mild detonating fuze from a primer. The shock strength is varied by the radius of the hemisphere. A witness plate provides evidence of whether a detonation occurred or not. The typical test setup is shown in Fig. 71.

Several investigators prefer this test because of the spherically diverging shock and because it correlates well with data from other tests, but the test has limitations. It is not very applicable to samples that have very large critical diameters or to samples having much damage.

Flying Plate Tests. Various flying plate impact tests exist in which a disc of material is propelled by a gun or explosive charge against the flat end of a cylindrical charge. By varying the composition, thickness, and velocity of the impactor, various levels and shapes of shock are possible.

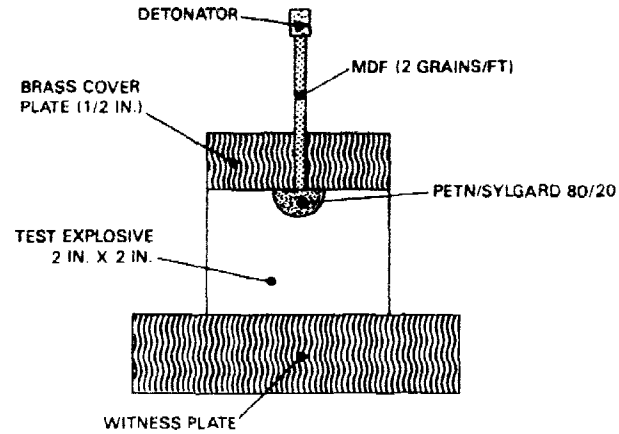

Fig. 71. Minimum Priming Charge Test.

Flying Foil Test. The flying foil test is a determination of the response of a energetic material to short-duration shock stimulus. In the test a mylar flyer (foil) is accelerated to high velocity by an electrically vaporized strip of aluminum. The mylar flyer impacts the sample, producing a strong shock wave in the sample. Samples are either cast in a steel confinement ring (washer) or cut to shape and inserted into the ring. Each sample is a 3.56-mm diameter by 3.06-mm high cylinder. Reaction (detonation) in the sample is detected by enlargement of the sample confinement ring. The quantity measured is the minimum voltage on the capacitor, used to vaporize the aluminum foil, that just causes detonation in the sample. Through the calibration of the device, voltage is related to flyer velocity. Velocity of flyer and shock properties of mylar and sample determine the pressure into the sample. Thus, the test determines the shock pressure that causes initiation. Unlike gap tests, the shock is planar, constant amplitude, and short (=5 ns, depending on the flyer thickness). The test has the advantage of requiring a small sample and is relatively inexpensive to perform. (The typical test setup is depicted in Fig. 72.)

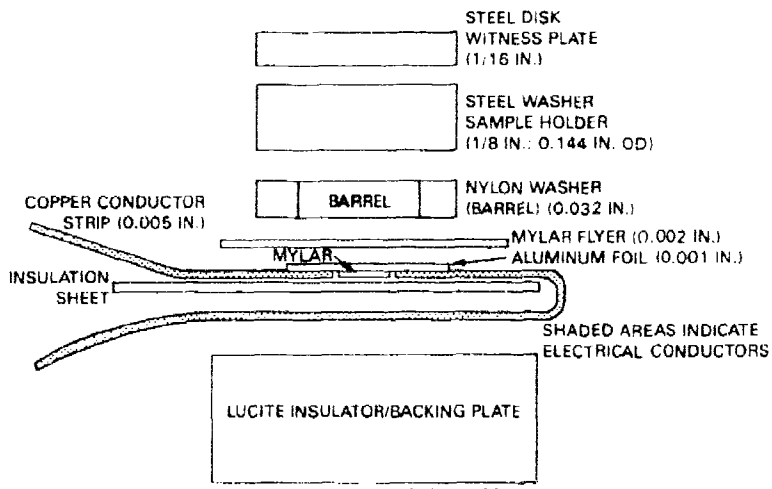

Fig. 72. Exploding Foil Assembly.

5.4.1.3. The Role Of Damage

Damaged energetic material behaves differently from its undamaged counterpart. Both the critical diameter and pressure required to initiate detonation are changed, causing increased sensitivity (smaller critical diameter and lower pressure). Figure 73 shows the increase in shock sensitivity as a function of void volume for one type of propellant. Information on the type and extent of damage is required if one is going to predict the hazard sensitivity of the damaged energetic material.

Fortunately, recent efforts (Lepie and Moran, 1985; Richter, Lepie and Adicoff, 1980; and Richter and Lepie as cited in Boggs et al 1988) have provided tools that characterize energetic materials in terms of the stress-strain behavior and the strain-volume dilatation (percent voids). Stress-strain behavior can be obtained using conventional techniques such as the Instron tester. While inferences of the onset of dewetting (the onset of damage caused by separation of the solid particles by the binder) can sometimes be made, use of a volume dilatometer provides quantitative information of the degree of damage.

Use of both tensile and shear dilatometers using both mercury and a Freon-type liquid has been demonstrated and discussed by Richter, Lepie and Adicoff (1980) and others.

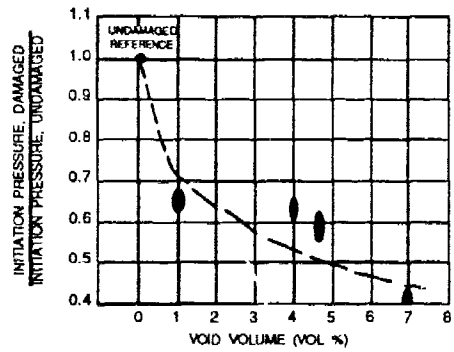

Fig. 73. Aquarium Gap Test Results - Normalized Pressure Versus Void Volume.

The work of Richter, Graham and others (as described in Boggs et al, 1988) on shock sensitivity of damaged propellants was accomplished using the Instron device to produce damage at the strain rate of 50 in/min (≈127 cm/min). The damaged samples were tested for shock initiation using an aquarium test. Supplemental tests using hydrostatic compression, as well as the strain-volume dilatation characterization, were used to estimate the damage present when the damaged samples were shocked (usually 15 to 20 minutes after the damage had been produced).

Future work is moving toward higher strain rates (up to 12,000 in/min--≈5.08 m/s) and decreased time between damage production and shock stimulus (as short as a few tens of milliseconds).

5.4.2. Deflagration-to-Detonation Transition (DDT)

This technical area considers whether or not a propellant reaction can transition from a burning reaction to a detonation. The considerations are shown in the flow chart (Fig. 74). The key requirement for this transition to occur is a sufficient surface to volume ratio and porosity of the energetic sample either through manufacture and loading, in the case of some gun propellants, or through large scale damage in the case of missile propellants. For missile propellants the first consideration then is the likelihood of the propellant being damaged either before or during the burn. This is a critical consideration because, with rare exceptions, it is impossible for a consolidated propellant at near theoretical maximum density (TMD) to undergo a DDT reaction.

The next consideration is whether or not sufficient surface-to-volume and porosity exist. Figure 75 presents the limits of DDT for granulated propellant samples (Butcher and others, 1979). This plot shows that you must have sufficient TMD - here about 49% TMD; any less will not sustain and accelerate the reaction. If the sample is too dense, the DDT reaction will not occur. Similarly there is a range of surface to volume required (100-700 inches^{-1}) if DDT is to occur. If these conditions, or similar conditions for other samples, are not met then a DDT reaction is extremely improbable. Although transition to detonation may not be probable, an explosion may still occur. In order to determine whether an explosion may occur, the pressure and the rate of pressurization caused by gasification must be determined and compared to the rupture characteristics of the motor case.

If the propellant is damaged and if the resulting %TMD and surface-to-volume ratio are in the "right" range then DDT is extremely likely. Whether or not the DDT occurs is determined by the pressure and pressurization rate within the vessel and the rupture characteristics of the vessel (motor case). If the motor case ruptures "too soon," then confinement is lost and the DDT reaction becomes unlikely. (The rupture may be a violent explosion.) The rupture characteristics of the vessel need to be determined experimentally and/or analytically but will not be discussed further in this paper.

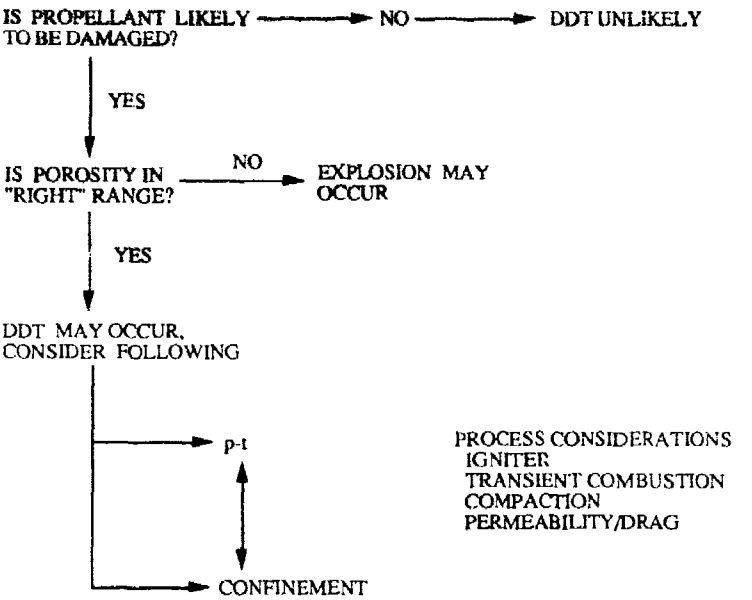

Fig. 74. Hazard Analysis Protocol for Deflagration to Detonation Transition.

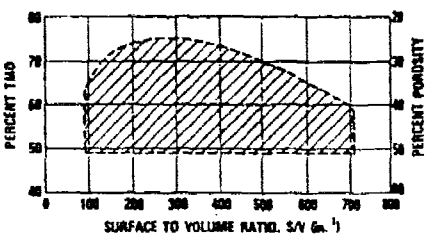

Fig 75. Limits of DDT for Granulated Propellant Samples (Butcher and others, 1979).

The pressure-time history of a DDT reaction is shown in Fig. 76. This figure shows several regions: the ignition, slow combustion build-up, combustion coupled with weak compaction wave, combustion coupled with strong compaction wave, shock formation, and detonation. The location of these events in the p-t plane are strongly influenced by several considerations. These include the degree of confinement, the strength or "brisance" of the ignition stimulus, the sample thermochemical and physical characteristics, the charge dimensions (diameter and column length), and the intrinsic detonability of the material. The physical characteristics of the sample include the size and shape of the damaged pieces, the porosity and gas permeability, and the compressibility. The thermochemical considerations include the chemical composition of propellant, pyrolysis products, and final products; the kinetics and energetics associated with the pyrolysis (solid propellant going to reactive intermediate species) process, and the kinetics and energetics associated with the conversion of the reactive intermediate gases to final products.

It must be stressed that the above items are listed separately but in fact the DDT process is a highly coupled interaction of these various considerations.

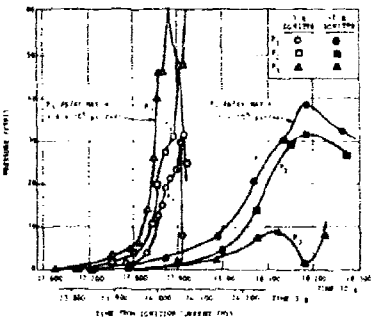

Fig. 76. Standard Test Unpressurized 12 g 2056D/Black Powder Bag and 3 g Mg-Teflon Test Comparison.

From the above discussion it can be seen that the following types of data are necessary in order to predict whether DDT is likely to occur:

- Strength and brisance of ignition stimulus
- Confinement and rupture characteristics of the case
- Compaction behavior of the sample - how the %TMD changes with pressure
- The compaction/drag/permeability - the compaction is caused by an imbalance of forces between the drag of the gases flowing over the particles and the particles ability to resist compression. As the sample is compacted, the permeability (the ability of gas to flow through the sample) is changed
- The kinetics and energetics associated with the pyrolysis and conversion to final products
- The compressive ignition characteristics of the compacted material
- The detonability of the propellant

In order to obtain these data various tests described below are used.

5.4.2.1. Tests

Various tests are used to determine the susceptibility of energetic materials to DDT. The tests determine the ease with which the energetic material may be damaged (friability) and, once damaged, how easy it is to transition from burning to detonation.

Shotgun Test

The friability of a propellant is usually determined using the shotgun test. In this test a sample of propellant (usually 8 grams - approximately 1.75 cm diameter by 1.85 cm long) is fired from a smooth bore gun (usually a 12 gauge shotgun) at a rigid target (usually a steel impact plate). The plate is located inside a catch box so that the damaged propellant can be collected for later firing in a closed combustion bomb (90 cubic centimeter closed vessels are often used). The apparatus is shown in Fig. 77. The velocity of the sample is recorded. The velocity is varied by varying the amount of shotgun powder used. The velocities ranging from those causing no sample break up to velocities where some of the sample weight is lost because some of the very fine material "flashes off."

The resulting damaged sample is then collected and fired in a closed bomb and the pressure-time history measured. The data are presented in several ways:

(1) Relative Quickness (dp/dt) - For a given run the maximum quickness dp/dt is determined (and sometimes compared to that of some standard material of known geometry). A high value of relative quickness shows large amounts of damage.

(2) Critical Impact Velocity (CIV) - This method takes quickness measurements one additional step. In this method the maximum dp/dt is plotted versus its impact velocity (see Fig. 78, Gould, 1981). The critical impact velocity (CIV) is that velocity where the straight line fitted through the data points crosses the dp/dt value of 2.5×10^6 psi/sec (1.74 MPa/s). This 2.5×10^6 psi/sec (1.74 MPa/s) value was the value of pressurization that caused DDT of cut propellants of known surface-to-volume ratios fired in closed pipe tests.

(3) Burn Area - While the above two techniques give some indication of the degree of damaged propellant, or friability, there are limitations. Neither method actually measures damage, or more importantly surface area. In addition, while friability can be compared within similar propellant families, it is almost impossible to compare quickness or CIV between widely different propellants (or

at least between propellants having widely different burn rates). Since dp/dt is a function of dm/dt and since $m = \rho A_b$ it is apparent that dp/dt is not an accurate characterization of burning surface (A_b) area between propellants having widely different values of density (ρ) and/or burn rate (r).

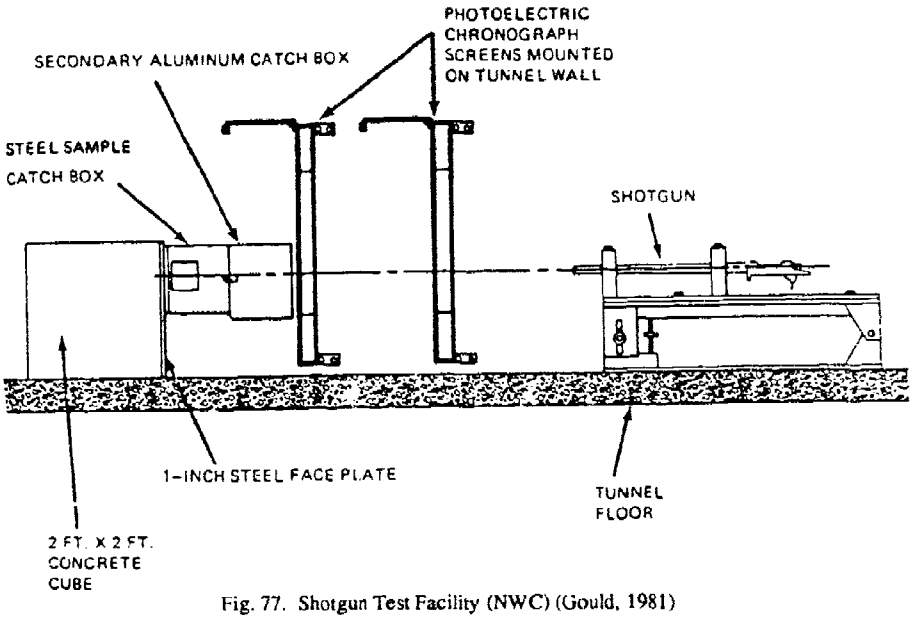

Fig. 77. Shotgun Test Facility (NWC) (Gould, 1981)

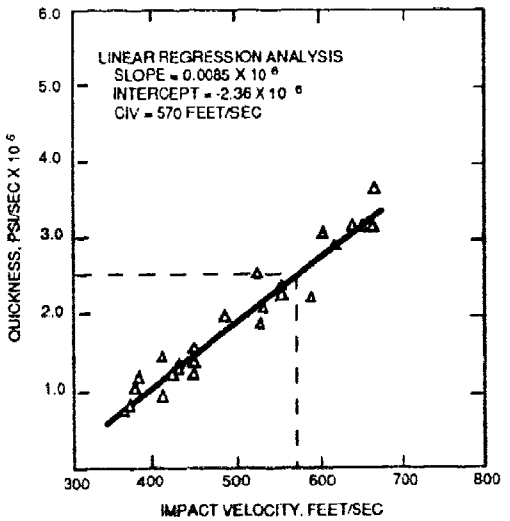

Fig. 78. Typical Shotgun/Quickness Test Results (Gould, 1981).

To overcome these deficiencies a technique, CBREDII (Price, et al., 1979), was developed that gives the burn area as a function of time and distance burned, as well as characteristic dimension of the damaged material. In this method an undamaged sample is burned in the closed bomb. Since the geometry is known the initial burn area can be assumed as well as a form function to describe the surface regression. From these runs the burning rate (surface regression rate as a function of pressure) can be determined. Having this burn rate-pressure parameter, and the propellant density, pressure-time data for damaged propellant can be reduced with assumptions of the thermochemistry to give burn area-pressure (and hence time) values. The burn area-time and burn area-distance burned

characteristics allow one to compare damage for propellants having different density and burn rates. The shape of the burn area-time curve allows determination of the type of damage (e.g., lots of fines that burn off quickly leaving a moderately damaged propellant to quiescently burn).

Closed Pipe Tests

Tests to determine the ease of transition from burning to detonation are usually done in a closed tube configuration, Fig. 79, with different stimuli. Various igniters have been used, ranging from "soft" (Butcher and others, 1982; Butcher, 1982; Butcher and Isom, 1982; Price and Boggs, 1983) to "hard" (Bernecker and others, 1982; Bernecker and Price, 1975; Price and Bernecker, 1975; Bernecker, 1978; Bernecker and others, 1976; Bernecker and others, 1985; Bernecker, 1984), to start the material in the ignitor end of the tube reacting. Driver sections, a burning material isolated from the rest of the bed by a gas impermeable barrier, have also been used as the stimulus (Campbell, 1980). Sandusky has used a piston driven into the tube to study compaction driven DDT (Sandusky and Bernecker, 1985; Sandusky, 1983). Various tube materials have been used and include Lexan and Steel.

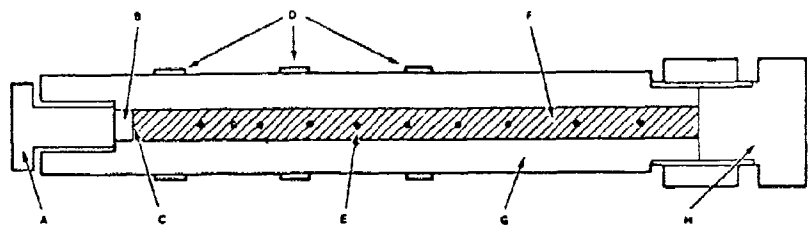

Fig. 79. Cross Section of DDT Tube. (A. Ignitor Bolt; B. Ignitor; C. Ignitor/Explosive Interface; D. Strain Gauges; E. Ionization Probe Location; F. Explosive Charge; G. Tube; H. Bottom Closure, Inner Diameter = 16.3 mm, Outer Diameter = 50.8 mm, Distance From Ignitor/Explosive Interface to Bottom Closure = 295.4 mm.) (Bernecker 1978)

Various types of instrumentation have been used in studying DDT in the closed tube configuration. The earliest tests were essentially go/no-go tests: a detonation occurred or did not occur as evidenced by numbers of fragments and type of fragmentation (e.g., "blueing" of metal). Strain gauges and/or event pins (ionization and/or closure pins) were added as shown in Fig.79 and wave speeds and event times could be determined. For example, Fig. 80 shows a compressive front traveling at 1.25 mm/μsec, forward and rearward running compression waves at approximately 2 mm/μsec (G, F-E-D) and onset of detonation at x = 153 mm followed by detonation wave at 7.29 mm/msec (Bernecker, et al., 1976).

With the use of transparent tubes (Lexan), continuous access streak cameras, continuous access framing camera, and flash x-ray instrumentation were used. Typical results are shown in Fig. 81, showing several events and associated velocities. The use of flash x-ray not only allowed identification of wave behavior but also provided quantitative values of the compaction (lead foils and/or balls were used as markers and the spacing between markers was used to determine the density).

The use of pressure transducers has been a significant improvement, providing quantitative data as opposed to just wave speeds, just as flash x-ray provided improvement over simple event gauges.

Both Butcher and others (1982) and Bernecker and others (1985) have used pressure transducers, extending our knowledge of DDT phenomena. They have investigated behavior resulting from igniter strength, bed compaction and pre-pressurization that affect nonequilibrium or transient combustion and hence DDT behavior (Butcher and others, 1982; Boggs and others, 1982).

Similar experiments, often called convection combustion experiments, have been done at various conditions in an effort to understand the first portion of the DDT phenomena (Atwood and others, 1986).

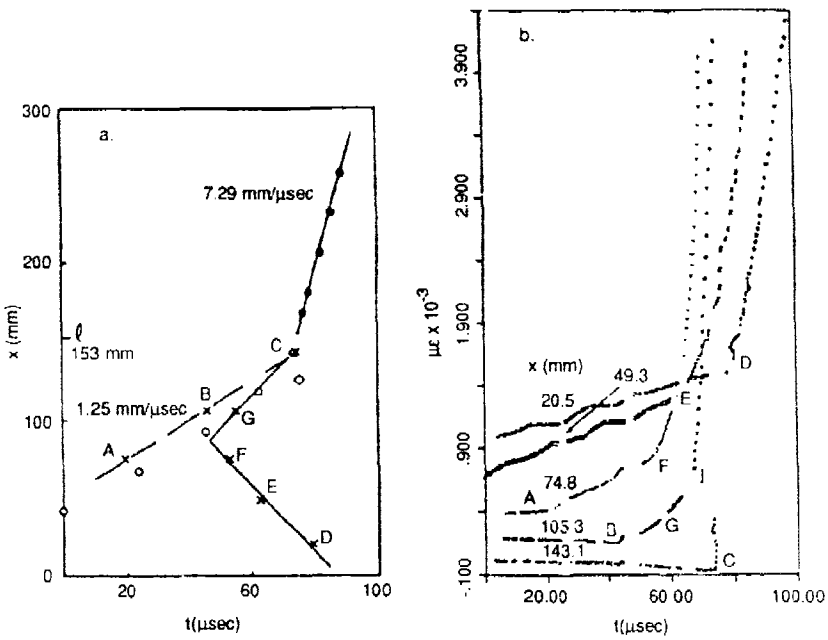

Fig. 80. Data for Shot 613 on 470μ Tetryl at 85%TMD, ρ_0 = 1.47 g/cc. [a. Distance-time plot (o custom-made probes, • commercial probes, X change in slope of ε-t curve of b, coalescence of isobars); b. Strain-time plots (change of slope shown by letters which also appear in a. Each curve except the lowest has been raised 0.2 x 10^{-3} υε, or an integral multiple thereof, for better data display.)] (Bernecker, et al., 1976)

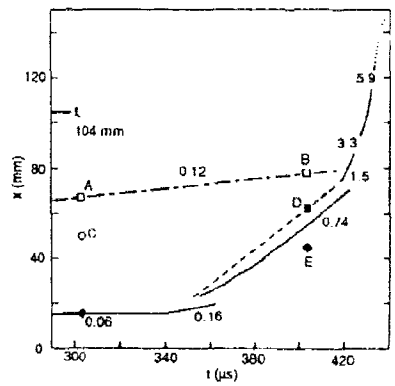

Fig. 81. Distance-Time Data From 61.0% TMD 1080 μm HMX, ρo = 1.16 g/cc (Shot A10). (—— luminous front in HMX; ····· luminous front in NaCl; ❑ head of weak compaction wave (WCW); ◊ head of 1.54 g/cc compaction regime; ◆ upstream end of compacted column; ■ head of strong compressive wave A(SCW); —·— path of WCW; - - - - estimated path of SCW. Numerical value is velocity of a front in mm/μs.)

Experiments in Support of DDT Modeling

Much of the modeling of DDT begins with first principles equations of mass, momentum, and energy conservation. The models try to describe phenomena consisting of highly coupled interactions between gasification of the solid, flow of gases past solids causing compaction, compaction restricting further flow, reaction of gases with various (thermal and mechanical) energy release mechanisms. A

complete description is improbable (and probably intractable) and so various constitutive relationships are used to describe the heat transfer, drag, compaction, gasification, etc. The parameters used in these relationships come from ancillary experiments such as compaction studies (Sandusky and others, 1982; Elban and others, 1981; Elban, 1982; Kooker and Costantino, 1986) ignition and transient combustion studies (Boggs and others, 1982; Boggs and others, 1984; DeLuca and others, 1976; Gerri and others, 1973; Krier and others, 1976), permeability and drag experiments (Atwood and others, 1986; Kuo and Nydegger, 1978; Jones and Krier, 1983; Ergun, 1952), burn rates (Boggs and others, 1980; Boggs and others, 1977; Parr and others, 1983), and flame spread and burning surface area (Price and others, 1979; Krier and others, 1976).

5.4.2.2. Mechanistic Understanding

Rapid progress in understanding the various processes occurring during DDT has been made in the last decade; however, much work needs to be done. The understanding of compaction behavior has increased markedly (Kooker and Costantino, 1986). The importance of using a fully transient combustion description instead of the previously used ignition criteria and steady state burning has been recognized (Boggs and others, 1982; Boggs and others, 1984; Price and Boggs, 1983; Hopkins, 1974, Keller, Horst and Gough, 1985; and Kim, 1984).

Another view of strong mechanical interactions between gas and condensed phases is also suggested by Leiber (1984). Discussion of the various models requires more scope than available in this publication. Interested readers are referred to Price and Boggs (1983), Beckstead and others (1977), Pilcher and others (1976), Pilcher and others (1977), Pilcher (1978), Krier and Gokhale (1978), Krier and Kezerle (1977), Baer and Nunziato (1984), Weston and Lee (1985), and Butler and others (1985) for detailed discussion of the various models.

Deficiencies in Understanding Chemical/Physical Phenomena

General: Most past descriptions of the DDT process have been cast in physical rather than chemical terms. Reactions were assumed to be either "off" or "fully on" with full and instantaneous equilibrium thermochemical energy release. This drove much of the experimental and analytical work. Indeed, experimental measurements largely consisted of wave speeds as determined by strain gauges and ionization or shorting pins down the length of the test bed. It has only been recently that pressure transducers have been used. The analyses were primarily the prediction of shock wave speed and amplitude.

5.4.2.3. Deficiencies in Experimental Work

Damage: The entire DDT process is predicated on materials having a high surface to volume ratio. For solid rocket propellants this requires damage, and rather extensive damage, of the propellant. This is the first and key consideration.

While we use tests such as the shotgun to give a ranking of a propellant's toughness or resistance to damage, we do not obtain much fundamental understanding from these tests. We must understand the mechanisms causing damage: how is damage formed (e.g., dewetting of crystalline ingredients from the rubbery matrix), what type of damage is formed, and to what extent.

DDT Tube Experiments

- Most of the DDT tube studies have been done using idealized systems: ball powders, HMX particles, cut or shredded propellant. It is now time to start testing real propellant having real damage.
- Our tests need to be better instrumented especially to detect and follow the thermochemical reactions. It has only been recently that we have started using pressure transducers and flash x-ray (to detect and follow compaction). The next step is to measure temperatures and hopefully some day have an indication of what species are present.
- Measurements need to start at time zero (with current to the igniter) not just near the detonation transition event. The processes occurring early in the event set up the DDT.

Collaborative Experiments to Provide Constitutive Equations and Parameters for These Equations

- We need more compaction experiments with emphasis on dynamic compaction of real propellants.
- We need more drag-compaction-permeability experiments with emphasis on higher Reynolds number flow.

- We need more transient combustion studies to determine kinetic and energetic parameters.
- We need to decouple the mechanical phenomena (compaction, fluid flow) from the combustion aspects and study each separately, and then merge phenomena in step wise fashion.

5.4.2.4. Deficiencies in Analyses

- We need better constitutive relations and assumptions.
- We need better thermochemical energy release description. Must replace ignition criteria followed by steady state burning with fully transient description.
- We must have better success in describing experiments modeling various parts of process.
  - Gas flow in tube
  - Gas flow in packed bed
    - compaction
    - permeability
    - piston driven compaction tests
    - "convective combustion" tests
    - DDT tube tests

As stated earlier, a complete analytical description of DDT based only on first principles is not currently possible: constitution equations and parameters are often used. These equations and parameters are developed based on experimental work.

5.4.3. Delayed Detonation (XDT)

Some shock input tests and some impact (and multiple impact) initiation tests exhibit a delayed detonation; that is the resultant detonation occurs at a time later than the normal transit time of the shock through the material. These reactions not only occur at times longer than characteristic of SDT, they also require a lower stimulus (e.g., as much as 50% lower impact velocity, see Fig. 82), and an increased number of cards in the card gap test (Fig. 83). These types of reactions have been called XDT, with the X reflecting an uncertainty with respect to the mechanisms involved.

Not only do these XDT reactions require lower values of input stimuli but they are also characterized by higher output. Figure 82 clearly shows this, and tests in France have shown that the output overpressure of XDT is always greater than that of SDT (generally 30% or more).

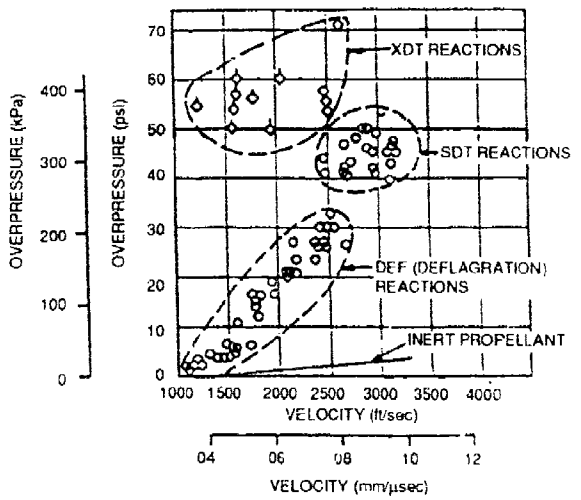

Fig. 82. Overpressure Versus Impact Velocity for Direct Impact Tests. Lines on XDT datum points imply higher overpressure than is indicated (Blomuer as cited in Energetic Materials Hazard Initiation, May 1987).

Sample size also determines the initiation threshold as seen in Fig. 84. Sample geometry and relation of sample orientation and stimulus are also important determinants of whether XDT will occur. For example, when a cylindrical sample of sufficient size (Fig. 84) travelling at sufficient velocity (Fig. 82) impacts head-on (axis of the cylinder perpendicular to the target plate) an XDT occurs; however, if the cylinder strikes side-on (axis of the cylinder parallel to the plate) XDT does not occur.

Sample mechanical properties are also important as indicated in Fig. and 85.

While initially unknown, the mechanisms responsible for XDT are becoming better understood. The process is generally thought to include fragmentation of the sample, recompression of the fragmented material, initiation of combustion, and subsequent build up to detonation.

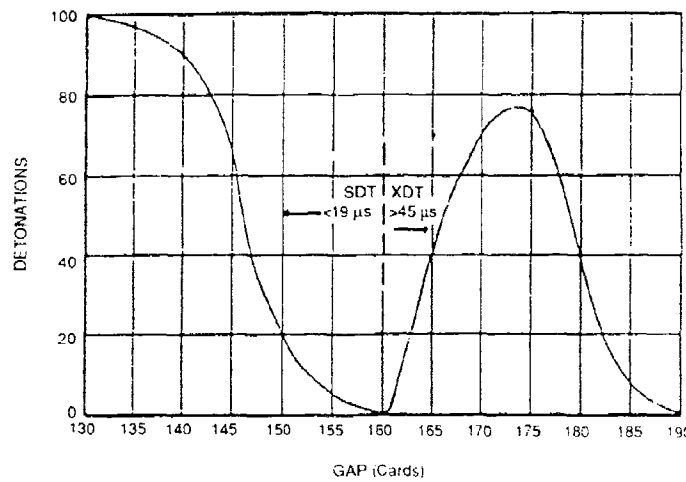

Fig. 83. Card Gap Test Results Showing SDT and XDT (from Keefe, 1981).

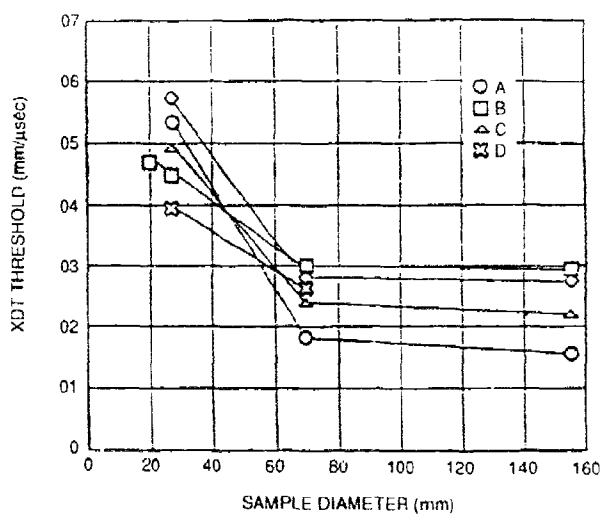

Fig. 84. Dependence of the Velocity Threshold for Observation of XDT on Sample Diameter for Various Propellants A Through E (Blommer as cited in Energetic Materials Hazard Initiation, May 1987).

This XDT phenomena has been observed for some propellants in several relatively small scale tests including the NOL card gap test (Keefe, 1981and Butcher and Isom, 1982), the shotgun test (Blommer as cited in Energetic Materials Hazard Initiation, May 1987 and Butcher and Isom, 1982).

projectile impact (Green, et al, 1981), and piston driven compaction of granulated propellant (Green, et al, 1981). It has been suspected that XDT type reactions may have been involved in some large scale mishaps. In these instances large rocket motors burst, expelling propellant from the motor and causing it to impact on adjacent test cell components/walls. Although the impact levels were not thought to cause SDT, it is thought that XDT occurred, causing widespread destruction.

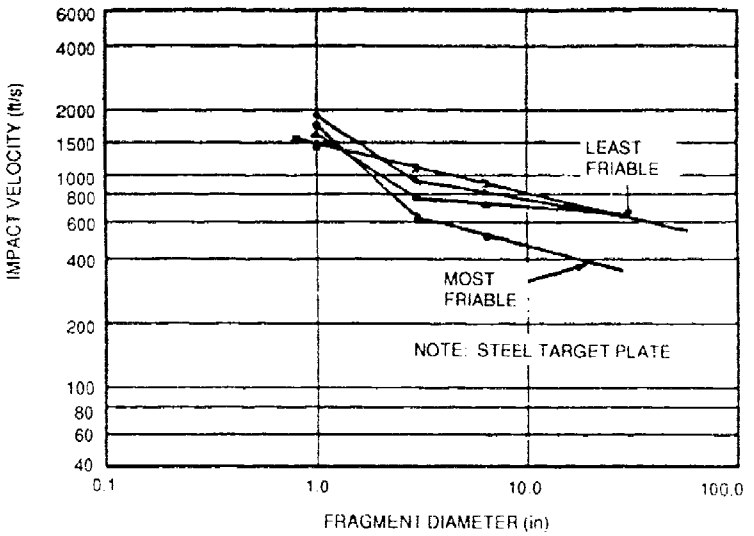

Fig. 85. Effect of Impact Fragment Size on Sensitivity to XDT (from Butcher and Isom, 1982).

5.4.4. Low Velocity Detonation

The preceding sections dealt with the transition from shock, deflagration, or sample break-up and recompression to a detonation (SDT, DDT, or XDT). Another possibility (Low Velocity Detonation) is described in Annex III.

5.5. PENETRATION MECHANICS AND BALLISTIC LIMITS

As was discussed in Chapter 4, if a fragment or bullet does not promptly cause a detonation by the SDT (or DDT or XDT) mechanism then the possibility of an explosion must still be considered. Whether the explosion occurs or not is dependent, as discussed in Chapter 4, on such considerations as ballistic limit (can the fragment/bullet penetrate the motor case), the ignitability of the propellant, the mass burn rate (includes surface regression rate and burn rate) of the propellant, the vent size(s) produced in the penetration and whether the reaction products can be vented rapidly enough to prevent the explosion. Tests in each of these areas are discussed below, but before discussing these individual considerations the scale model rocket motor tests of projectile impact used in the United Kingdom are discussed.

In the UK work on vulnerability of rocket motors to fragment attack has made extensive use of a model scale rocket motor (MSM) (Fig. 86). A standard target cylindrical tube, external diameter 127 mm, length 254 mm, of any desired material, forms the case for the propellant charge. This may be an externally inhibited loose charge, or case-bonded with or without an inhibitor as appropriate; it may be a solid charge, or with any web configuration desired; an igniter may be included. The cylinder is closed by massive steel caps, which overlap the ends of the cylinder and incorporate O-ring seals. These end-caps are connected by four external tie-rods, regularly spaced around the cylinder. Usually an appropriate nozzle and venturi are fitted into one end-cap. Attack is by means of a single 17 g steel cylinder (representative fragment) presented end-on at a point, halfway along the length of the cylinder and midway between two tie-rods; this cylinder is fired from a smoothed-bore 0.5" Browning barrel at one of two velocities, viz 525 ± 25 or 925 ± 25 m/s. Even the lower velocity range has been sufficient to overcome the ballistic limit of the case except in one or two low-temperature experiments on propellant in steel cases. Ignition has otherwise occurred in every trial, even if the fragment has completely traversed the case.. The main assessment of violence of response is from the state of the tube after the event. Instrumentation includes velocity screens to measure the exact impact velocity;

blast overpressure gauges; internal pressure (Kistler) gauges in some experiments, and cine photography at 2000 pps.

The results in terms of tube fragmentation are divided, for the purposes of the research, into six categories, but nearly all are burnings or deflagrations, though a few of the most violent are in the mild explosion category. No detonations have been observed. This test is now standard for qualification of rocket motor propellants in the UK.

The results of nearly 200 MSM experiments, involving 5 propellants (one extruded double-base (EDB), one cast double-base (CDB), one composite modified cast double-base (CMCDB), one elastomer-modified cast double-base (EMCDB), and one hydroxy-terminated polybutadiene (HTPB), all U.K. Hazard Division Class 1.3 compositions) [NOTE: 1.3 hazard classification by United Kingdom RARDE Scaled Vessel Test, see page 59. France and the United States use card gap tests to determine hazard classification of propellants. The Netherlands use the TNO tube test], 6 tube materials (mild steel, aluminum alloy, fiberglass, steel strip-laminate, carbon-fibre reinforced plastic (CFRP), Kevlar-overwrapped light alloy) and a range of temperatures may be summarized as follows:

1. Increasing the frangibility of the propellant (without temperature change) tends to increase violence of response (EDB>CDB>EMCDB; CMCDB>HTPB).

2. Increasing calorimetric value of propellant tends towards more violent response.

3. Making cases able to vent more quickly tends to reduce violence of response, e.g., Kevlar-overwrapped light alloy containing HTPB. Steel strip-laminate is not however very effective.

4. An inhibitor/insulator layer (as opposed to simple gluing) may reduce violence of response for case-bonded charges (observed for CMCDB where case-bonding is probably improved; no change for HTPB where use of glue is standard).

5. The presence or absence of an igniter is unimportant; even hitting the igniter with the fragment had no effect on the result.

6. For CMCDB and HTPB (case-bonded) more violent responses are obtained with star-centered conduit charges than with solid charges; for EDB (loose, inhibited) there is little difference.

7. A fragment which completely traverses the MSM gives a less violent response than a somewhat slower one which remains inside.

8. Lowering the temperature produces a sharp increase in response as the temperature passes through a value related to (but somewhat above) the glass transition temperature for the propellant under test (as measured at low strain rates).

These results in general underline the importance of crack-propagation (and branching) in enhancing the violence of the response (nos. 1,8); the role of support of the charge in reducing either crack propagation or the effectiveness of cracks in increasing the burning surface (no. 6, EDB charges being loose and being very brittle perhaps shatter in any case); the more damaging effect of the use of higher-energy propellants (the higher flame temperatures producing higher gas pressure in the MSM - no. 2); the importance of effective case-bonding (no. 4); and the value of quick venting in reducing the response (nos. 3,7).

No standardized test procedure is available in the UK to test stress/strain characterization under the high strain rate conditions involved in fragment attack; the "glass temperature" is definitely a function of strain rate and also probably of extensibility. Work is in progress on crack-propagation and is expected to be extended to crack-branching, which is probably equally important for propellant fragmentation.

Projectile Attack Full-Scale Trials

The MSM work described above has been followed up by a series of trials using single projectiles, ranging from 3.1 g steel cube, through 7.62 mm bullet, 17 g steel cylinder presented end on (as in the MSM work) and 0.5" AP bullet (single shot) to 20 mm HE to attack NATO Bullpup motors (which contain 49 kg low-performance CDB propellant) withdrawn from service. The results, assessed in terms of case damage, showed increased response with increasing projectile kinetic energy and decreased response with increasing presented area of the projectile (i.e., with projectile entry hole size). (The latter indicates the importance of venting in the area of impact, while the former presumably shows the importance of damage to the charge in this situation, where none of the projectiles traversed the motor completely.)

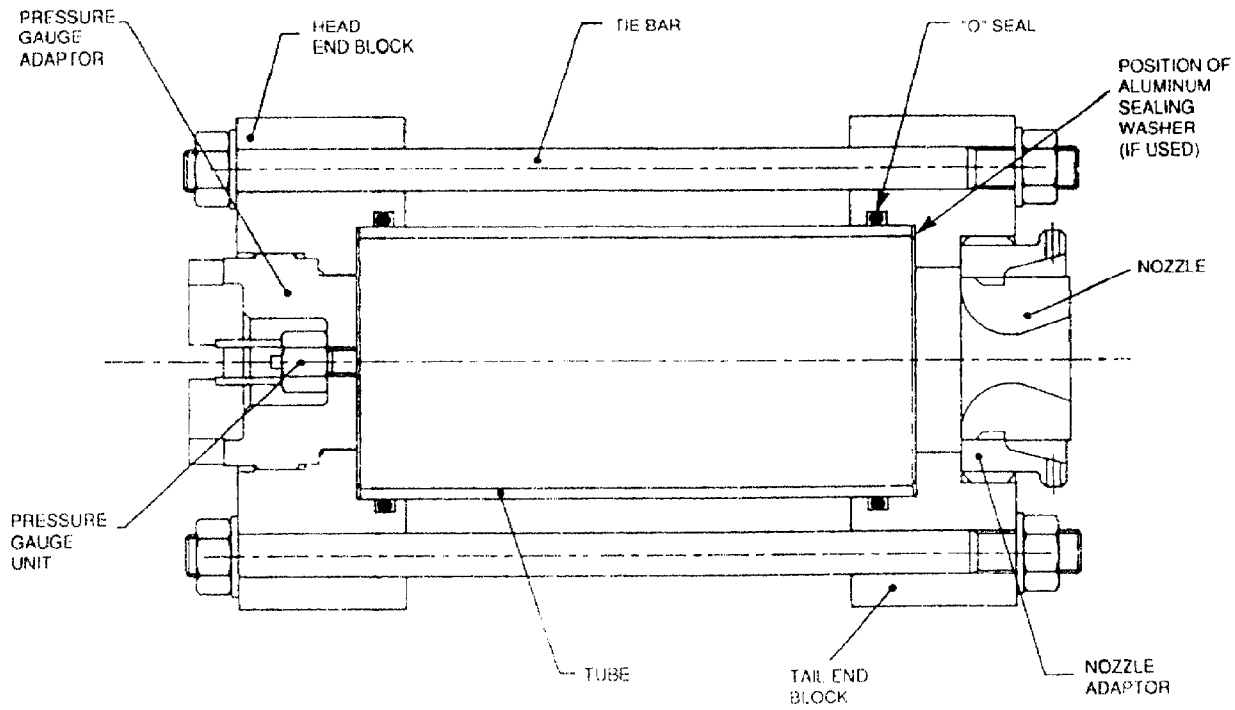

MODEL SCALE ROCKET MOTOR FRAGMENT ATTACK

The exception was the 20 mm HE where there was little damage to the case other than that in the immediate neighborhood of the point of impact, where the damage was sufficient to provide more than adequate venting. No detonations were observed. Attack by HE rounds or motors containing more energetic propellants would certainly raise the possibility of detonating the propellant. This would depend critically on whether the diameter or characteristic dimension of the projectile were greater or less than the critical diameter of the propellant (see Fig. 11).

Some trials with .30 caliber ball, .50 caliber ball, .50 caliber API, 20 mm API, and 23 mm HEI-T against US Class 1.3 and Class 1.1 (see previous Note) composite propellants in a 20 cm diameter motor are reported in AGARD Conference Proceedings No. 367, p. 2-2. These resulted in ignition only (the Class 1.1 propellants giving less violent fires) except with the 23 mm HEI-T, which detonated the Class 1.1 compositions.

The relevance of the MSM work to full scale motor vulnerability is accepted by the UK government for purposes of propellant qualification on the basis of evidence from full scale bullet attack trials (mostly single-shot 0.5 inch AP). There is limited UK evidence that with fairly large motors (3 m long, propellant as 186 kg) single bullet attack gives more violent response at the head end than at the nozzle end or half-way along the motor. This is not unexpected in terms of confinement of the propellant. There has also been a little work in the UK on the effect of multiple attacks (burst of three 0.5" AP bullets), the results suggesting that much greater violence can be developed than with a single shot. Trials have also been carried out against the NATO Bullpup motor in its carrying box, and the effect of venting the box in mitigating the response has been demonstrated.

Investigators in the US are measuring the ballistic limits of various case materials (steel, aluminum, and composite) and various thicknesses backed by simulated propellant subjected to various fragment masses, velocities, angles of obliquity, and fragment shape.

Ballistic Limit of Case. A key consideration in Fig. 13 was whether a fragment of a given mass and orientation has sufficient velocity to penetrate the motor case. Sewell and Graham have presented a simple penetration equation of the form

$$T_c \sec\theta = \frac{K m v_i}{A}$$

where

T_c = thickness of case which will be perforated in the impact
θ = obliquity angle (angle of incidence)
K = a materials property constant of the case (see Table 18)
m = fragment mass
v_i = impact velocity
A = effective frontal area of fragment

For the various systems of units, the constants in Table 18 can be applied to the above equation

Table 18. Ballistic Limit Coefficient for Two Steel Case Materials.

Variable	Units		
	Engineering	CGS	SI
q	degrees	degrees	radian
m	grains	grams	kg
v_i	ft/s	cm/s	m/s
A	in^2	cm^2	m^2
T_c	in	cm	m
Value of K			
1. Mild Steel	1.90×10^{-7}	1.58×10^{-6}	1.58×10^{-3}
2. Brinell 300 steel	1.47×10^{-7}	1.22×10^{-6}	1.22×10^{-3}

NOTE: When T_c is equivalent to the case thickness, the velocity is the ballistic limit for the case.

3.6 ELECTROSTATIC DISCHARGE (ESD)

Several parameters were identified in the ESD hazard protocol, as being necessary to being able to predict ESD sensitivity (Covino and Hudson, 1990; and Covino and Dreitzler, 1988). These include volume resistivity, dielectric breakdown, and dielectric constants. This section describes how these quantities are measured, as well as discussing a resistor-capacitor (RC) discharge apparatus and the percolation theory.

5.6.1. Resistivity Measurements as Applied to ESD

French experiments suggested that propellant volume resistivity (ρ_v) as a function of temperature behavior may be important in the ESD sensitivity of a propellant. For all the compositions tested by the French, it was found that the propellant volume resistivity measurements from -40 to +80°C (-40 to +176°F) could show one of three different laws of resistivity versus temperature.

When plotting the ln (ρ_v) versus 1/T for propellant samples, the French found all of the three behaviors shown in Fig. 87. Based on semiconductor theory, the existence of two straight intersecting lines points to a change in the type of conduction. It was observed that the compositions which react to capacitive discharges follow a type I behavior (i.e., the ratio of slopes, M_1/M_2, is greater than 1) whereas the propellant compositions which do not react have a type II or III behavior (i.e., M_1/M_2 is less than or equal to 1).

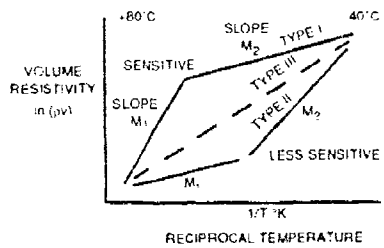

Fig. 87. Plot of the ln(ρ_V) Versus 1/T °K Showing the Three Types of Behavior.

In the U.S. instrumentation to measure both volume resistance and surface resistance of propellants and propellant ingredients as a function of temperature and relative humidity has been built. Temperatures ranging from -30°C to 100°C (-22°F to 212°F) can be achieved with a Tinney T and H Jr. chamber. Surface and volume resistance on propellant samples as small as 3.43 cm can be measured on either copper or stainless steel electrodes. A Keithley Model 617 digital electrometer capable of reading 10^{-15}A is used to make the current measurements. Applied voltages ranging from 45 to 2,000 V can be used. The determination of surface and volume resistivities consists of measuring surface and volume resistances followed by calculations of the corresponding resistivities with the use of known sample and electrode dimensions. The volume resistivity is defined as the ratio of potential gradient parallel to the current in the material to the current density in units of ohm m (Keithley Instruments, 1984; and ASTM, 1983). The surface resistivity (ρ_S) is defined as the ratio of potential gradient parallel to the current along a surface to the current per unit width of the surface in units of ohm m (Keithley Instruments, 1984; and ASTM, 1983).

Figure 88 shows electrode configuration to measure surface resistance. The measurement is performed by applying a set voltage on the surface of the sample and obtaining a current reading. The following equation is used to calculate the surface resistivity (ρ_S):

ρ_S = K_S*(V/I) (Ω)
V = Voltage (volts)
I = Current reading (amperes)
K_S = A geometrical factor arising from electrode geometry (unitless)

The geometric factor is an effective perimeter of the guarded electrode divided by the gap between the guarded electrode and the guard.

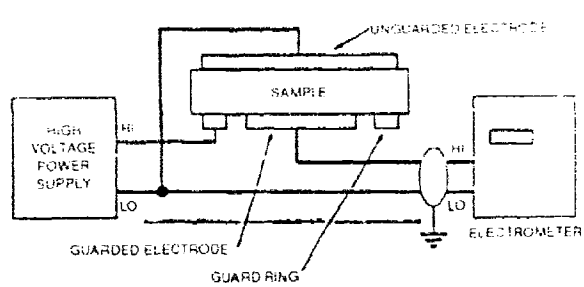

Fig. 88. Surface Resistivity Electrical Diagram (sample is disk shaped).

Figure 89 shows electrode configuration to measure volume resistance. The measurement is performed by applying a set voltage through the sample and obtaining a current reading after a set time interval of one minute. The following equation is used to calculate volume resistivity (ρ_v):

ρ_v = K_v*(V/I), (Ω-cm)
V = Voltage (volts)
I = Current reading (amperes)
K_v = A geometric factor arising from electrode geometry (cm)

The geometric factor is an effective area of measuring electrodes divided by the sample thickness.

In order to calculate the geometric factors, K_s and K_v, specific electrode dimensions and sample thickness are needed. Figure 90 illustrates the electrode geometry used at NWC. To calculate the surface geometric factor, K_s, the following equation is used:

$$K_s = P/g = (\pi D_0)/g$$

where:

P = the effective perimeter of the guarded electrode for the particular arrangement used (m)
g = gap (m)
D_0 = See Fig. 90

To calculate the volume geometric factor, K_v, the following equation is used:

K_v = A/t
A = $[\pi(D_1 + g)^2]/4$
D_1 = Diameter of inner ring on Fig. 90

where:

A = the effective area of the measuring electrode for the particular arrangement used (m^2)
t = the average thickness of the sample

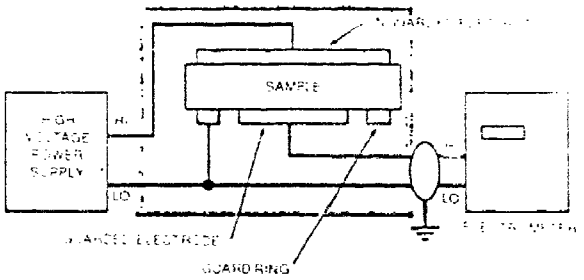

Fig. 89. Volume Resistivity Electrical Diagram.

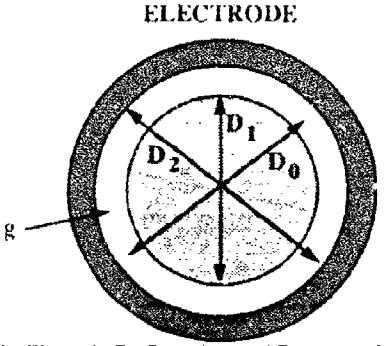

Fig. 90. Shows the Electrode Configurations and Parameters Needed for the Geometric Calculations for Surface and Volume Resistivity.

Figure 91 shows surface resistivity data versus time for an HTPB binder propellant containing ammonium perchlorate and aluminum. The surface resistivity increases exponentially as a function of time.

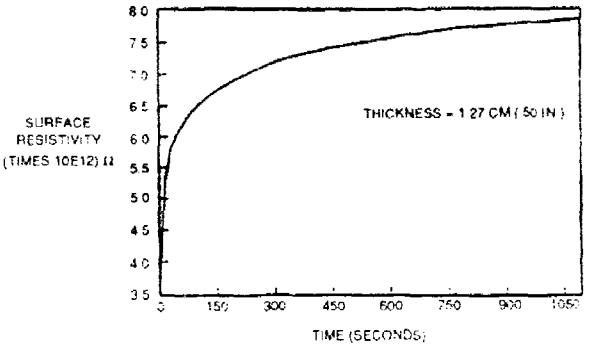

Fig. 91. Surface Resistivity Vs. Time at 69.1°F(20.61°C), 23.3% RH and 100 V.

Figure 92 shows volume resistivity data for the same propellant. The overall behavior for the volume resistivity data is also an exponential rise as a function of time.

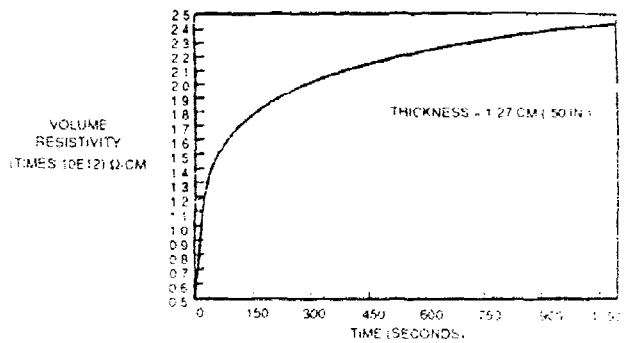

Fig. 92. Volume Resistivity Vs. Time at 69.5°F (20.83°C), 22.7% RH and 100 V.

Figures 93 through 96 illustrate $\ln(\rho_V)$ versus 1/T for the same propellant. This data is presented at 100V (after 1 minute) and 500V (after 1 minute) and at sample thicknesses of 0.25" (0.634 cm) and 0.50" (1.27 cm).

It should be noted that the data reported in these graphs were taken after 1 minute. From Fig. 92 we can see that within a few seconds these materials reach a maximum volume resistance and at 1 minute the propellant is totally charged. However, the time at which maximum volume resistivity is reached is material dependent and can change from one propellant to another.

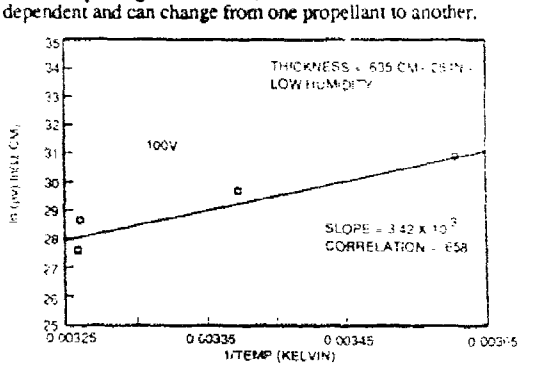

Fig. 93. Volume Resistivity Vs. Temperature For Data Taken After 1 Minute, at 100 V and Low Relative Humidity.

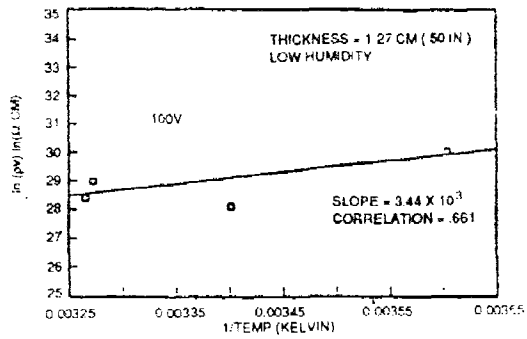

Fig. 94. Volume Resistivity Vs. Temperature For Data Taken After 1 Minute, at 100 V and Low Relative Humidity.

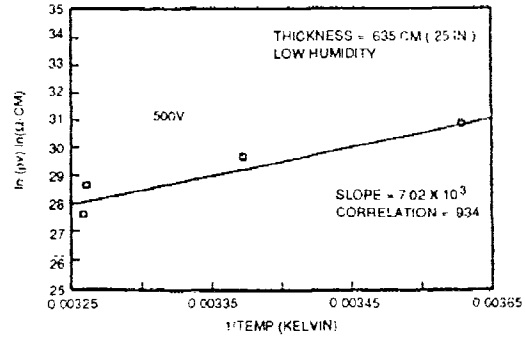

Fig. 95. Volume Resistivity Vs. Temperature For Data Taken After 1 Minute, at 500 V and Low Relative Humidity.

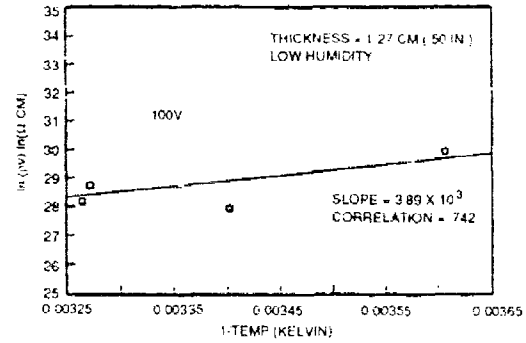

Fig. 96. Volume Resistivity Vs. Temperature For Data Taken After 1 Minute, at 500 V and Low Relative Humidity.

Overall the propellants display a linear dependence when plotting $\ln(\rho_v)$ versus temperature.

5.6.2. Dielectric Breakdown $\left(\frac{dE}{dt}\right)$

The dielectric breakdown of a material is defined as the failure of a dielectric under electric stress. The dielectric breakdown of a material is measured by following the ASTM D149 procedure (ASTM, 1981; and IEEE Standard, 1969).

In summary, the dielectric breakdown data presented in this paper was obtained by applying a ramped DC voltage to the propellant sample and watching the material's electrical response. The voltage is increased from zero at approximately 600 volts per second until dielectric failure of the test specimen occurs.

A schematic of the test circuit used at NWC is shown in Fig. 97. The test voltage applied can be programmed to increase from 0-40 kV at any predetermined rate.

Dielectric breakdown data was obtained at different temperatures and at sample thickness of approximately 0.5" (1.27 cm) and 0.25" (0.635 cm). Sample data is tabulated in Table 19. As can be seen from the data presented, the breakdown voltage is virtually independent of temperature. The data shows that both propellants, although different in composition break down at the same voltage. It is planned to look at this with more sensitive electronic as well as monitor current during breakdown to see if these data are real.

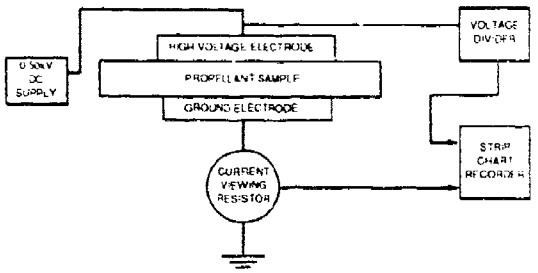

Fig. 97. Dielectric Breakdown Measurement Circuit. Voltage application can be ramped at a variety of rates from 0-40 kV. Measurement can be performed as a function of temperature and relative humidity. During the dielectric breakdown, measurement of applied voltage on the sample and current going through the sample are recorded.

Table 19. Dielectric Breakdown Data*.

Temperature (RH Low - < 30%)	Sample Thickness	Measured Breakdown Voltage	Breakdown Voltage per cm
40°F	1.301 cm	11 kV	8.5 kV
40°F	0.663 cm	5 kV	7.5 kV
70°F	1.202 cm	15 kV	12.5 kV
70°F	0.712 cm	8 kV	11.2 kV
90°F	0.639 cm	5 kV	7.8 kV
90°F	1.328 cm	12.5 kV	9.4 kV

*Breakdown voltage ranges presented in this table are within the detection limit of our present instrumentation.

5.6.3. Dielectric Constant Measurements

Dielectric properties may be defined by the behavior of the material in a parallel plate capacitor. This is a pair of conducting plates, parallel to one another and separated by a distance, d, that is small compared with the linear dimensions of the plates. With a vacuum between the plates, the capacitances C_o is defined as:

$$C_o = \frac{e_o A}{d}$$

where e_o is the permittivity of free space, 8.854×10^{-12} Fm^{-1}, and A is the area of the plates. Since e_o, A, and d are constants the capacitance depends only on the dimensions of the capacitor. On applying a potential difference, V, between the plates, a quantity of charge, Q_o, is stored on them, given by:

$$Q_o = C_o V$$

If a dielectric substance is now placed between the plates and the same potential difference applied, the amount of charge stored increases to Q_1 and the capacitance therefore increases to C_1. The dielectric constant or relative permittivity, ε', of the dielectric is related to this increase in capacitance by:

$$\varepsilon' = \frac{C_1}{C_o}$$

The magnitude of e' depends on the degree of polarization or charge displacement that can occur in the material. For details on dielectric theory see Smyth (1955), West (1984), and ASTM (1971).

The dielectric constant of propellants and propellant ingredients as a function of frequency, temperature, and relative humidity is an important material property to obtain. When looking at ESD sensitivity of solid propellants the dielectric constant gives an indication of the energy storage capability as well as energy discharge of the propellant. The following schematic, Fig. 98, illustrates how the measurement is made. Two copper descs (76 mm diameter) form the capacitor. In order to compensate for the fact that the propellant samples are not 100% parallel, the plates can move up and down and pivot from side to side. Details of the dielectric constant measurements can be found in Covino and Hudson (1987). A summary of the dielectric constant data for the propellant at different sample thicknesses is shown in Figure 5.84.

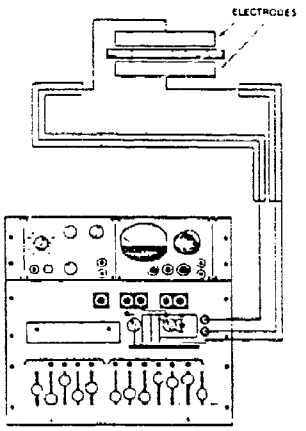

Fig. 98. Dielectric Constant Measuring Circuit. A capacitance measuring assembly. Measurements can be made from 50 Hz to 10 kHz. Measurements can be performed as a function of temperature and relative humidity.

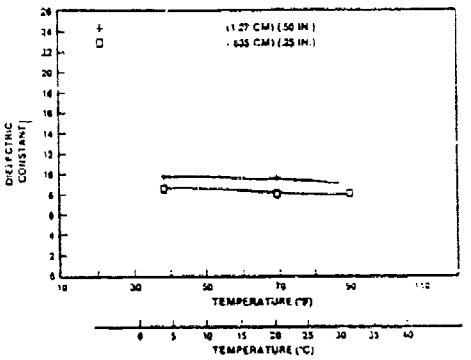

Fig. 99. Dielectric Constant Vs. Temperature at 1 kHz.

5.6.4. The RC Discharge Test Apparatus

ESD is a phenomenon that arises by the discharge of static electricity across a conductive path from a region of higher potential to a region of lower potential. The "French-like" ESD test is an RC discharge through representative propellant samples with cylindrical geometry of 9.0 cm diameter and 10.0 cm long. "Go" or "no/go" results as a function of temperature and humidity can be obtained from such test. The basic features of the RC discharge test are:

1. A known energy is applied through a point brass electrode and allowed to dissipate through the propellant to a plate brass electrode.

2. A typical test series is 30 consecutive discharges on each of three identical specimens at 15.6J (30 kV and 34.7 nF).

If any of the 90 discharges results in "cracking", "popping", smoke or fire, then the formulation is considered sensitive to ESD.

Figure 100 shows a schematic of the electrostatic discharge test at NWC. It should be noted that electrode contact to the propellant is ensured by slightly forcing the tip of the brass electrode into the propellant (approximately 1 mm) and by the use of a conductive silver paint to contact the plate electrode with the propellant. Figure 101 illustrates an electrical circuit representation of the NWC ESD RC discharge test apparatus.

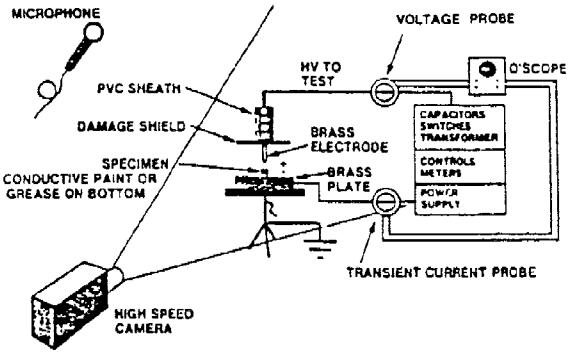

Fig. 100. A Schematic of the NWC Electrostatic Discharge Apparatus Modeled After the SNPE Design.

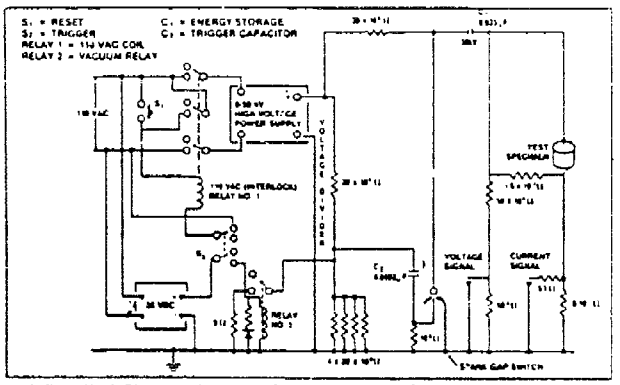

Fig. 101. A Detailed Circuit Diagram of the NAVWPNCEN ESD RC Discharge Apparatus.

It should be noted that a voltage range of 0-40 kV, currents up to 2.0 mA, and a maximum capacitance of 35 nF are available on this instrument. Energies of up to 15.6J can be stored into the capacitors and then allowed to discharge through the propellant.

Table 20 lists the capacitors and the theoretical maximum energy for each capacitor, calculated from $E = 1/2\ CV^2$.

Table 20. Capacitors and Energies Available on the NWC Electrostatic Discharge Apparatus.

General Specifications	
Voltage Range	0-30 kV
Current Range	2mA Max
Fixed Capacitors	4.7nF
	10nF
	20nF

Capacitances (nF)	4.7	10	14.7	20	24.7	30	34.7
Energies (J)	2.1	4.5	6.6	9	11.1	13.5	15.6

Electrostatic discharge testing was carried out on the propellant previously discussed as a function of temperature. Propellant sample sizes averaged 9.02 cm in diameter by 10.16 cm tall (3.55 in. diameter x 4.0 in tall). Data for these experiments are summarized in Table 21 and in Fig. 102. From the data presented, it can be seen that the propellant is ESD sensitive.

Table 21. Electrostatic Discharge Data on Propellant, RC-Discharge Test.
(90 mm diameter x 100 mm high, right cylinders were used)

Temperature °F	Temperature °C	Relative humidity, %	Energy, Joules	Reaction
-17	-27.2	<30	15.8†	Go 4 out of 5 shots were positive.
-17	-27.2	<30	15.8†	Go All 30 shots were positive.
-10	-23.3	<30	15.8†	Go All 30 shots were positive.
-10	-23.3	<30	15.8†	Go 1 out of 1 shot was positive. Sample moved away from electrode - test terminated
2	-16.7	<30	9.0¶	No Go
7	-13.9	<30	15.8†	Go 1 out of 1 shot was positive. Sample ignited and continued to burn.
20	-6.7	<30	15.8†	Go 4 out of 30 shots were positive.
30	-1.1	<30	15.8†	Go 3 out of 30 shots were positive.
40	4.4	>30	15.8†	Go 1 out of 10 shots were positive. Sample moved away from electrode - test terminated.
70	21.1	<30	9.0†	Go Small cracks were visible at end of test.
120	48.9	>30	15.8†	No Go

† 0.035 μF, 30 kV ¶ 0.02 μF, 30 kV

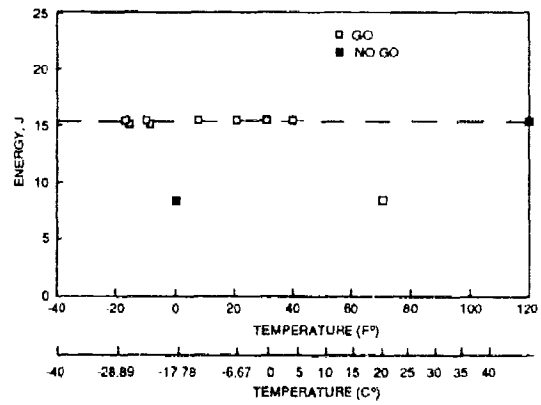

Fig. 102. RC Discharge Test Results for Propellant.

5.6.5. Percolation Calculations as Applied to ESD

In an attempt to understand why certain propellants were ESD sensitive and others were not, the French implemented the Percolation Theory (Hammersley and Handscomb, 1964; Hammersley and Broadbent; and Hammersley). A factorial examination of the propellant active ingredients was carried out. The results of such investigations showed that the aluminum particle size and the electrical properties of the binder (binder = prepolymer + miscellaneous additives) were major components in determining the propellant electrical properties. From experimental obse:vations of discharge tests, the French found that, at a constant aluminum concentration, as the particle size decreases (i.e., increase in number of aluminum particles) propellant sensitivity to capacitive discharge increases.

Percolation, as theoretically defined, is independent of the applied voltage and allows (for a given conducting and insulating particle system) determination of a critical ratio between conducting and nonconducting particles (N_c/N_i), above which, the entire system is fully conducting. In the case of a composite propellant, it does not seem possible to obtain such a level exactly, because the oxide-covered aluminum particles are working as insulators, although conductive inside.

Recently at SNPE, Kent and Rat (1980) indicated that they have adopted a refined "P breakdown percolation" coefficient equation which so far proves to be more discriminating. The improved percolation breakdown coefficient is defined as follows:

$$P_{Imp} = \left(\frac{\rho_n}{\rho_c}\right) \cdot \left(\frac{\%\,C}{\%nf}\right) \cdot \left(\frac{d_{nf}}{d_c}\right)^3 \left[\frac{\rho_b}{\%_b}\left(\frac{\%\,C}{\rho_c} + \frac{\%n}{\rho_n}\right) + 1\right] \rho_{vb}$$

where:

ρ_n = density of nonconducting particles
ρ_c = density of conducting particles
% C = wt. percent of conducting particles
%nf = wt. percent of finest fraction of nonconducting particles
d_{nf} = diameter of finest fraction of nonconducting particles
d_c = diameter of finest fraction of conducting particles
ρb = density of the binder
$\%_b$ = wt. percent of the binder
%n = wt. percent of all nonconducting particles
ρ_{vb} = volume resistivity of the binder in Ω-m

It was found by the French that if P_{Imp} was greater than 10^{10} Ω-m and if weight percentage of conducting particles was greater than 15% the propellant was considered to have an ESD hazard.

A sample calculation for P_{Imp} using a hypothetical propellant composition and particle sizes is performed below in an attempt to clarify the calculation and to point out some of the inherent assumptions which are made. Table 22 lists the data used for this sample calculation.

Table 22. Hypothetical Propellant Composition.

		Al	AP	HTPB
% C	wt %	10	70	20
d_c	diameter of particles	10 mm	20 mm	--
ρ_c	density (g/cc)	2.7	1.95	0.93
ρo_b	volume resistivity (W-m)	--	--	3×10^{10}
	Initial assumption made: 1. Al is the only conducting species 2. AP is the only nonconducting species			

$$P_{Imp} = \left(\frac{1.95\ g/cc}{2.7\ g/cc}\right)\left(\frac{10}{70}\right)\left(\frac{20\ \mu m}{10\ \mu m}\right)^3\left[\frac{0.93\ g/cc}{20}\left(\frac{10}{2.7\ g/cc} + \frac{70}{1.95\ g/cc}\right) + 1\right] \cdot 3 \times 10^{10}\ \Omega\text{-m}$$

$$P_{Imp} = 7.04 \times 10^{10}\ \Omega\text{-m}$$

Since this value is greater than 10^{10} Ω-m, if the % of conducting particles is less than 15% this propellant would not be considered sensitive to ESD.

If a small change in the aluminum particle size (10 to 40 μm) was made to this theoretical propellant formulation, the P_{Imp} would calculate to be 1.10×10^9 Ω-m. Since this value is less than 1×10^{10} Ω-m, this propellant would be considered less sensitive to ESD. For the propellant previously prescribed $P_{Imp} = 1.29 \times 10^{12}$ Ω-m.

It should be noted that the percolation breakdown coefficient calculation does not include many critical propellant parameters and therefore cannot describe the propellant system accurately. Among some of these parameters are: aluminum particles which are assumed to be conducting have a highly resistive oxide coating and particle shapes are not accounted for. The $P_{critical}$ has been simply determined by experimental results. There is not yet a physical interpretation of why it was 10^{10} Ω-m for the critical P breakdown coefficient. Furthermore, today's solid rocket propellants are quite complex. For example, they might contain two or more nonconducting species (i.e., AP and AN) which have fine particles, thus having different contributions to the percent of nonconducting particles. In the percolation equation, all the nonconducting particles are lumped together except for the finest fraction of nonconducting particles. Conducting species can also be of a different nature and

thus have different chemical and physical properties. For example, both aluminum and carbon which are highly conductive are common propellant additives. However in the percolation equation all the conducting species are treated uniformly. Lastly, the binder itself is a complex network, having different chemical species with different chemical properties. However, it too is treated as one entity in the percolation calculation. In the percolation equation, r_{vb} (volume resistivity of the binder) is a term which most dramatically affects the magnitude of the P factor. This term is measured experimentally and it is temperature- and humidity-dependent as well as time-dependent, thus quite prone to experimental inconsistencies.

However it is not claimed that the equation gives an exact treatment. It only gives a preliminary indication of whether an ESD hazard might be expected, which is useful when new propellants are being designed. The value of P_{Imp}, in conjunction with the percentage of conducting particles gives valuable guidance.

5.7. SHAPED CHARGE JET

5.7.1. Description of a Shaped Charge Warhead

A modern rotationally symmetric shaped charge consists of a high-performance high explosive charge which at the end facing the target usually has a conical cavity (Fig. 103). This shaped cavity, or hollow space, inspired the name of "shaped charge" or also "hollow charge," for this type of explosive body. Nowadays, this cavity is usually lined with an axially symmetric layer of copper having a thickness of, say, 2 mm. This type of charge is then termed a "lined shaped charge."

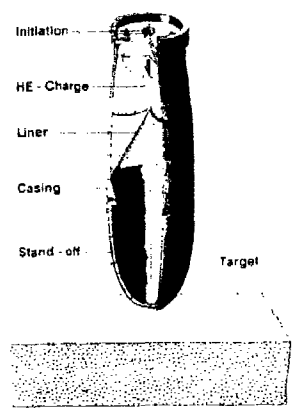

Fig. 103. Shaped Charge Components.

Precisely axial initiation is essential for high penetration performance from a rotational symmetric shaped charge; this initiation is achieved by a suitable booster charge. Today, there is always a space in front of the cavity, because the shaped charge reaches its highest penetration performance at a certain stand-off distance from the target. The initiation elements, the high explosive charge, the liner, and the space are all held together by a casing.

Penetration capability is considerably reduced if the rotational symmetry of even one of these four fundamental parameters (point of initiation, high explosive charge, liner, or casing) is disturbed. In such cases one will obtain a cutting action with less axial penetration. So-called cutting charges, or linear shaped charges, are often used as flexible linear shaped charges (FLSC) in controlled cutting of structure elements and large charges in the demolition of steel girders and reinforced-concrete bridge members.

5.7.2. The Phenomenology of the Shaped Charge (Held, 1981a)

A cylindrical high explosive charge placed directly (with no stand-off distance) upon a thick steel block will, on detonation, create a shallow depression in this target block, and the width of the depression is about the same as the diameter ("caliber") of the charge (Fig. 104 - left picture). When the charge has a conical cavity at the end facing the target, the result is, surprisingly enough (von Förster, 1883), a crater about 1 caliber deep, although the amount of high explosive is now less than with a full cylinder (Fig. 104 - center picture). The deeper, though narrower hole in the target block is produced precisely opposite the cavity in the explosive charge. About the same time, Munroe (1888a

and 1888b) also discovered the effect of hollow-charge once more. Munroe not only made imprints of elm and maple leaves in steel plates to decorate the fireplace at the Cosmos Club, but he also tied sticks of dynamite around a tomato can and blew a hole in a safe door. Photographs of the results were published in Popular Science in 1900 (Munroe, 1900).

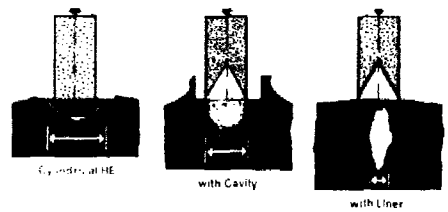

Fig. 104. Concentration Effect of Unlined and Lined Shaped Charges Compared to a Cylindrical High Explosive Charge.

Comparing this effect with that of a lined shaped charge (Fig. 104 - right picture) one will find a crater which now is 2 to 3 calibers deeps, although its diameter is now still smaller than that produced by the solid cylinder of the unlined shaped charge (Thomanek, 1938).

An engineer familiar with general demolition blasting, but not having any particular knowledge of the shaped charge effect, would have expected increasingly smaller penetrations. For one thing, the amount of explosive has become less than in the unlined shaped charge, for another, the center of gravity of the charge has moved away from the target somewhat, and thirdly the liner material shields the cavity from the effects of the pressure. The increase in depth of penetration in spite of all this is surprising indeed and goes to show that special effects have come into play.

A comparison of the crater-diameters related to the various configurations of charges indicates that the introduction of a cavity, and employment of a liner have caused a focusing effect, resulting in an enhanced depth of penetration at the expense of the width of the crater.

Measurement of the time history of cratering (Held, 1981b) by means of electrical make-contact probes installed in the target gives a time-versus-distance diagram of cratering, such as the one shown in Fig. 105. A time of approximately 400 μs is needed to perforate approximately 600 mm of RHA. This means that the mean velocity of cratering is 1.5 mm/μs, or 1500 m/s. This astonishingly high mean cratering velocity can be as high as about 4000 m/s at the beginning of the penetration process. Such a high cratering velocity indicates that the perforation of RHA plates by means of shaped charges cannot be a thermal process, because the phenomena of heat conduction and melting could not possibly propagate at such a high speed.

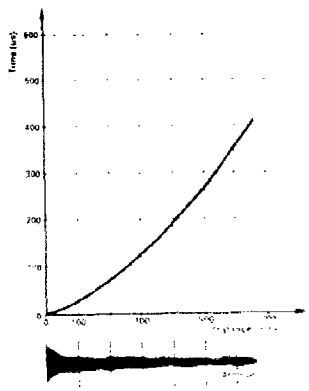

Fig. 105. A Shaped Charge Acts About 40 Times Longer Than a HE Charge in Contact.

On the other hand, the detonation head of a detonating cylindrical high explosive charge of the same diameter, in contact with the target plate, would act only for about 10 µs (Cook, 1959). This means that a shaped charge acts against a target about 40 times longer than a cylindrical charge in contact would do.

The "concentration," and the "prolonged duration" of the effects appear to be two features that are essential for the high penetration capability of shaped charges.

What is known as the stand-off curve is another characteristic feature the shaped charge (Fig. 106) (Held, 1983a). The depth of penetration increases with increasing distance from the shaped charge base to the target, up to a distance of 4 to 8 base diameters (calibers); but it decreases again when the distance is increased further. This phenomenon shows that there is an agent transferring the effect between the shaped charge and the target and causes maximum penetration at a certain stand-off distance.

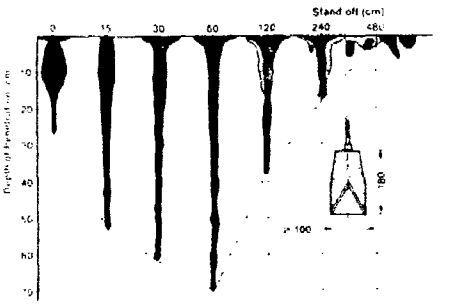

Fig. 106. Typical Stand-Off Curve of a Shaped Charge.

This transfer agent can be recorded and analyzed with the aid of X-ray flash photography. Although the light flash of a detonation is extremely bright, the reaction products obscure the optical view, but X-ray-flash photography permits the observation of the deformation of the shaped charge liner and the formation of a jet from it under the high pressure of detonation. Figure 107 shows a sequence of flash radiographs taken at different times after the arrival of detonation at the tip of the conical liner and X-ray flash exposure.

One can clearly see the copper liner being accelerated towards the axis and collapsing into a lump spread out along the axis. From this lump emerges a "shaped charge jet" made up of some 10 to 20% of the mass of the liner, attaining tip velocity of over 9000 m/s with copper as a liner material. The remainder of the lump, which constitutes the balance of the mass of the liner, and which is termed the "slug," has a velocity of the order of 300 to 1000 m/s. This means that there is a gradient in velocity from the tip of the jet to the slug, and this gradient leads to a continuous lengthening of the jet in flight.

The three shaped charge phenomena mentioned above can be explained with the aid of this flash X-ray sequence (Fig. 107):

- concentration effect by the acceleration of the liner towards the axis and the resulting formation of the high-velocity jet,
- long-lasting action through the long jet (in effect a long projectile) interacting with the target for an extended period of time,
- greater effect at longer stand-off distance, where the jet has become longer under the influence of its own velocity gradient.

Unfortunately, the copper jet does not lengthen indefinitely, but will break up into particles after a certain time, or within a certain interval of time, depending on the liner-material and on several other, but less important parameters (Fig. 108). The shaped charge jet is then called a "particulated" jet.

Before this breakup, copper-like materials undergo an elongation more than 1000%. This is a phenomenon that has not been explained up to now: why does copper, which in static tests gives an elongation of not more than 80%, undergo elongations that are 10 to 15 times greater, under conditions of such extreme mechanical loading?

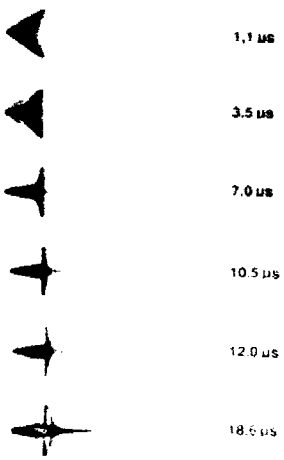

Fig. 107. Flash X-Ray Pictures of Jet Formation, Which Show the Concentration Effect and Formation of a Long Jet at Longer Distances.

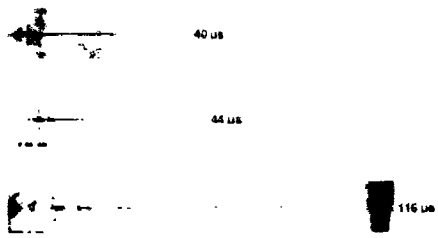

Fig. 108. The Stretching, Initially Continuous Jet, Particulates Only Once.

Particulation occurs only once. Thereafter, the length of the jet or, more precisely, the sum of the lengths of the individual jet particles remains constant. From particulation onwards, the depth of penetration of the shaped charge jet should actually remain unchanged, to a first approximation. However, aligning the shaped charge jet precisely along the charge axis is one difficulty, and further problems are the tumbling and transverse drift effects caused by shear fracture during the particulation, which cause the jet, or the jet particles, to deviate from the axis. And as the distance from the shaped charge to the target increases, these angular deviations lead to even greater transverse deviations that will cause the jet or its particles to hit the walls of the hole being generated, if the hole diameter is small. With the high impact velocities involved, the jet portions or particles concerned will become pulverized on impact and will therefore no longer contribute to an increase in penetration. This explains the ever decreasing penetration performance as the stand-off distance increases beyond the optimum value.

When a continuous and still-coherent shaped charge jet hits a target plate, the stagnation pressure produced as a result of the velocities of several 1000 m/s will be of the order of more than 100 GPa, or 1 Mbar, or 10.000 Kp/mm^2. Such a pressure by far exceeds the strength of even the toughest, armor steel. An impression of the penetration of a continuous and coherent shaped charge jet into a DURAL block can be gathered from Fig. 109. Particular mention should be made of the narrow hole through which the jet must pass without touching the walls in order to be able to convert its energy into further penetration.

A particulated shaped charge jet can also have a good penetration performance into a target, if the particles are well-aligned, so that they will all arrive at the crater bottom (Fig. 110). In this case, each individual jet particle makes its own bubble-shaped hole.

The jet parameters, e.g., jet tip velocity, mass, particulation time, diameter, etc., depends on a lot of design rules and cannot be described here. Generally mass, particulation time and diameter of a jet

is a linear function of shaped charge diameter and the tip velocity which is strongly correlated with the liner angle (Fig. 111).

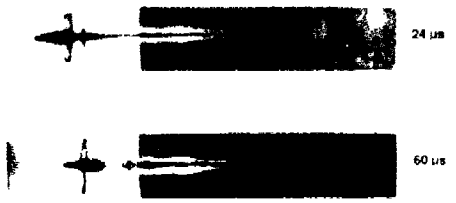

Fig. 109. Continuous Copper Jet Penetrating Into a DURAL Block.

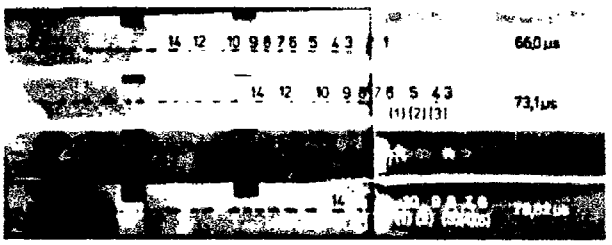

Fig. 110. The Individual Particles of a Jet Produce Individual Bubbles in the DURAL Target.

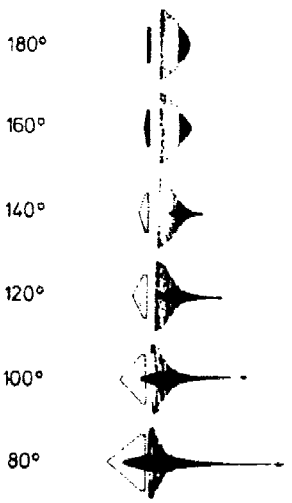

Fig. 111. Jet and Slug Formation of Shaped Charges with Different Liner Angles.

The differences in design between rotational symmetric hollow charges (RSC) and linear shaped charges (LSC) and planar symmetric hollow charges (PSC) with cutting performance are shown in Fig. 112.

In the "rotational symmetric hollow charge (RSC)" a rotational symmetric liner is positioned coaxially to the axis of the high explosive charge and the initiation takes place exactly in the axis opposite to the liner.

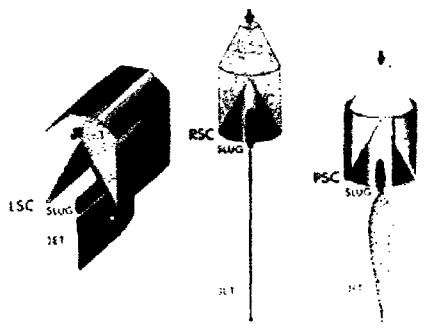

Fig. 112. Typical Shaped Charges and Their Jet Forms.

In the "linear shaped charge (LSC)" a prismatic liner is inserted in the cavity of the high explosive charge. The initiation can either take place at the front end of the charge or in the middle of it. The liner itself can be formed semi-circular or as circular arc, or it can be roof shaped with a smaller or larger angle.

In the "planar symmetric hollow charge (PSC)" the rotational symmetry is modified for example by eccentric initiation or by planar symmetric confinement, etc.

At the detonation of the high explosive the liner of the linear shaped charge is accelerated towards the plane of symmetry whereby it is transformed along the collapse line into a jet and a slug. The velocity of the jet tip is 2000 m/s-3000 m/s at cutting charges with a liner angle of about 90°. The slug velocity is 200 m/s-500 m/s. As a result of the velocity gradient the "cutting edge" is more and more extended, the greater the distance from its origin. Consequently, the initially continuous jet will break up in the direction of flight and small "rods" are formed.

Because of the two confinements at planar symmetric hollow charges the duration of the shock wave pressure is longer on the corresponding liner elements and therefore these liner elements are accelerated to higher velocity towards the axis, so that the jet is directed planar symmetrically towards the two unconfined sides and spreads out planar symmetrically.

5.7.3. Hydrodynamic Theory of Shaped Charge Jet Penetration

5.7.3.1. Constant Velocity of a Projectile, or Jet

To simplify matters, let us say as a first assumption that no lengthening or elongation of the jet occurs. This means that there is a projectile with given length L, which hits the target with high velocity (Fig. 113, bottom). Furthermore, purely hydrodynamic penetration will be assumed, i.e. the mechanical strength of both the projectile (jet) and the target material can be completely neglected. Because of the high stagnation pressure occurring at the high velocities involved, this simplification is certainly valid to a first approximation, because experimental evidence from cratering measurements are in good agreement with theoretical predictions based on this simplification. The projectile, or shaped charge jet, which penetrates into the target material with high velocity, is itself eroded in this process from it tip (Fig. 113, middle).

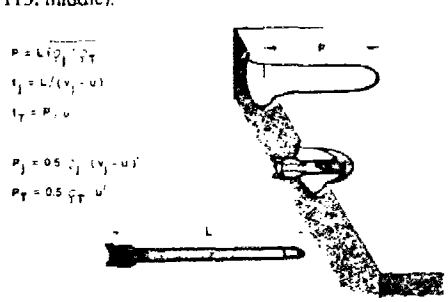

Fig. 113. Hydrodynamic Penetration of a Projectile or Nonstretching Jet.

In a laboratory system of coordinates, this is actually an unsteady process, but it can be made "steady" from the point of view of the stagnation point, or from the crater bottom, by means of a Galilei transformation. In this case, target material of density ρ_T is flowing with the crater bottom velocity, u, towards the stagnation point. The projectile, or the jet, with density ρ_j flows also towards this stagnation point with the difference between jet velocity, v_j, and the crater bottom velocity, u, i.e. with $v_j - u$ (Fig. 113, middle).

The stagnation pressure, p, which must be the same for the projectile, or jet, and the target material, can be calculated from the Bernoulli equation:

$$p = 1/2 \cdot \rho_j \cdot (v_j - u)^2 = 1/2 \cdot \rho_T \cdot u^2 \tag{5.25}$$

Rearrangement of this equation leads to the crater bottom velocity

$$u = \frac{v_j}{1 + \sqrt{\frac{\rho_T}{\rho_j}}} \tag{5.26}$$

For the special case that the jet and target materials have identical densities, the crater bottom velocity, u, half the impact velocity, v_j.

With the jet velocity v_j assumed to remain constant during penetration and, hence, also the crater bottom velocity u remaining constant, the depth of penetration P can be calculated from the length L of the projectile or of the jet. The time t required for complete erosion, i.e. until the projectile or jet with length L has been completely consumed, can be equated to the time when maximum depth P of the crater has been reached. Hence,

$$t = \frac{L}{v_j - u} = \frac{P}{u} \tag{5.27}$$

Rearranging Eq. (5.11) and replacing the velocities by the densities from Eq. (5.17) leads to the following relation:

$$P = L\frac{u}{v_j - u} = L\sqrt{\rho_j/\rho_T} \tag{5.28}$$

This is very well known and frequently used formula for hydrodynamic penetration, representing the depth of penetration as the product of length of the projectile, or of the jet, multiplied by the square root of the ratio of projectile or jet density and the density of the target material. The impact velocity has no effect on the hydrodynamic penetration depth. However, Eq. (5.28) was derived under grossly simplifying assumptions, such as the absence of velocity gradient and, thus, a constant length of the jet; therefore, its predictions for the depth of penetration of shaped charge jets are not very accurate in practice, but it is very useful and illustrative for qualitative considerations.

According to Eq. (5.28), the depth of penetration P_X into a given target having density ρ_{TX} would differ from the penetration P_S in a standard target, say, steel with density ρ_{TS}, as the ratio

$$P_X/\rho_S = \frac{L\sqrt{\rho_j/\rho_{TX}}}{L\sqrt{\rho_j/\rho_{TS}}} = \rho_{TS}/\rho_{TX} \tag{5.29}$$

if the charge parameters, i.e. the length L and the density ρ_j of the jet, were to remain unchanged. With the density ρ_{TS} set equal to that of steel, i.e. 7.85 g/cm^3, the above formula would predict penetrations that are higher by a factor of 1.7 in Aluminum (density 2.75 g/cm^3) and by a factor of 2.1 in propellant (density 1.7 g/cm^3) than the penetration in steel. However, the values observed in practice are different than these, confirming the above reservations.

5.7.3.2. Hydrodynamic Penetration of a Shaped Charge Jet With a Velocity Gradient

In order to keep the derivation of the formulae below to a level that is readily understood, we shall, for simplicity, assume that the jet is generated at an instant in time and at one definite location, specifically at its "virtual origin." The distance from this virtual origin to the target will be denoted by

Z_0, and this distance differs slightly from the stand-off distance in that the latter is measured from the shaped charge base (Fig. 114). Furthermore, the jet which at first is continuous and which stretches under the influence of the velocity gradient, will--also for simplicity--be assumed to break up into particles at an instant in time t_p which is called the particulation time and which is determined experimentally.

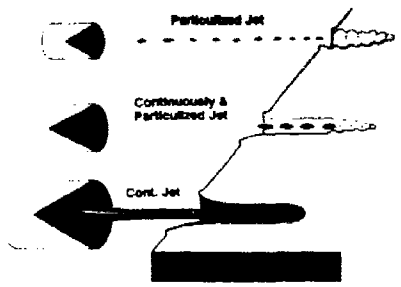

Fig. 114. The Three Different Cases for Penetrating Shaped Charge Jets.

Three different cases have to be distinguished in the formation of a crater by a shaped charge jet (Fig. 114):

Case 1: Cratering by a continuous, stretching shaped charge jet, which in practice implies a very short stand-off distance.

Case 2: Cratering by a continuous, stretching shaped charge jet at first, and then cratering continued by the particulated shaped charge jet. This is certainly the case most frequently encountered in practice.

Case 3: Cratering solely by a particulated shaped charge jet, which implies a long stand-off distance from the shaped charge to the target.

d_t = diameter of jet at time t
d_p = diameter of particulated jet
P = depth of penetration
T = plate thickness in the direction of perforation
t = time
t_0 = time for the jet tip from the virtual origin to the target ($t_0 = Z_0/v_{j,0}$)
t_p = particulation time from the virtual origin to the particulation of the shaped charge jet
$v_{j,0}$ = jet tip velocity
$v_{j,min}$ = velocity of efficient residual jet
Z_0 = distance of target to the virtual origin

γ = $\sqrt{\rho_T/\rho_j}$, with ρ_T and ρ_j denoting the densities of the target and of the jet, respectively

The associated formulas for cratering P(t) as a function of time are:

$$\text{Case 1: } P(t) = Z_0 \{(t/t_0)^{1/(1+\gamma)} - 1\} \tag{5.30}$$

$$\text{Case 2: } P(t) = Z_0 \{(1+\gamma)(t_p/t_0)^{1/(1+\gamma)} t/(t_p + \gamma t) - 1\} \tag{5.31}$$

$$\text{Case 3: } P(t) = Z_0 (t/t_0 - 1) t_p/(t_p + \gamma t) \tag{5.32}$$

The achievable penetration as a function of the minimum jet velocity $v_{j,min}$ is essential for quantitative statements. The corresponding formulas are obtained by eliminating the variable time t from Eqs. (5.30-5.32) as

$$t = (P + Z_0)/v_{j,min} \tag{5.33}$$

and then rearranging:

$$\text{Case 1: } P(v_{j,min}) = \{ Z_0 (\frac{v_{j0}}{v_{j,min}})^{1/\gamma} - 1 \} \tag{5.34}$$

$$\text{Case 2: } P(v_{j,min}) = \{(1+\gamma)(v_{j0}t_p)^{1/(1+\gamma)} \cdot Z_0^{\gamma/(1+\gamma)} - v_{j,min} \cdot t_p\}/\gamma \cdot Z_0 \tag{5.35}$$

$$\text{Case 3: } P(v_{j,min}) = (v_{j0} - v_{j,min}) \cdot t_p/\gamma \tag{5.36}$$

5.7.3.3. Residual Jet Tip Velocity and Diameter of Jet

The threshold for a reaction or the initiation in an energetic material protected by a plate is correlated with the residual jet velocity after the perforation of a plate of line of sight thickness T and the jet diameter D_j.

The residual jet velocity v_j after a perforation of a plate of thickness T can be calculated with the following equations. For this $P(v_{j,min})$ is to replace by T and $v_{j,min}$ by the residual jet velocity v_j in the equations (5.34 through 5.36) and then rearranging

$$\text{Case 1: } v_j = v_{j0}\,[Z_0/Z_0 + T)]^{\gamma} \tag{5.37}$$

$$\text{Case 2: } v_j = \{(1+\gamma)(v_{j0} + t_p)^{1/(1+\gamma)} Z_0^{\gamma/(1+\gamma)} - \gamma(Z_0 + T)\}/t_p \tag{5.38}$$

$$\text{Case 3: } v_j = v_{j0} - \gamma T/t_p \tag{5.39}$$

The diameter of the continuous jet can be predicted with the following equations, if direct measurements are not available. As soon as the jet has broken up, it no longer stretches and, hence, its diameter d_p does no longer change. All that changes is the distance between the individual particles owing to their different velocities.

Let us consider the jet length l_t to the time t, whereby the time t_t is shorter than the particulation time t_p. Further the jet has the diameter d_p during (or after particulation), also on the time t_p. The mass of the jet is given under these two time conditions to

$$V = \rho_t \cdot \frac{d_t^2 \cdot \pi}{4} \cdot l_t = \rho_p \frac{d_p^2 \cdot \pi}{4} \cdot l_p \tag{5.40}$$

For constant jet densities to the time t and t_p, Eq. (5.40) can be written

$$d_t^2 = d_p^2 \cdot l_p/l_t \tag{5.41}$$

The length of the jet - or jet element - for equal considered jet velocity is given for the two times to

$$l_t = v_j \cdot t, \text{ respective } l_p = v_j \cdot t_p \tag{5.42}$$

This gives

$$l_p/l_t = t_p/t \tag{5.43}$$

Equation (5.43) can be introduced in Eq. (5.41)

$$d_t = d_p \sqrt{t_p/t} \tag{5.44}$$

This will give a first and normally adequate approximation for determining the jet diameter as a function of distance for the continuous jet, if direct measured results are not available.

5.7.4 Initiation by Shaped Charge Jets

5.7.4.1. History

The reaction of high explosive charges to shaped charge jet attack has been investigated for a long time. But the number of open literature published papers is rather limited.

In 1945, workers (Armament Research Department) in the UK reported on using flash radiography to study the initiation of bare tetryl pellets by a metal jet generated by a shaped charge. The study showed that the jet initiated the explosive long before the arrival of the slow moving slug. It was difficult to find the origin of the detonation. It was reported that initiation occurred after an estimated 5 mm penetration of the tetryl by the jet. It was also reported, that detonation of the tetryl was capable of disturbing or destroying the head of the jet, and that in no case was the jet seen to emerge beyond the pellet.

In 1955, Zernow et all, using 42-mm and 105 mm diameter shaped charge undertook a preliminary investigation into the jet initiation of Composition B charges of different lengths either bare or with various thicknesses of steel cover plates and/or with side confinement. The study concluded that the coverplate thickness, explosive charge lengths, and degree of confinement affected the jet initiation of explosives. Photography of the exterior of the charge indicated that as steel cover plate thickness was increased, the onset of detonation occurred further down the charge. The limited nature of the investigation did not allow this observation to be explained. Interpretation of the results was complicated by the spread of results obtained for a given cover plate thickness and length of explosive.

In 1968, Held reported the initiation of bare high explosive charges by jets from shaped charges of 22 mm, 32 mm, 64 mm, and 96 mm diameter. The charges were fired from a 50 mm standoff through a steel barrier to produce jets of varying exit velocities. Prior to hitting the high explosive charges the jets became particulated and the length, diameter, and velocities of the jet particles were measured using flash radiography. The critical velocity to detonate bare high explosive charges of the composition TNT/RDX 35/65 were determined for the various diameter shaped charges. It was found that the critical velocity v of the jet particles was related to the jet diameter d by the relationship v^2d = constant, where the constant was 5.81 $mm^3/\mu s^2$ for the tested charges. Held (1983b) has shown that the v^2d-criterion for detonation has been generally confirmed in other work on blunt-projectile and flying foil impact tests against various high explosives.

In 1981, Mader and Pimbley reported work by Campbell using bare PBX-9404 and PBX-9502. The results supported Held's v^2d-critical initiation criterion for particulated jets. Mader modeled the process numerically by treating the jet as a solid cylinder of metal impacting the bare explosive. The result showed that either detonation occurred promptly or the charge failed to detonate. For a detonation to occur the jet was required to produce a shock of sufficient magnitude and duration.

Mader (1968) nicely summarized recent advances in numerical modeling of jet initiation and penetration of explosives as follows:

> "The two-dimensional Eulerian hydrodynamic code 2 DE, with the shock initiation of heterogeneous explosive burn model called Forest Fire, Mader has used to model numerically the interaction of jets of steel, copper, tantalum, aluminum, and water with steel, water, and explosive targets. The 2 DE code and the Forest Fire Heterogeneous explosive burn model are described in Mader (1978).
>
> From the numerical modeling studies, it was concluded
>
> (a) For engineering purposes, the initial jet penetration velocity into an inert substance can be estimated, using the shock impedance relationship $v_j/u = 1 + \rho_T U_T/\rho_j U_j$ and $p = \rho_T U_T \cdot u$. Final penetration velocity can be estimated, using Bernoulli's theorem ($v_j/u = 1 + \sqrt{\rho_{uc}/\rho_j}$). The interface pressure, p, at the jet tip is estimated using $p = 1/2 \cdot \rho_T \cdot u^2$.
>
> (b) The calculated penetration velocity into explosives that are initiated by low-velocity jets is significantly less than for nonreactive solids of the same density. Reaction products near the jet tip have a higher pressure than in inert materials of the same density, and thus impede the jet penetration. The effect is less important as the jet velocities increase. Thus when the target is a high explosive, the Bernoulli equation needs an additional term, p^*, $[1/2\rho_j(v_j - u)^2 = 1/2\rho_t u^2 + p^*]$,. where p^* is approximately 4.0 GPa for the explosives studied.
>
> (c) The critical jet or projectile velocity for initiating propagating detonation can be estimated using projectile diameter and the Held (1968) critical v^2d expression where v is jet velocity and d is jet diameter. In PBX 9502, the jets initiate an overdriven detonation smaller than the critical diameter while the overdriven detonation decays to the C-J state. In PBX 9404, the jet initiates a detonation that propagates only if it is maintained by the jet for an interval sufficient to establish a

stable curved detonation front. A critical expression independent of the projectile material is $\rho v^2 d$, where ρ is the projectile density.

(d) The above methods are approximate, if jet or projectile velocity is not substantially constant, or if the projectile length is not much greater than the diameter, numerical calculations will be necessary. The Held criterion may be useful even when the projectile length is the same as the diameter.

(e) A jet with a penetration velocity greater than the C-J detonation velocity of the target explosive gives an overdriven detonation wave proceeding ahead of the jet with a velocity near that of the jet.

(f) If the jet diameter and velocity histories are known, all the experimentally observed jet penetration behavior of metals or explosives can be modeled numerically. Also, if the jet or projectile length is known, the penetration depth and hole diameter may be calculated."

Chick and Hatt (1981a, 1981b, and 1983) using x-ray flash radiography have reported the initiation of covered, but otherwise unconfined, high explosive charges by means of a jet of a 38 mm shaped charge, the high explosive being in direct contact with the cover material in some of the experiments, but with a 15 mm air gap in others. It was found that a TNT/RDX/Wax 44/55/1 charge immediately in contact with the barrier, or cover material, would be initiated by a shaped charge jet if the barrier thickness did not exceed a limit of 63.5 mm. Surprisingly enough, with a 15 mm air gap between the charge and the cover plate, initiation was observed even with a cover thickness of 89 mm-102 mm. This means that a high explosive, which is in contact with the barrier, requires a higher jet velocity for initiation than one with an air gap. Chick and Hatt suggested that this was due to the high explosive charge in contact with the barrier being compressed by a shock wave preceding the cratering process rendering it less sensitive because of its higher density and/or the smaller number of hot spots resulting from this precompression. More recently doubt has been expressed regarding the original explanation of a desensitizing by a precursor shock wave. These follow tests (Chick and MacIntyre, 1985) with different barriers, viz. aluminum and acrylic glass instead of steel only, as well as steel/acrylic glass combinations, and spaced acceptor charges or air gaps in the charges. The results of these studies indicate that a substantial reaction in a bow wave will not insignificantly affect the initiability of the acceptor charges. The v^2d-criterion for attack on bare charges was also confirmed with jets of 38 mm and 81 mm shaped charges (Chick et al, 1986a) or replaced for the covered acceptor charges with u^2d, where u is the crater velocity. Critical steel cover thickness and critical jet velocities for creamed and pressed TNT, Composition B, H-6, and pressed tetryl were also measured. A summary of the Australian jet initiation mechanisms for covered, but unconfined high explosive charges is given by Chick et al (1986b) as follows:

"When the jet hits the surface of the cover a large impact shock is produced. The impact shock propagates through the cover ahead of the jet but decays very rapidly. The penetrating jet sets up a bow wave that overtakes the impact within a few jet diameters of the cover surface. The characteristics of the bow wave are independent on the properties of the jet and the host material. The jet and its bow wave continue steady penetration towards the cover/explosive interface. After passing through the interface either the decaying impact shock or the bow wave can alter the state of the explosive so that it is desensitized to the following jet. The stagnation pressure at the jet tip in the explosive is several times the magnitude of the bow wave pressure. It can also be several times the magnitude of the critical initiation pressure without detonation occurring. Thus bow wave desensitization is a major effect. When the jet penetrates the explosive a new bow wave is set up. Reaction occurs within the thickness of the bow wave and in sufficiently strong bow wave builds up to detonation.

Depending on the velocity of the jet and the cover thickness several types of events are possible:

(a) For very thin covers and high jet velocities the impact shock can cause detonation. This occurs within a few millimeters of the explosive surface and before the arrival of the jet.

(b) If the cover is more than a few jet diameters thick then the impact shock is attenuated before it reaches the explosive and the bow wave from the jet penetrating the explosive becomes the dominating mechanism for initiation. Strong bow waves will cause detonation within a few millimeters of the explosive surface.

(c) As the jet velocity decreases with increasing cover thickness, the strength of the bow wave in the explosive decreases and the run distance and time to detonation increases. Thus near the critical condition, detonation in Composition B can take 11 μs and 40 mm for initiation by the 38 mm diameter shaped charge jet.

(d) For bow waves below the critical condition the explosive fails; the jet penetrates through the explosive with the bow wave causing disruption and/or reaction.

(e) Jet bow waves reflected back into the explosive from a steel surface at the far end of short test samples can cause detonation. This has been observed near the critical jet initiation condition with explosive samples of up to 50 mm long for jets from the 38 mm charge and with samples up to 100 mm long for jets from an 81 mm shaped charge. This must be considered as a potential mechanism for initiation in munition systems, at least in smaller geometries with heavy confinement near the jet initiation threshold.

For covered explosives the studies have never observed initiation occurring directly at the jet tip; it has always occurred in the shock ahead of the jet or not at all. All of these mechanisms are a mode of shock initiation."

Vigil (1985) has also performed initiation tests with very small shaped charges (1.73 mm to 3.46 mm cone diameter) against a great number of acceptor charges, and confirmed the v^2d-criterion.

Held (1987a, 1987b, and 1987c) has reproduced the tests made by Chick and Hatt (1981a, 1981b, 1983) and Chick and MacIntyre (1985) with similar size shaped charges and with acceptor high explosive charges having a similar geometry and sensitiveness. However, this time the diagnostic instrument was not X-ray flash radiography, but a simultaneous framing and streak recording rotating mirror camera. To demonstrate the different effects the air gaps between the barrier and the high explosive charge were varied and the barriers and/or the acceptor chargers were spaced and/or interrupted by air gaps. These investigations lead to modified explanations of the phenomena reported by Chick et al (1986a and 1986b) as reproduced above.

5.7.4.2. Build-Up Distances and Run-Up Times

The test set-up for the measurement at the initiability of an unconfined high explosive charge, covered by a steel block either in direct contact with the explosive or with a given air gap between, and the impact of a penetration shaped charge jet is shown in Fig. 115 (Held, 1987a). These types of tests with unconfined charges are solely to establish the threshold between a "reaction" and a "detonation" of the acceptor charge, the so-called "initiability" by a shaped charge jet.

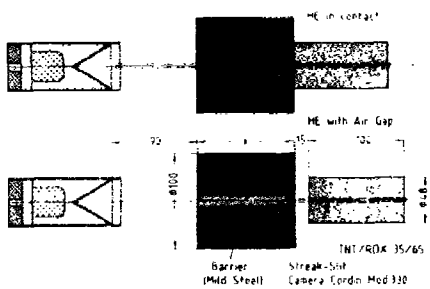

Fig. 115. Experimental Set-Up of Shaped Charge, Barrier, and Unconfined High Explosive Charge, in Contact With the Barrier or With a 15 mm Air Gap Between.

The experimental results regarding the build-up distances, Δs, the run-up times, Δt, and the initiation times, t_i, for these two different arrangements of the barrier relative to the acceptor charge, as a function of the residual jet tip velocity after the barrier are summarized in Fig. 116 for the acceptor charge in direct contact with the barrier, and Fig. 117 for a 15 mm air gap between the acceptor charge and the steel barrier (Held, 1987c). Chick and Hatt (1981a, b, c) also have roughly determined, with the aid of radiographs, the build up distances and delay times for the initiation of Composition B as a function of cover plate thickness. The build-up distances Ds and/or the run-up times t_i of the tests with the charges in contact with the barrier (only for these were data from Chick and Hatt available) are in fairly good agreement. Initiation time, t_i, is defined from measured run-up time Dt minus the time t_D, which is necessary for the detonation wave to propagate from the axis to the surface of the charge ($t_D = R/D$ where R = radius and D = detonation velocity of the acceptor charge).

The high explosive charge directly in contact with the barrier is less easily initiated than the one with an air gap between. The reasons for this are:

- The acceptor charge is being preshocked by preceding waves (in the author's opinion this is only of minor importance, because these shock waves are comparatively weak).
- the high explosive is precompressed by the barrier plate's bulging as the shaped charge jet perforates it
- relatively slow loading of the test charge generated by the bulging target plate and by the pressure of the cratering jet and there is no such high, one-dimensional pressure as in the case of a free jet
- the high explosive charge in contact with the barrier is exposed in a smaller area than the charge with an air gap between, because the emerging shaped charge jet forms a large-area spray of fragments.

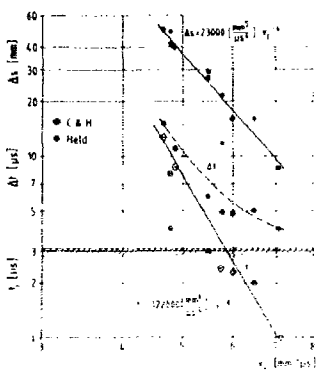

Fig. 116. Build-up distances Δs, run-up times Δt, and initiation times t_i as functions of the residual jet velocity v_j, for the arrangement with the high explosive charge in contact with the barrier.

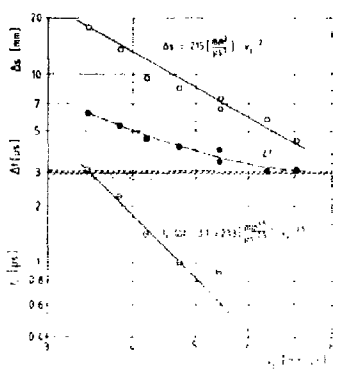

Fig. 117. Build-up distances Δs, run-up times Δt, and initiation times t_i as functions of the residual jet velocity v_j, for the arrangement with a 15-mm air gap between the high explosive charge and the barrier.

The three listed effects appear to be responsible for the differences in initiability of a covered and an uncovered acceptor charge. However, the test set-up and the sensitivity of the acceptor charge might also play a critical role as to which of these three effects will be more or less dominant.

The diameters of the particles of a shaped charge jet that had already broken up into particles were analyzed in detail using an orthogonal-synchro-streak record (Fig. 118). The diameter of the continuous jet in relation to its velocity was calculated from this diagram by means of the following formula:

$$d_j = d_p(t_p/t_j)^{0.5} \tag{5.45}$$

where d_j is the diameter of the jet in the velocity range v_j at time t_j, d_p is the diameter of the particulated jet with velocity v_j, t_p is the time of particulation, and t_j is the time required to pass across the barrier.

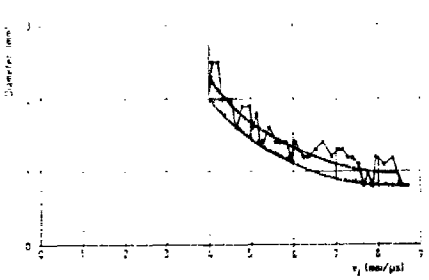

Fig. 118. Diameter of Jet as a Function of Jet Velocity v_j.

The value of d_p is measured, v_j and t_j were calculated for the given barriers and hence are known, so d_j can be calculated from these quantities.

In Fig. 119 a representation is given of the build up distance, Δs, of the measured delay time, Δt, and of the initiation time, t_i, as a function of $v_j^2 d_j$ for the given acceptor charge in contact with the barrier, and in Fig. 120 this is shown for the acceptor charge at an air gap of 15 mm behind the barrier.

Surprisingly, such a log-log representation gives a straight line in first approximation, and Ds and t_i can be written as follows for the case of the high explosive charge in contact (Fig. 119.

$$\Delta s = 160 \times 10^3 (v_j^2 d_j)^{-2} \tag{5.46}$$

$$t_i = 16.8 \times 10^3 (v_j^2 d_j)^{-2} \tag{5.47}$$

With a good fit of the measured points, the result for the 15 mm air gap arrangement is (Fig. 120):

$$\Delta s = 373(v_j^2 d_j)^{0.91} \tag{5.48}$$

or ,still in fair agreement with a perhaps more plausible exponent:

$$\Delta s = 560(v_j^2 d_j)^{-1} \tag{5.48}$$

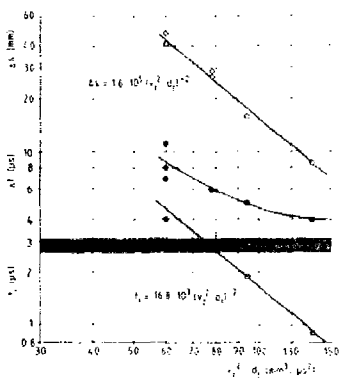

Fig. 119. Build-up Distances Δs, Run-Up Times Δt, and Initiation Time t_i as Functions of $v_j^2 d_j$ for the Arrangement With the High Explosive Charge in Contact With the Barrier.

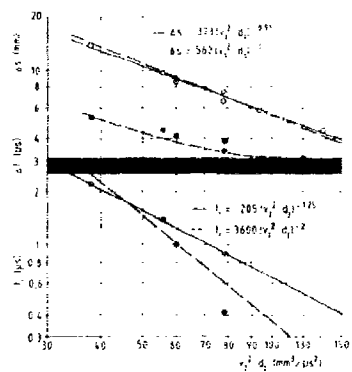

Fig. 120. Build-up Distances Δs, Run-Up Times Δt, and Initiation Time t_i as Functions of $v_j^2 d_j$ for the Arrangement With a 15 mm Air Gap Between the High Explosive Charge and the Barrier.

The measured initiation times t_i, which show an even greater dispersion, can be described approximately by the equations

$$t_i = 205(v_j^2 d_j)^{-1.25} \tag{5.49}$$

resp.

$$t_i = 3600(v_j^2 d_j)^{-2} \tag{5.49a}$$

McAfee (1987) has obtained similar streak records to find the build-up distances or corner-turning distances (CTD) for the initiation of PBX 9502 with copper jets of the LAW warhead (66 mm diameter, 42° angle). Detailed streak measurements are much more accurate compared to the simple use of witness plates to indicate the promptness of the initiation (Campbell, 1981).

5.7.4.3. Confined Acceptor Charges

A few tentative trials were made in order to find out whether the initiation behavior would change if the acceptor charge were fully confined, and where the threshold between reaction and no reaction of the acceptor charge would lie in such a case.

A TNT/RDX 35/65 test charge, 48 mm in diameter and 100 mm long was fitted into a 6 mm thick and 120 mm long steel casing (Fig. 121). The end faces of the high explosive charge were covered with 10 mm thick steel disks. This whole confinement was mild steel.

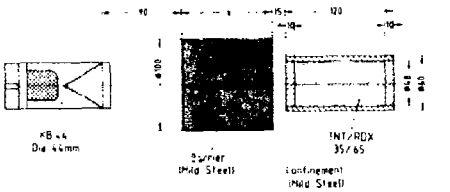

Fig. 121. Test Set-Up With Confined Acceptor Charge.

The results of four trials are listed in the table below:

Barrier X [mm]	X + 10 mm [mm]	v_j [mm/ms]	Reaction
100	110	4.05	Det.
140	150	3.4	Det.
165	175	3.2	Defl.
190	200	2.9	Defl.

An "unconfined" high explosive charge behind a 100 mm barrier, or even one covered with 10 mm, showed no detonation, whereas the confined charge came to a full detonation. The same occurred also after a total of 150 mm had been perforated (Fig. 122).

A strong reaction occurred even after a total distance of 175 mm had been perforated and only slightly less violent reaction even after a total perforation thickness of 200 mm.

These results show that the confined test charge will be detonated by a lower velocity residual jet than the unconfined charge. The limit of initiation of the unconfined charge, being in contact with the barrier, by this type of shaped charge was found to be 4.8 mm/ms, while the confined charge is still initiated by a jet having a velocity as low as 3.4 mm/μs. A very violent reaction occurs even at a jet velocity of approximately 3.2 mm/μs, the evidence being the type of fragments generated; a full deflagration is still obtained with a 2.9 mm/μsec jet velocity (Fig. 123).

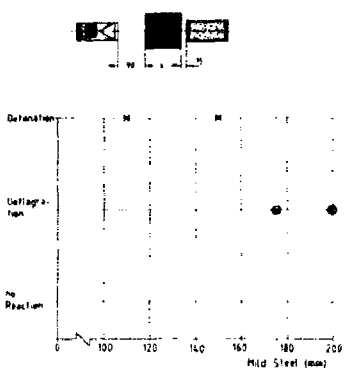

Fig. 122. Type of Reaction as a Function of Barrier Thickness.

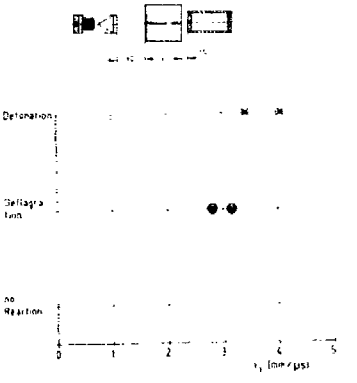

Fig. 123. Type of Reaction as a Function of Jet Velocity.

The times for a reaction in the case of an unconfined charge must be relatively short. The high explosive charge must react before it is broken by the perforating jet or by the pressure developing

internally from reaction associated with the jet path. Under confinement, the charge has much more time to react and can detonate through a DDT process.

These preliminary tests with confined acceptor charges and the comparison with unconfined acceptor charges demonstrated the important fact that unconfined charges are suitable only for establishing the initiability, because the perforating jet and the internal reaction it causes will rapidly destroy the test charge.

Confinement holds the test charge together for a considerably longer time, so that a reaction that starts more slowly can still run up to a full detonation. Therefore, the threshold between detonation and reaction, and the threshold between reaction and no reaction, will in the case of confined charge be at considerably lower jet penetration velocities.

5.7.4.4. v^2d - Criterion

The v^2d criterion with v as the threshold velocity and d as the diameter of the jet or projectile, generally expressed in $mm^3/\mu s^2$, is also very often written as $v\sqrt{d}$ criterion in $mm^{3/2}/\mu s$ and also as $v^2\sqrt{A}$, with A being the impacted area or projectile area. The constants can be transformed simply in the following way:

v^2d	=	c_1	into	$v\sqrt{d}$	=	$\sqrt{c_1}$
v^2d	=	c_1	into	$v^2\sqrt{A}$	=	$0.886c$
$v\sqrt{d}$	=	c_2	into	v^2d	=	c_2^2
$v\sqrt{d}$	=	c_2	into	$v^2\sqrt{A}$	=	$0.886c_2^2$
$v^2\sqrt{A}$	=	c_3	into	v^2d	=	$1.128c_3$
$v^2\sqrt{A}$	=	c_3	into	$v\sqrt{d}$	=	$1.128\sqrt{c_3}\sqrt{d}$

Figure 124 gives the critical threshold velocity for the initiation of different high explosive charges as a function of the diameter of shaped charge jets or projectiles. Experiments with flying foils with different diameters and theoretical predictions are also included. Summarizing, one can say that the support for v^2d criterion is strong.

In early experiments (Held, 1968) with shaped charges, having different base diameters and, hence, also different jet diameters, which were fired against unconfined charges made of TNT/RDX 35/65, the critical velocity of impact was found to be inversely proportional to the square root of the jet diameter.

Campbell performed tests in 1978 and 1979. A summary of these tests is given in Campbell (1988). The data are included in Fig. 124 and in arguments for using v^2d as the critical parameter for shaped charge jets are as follows:

> "In all of the experimental work to date, in which jets have been attenuated by penetrating metal plats, there has not been an instance where there has been an inversion of results.
>
> There has not been a case in which a jet has failed to initiate particular explosive and a similar but slower jet has produces initiation. This experience is based on work with three sizes of shaped charges and explosives including PBX-9404, Composition B, Cyclotol 75/25 and PBX-9502. Thus, it is concluded that the method of assigning jet diameters and the resultant scatter in diameters are not entirely meaningful, or inversions in results would have occurred. Until the process of jet initiation of explosive is better understood, it seems necessary to use a present method of smoothing diameter data, and it is anticipated that the concept of critical value for v^2d will permit prediction of the performance of copper jets from untested shaped charges."

Vigil (1985) has used jets of very small rotationally symmetric shaped charges (RSC) to initiate four different secondary explosives. The RSC-jet velocities have been varied between 3.6 and 6.5 mm/μs. The jet tip diameters ranged from 0.041 mm to 1.1 mm. The explosive acceptor diameters were varied between 1.90 mm and 19.1 mm. The lateral confinement of the acceptor explosive was minimal. The threshold initiation parameter v^2d for LX-13 (80% PETN and 20% Sylgard), PETN, PBX 9407, and Tetryl were experimentally determined to be 11, 13, 31, and 44 $mm^3/\mu s^2$ or 3.3, 3.6, 6.4, and 6.6 $mm^{3/2}/\mu s$, respectively, for copper jets impacting bare explosive acceptors. The lower values for the LX-13 and PETN indicate that these two explosives are more sensitive to jet initiation than PBX-9407 and Tetryl explosives.

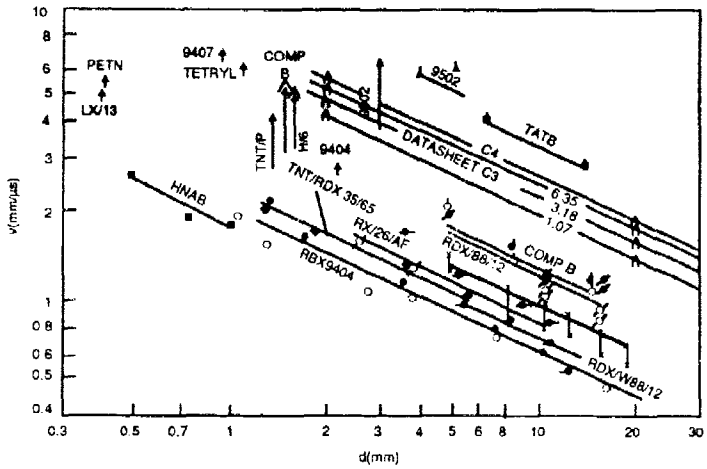

Legend:

Full Initiation: ▲ ● ■; No Initiation: △ ○ □

Jet Attack	◆	Held - 1968 <13>	TNT/RDX 35/65
	◭ △	Campbell - 1979 (<28> - <29>)	PBX 9502 (TATB)
	↑	Vigil - 1985 <16>	Different HEs
	⇧ ↑	Chick et. al. - 1981 (<19> - <24>) (⇧ covered, ↑ uncovered)	Different HEs
	⇑	Weickert - 1987 <32> (in thin sandwiches)	Datasheet and C-4
Projectiles	◆	Griffiths et. al. - 1963 <33>	RDX/WAX 88/12
	● ○	Bahl et. al. - 1981 <34>	PBX 9404
	◆ ◇	Bahl et. al. - 1981 <34>	RX-26-AF
	◭ △	Moulard - 1981 <35>	Comp. B
	◢ ◿	Moulard - 1981 <35>	RDX/Binder 88/12
Explosive Foils	▲	Weingart et. al. - 1976 <36>	TATB
	■	Hasman et. al. - 1986 <37>	HNAB
Theory	⟊	Starkenberg et. al. - 1984 <38>	Comp. B
	⟊	Huang et. al. - 1985 <39>	Comp. B

Figure 124. Threshold or Impact Velocity as a Function of the Diameter of Shaped Charge Jets, Projectiles, or Flyer Foils for Different Hish Explosive Charges.

Chick et al (1986a) have also examined Composition B, H-6, PBX-9502 and pressed TNT with jets from 38 mm and 81 mm diameter shaped charges. They have looked at the sensitivity of bare and covered acceptors. The jet diameters had not been measured for each firing; a diameter of 1.5 mm had been assumed for all small shaped charge jets, and one of 3 mm for the large shaped charge jets. Nevertheless the values are within the range of the other data (Fig. 124). Important is the fact that they have shown for the first time that bare high explosive charges can be initiated by a jet at about half the tip velocity required by a covered charge attacked by a similar jet. In both cases the explosive is still unconfined.

Weickert (1987) has also confirmed the v^2d criterion using four different shaped charge diameters, namely 25.4 mm, 50.8 mm, 76.2 mm, and 101.6 mm against relatively thin layers of confined high explosive charges in metal/explosive/metal sandwiches. The metal layers of cold-rolled steel 4140 were 3.18 mm thick. Two types of high explosive layers were used, consisting of Datasheet C with thicknesses of 1.07 mm, 3.18 mm, and 6.25 mm and Composition C-4, 3.18 mm thick. The shaped charge jet particles were very irregular in shape, or they were multiple particles. Still, the Detonation/No Detonation results show that the relation $v_j^2 d$ = constant can be used for the shaped charge jet initiation of explosive/metal sandwiches. The spread of Weickert's data points about his best fit line is considerable. This can be attributed to the uncertainty in the measurement of the diameter d. In order to determine the sensitivity of the results to the diameter measurement technique,

Weickert has used various alternative diameters d: (i) the largest dimension of the lead jet particle; (ii) a mean cylindrical diameter, and (iii) the diameter of a circle with area equivalent to that of the lead particle. The results using any of these diameters were consistent with the $v_j^2 d$ = constant relationship and shifted the jet particle velocity v_j intercept on the v_j versus d plot by a maximum of 15% compared to that obtained using the diameter based on the projected area.

The influence of varying the explosive thickness is interesting. As the thickness of Datasheet-C3 is increased, the critical $v_j^2 d$ value increases, indicating a reduction in initiation sensitivity of the sandwich.

Datasheet - C3

Thickness mm	$v_j^2 d$ mm^3/ms
1.07	35
3.18	46
6.35	58

This gives an almost linear relationship between $v_j^2 d$ and the sheet thickness t:

$$v_j^2 d = 31 + 4.41\ t$$

This relationship is valid for the limited range of explosive thicknesses tested. However, the critical $v_j^2 d$ value will be bounded by the critical diameter of the explosive for a thin explosive layer and by the value for the semi-infinite configuration for a thick explosive layer.

The $v^2 d$ criterion has also been confirmed for projectile impact on bare high explosive charges.

Griffiths et al (1963) have published earlier work of Whitbread on the threshold velocities with projectiles of 12.7 mm, 10.67 mm, 8.13 mm, and 5.60 mm diameter against charges of RDX/Wax 88/12. It was shown that the length of the projectile did not affect the probability of detonation. They have tried to find a correlation between v and r^2. But the four points do not make a straight line on the diagram.

Bahl et al (1981) have measured the initiation thresholds of bare and covered PBX 9404 and an HMX/TATB explosive, called RX 26-AF. Steel projectiles of flat and rounded front were used in the velocity range of 0.5-2.2 mm/μs. All their experimental values for bare high explosive charges of PBX 9404 and RX-26-AF are presented in Fig. 124. The regression line gives a straight correlation for the $v^2 d$-criterion, but with a constant twice as high. These values are not presented in Fig. 124.

Moulard (1981) has made additional tests with projectiles of rectangular and ring-shaped front ends. If these areas are transformed into diameters (representing the area) then the corresponding points are also on the $v^2 d$-line.

Foil tests also demonstrate the $v^2 d$-criterion if the flying foil thickness, related to the diameter, is not too small. The ratio should be greater than 1/5. Two velocities have been added to Fig. 124 from published papers by Weingart (1976) who had used 0.255 mm thick flyers of Mylar against TATB.

Hasman (1986) has published the critical energy for initiation, using flyer diameters of 0.5 and 1 mm, and 76 μm thick Mylar foils against HNAB [Hexanitroazobenzene, bis(2,4,6-trinitropheynil)-diazene] of 5 μm grain size and 1.6 g/cm^3 density.

The experimental values of the $v^2 d$-criterion also are confirmed by the numerical 2D simulations of Mader (1983 and 1986), Starkenberg, et al (1984), and Huang et al (1985). The latter values are also given in Fig. 124 for Composition B, which correlates very well with the trend, but not so well with the constants compared to the experimental data for Composition B. Also Green (1981) has made relatively simple considerations for the shock and release wave behavior and has found a good correlation to the $v^2 d$-criterion.

In conclusion, one can say that for "jet attack" against high explosive charges, the $v^2 d$-criterion in fact describes the detonation threshold of the high explosive charges in terms of the threshold velocity as a function of jet diameter. This is confirmed by "projectile" impact results which, however,

involved larger diameters and correspondingly lower velocities and also by flying foils, if the ratio of foil thickness to diameter exceeds 1/5. This criterion is also confirmed by simulation of the high explosive charge behavior with numerical codes.

5.7.4.5. Solid Propellant Rocket Motor Attacked by Shaped Charge Jets

In the open literature, few tests are published relating to shaped charge attack against propellants, propellant grains, or even rocket motors. Nevertheless, conclusions can be drawn from test results against high explosive charges together with simple considerations concerning the behavior of the explosive materials under shaped charge jet attack.

The behavior of charges of different types of propellant under shaped charge attack has been investigated (Held et al, 1978). Various compositions with the following ingredients were used:

- RDX and PETN as energetic materials,
- Nitroguanidine, Oxamide, Ammonium oxalate, as gas-producing materials,
- Nitroglycerine as an energetic plasticizer,
- Polyurethane and Nitrocellulose as binders,
- Carborundum as a combustion instability suppressant.

These propellant materials have been tested in a large variety of combinations in sandwiches between steel plates with 60° obliquity with copper jets, with a base diameter of 64 mm. With high content of sensitive materials the entire grain fully detonates. If the propellant was less sensitive, only the portion of the sandwich having a smaller angle between the jet and direction of detonation, detonated (upper part of Fig. 125b). With much less energetic material, reaction only occurred around the jet (Fig. 125c).

(a) (b) (c)

Fig. 125. The 3 possible Types of Reaction of Solid Propellants Under Shaped Charge Jet Attack: (a) "Full Detonation," (b) "Partial Detonation" (in the upper region only), and (c) "partial reaction."

The conclusion from these tests is, that depending of the sensitiveness, the composition can come to a full detonation, or a partial detonation, or only a reaction in a limited region around the jet impact.

No doubt, the initiability is correlated with the critical diameter of the tested material. The jet is generally very small in diameter. The "stagnation" pressure radially decreases and follows the penetrating jet. If, over a dimension less than the critical detonation diameter of the material, the shock pressure in the bow wave around the jet becomes less than the initiation threshold pressure, a high-order reaction of the propellant cannot be expected. Chick and Bussell (1987) have drawn the following conclusion from jet attack against explosives:

> "The method of increasing the power output from solid rocket propellants by the incorporation of secondary high explosives such as PETN, RDX, and HMX has resulted in compositions which exhibit a significant decrease in critical detonation diameter when compared to conventional propellants. This is demonstrated by the following table where the results of a literature survey show that the composition containing secondary explosives have critical diameter D of only a few millimeters. The application of the D/d criterion (critical detonation diameter D/jet diameter d) suggests that many bare and thinly covered traditional solid propellants would not be expected to be initiated by the jet impact mechanisms from conventional shaped charges. These materials generally have shock sensitivities considerably less than TNT and may only be expected to be detonated by the bow waves from higher velocity elements of the larger diameter jets. The compositions with exceptionally large critical detonation diameters (which are also generally extremely insensitive to shock) would not be expected to be detonated by conventional shaped charge jets since the bow wave may not spread to a sufficiently large diameter and/or be strong enough."

Table 23. Critical Detonation Diameters Estimated From the Available Literature For Several Types of Explosives (Chick and Bussell, 1987).

Type of Explosive			Literature Critical Detonation Diameter D (mm)
High Explosive	Pressed	(1.52 g/cm^3)	2.6
	Composition B	(1.65 g/cm^3)	4.3
	PBX 9502	(1.90 g/cm^3)	9
	Octol	(1.78 g/cm^3)	< 6.4
	H-6	(1.74 g/cm^3)	≈ 6.4
	Composition B	(1.65 g/cm^3)	4.3
	Cast TNT	(1.57 g/cm^3)	14.6
Propellants	Conventional Composite		Very large, between 50-500 mm depending on composition.
	Cast Double Base		Little information available, 36 mm confined samples detonate
	Aluminized Composite		20-35
	Composite Containing PETN (≈ 75%)		< 3
	Composite Containing RDX (≈ 75%)		3-4.5

If no detonation results from the shaped charge impact and perforation, then a burning reaction will occur. Depending on the strength of the casing this reaction will be mild or strong. Asay et al (1987) have described this behavior quite adequately. They have given a good schematic model (Fig. 126) which helps to define the regions of interest in the case of detonation failure:

"The jet impacts the propellant and initiates a detonation in the immediate vicinity of the jet tip. Detonation proceeds for a certain distance and a transition to a violent deflagration occurs. This reaction propagates until a transition to a mild burn occurs. The delineation between these regions may or may not be clear-cut and this description is necessarily, in the absence of experimental evidence, overly simplified. However, this idea is conceptually sound."

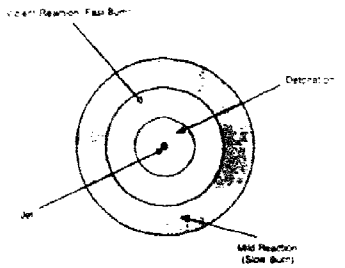

Fig. 126. Schematic of Regions of Interest in the Case of Detonation.

5.7.5. Summary

A shaped charge jet of a HEAT weapon has generally enough power to bring any type of propellant charge to a reaction, even after perforation of a casing.

This residual jet tip velocity can be calculated from the jet tip velocity, the stand-off distance, or the distance of the target from the virtual origin, the casing thickness along the perforation line and the target density.

The type of reaction depends on the sensitiveness of the propellant charge, which is correlated with the critical detonation diameter D, the residual jet velocity v, and the jet diameter d; this is expressed by the v^2d-criterion.

The conventional composite propellants will normally not be initiated by a shaped charge jet, because their sensitiveness is low and their critical detonation diameter is relatively large. Composites containing PETN, RDX, or HMX will normally detonate, especially if these materials are added in large proportions.

CHAPTER 6. MITIGATION OF RESPONSES

6.1. INTRODUCTION

The previous chapters have presented (1) the general response of rocket motors to various stimuli (thermal resulting in cook-off and inadvertent ignition, fragment impact, bullet impact, electrostatic discharge, etc.), (2) the scientific/technical areas such as shock to detonation transition, deflagration to detonation transition, burn to explosion, etc., (3) the parameters necessary to describe or predict effects in each of the scientific/technical areas and various test techniques used to obtain these parameters.

This chapter seeks to provide help on options available to mitigate unwanted reactions. That is, after you have used the methods and information presented in the previous chapters, and determined that you have a hazards problem, what can you do to lessen or eliminate the problem.

6.2. THERMAL STIMULI

Cook-off of confined energetic materials will inevitably occur if these materials are subjected to elevated temperatures for prolonged periods of time. Obviously, the first mitigation consideration should be suppression of the heat flow from the heat source to the munition, giving valuable time to attempt to extinguish the fire. Obviously, much less time is available in the fast cook-off situation, but the slow cook-off reaction, if it occurs it is usually more violent than fast cook-off.

To prevent or reduce the heat flow from an external heat source into a rocket system a number of options are open to the designer. The most important ones are listed below.

1. In storage, rocket systems can be protected by selecting proper fire-resistant package materials of low thermal conductivity. In addition, heat shields can be used to further decrease the heat transfer.

2. If the rockets are out of their protective packaging the outer casing can be coated with special heat insulation materials such as intumescent paints. For example an ammonium salt of a sulfonic acid embedded in an epoxy polysulfide binder can be loaded with mica flakes and used as a radiation shield which in the case of fire will react to form a protective foam layer of poor thermal conductivity (Crowley, 1978).

3. Inside the rocket motor a good heat insulation can be accomplished by means of suitable liner materials (McQuaide, 1976, and Miguel, 1977).

The liner will give the necessary mechanical strength and case bonding against stress (McQuaide, 1976). An additional advantage of some liner materials is that they slowly decompose, leading to a pressure build-up which may disrupt some rocket motor casing before the propellant will ignite. Also, the reaction gases may act as a heat insulating layer which will further increase the time to ignition.

4. Careful selection of propellant materials is another important way to prolong the time to ignition and to reduce the effects of cook-off. Typically, double base propellants will start to decompose at temperature ranging from about 150 up to 170°C. In large rocket motors the decomposition can start at an ambient temperature of 90°C whereas composite propellants decompose at considerable higher temperatures (250-300°C) (Rideal and Robinson, 1948), although in recent U.S. tests with full scale rocket motors with composite propellants reactions have occurred at oven temperature between 160-211°C. Besides the use of thermally stable elastomers (Sutton and Wellings, 1964), flame retardants can be added to inhibit the decomposition reactions of the energetic material in composite propellants (Gidhar and Aroca, 1978). Finally, stable binder materials will increase the thermal stability of the propellant (Vetter, 1977).

5. In the areas near the wall of the rocket motor the heat flow into the propellant will be the greatest. So in these areas ignition is most likely to occur. Therefore to increase the time to ignition one should increase the thermal conductivity of the propellant to divide the heat over the entire propellant grain (Rat and Kent, 1982).

However, delaying the ignition by the use of heat insulating packages or external or internal liners may increase the violence of the event when it does eventually take place. This is because the lower rate of heat flux into the propellant will result in a less steep temperature gradient within the propellant so that when ignition takes place near the motor wall, the inner part of the propellant grain will ignite more readily and the event will develop more rapidly. This assumes of course that the motor case does not degrade during this longer time-scale. (Also, pre-ignition reactions may complicate the issue.)

If the countermeasures described above have failed, a thermal explosion of the propellant is to be expected. In order to minimize the risk of such an event, some additional countermeasures can be taken.

All the concepts presented below are based on the idea preventing a pressure buildup inside the casing (Vetter, 1977). This can be achieved by including vent holes in the motor casing, by providing relief ports or to chose a relatively weak material for the casing, i.e. using the strip laminated technique.

PASSIVE MITIGATION DEVICES

Partial Ins ' .tion Technique (PIT): This concept uses an external insulative coating applied over most of the munition's case, leaving only a bare strip down the length of the component. When the munition is exposed to fast cook-off, heat transfers into the item through the uncoated area. The heat weakened part of the case then fails longitudinally when the underlying liners/insulators or energetic material undergo thermal decomposition. The advantages of the approach are that it is easily and inexpensively applied and uses no moving parts or energetic materials. Disadvantages include a small weight penalty and center-of-gravity shift of the munition, possible handling and fitment problems, and that it provides protection against only a truly fast cook-off.

Case Stress Riser: This concept consists of mechanically grooving a metallic case containing energetic material. As the material is heated and expands or the liner pyrolizes, the internal pressures will crack open the case in a controlled manner at acceptably low pressures.

ACTIVE MITIGATION DEVICES WITHOUT IGNITION

Thermally Initiated Venting System (TIVS): This device uses a linear shaped charge to explosively cut through a munition component case. The explosive is sized to crack open the case without igniting the underlying energetic material. In order for it to function, the TIVS must be connected to a thermal sensor and initiation trigger. When used on weapons subject high free flight aerodynamic heat, there must be a launch energized out-of-line device placed between the detonation mechanism and the linear shaped charge. TIVS has demonstrated good results on AMRAAM and Maverick. The TIVS has the advantage that it may be modified to work in both fast and slow cook-off environments. The disadvantages with TIVS include complexity (when including sensor/triggers and out-of-line mechanisms) and potential safety problems when associated with its external location. An addition, although unlikely, safety hazard is accidental and unnoticed TIVS initiation when u'ed on a rocket motor. Subsequent missile firing would probably result in an immediate motor explosion. The AMRAAM TIVS is designed to disable the motor firing circuit given TIVS initiation.

ACTIVE MITIGATION DEVICES WITH IGNITION

The U.S. Navy position is that these type of devices will not be allowed.

Thermite Case Penetrator (TCP): This approach uses thermite to melt through a munition case and ignite the underlying energetic material. (It is possible to design this device to melt through a case without igniting the underlying energetic material; such an approach would then be classified as active without ignition.) The thermite is located outside the case in retrofit designs. The external version consists of a thin metal cup filled with a strip of thermite. Inside the cup is a small piece of rocket propellant which is autoignited during fire exposure. The burning propellant then ignites a "transfer charge" of finely ground thermite which, in turn, ignites the thermite main charge. The external TCP has proven to be reliable in providing mild fast cook-off reactions to rocket motors. With additional thermite ignition work (thermal batteries) it may provide acceptable slow cook-off reactions for at least some types of ordnance. Safety is an issue with this approach because the device has the potential to cause accidental ignition of energetic material in munition components. The thermite igniter is thermally exposed to the outside environment but will only function when heated to above 260°C. On the tested ordnance item, functioning of the device occurred about 15 seconds before the munition would otherwise have reacted. Safety concerns should only apply to the identification of accidental ordnance heating situations, and probabilities thereof, which could function the thermite igniter without also reacting the munition.

Ignition: This applies only to rocket motors and consists of deliberately igniting the motor through use of its built-in ignition system. This would usually also require some sort of motor case opening system. It would generally only be used in a slow cook-off situation when a sensor determined that the propellant was in imminent danger of detonating.

THERMAL SENSORS FOR ACTIVE MITIGATION DEVICES

Thermally Activated Safe-Arm Device (TASAD): This is a device being developed under the U.S. Navy's "Insensitive Munitions" Advanced Development Air-Launched Ordnance Section Program

which will identify and classify a fast or slow cook-off event and provide output signals to appropriate mitigation devices such as TIVS. The first working prototype has demonstrated that it will identify and discriminate between fast and slow cook-off. It can be set to identify slow cook-off as any heating history which will cause an ordnance item to react in about 30 minutes or longer. This generic model will require modification and development for direct application to a specific munition. It also requires detailed energetic material's characterization work in order to correctly establish the specific heating histories which cause transition from fast cook-off type reactions to slow cook-off reactions.

Thermal Batteries: This is a new and alternate approach to TASAD. It used thermal batteries as a combined heat detector and power source to function a mitigation device such as TIVS. Two different thermal batteries are used. One has a fairly high melt temperature electrolyte which energizes in a fast cook-off environment. The other battery uses a lower melt temperature electrolyte combined with external insulation sufficient to prevent it from energizing in fast cook-off. In slow cook-off, the slower external heating rates provide the time for the heat to transfer to the electrolyte and function the battery. Thermal switches are also required to allow the batteries to reach full charge prior to activation. This approach is still in early development and has not yet been demonstrated to work.

6.3. DETONATION

Earlier chapters discussed how fragment impact and bullet impact could lead to a detonation either through the shock to detonation transition (SDT) or through deflagration to detonation transition (DDT).

Obviously one primary way to prevent the detonation is to prevent materials impacting the motor, or if impact does occur, slowing the fragment down or decreasing its mass (e.g., via fragmentation) so that it does not impact the motor with sufficient mass-velocity to cause SDT. Shielding materials or spacing ordnance is the most common mitigation methods, however one often pays an operational penalty for this mitigation. Parsons et al (1988) discusses operational considerations of separation distances and shielding materials, as does Swisdak et al (1987). However, in some instances the barrier material does not have to be excessively thick or heavy. Some recent work at NWC (unpublished at present) has shown that in some instances the shipping container or launch tubes may provide sufficient barrier. In some shipping configurations storage of the missile wings/fins (unattached during shipping) between adjacent missiles can provide sufficient mitigation. In other instances, plastic materials and/or scoria like materials are being considered for attenuation media between rounds.

Good progress has been made in applying various hydrodynamic computer codes to predict the effectiveness of various barrier materials and spacings in attenuating shock input to the munitions. Since the applications are very system dependent, and quickly become weapon system vulnerability issues (that are classified) they are not included in this AGARDograph. However the reader should know that techniques are available.

Other areas of mitigation of direct SDT involve the response of the munition itself. In the propulsion area some work has been started to look at the role of motor case itself, but most of the work has been devoted to providing less sensitive propellant. This can be accomplished in several ways as outlined in the fragment impact hazard protocol (Section 4, Fig. 11) by increasing the critical diameter of the propellant, by increasing the shock initiation threshold, by increasing the run distance to detonation, and by providing void-free, hard to damage (environmental effects included) propellant.

For many propellants the critical diameter is quite large, especially when compared with the diameter of the motor (although the discussion of Section 5.4.1.1 should be reviewed). However the critical diameters for advanced solid rocket propellants may be relatively small (Brunet and Salvetat, 1988), especially for those containing some burn rate modifiers and/or energetic binder and/or nitramine ingredients. The effect on SDT sensitivity due to critical diameter can be seen in Fig. 127. This figure presents the results of calculations done for an actual propellant that had a critical diameter of approximately 1.3 cm and a shock sensitivity of approximately 120 U.S. cards (1.2 inch, 3.05 cm, of PMMA) in the NOL card gap test. In the analytical study, the critical diameter was varied from 1/2 inch (1.27 cm) through 2 inches (5.08 cm). The initiation threshold pressure was not changed during the calculations. As shown in the figure increasing the critical diameter of the propellant significantly decreases the susceptibility to combinations of projectile mass and velocity that would cause SDT.

From the discussions of deflagration-to-detonation transition (Section 5.4.2), successful prevention of this phenomena primarily depends on preventing damage to the propellant (e.g. making tough, nonfriable propellant), preventing ignition and flame spread, and relieving confinement before the reaction can transition to a detonation. A discussion on how to make tough propellants is beyond the scope of this volume. The method usually used to determine if tough propellant has been made is

the shotgun test that was discussed in Section 5.4.2.1. Methods to relieve confinement are similar to the techniques used to relieve confinement to prevent explosion as discussed below.

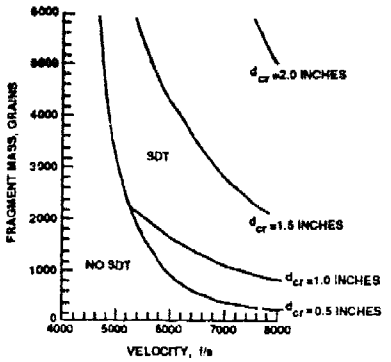

Fig. 127. Effect of Critical Diameter, d_{cr}, on Fragment Induced Shock to Detonation High Energy Propellant in 3/16" Steel Case, Blunt Cylinder Impactor.

6.4. EXPLOSION

As discussed in Section 4.6, if a fragment does not have sufficient mass or velocity to cause prompt shock-to-detonation transition we must still be concerned about a burn to explosion reaction. In terms of Fig. 13 the possible routes of mitigation (i.e., to reduce vulnerability) for an event less violent than detonation would appear to be:

1. Consider the mass and/or velocity of the fragment. In many cases this means reducing the mass or velocity through the use of barriers or cases. However one must be careful. If one is in the region where the fragment completely passes through the motor without igniting the propellant, or even when with ignition the holes produced are sufficient to vent the reaction [the exit hole is usually very much greater than the entry hole] a reduction of mass and/or velocity may cause the undesired burn-to-violent reaction.

2. Change the ballistic limit of the case.

3. Reduce the ignitability of the propellant.

4. Reduce the temperature coefficient of the propellant burning rate.

5. Reduce the pressure exponent of the propellant burning rate.

6. Improve the mechanical strain rate behavior (i.e., reduce the frangibility) of the propellant.

7. Modify the thermochemistry and energetics to reduce the pressure rise rate following ignition by fragment impact. (This usually is not a viable option since the ballistics of the motor would also be changed.

8. Improve the venting of the motor case.

Of these, (1), (2), and (3) might, in the event of attack of a non-ignited motor, eliminate the event altogether, while any except perhaps (3) could reduce the violence of the event.

However, requirements related to performance may limit the practicalities. The introduction of plates or containers to achieve (1) may not be practicable because of weight configuration and the same may apply to (2); in any case, some ways of achieving (2) will be counterproductive in terms of venting if the projectile does get in. Since propellants have to be readily ignitable there is a definite limit to what can be achieved in (3). Option four is certainly desirable but in practice will be tied up with (5) and (7), again in connection with performance. The principal options for mitigation of response would therefore appear to lie in modifying the propellant behavior under attack by (6) and improving case venting by (8).

The conclusions are generally in accord with those from the UK MSM work (which has also considered the effect on response of temperature variation) and the UK has therefore developed the

LOVUM program to investigate the possibilities, using a matrix of four propellants of different chemical types (one as control) and three case materials.

THE LOVUM PROGRAM

The program is designed to assess the effect of changes in the propellant formulation and motor case material on the results of 0.5 in AP bullet attack, standardized fuel fire and slow cook-off trials relative to those of analogous cast-double-base propellant motors (Bascombe and Manners, 1987). Four different propellant compositions in all and several case materials are being assessed.

The application is a single thrust (boost) radially burning motor with the highest performance possible in keeping with a reduction in vulnerability to attack.

An outline sketch of the LOVUM motor is shown in Fig. 128. All variations of the motor are designed to have as similar performance as possible and commonality of design as follows:

1. Slotted tubular charges; the HTPB charge has 3 slots, the rest 4.

2. Similar web thicknesses.

3. Mean working pressure at 20°C: 10 MPa.

4. Ratio static bursting pressure to tube maximum working pressure at 60°C: > 1.33, with not more than 10% variation between various designs of motor case.

5. Burning times: 2 to 4.5 secs at 20°C.

6. Specific impulses: 220 to 240 s.

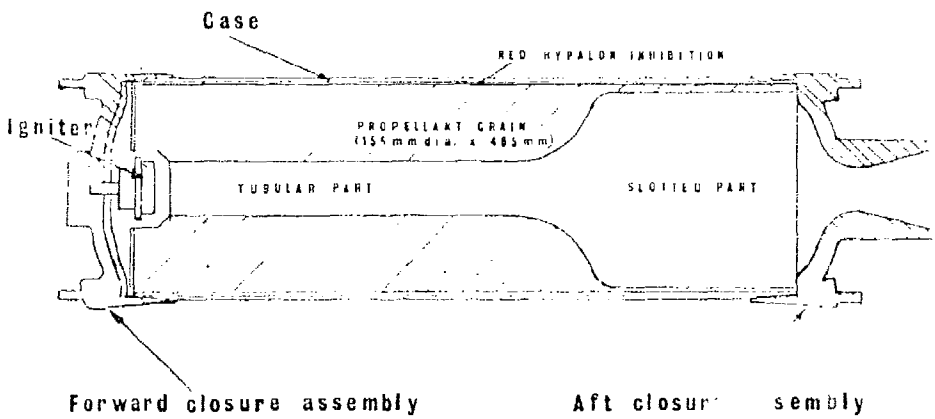

Fig. 128. LOVUM Motor.

The four propellants used in the tests are standard cast-double-base propellant (C[illegible]ntrol), a nitramine loaded cast-double-base propellant (CDB/RDX), both as cartridge-loaded cha[illegible]an elastomer-modified cast-double-base propellant (EMCDB) and a hydroxy-terminated-poly[illegible]adiene propellant (HTPB), both as case-bonded charges.

The case materials used in the tests are:

1. Carbon-fibre-reinforced plastic (CFRP).

2. Steel strip-laminate (SSL).

3. Kevlar-overwound aluminium alloy (KOW).

4. KOW (designed primarily for low response to fragment attack) plus a rapid venting system to activate in a fire and vent the case before a serious reaction could occur. Systems under investigation at the moment are thermite tabs (TT) and line cutting charges (LCC).

Each motor is checked radiographically for integrity of propellant/inhibition bonding, and each propellant/motor case combination is checked for performance (thrust and pressure) by firing one motor at -30°C and another at +60°C.

TRIALS PROGRAM

The full set of intended tests is given in Table 24. BA denotes bullet attack (2 trials) - single shot 0.5" AP, service velocity (≈850 m/s), one trial against a motor conditioned at 60°C and one against a motor conditioned at -30°C, except for the additional tests where a single attack at -50°C is intended. Approximate measurements of blast overpressure are obtained from 4 foil gauges arrayed round the store, 1 m from the center, and a pressure transducer is installed in the motor. High speed cine (100 and 1000 pps) and video are also used. FF denotes fuel fire (single trial) using AVCAT or commercial kerosene grade B to give a ten-minute fire in a steel tray 1.58 m x 1.15 m x 0.10 m deep in a suitable emplacement to keep out the wind. Instrumentation includes thermocouples to measure flame temperatures inside the motor, with a cine camera at 16 pps and video. SCO denotes slow cook-off; the motor is heated, in a disposable air-circulation oven, at temperatures increasing from ambient at 3.3°C per hour until an event occurs.

Table 24. LOVUM Test Matrix.

Propellant / Case	CDB	CDB/RDX	EMCDB	HTPB
1. CFRP	BA FF SCO	BA FF SCO	BA FF SCO	BA FF SCO
2. SSL	BA FF SCO	BA FF SCO	BA FF SCO	BA FF SCO
3. KOW	BA FF SCO	BA FF SCO	BA FF SCO	BA FF SCO
4. No 3 plus TT or LCC	FF SCO	FF SCO	FF SCO	FF SCO

+ additional test (BA - 50°C)

The full range of tests is programmed for motors using cases 1, 2 and 3 but curtailed for case 4 motors; case 4 is a modification of case 3 to improve the response to fuel fire and slow cook-off so the BA test is superfluous.

Bullet attack at -50°C will be carried out for those propellant/case combinations where a maximum non-detonating response (Explosion) is not achieved in the fragment attack test at -30°C. These rubbery propellants have a much lower glass transition temperature (Tg) than the standard double-base propellants (filled or unfilled) and a temperature much lower than -30°C is needed to make them brittle under these attack conditions.

The UK has little experience of rocket motor detonation but clearly methods of mitigating such an event would vary depending on whether the event was a DDT. Once the detonation is established there can be no means of stopping it, so for DDT it is necessary to work on the initial deflagration phase and considerations similar to those above should apply. For SDT it is necessary to attenuate the affect of the shock, either by interposing a liner between propellant and motor case (imposing a mass penalty and possibly increasing the prospects of DDT by increasing the confinement) or if possible by changing the propellant system for a composition of greater critical diameter.

6.5. ELECTROSTATIC DISCHARGE

All parts of the system must be at the same voltage. The first requirement is to have a properly designed, installed, and frequently checked earthing system.

Where possible, conductive cases should be used along with the least sensitive (to electrostatic discharge) propellants.

Where other requirements preclude the prevention of electrostatic charge generation, conditions favorable to high charge leakage rates, such as relative humidities in excess of 40%, should be introduced.

Solid propellant sensitivity can be reduced by using large sized conductive (Al) particles and spheroidal rather than platelet conductive particles.

CHAPTER 7. NATO STANDARDIZATION ACTIVITIES TO PROMOTE MUNITION SAFETY

7.1. BACKGROUND

The purpose of this chapter is to briefly outline NATO supported activities dealing with solid propellant rocket motor hazards or the more general area of munition safety.

One aim of NATO is to achieve increased military effectiveness through the efficient use of resources allocated by nations for their defense. This includes funds allocated for multinational development of weapons and cross procurement of weapons between nations. In the case of weapons and stores containing energetic materials, an economy of resources can be realized if there is a common approach for the design of a weapon and the test requirements necessary to demonstrate acceptable safety limits.

7.2. ORIGIN OF AC/310 IN NATO

Prior to 1979, NATO addressed munition safety needs through activities within AC/225, "NATO Army Armament Group" and AC/258, "Group of Experts on the Safety Aspects of Transportation and Storage of Military Ammunition and Explosives." In 1979, the Conference of National Armament Directors (CNAD) acknowledged that munitions safety was one of the greatest impediments to weapon interoperability within NATO nations. Accordingly, NATO formed AC/310, "Group on the Safety and Suitability for Service of Munitions and Explosives," and tasked this Group to address safety standardization associated with the different phases of the research, development, and weapon procurement cycle. The Terms of Reference for AC/310 (NATO, 1987) more clearly define the activities of this group.

"The areas of concern are:

- The design principles to be adapted to ensure the safety of munitions,

- The criteria and tests to be applied for the assessment of the safety and suitability for service of munitions, and

- The service environments with special emphasis on munitions.

These areas of concern include the basic properties, characteristics and qualification of explosives, including new materials not yet applied.

These concerns are valid throughout the design to acceptance-for-service stages of weapon development."

7.3. AC/310 WITHIN THE NATO ORGANIZATION

A partial NATO organization chart, presented in Fig. 129, shows the relationship of AC/310 relative to other groups involved in different aspects of safety standardization.

NATO AC/310 is one of six CADRE groups reporting to the Conference for National Armament Directors (CNAD). The activities of AC/310 are of interest to all other groups in the CNAD structure dealing with munitions. The primary groups with which AC/310 interacts are as follows:

- NATO Navy Armament Group (NNAG), AC/141
- NATO Air Force Armament Group (NAFAG), AC/224
- NATO Army Armament Group (NAAG), AC/225
- NATO Group of Experts on the Safety of Transportation and Storage of Ammunition and Explosives, AC/258
- NATO Industrial Advisory Group (NIAG)

The activities of the three armament groups involve NATO cooperative munitions programs (e.g., NATO Sea Sparrow, NATO Sea Gnat, NATO 155 mm Self-Propelled Howitzer, Milan Guided Anti-Armour Weapon, the NATO Patriot Program, etc.). Obviously, all NATO munitions development programs must abide by standard safety requirements and standards arising from AC/310. The NIAG is a high level consultative body of senior industrialists of NATO member nations. Among other goals, the NIAG fosters government-to-industry and industry-to-industry armament cooperation within NATO.

For technical issues associated with munitions using propulsion components, AC/310 interacts with the Propulsion and Energetic Panel of the Advisory Group for Aerospace Research and Development (AGARD). This AGARD Panel is the sponsor for this AGARDograph.

NATO AC/315 is a high level group tasked by the NATO Council to coordinate the overall NATO standardization program.

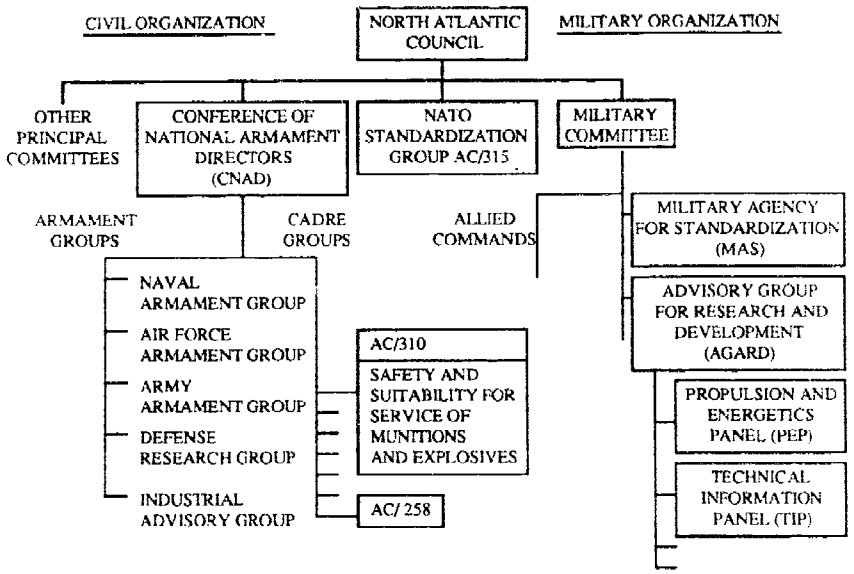

Fig. 129. AC/310 in NATO Organization

7.4. STRUCTURE OF NATO AC/310

NATO AC/310 is a tri-service group and considers all elements of a weapon or store containing explosives (or energetic materials). The organization of AC/310 is presented in Fig. 130. It is comprised of a Main Group and four supporting Sub-Groups.

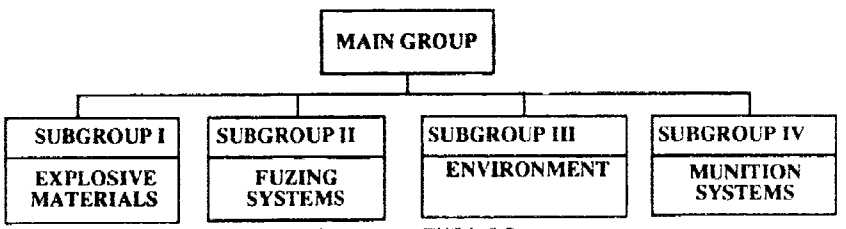

• EXPLOSIVES = ALL ENERGETIC MATERIALS
• MUNITIONS = ALL DEVICES CONTAINING ENERGETIC MATERIALS

Fig. 130. NATO AC/310 Organization.

7.4.1. The Main Group. The Main Group of AC/310 is the permanent policy and management body for AC/310. It is responsible for accepting and assigning tasks for AC/310. It directs, coordinates, and integrates the program of work within AC/310 as well as in relation to the function of AC/310 within NATO, and in consequence, directs the planning and execution of the work of its subordinate bodies.

7.4.2. The Sub-Groups

The Main Group has established four permanent Sub-Groups to deal with specific long term tasks of AC/310. The Sub-Groups may undertake tasks within the framework of the TOR and the policy established by the Main Group.

Sub-Group I concentrates on the safety and suitability for service of explosive materials (high explosives, propellants, and pyrotechnics).

Sub-Group II is concerned with design safety principles and test methods for ignition systems, fuzing, and safety and arming systems.

Sub-Group III has the responsibility for achieving a common, agreed definition of climatic, mechanical, and specialized electrical environments. The latter includes radio frequency(RF), static electricity, and lightning aspects.

Finally, Sub-Group IV is concerned with developing methodology for the assessment of the safety and suitability for service of munition systems. To accomplish this, Sub-Group IV draws on the fundamentals developed in the other three Sub-Groups and applies these to three generic classes of munition systems: underwater, surface and air launched. In addition to safety test requirements for different munition systems, Sub-Group IV is publishing safety design criteria documents for specific munition components and subcomponents.

The frequency of meetings for the Main and Sub-Groups is twice a year, but each Sub-Group has the authority to establish ad hoc working groups of specialists to deal with particular problems.

7.5. NATO "INSENSITIVE MUNITIONS" INFORMATION CENTER (NIMIC)

In recent years, increased attention has been given to weapon platform vulnerability with special emphasis on the adequacy of a munition's safety in a combat environment. For both new and existing munitions, the desire is to minimize a munition's sensitivity to those stimuli associated with combat environment and to minimize the munition's response if it should be initiated by these stimuli. Munitions designed according to these needs are termed "Insensitive Munitions."

Because of the increased level of interest nations were directing to different aspects of "Insensitive Munitions", AC/310 recognized the need to coordinate multinational efforts to minimize unnecessary duplication, share in new methods for achieving safety, and provide the basis for an acceptable level of standardization. To accomplish these needs, AC/310 proposed that a NATO "Insensitive Munitions" Information Center (NIMIC) be created.

The concept of a NIMIC was introduced at an AC/310 sponsored workshop held October 1986 in London, England (Proceedings, 1987). The workshop was conducted for members of NATO groups that would be interested in the creation of a NIMIC and could provide AC/310 with constructive feedback regarding the value of such an information center relative to existing NATO efforts. Representatives from the key NATO groups shown in Fig. 129 were present at the workshop.

The workshop discussions resulted in a recommendation that a NIMIC be formed. More specifically, the recommendation supported a proposal for first establishing a Pilot NIMIC (PNIMIC) which would be located at Applied Physics Laboratory/Johns Hopkins University, Maryland. After the PNIMIC had evolved into an operational information center the PNIMIC would be transferred to NATO Headquarters.

> The PNIMIC was created when the National Armament Directors for France, Netherlands, Norway, the United Kingdom, and the United States signed a Memorandum of Understanding at the April 1988 CNAD Meeting in Brussels, Belgium. The objectives of the PNIMIC are to receive, analyze, generate, store, and supply technical information on the following topics:

(a) Technical requirements for "Insensitive Munitions,"

(b) Methods and systems for assessing and improving munitions to meet these requirements,

(c) Databases of sensitivity tests using explosives and munitions,

(d) Insensitive munition technology deficiencies that prevent requirements from being achieved and proposals for remedial actions,

(e) Recommendations for possible solutions or design approaches to meet "Insensitive Munitions" development requirements, and

(f) Techniques for facilitating interactions among designers.

The operation of the PNIMIC is depicted in Fig. 131. Participating nations, shown to the right of the figure, each have munition specialists working at the PNIMIC.

Munition safety data related to "Insensitive Munitions" is provided to the PNIMIC through the resident specialist who shares the data with other specialists at the Center. The PNIMIC staff does more than provide a library function; rather, the staff collects and provides analysis resulting in a

product focused at accomplishing the objectives of the Center. Information and results in the PNIMIC are available to participating nations as shown in Fig. 131. The transfer of any information from the PNIMIC to nonparticipating nations must be approved by the PNIMIC Steering Committee which consists of representatives from each participating nation. Other NATO nations may join the PNIMIC; these nations are depicted by the boxes on the left of Fig. 131.

It is anticipated that PNIMIC will transition to NATO Headquarters in the Spring of 1991 at which time it will become the NATO "Insensitive Munitions" Information Center (NIMIC).

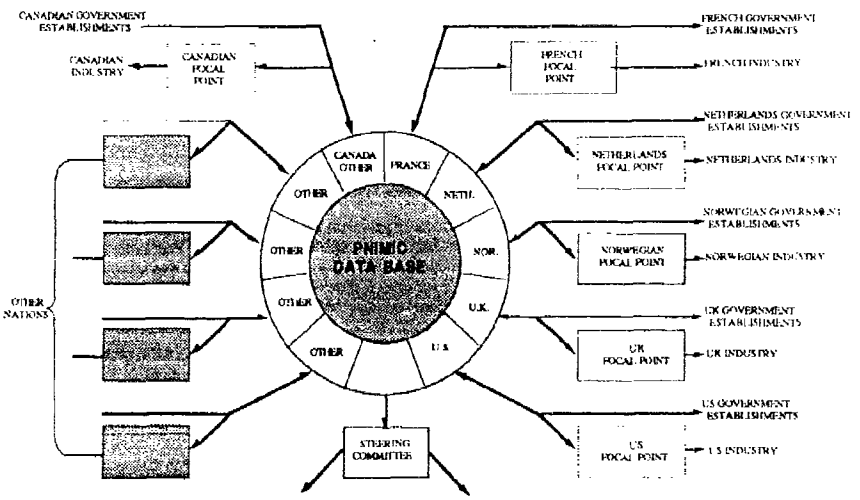

Fig. 131. Pilot NATO "Insensitive Munitions" Information Center.

8. FUTURE NEEDS

8.1 INTRODUCTION

This AGARDograph does not present the final understanding for hazards associated with solid propellant rocket motors. Rather it represents the status of hazards of solid propellant rocket motors as of 1 January 1989. Progress has been rapid in this field in the last several years and it is anticipated that this acceleration will continue and increase.

Perhaps the most significant contribution the AGARDograph makes is to put fundamental technical areas in perspective relative to rocket motor hazards threat areas. This is done through the introduction of the Hazard Analysis Protocol concept (see Chapter 4). This concept presents a logical, technically sound approach for addressing threats. It introduces the fundamental technical areas important to hazards are introduced through the identification of test methods and analysis.

8.2 HAZARD ANALYSIS PROTOCOL CONCEPT

The Hazard Analysis Protocols have not been completed for all threats of importance to solid rocket motors. In this AGARDograph, only fragment impact is complete in that it includes all four phases of the concept. Since the time this AGARDograph was assembled, much further work has been conducted on the fragment impact protocol (notably by James and co-workers in the United Kingdom), the shaped charge jet protocol (Chick of Australia, Frey of the United States, and James of the United Kingdom), electrostatic discharge (Covino and Dreitzler of the United States, Hamment of the United Kingdom). In addition protocols for cook-off and sympathetic detonation have been developed. Much of this protocol development as well as identification of deficiences and establishment of technical collaborative studies to overcome the deficiences has been done within the Technical Cooperation Program W Action Group 11 on The Hazards of Energetic Materials and their Relation to Munitions Survivability.

Work is continuing in all of these areas and it is anticipated that the protocols will continue to evolve as additional knowledge is gained.

8.3 LABORATORY TESTS AND ANALYSIS

Many test methods used to evaluate energetic material, such as solid propellants, are of a go/no-go nature and do not provide the necessary quantitative data to allow calculations and analyses prescribed by the Hazard Analysis Protocols. A need exists to address all of the threat Hazard Analysis Protocols and identify deficiencies and weaknesses from a test and analysis standpoint. Where weaknesses are identified, research studies should be initiated to provide the data necessary to eliminate the deficiencies. Chapter 5 presents some of the most significant areas where additional data are needed and research studies are being conducted.

8.4 MITIGATION APPROACHES

Chapter 6 presents some methods for mitigating unwanted reactions when solid rocket motors are subjected to threats. As more is learned about the fundamental nature of solid rocket behavior in a threat environment, new mitigation methods will be made available. Since Chapter 6 was written, several efforts in mitigating sympathetic detonation have been performed. The one effort, utilizing the Hazard Analysis concept, uses a computer program called FRAGMAP. This progam has been presented to the NATO Insensitive Munitions Information Center (NIMIC) (Wagenhals, 1990). A separate area of study that must be addressed in the future is the understanding of tradeoffs between hazard mitigation and parameters such as cost, performance, and producibility of rocket motors.

8.5 FUTURE PROPELLANTS

Past methods for ranking solid propellants are inadequate for discussion involving solid rocket motor hazards. In the past, solid rocket propellants were distinctly different from high explosives. Today, the ingredients and formulations for solid propellants, used in rockets, and high explosives, used in warheads and bombs, are not markedly different for some systems. Accordingly, classification of propellants separate from high explosives doesn't recognize the fact that some solid propellants and high explosives have almost the same combination of ingredients.

New approaches are needed for ranking solid propellants, and perhaps all energetic materials. One possible scheme to classify cast double-base propellants, proposed by a principal propellant developer in the UK, is presented in the following paragraphs.

8.5.1 Families of Propellants

A propellant developer will generally be involved simultaneously in work on a number of formulations of the same general type, i.e., based on the same manufacturing process, and using the same chemical system as the principal source of energy and gaseous products, but differing in minor ingredients (stabilizer, burning rate catalyst, etc.) and in the proportions of the various ingredients. In connection with qualification in terms of STANAG 4170 he will seek guidance from the National Authority on which of these constitute new propellants; he will wish to minimize the number of propellant compositions subjected to a detailed qualification program since this is an expensive and time-consuming process, involving a wide range of testing procedures. This problem has been receiving attention. The aim of a National Authority should be to give advice as early as possible and this conflicts with the need to ensure that the assessment is conducted on data which apply to the propellant actually going into service. Changes in formulations may occur late in development, for example to facilitate production or to adjust performance characteristics, etc. A re-evaluation of any earlier safety assessment is then required and consideration must be given to the need for repeat, albeit limited, testing of compositions.

It is clear therefore that an overall aim to provide a wide range of potentially "on the shelf" qualified propellants to meet the needs of weapons programs cannot be achieved without resorting to classification by analogy. It should be possible to establish a base line of safety and suitability characteristics for the most common formulations. For example, in this a scheme proposed by a principal propellant developer in the U.K. and agreed to by the British National Authority, their range of cast double-base propellants are classified based on binder/filler combinations with selections of additives. Six propellant composition groups have been identified and the principle of "worst case" testing has been proposed, i.e., the minimum and maximum nitrocellulose/nitroglycerine ratios of each group are taken and, where appropriate, the maximum filler content envisaged in practice. The resulting total of 12 compositions is considered a minimum to establish a base line for this scheme which is outlined in Table 25. Some testing after aging is also involved. Any new ingredient thereafter will be judged on its merits at the time of its proposed introduction and any requirement for testing appraisal propellant formulations containing it will need to be decided. In this way it is hoped by the U.K. to reduce the testing and assessment of the large numbers of possible cast double base formulations that exist to manageable levels. To place such compositions in a scheme of this kind is a major undertaking. On completion of this program, it is anticipated that the degree of classification by analogy will require review and the feasibility of new guidelines will be examined by the National Board for the definition of new cast double-based propellants. It has to be stressed, however, that all propellants must be considered on their merits by the National Board, when they are presented as candidates for UK service. It will not be possible to give blanket clearance in advance and, for individual cases, the National Board may require a written submission from the developer presenting the arguments for classification by analogy. On the basis of the greatly enlarged database, it is hoped that a quick response will be possible from the National Board in most circumstances.

8.6 CONCLUDING REMARKS

The various authors hope that this AGARDograph makes contributions to the munition user, designer, and scientist, hopefully bringing these groups closer together in understanding. We are also aware of many deficiencies and have attempted to point out some of these in the various chapters. For example, there is a critical need for well defined, standardized test methods, especially small scale tests that can be performed early in the development cycle that provide data for the designers. These results must give good comparison to actual full scale tests. Computer simulation and modeling of the large scale tests is critically needed so that we don't have to run so many costly large scale tests. These predictions should also allow us to better understand the phenomena in cause and effect fashion, and to extrapolate results from one regime to others. We also need better ancillary experiments that allow us to determine parameters from laboratory experiments, and then fix these parameters in other analyses.

We hope that this AGARDograph is helpful to the users and stimulates others to continue work in these areas.

Table 25 Proposed Scheme of Propellant Composition Groupings. (Example)

	Conventional CDB			Elastomer Modified (EDM) CDB		
	Group 1	Group 2	Group 3	Group 4	Group 5	Group 6
Double-Base Content	NC/NG Ratio 6.0/1 to 1.4/1	As Group 1	As Group 1	NC/NG Ratio 1/2.2 to 1/1.3	As Group 4	As Group 4
Inert Content	6.0 to 12.0%	As Group 1	As Group 1	As Group 1	As Group 1	As Group 1
Explosive Loading	Nil	0 to 40% nitramine (such as RDX)	0 to 40% nitramine (such as RDX) Aluminum/ Ammonium Perchlorate	Nil	As Group 2	As Group 3

[NOTE: Some concern has been expressed over grouping in the same family propellants having 0 to 40% nitramine (such as RDX).]

Similar classifications into groups can be made for extruded and rubbery composite propellants and some progress on base line characterization has been made in these areas.

REFERENCES

V. G. Abramov, A. G. Merzhanov, and V. T. Gontkovskaya. Izv. Akad. Nauk SSSR, Ser. Khim., 3, 427, 1966.

V. G. Abramov, A. G. Merzhanov, and V. T. Gontkovskaya. Izv. Akad. Nauk SSSR, Ser. Khim., 5, 823, 1966.

G. Adomeit and W. Hocks. AIAA Journal, Vol. 20, pp. 1579-1585, 1982.

G. Adomeit and W. Hocks. FRG Symposium on Ballistics, Mannheim, October 1987.

Allied Ordnance Publication (AOP) No. 7, NATO, Bruxelles (1982).

American Society for Testing and Materials. "Standard Test Methods for D-C Resistance of Conductance and Insulating Materials," Standard D257-78, reapproved 1983.

American Society for Testing Materials. "Standard Test Method for Dielectric Breakdown Voltage and Dielectric Strength of Solid Electrical Insulating Materials at Commercial Power Frequencies," Standard D149-81, 1981, pp. 1-13.

American Society for Testing Materials. "Standard Methods of Test for A-C Loss Characteristics and Dielectric Constant (Permittivity) of Solid Electrical Insulating Materials," Standard D150-70, 1971, annual book of ASTM Standards by American Society for Testing and Materials, p. 27.

A. P. Amosov, S. A. Bostandzhiyan, V. P. Volodin, A. N. Gryadunov, and S. M. Muratov. Combustion, Explosion, and Shock Waves, Vol. 14, pp. 644-648, 1979.

W. H. Anderson. Combustion Science and Technology, Vol. 24, pp. 143-159, 1980.

W. H. Anderson, L. J. Irwin, and N. A. Louie. Combustion Science and Technology, Vol. 20, pp. 1-4, 1979.

W. H. Anderson and N. A. Louie. Combustion Science and Technology, Vol. 20, pp. 153-160, 1979.

W. H. Anderson and G. P. Stillman Combustion Science and Technology, Vol. 32, pp. 237-244, 1983.

Armament Research Department. "The Initiation of an Exploder by a Munroe Jet (Flash Radiography)," ARD Met. Report 45, April 1945.

B. W. Asay, J. B. Ramsay, and A. W. Campbell. "Response of Propellants to Hypervelocity Attack," LA-UR-87-3171, 1987.

A. I. Atwood, C. F. Price, D. E. Zurn, and T. L. Boggs. "Frangible Tube Convective Combustion Tests," 1986 JANNAF Propulsion Systems Hazards Subcommittee Meeting, CPIA Publ. 446, Vol. I, pp. 197-204, March 1986.

A. I. Atwood, C. F. Price, D. E. Zurn, and T. L. Boggs. "The Determination of Permeability/Drag of Systems Described by DDT Analysis," 1986 Propulsion Systems Hazard Subcommittee Meeting. CPIA Publ. 446, Vol. I, pp. 99-106, March 1986.

A. I. Atwood, D. E. Zurn, T. L. Boggs, C. F. Price, and L. M. Stayton. "The Effects of Artificial and Normal Aging on the Ignitability and Burn Rate of a High Energy Propellant, 20th JANNAF Combustion Meeting, Monterey, CA. October 1983. (CPIA Publication 383.)

M. R. Baer and J. Nunziato. "A Theory for Deflagration-to-Detonation Transition (DDT) in Granular Explosives," SAND82-0293, Sandia National Laboratory, Albuquerque, NM, December 1983 and M. R. Baer and J. Nunziato, "A Study of Deflagration-to-Detonation Transition (DDT) in the Granular Explosive, CP," SAND83-1929, Sandia National Laboratory, Albuquerque, NM, February 1984.

K. L. Bahl, H. C Vantine, and R. C. Weingart. "The Shock Initiation of Bare and Covered Explosives by Projectile Impact," 7th Detonation (International) Symposium, pp. 325-335, 1981.

W. E. Baker, P. A. Cox, P. S. Westine J. J. Kulidge, and R. A .Strehlow. "Explosion Hazards and Evaluation," Elzevier, 1983.

K. N. Bascombe and D. J. Manners. "UK Work on Low Vulnerability Rocket Motors," Workshop on Insensitive Munitions Information Exchange, NATO AC/310 Conference Proceedings No. 001, March 1987.

M. W. Beckstead, N. L. Peterson, D. T. Pilcher, B. D. Hopkins, and H. Krier. "Convective Combustion Modeling Applied to Deflagration-to-Detonation Transition of HMX," Comb. and Flame, Vol. 30, pp. 231-241, 1977.

P. Benhaim and J. Goliger. "Deflagration Rate of Composite High Explosive and Composite Propellants at Pressure Above 1 Kilobar," 6th Symposium on Detonation, San Diego, CA, 1976.

R. R. Bernecker. "Experimental Techniques and Results for Propellant and Explosives," ONR/AFOSR Workshop on Deflagration-to-Detonation Transition, CPIA Publ. 299, pp. 187-216, September 1978.

R. R. Bernecker. "The DDT Process for High Energy Propellants," Hazard Studies for Solid Propellant Rocket Motors," AGARD Conference Proceedings, No. 367, NATO, May 1984.

Naval Ordnance Laboratory. "Sensitivity of Explosives to Transition from Deflagration to Detonation," by R. R. Bernecker and D. Price, 7 February 1975, NOLTR 74-186.

R. R. Bernecker, D. Price, J. O. Erkman, and A. R. Clairmont, Jr. "Deflagration to Detonation Transition Behavior of Tetryl," Sixth Symposium (International) on Detonation, Arlington, Virginia, Office of Naval Research, ACR-221, pp. 426-435, 1976.

R. R. Bernecker, H. W. Sandusky, and A. R. Clairmont, Jr. "Deflagration-to- Detonation Transition Studies of Porous Explosive Charges in Plastic Tubes," Seventh Symposium (International) on Detonation, pp. 119-138, 1982.

R. R. Bernecker, H. W. Sandusky, and A. R. Clairmont, Jr. "Deflagration-to- Detonation Transition DDT Studies of a Double Base Propellant," Eighth Symposium (International) on Detonation, Naval Surface Weapons Center, NSWC Preprint CONF-850706, Vol. 2, pp. 712-723, 1985.

G. S. Biasutti. History of Accidents in the Explosives Industry, Vevey, 1985.

A. Birk and L. H. Caveny. AIAA Journal, Vol. 18,, pp. 1363-1370, 1980. (See also AIAA Journal Vol. 21, pp. 579-585, 1983.)

E. J. Blommer as cited in Energetic Materials Hazard Initiation: DoD Assessment Final Report, May 1987

A. B. Bofors and Nobel Kruit. Analytical Methods for Powders and Explosives, Bofors, Sweden, 1960.

T. L. Boggs, A. I. Atwood, K. J. Graham, A. H. Lepie, C. F. Price, H. P. Richter and D. E. Zurn. "Hazards of Solid Rocket Propellants," in Proc. Eastern States Combustion Meeting, November 1986, pp. B1-B12.

Naval Weapons Center. "Combustion Bombs: A Review and Recommendation for Use in High-Energy Propellant Safety Program," by T. L. Boggs, H. H. Bradley, Jr., T. S. Eitzen, and D. E. Zurn. China Lake, CA, NWC, August 1976. (NWC TM 2922, publication UNCLASSIFIED.)

T. L. Boggs, C. F. Price, A. I. Atwood, D. E. Zurn, and R. L. Derr. "Role of Gas Phase Reactions in Deflagration-to-Detonation Transition," Seventh Symposium (International) on Detonation," Naval Surface Weapons Center, NSWC MP-82-834, pp. 216-224, 1982.

T. L. Boggs, C. F. Price, A. I. Atwood, D. E. Zurn, and R. L. Derr. "Preignition of High Energy Propellants," 16th JANNAF Combustion Meeting, December 1979. (CPIA Publication 308.)

T. L. Boggs, C. F. Price, A. I. Atwood, D. E. Zurn, and R. L. Derr. "Role of Gas Phase Reactions in Deflagration to Detonation Transition," 7th Symposium (International) on Detonation, White Oak, MD, June 1981. (NSWC MP 82-334.)

T. L. Boggs, C. F. Price, A. I. Atwood, D. E. Zurn, and J. L. Eisel. "The Combustion of HMX," 17th JANNAF Combustion Meeting, CPIA Publ. 329, pp. 432-440, November 1980.

T. L. Boggs, C. F. Price, and R. L. Derr. "Transient Combustion: An Important Consideration in Deflagration to Detonation Transition," Hazard Studies for Solid Propellant Rocket Motors, AGARD Conference Proceedings, No. 367, NATO. May 1984.

T. L. Boggs, C. F. Price, H. P. Richter, A. I. Atwood, A. H. Lepie, N. G. Zwierzchowski, and L. R. Boyer. "Detonation of Undamaged and Damaged Materials," in Combustion and Detonation Phenomena, 19th International Annual Conference of ICT, pp. 30-1 to 30-13, 1988.

T. L. Boggs, C. F. Price, D. E. Zurn, R. L. Derr, and E. J. Dibble. "The Self-Deflagration of Cyclotetramethylenetetranitramine (HMX)," AIAA/SAE 13th Joint Propulsion Conference, Preprint 77-859, July 1977.

T. L. Boggs, D. E. Zurn, and R. L. Derr. "The Burning Rates of Damaged High Energy Solid Propellants," in Proceedings of ONR/AFOSR Workshop on Deflagration-to-Detonation Transitions, CPIA Publ. 299, pp. 89-94, 1978.

F. X. Boisseau, Department of Defense Explosives Safety Board Meeting, DDESB, 1986.

F. P. Bowden and O. A .Gurton. Proc. Roy. Soc. Lond. A198, p. 337, 1949.

F. P. Bowden and A. D. Yoffe. "Initiation and Growth of Explosion in Solid and Liquids," University Press, Cambridge, 1952.

H. H. Bradley. "A Unified Theory of Solid Propellant Ignition," NWC TP 5618, China Lake. California, 1975.

J. Brunet and B. Salvetat. "Detonation Critical Diameter of Advanced Solid Rocket Propellants," Joint International Symposium on Compatibility of Plastics and Other Materials with Explosives, Propellants, Pyrotechnics and Processing of Explosives, Propellants, and Ingredients, New Orleans, Louisiana, 18-20 April 1988.

Burlot. 1930 Memoires Artillerie Francais, 1930, 9:799.

A. G. Butcher. "Advancements in DDT Research Using the Plastic Pipe," 1982 JANNAF Propulsion Systems Hazard Meeting, CPIA Pub. 356, Vol. 1, pp. 155-163, April 1982.

A. G. Butcher, B. D. Hopkins, and N. J. Robinson. "Fundamental Experiments of DDT," 15th JANNAF Combustion Meeting, CPIA Publ. 297, Vol. III, pp. 75-102, February 1979.

A. G. Butcher and K. B. Isom. "Combustion Behavior During DDT Run-up," 19th JANNAF Combustion Meeting, Vol. II, pp. 203-216, October 1982.

A. G. Butcher, R. L. Keefe, N. J. Robinson, and M. W. Beckstead. "Effects of Igniter and Compaction on DDT Run-up in Plastic Pipes," Seventh Symposium (International) on Detonation. Naval Surface Weapons Center, NSWC MP 82-334, pp. 143-150, 1982.

P. B. Butler, M. F. Lembeck, and H. Krier. "Modeling of Shock Development and Transition to Detonation Initiated by Burning in Porous Propellant Beds,"Combustion and Flame, Vol. 46, p. 75, 1982. (Also see enclosed References 1-6 for earlier versions of DDT model and C. Cudak, P. Butler, and H. Krier, "A Model for Shock Initiation of Porous Propellants by Ramp Induced Compression Processes," Eighth Symposium (International) on Detonation, Preprint Vol. 2, p. 658, 15-19 July 1985 (Albuquerque, NM).

A. W. Campbell. "Jet Attack of PBX-9502," LANL Int. Report M-3-QR-78-4, 1978 and M-3-QR-79-1, 1979.

A. W. Campbell. "Deflagration-to-Detonation Transition in Granular HMX," 1980 JANNAF Propulsion Systems Hazard Meeting, CPIA Publ. 330, Vol. 1, pp. 105-130, December 1980.

A. W. Campbell. "The Use of Witness Plates to Assess the Promptness of Initiation of PBX-9502 by Jets," LA-UR-81-3545, 1981.

A. W. Campbell. "Jet Attack of PBX-9502," LA-UR-88-458, 1988.

D. Casenave and P. Racimor. Proc. AGARD Conf. 367, 20-1, Lisse, 1984.

E. Catalano, R. R. McGuire, E. L. Lee, E. W. Wrenn, D. Ornellas, and J. Walton. Proc. 6th Symp. (Int.) on Detonation, 214, Arlington, 1976.

M. C. Chick and T. J. Bussell. "The Importance of Critical Detonation Diameter in Determining the Response of a Munition Filling to Shaped Charge Jets," Second Australian Explosive Safety Seminar. Canberra, 1987.

M. C. Chick, T. Bussell, R. B. Frey, and G. Boyce. "Initiation of Munitions by Shaped Charge Jets," 9th International Symposium on Ballistics 2, pp. 421-430, 1986a.

M. C. Chick and D. J. Hatt. "The Mechanism of Initiation of Composition B by a Metal Jet," 7th Symposium (International) on Detonation, 1981 [Proc.], pp. 352-361, 1981a.

M. C. Chick and D. J. Hatt. "Metal Jet Initiation of Bare and Covered Explosives; Summary of the Mechanism, Empirical Model and Some Applications," Department of Defence, Material Research Laboratories, Melbourne, Victoria, Australia, Report, MRL-R-830, 1981b.

M. C. Chick and D. J. Hatt. "The Initiation of Covered Composition B by a Metal Jet," Propellants, Explosives, Pyrotechnics, Vol. 8, pp. 121-126, 1983.

M. C. Chick and J. B. MacIntyre. "The Jet Initiation of Solid Explosives," 8th Symposium (International) on Detonation, 1985 [Proc.], pp. 20-28, 1985.

M. C. Chick, M. G. Wolfsan, and L. A. Learmonth. "A Calibrated Test for the Assessment of the Sensitivity of Explosives to Shaped Charge Jets," MRL-Report-1016, 1986b.

"Compilation of Damage Models," Ministry of Housing, Physical Planning, and the Environment, the Netherlands, to be published 1989.

M. A. Cook. "The Science of High Explosives," Reinhold Publishing Corporation, 1959.

J. Covino and D. R. Dreitzler. "Electrostatic Discharge (ESD) Hazards of Energetic Materials and Propulsion Systems," 19th ICT Conference, Combustin and Detonation Phenomena, pp. 80-1 to 80-14, 1988.

J. Covino and F. E. Hudson, III. "Current Assessment Methodology for Electrostatic Discharge (ESD) Hazards of Energetic Materials," to be published by AIAA Journal of Propulsion and Power, 1990.

D. P. Crowley. U.S. Patent 4, 114, 369 9/1978 60/100 A.

J. E. Crump, A. I. Atwood and D. E. Zurn. Combustion Instability and Ignition Testing of NOS/IH Extruded Composite Propellant (Hycar Formulation, Mix 8514)," China Lake, CA, NWC, December 1984 (NWC TP 5427, publication UNCLASSIFIED).

L. DeLuca, L. H. Caveny, T. J. Ohlemiller, and M. Summerfield. "Radiative Ignition of Double-Base Propellants: I Some Formulation Effects, II Pre-Ignition Events and Source Effects," AIAA J., Vol. 14, No. 7, pp. 940-946, July 1976, Vol. 14, No. 8, pp. 1111-1117, August 1976.

A. V. Dubovik and M. V. Kisanov. Combustion, Explosion, and Shock Waves, Vol. 21, pp. 459-464, 1985.

A. S. Dyer, P. J. Haskins, P. J. Hubbard, and C. D. Hutchinson. "The Growth and Decay of Explosive Deflagrations in Munition in Simulated Factory Accident Scenarios," in 8th Symposium (International) on Detonation, 1985 Preprint Volume 850706, Vol. 1, pp. 29-38.

W. L. Elban. "Quasi-Static Compaction Studies for DDT Investigations: Ball Propellants," submitted to Propellants, Explosives, and Pyrotechnics, 1982.

W. L. Elban, S. B. Gross, and R. R. Bernecker. "Quasi-Static Compaction of Porous Columns of Inert Materials," Naval Surface Weapons Center, NSWC TR-81-113, 1981.

R. B. Elwell, O. R. Irwin, and R. W. Vail, Jr. "Project SOPHY - Solid Propellants Hazards Program," AFRPL-TR-67-211, Vol. I, 1967, AD 819299.

S. Ergun. "Fluid Flow Through Packed Columns," Chem. Eng. Progress, Vol. 48, pp. 89-94, February 1952.

T. Erneux, J. Arys, and R. Meysmans. Prop. Explo. and Pyr., 8, 199, 1983.

G. I. Evans, J. F. Bingham, J. H. Sindall. Proc. AGARD Conf. 367, 8-1, Lisse, 1984.

S. A. Finnegan, et al. "Characterizing the Fragment Impact Hazards of Warheads and Solid Propellant Motors," Proceedings from the Tenth International Symposium on Ballistics, San Diego, California, October 1987.

R. W. Fleming and R. L. Derr. "An Investigation of Nonreactive Surface Coatings for Use in Solid Propellant Arc-Image Ignition Studies," China Lake, CA, NWC, December 1975 (NWC TP 5828, publication UNCLASSIFIED).

C. A. Forest. "Burning and Detonation," Seventh Symposium (International) on Detonation, NSWC MP 82-334, Naval Surface Weapons Center, White Oak, Silver Spring, Maryland, pp. 234-243, 1981.

D. A. Frank-Kamenetsky. Diffusion and Heat Exchange, Princeton University Press, Princeton, 1955.

D. A. Frank-Kamenetsky. Dokl. Akad. Nauta SSSR, 18, 411, 1938; Zh. Fix. Komm., 13, 868, 1939.

D. A. Frank-Kamenetsky. Diffusion and Heat Transfer in Chemical Kinetics, Plenum Press, New York, 1969.

N. J. Gerri, S. P. Pfaff, and A. E. Ortega. "Gas Flow and Flame Spreading in Porous Beds of Ball Propellant," 11th JANNAF Combustion Meeting, CPIA Publ. 261, Vol. 1, pp. 177-198, December 1974. Also see BRL-IMR-159, 1973.

T. R. Gibbs and A. Popolato. "LASL Explosive Property Data," University of California Press, 1980.

H. L. Gidhar, A. J. Aroca. Combustion and Flame, Vol. 31, pp. 245, 1978.

I. Glassman. "Combustion," Academic Press, New York, 1977.

A. Gomez and G. C. Wake. Combustion and Flame, Vol. 61, pp. 177-187, 1985.

R. A. Gould. "Progress Report on JANNAF Panel on Shotgun/Relative Quickness Testing," 1980 JANNAF Propulsion Systems Hazards Subcommittee Meeting, CPIA Publ. 330, Vol. I, pp. 289-301, December 1981.

L. Green. "Shock Initiation of Explosives by the Impact of Small Diameter Cylindrical Projectiles," 7th Detonation (International) Symposium, pp. 273-277, 1981.

N. Griffiths, R. McN Laidler, and S. T. Spooner. "Some Aspects of the Shock Initiation of Condensed Explosives," Combustion and Flame, Vol. 7, pp. 347-352, 1963.

Th.M. Groothuizen, E. W. Lindeyer, and H. J. Pasman. "Investigation into the Cause of the Explosion in the TNT Melting Shop of the KNSF at Muiden," Explosivestoffe, May 1970.

J. M. Hammersley and D. C. Handscomb. Monte Carlo Methods, 1964, Spottiswoode, Ballentyne and Co. Ltd., London and Colcrester, pp. 134-141.

J. M. Hammersley and S. R. Broadbent. "Percolation Processes. I. Crystals and Mazes," Proc. Comb. Phil. Soc., 53, pp. 629-641.

J. M. Hammersley. "Percolation Processes and Related Topics," J. Soc. Indust. Appl. Math, 11, pp. 894-918.

E. Hasman, M. Gvishi, and Y. Carmel. "Measurement of Shock Initiation Threshold of HNAB by Flyer Plater Impact," Propellants, Explosives, Pyrotechnics, Vol. 11, pp. 144-149, 1986.

M. Held. "Initiierung von Sprengstoffen, ein Vielschictiges Problem der Detonationsphysik," Explosivstoff, Vol. 5, pp. 2-17, 1968.

M. Held. "Cutting Charges," V International Symposium on Ballistics, pp. 1-8, 1980.

M. Held. "Hohlladungen," in Handbook, Munitionsbewertung, BWB-WM IV 2, 1981a.

M. Held. "Evaluation of Shaped Charge Jet Penetration Efficiency by Advanced Diagnostic Techniques," IV International Symposium on Ballistics, pp. 480-493, 1981b.

M. Held. "Characterizing Shaped Charge Performance by Stand-Off Behaviour," VII International Symposium on Ballistics, pp. 331-339, 1983a.

M. Held. "Critical Area for the Initiation of High Explosive Charges," Shock Waves in Condensed matter, Santa Fe, NM, 1983 [Proc.] Chapter XII, pp. 555-557, 1983b.

M. Held. "Experiments of Initiation of Covered, but Unconfined High Explosive Charges by Means of Shaped Charge Jets," Propellants, Explosives, Pyrotechnics, Vol. 12, pp. 35-40, 1987a.

M. Held. "Experiments of Initiation of Covered, but Unconfined HE Charges Under Different Test Conditions by Shaped Charge Jets," Propellants, Explosives, Pyrotechnics, Vol. 12, pp. 97-100, 1987b.

M. Held. "Discussion of the Experimental Findings From the Initiation of Covered, but Unconfined High Explosives Charges With Shaped Charge Jets," Propellants, Explosives, Pyrotechnics, Vol. 12, pp. 167-174, 1987c.

M. Held, F. Schedelbauer, and H. Schubert. "Aktive Schicht Für Schutzanordnungen Gegen Hohlladungsund Wuchtgeschosse," Patent DBP 2 931 415, 1978.

C. E. Hermance. "Fundamentals of Solid Propellant Combustion, ed. K. K. Kuo and M. Summerfield, AIAA Inc., New York, pp. 239-304, 1984.

J. D. Hightower. "An Investigation of the Effect of Environmental Gases and Pressure on the Ignition of Solid Rocket Propellants," China Lake, CA, NWC, October 1967 (NWC TP 4431, publication UNCLASSIFIED).

Naval Weapons Center. "A Unified Theory of Solid Propellant Ignition," by B. D. Hopkins, Jr., China Lake, California, NWC TP 5618, August 1974.

P. M. Howe, Y.. K. Huang, and A. L. Arbuckle. "A Numerical Study of Detonation Propagation Between Munitions," Seventh Symposium (International) on Detonation, pp. 1055-1061, 1981.

P. M. Howe. "Insensitive Munitions: Can We Have our Cake and Eat It, Too?" in Report on Working Group Meeting, Sensitivity of Explosives, March 15-18, 1987, Socorro, New Mexico, published by U.S. Army Research Office, P. O. Box 12211, Research Triangle Park, North Carolina.

Y. K. Huang, J. J. Starkenberg, and A. L. Arbuckle. "Some New Computed Results for Projectile-impact Shock Initiation of Solid Explosives," 8th Detonation (International) Symposium, pp. 307-317, 1985.

C. D. Hutchinson. 8th Symp. on Detonation, 480, Albuquerque, 1985.

IEEE Standard Techniques for High-Voltage Testing, 16th Edition, IEEE Standard 4-1969, pp. 37-125.

International Herald Tribune of August 30, 1986.

M. J. Isler. "Contribution Du Mode De Combustion Des Explosifs Compacts Au Processus De Transition Combustion-Deflagration-Detonation," Combustion and Detonation Phenomena, pp. 18-1 to 18-13, 1988.

P. E. Jarrett. "Derivation of the British Explosives Safety Distances," in Prevention of and Protection Against Accidental Explosion of Munitions, Fuels, and other Hazardous Mixtures, E. Cohen, editor, Annals of the New York Academy of Sciences, Vol. 152, Art. 1, pp. 18-35, 1968.

D. P. Jones and H. Krier. "Gas Flow Resistance Measurements Through Packed Beds at High Reynolds Numbers," Journal of Fluids Engineering, Vol. 105, pp. 168-173, June 1983.

R. L. Keefe. "Delayed Detonation in Card Gap Tests," Seventh Symposium (International) on Detonation, pp. 265-272, 1981, NSWC MP 82-334.

Keithley Instruments, Inc. Low Level Measurement For Effective Low Current, Low Voltage, and High Impedance Measurements, 3rd Edition, 1984, Cleveland, Ohio, pp. 63-66.

G. E. Keller, A. W. Horst, and P. S. Gough. "A Study of Ignition Dynamics for a LOVA-Type Propellant Using XNOVAK," Proceedings of the 22nd JANNAF Combustion Meeting, CPIA Publ. 432, 1985.

R. Kent and M. Rat. "Etude Des Phenomenes D'electricite Statique Dans la Frabrication et la Manipulation des Propergols Solides," Note Technique No. 94/80/CRB/DR, SNPE, 7 November 1980, (DIFFUSION RESTREINTE).

R. Kent and M. Rat. "Explosion Thermique (Cook Off) des Propergols Solides," Propellants, Explosives, Pyrotechnics, Vol. 7, pp. 129-136, 1982.

K. Kim. "Numerical Simulation of Convective Combustion of Ball Powders in Strong Confinements," AIAA J., Vol. 22, p. 793, 1984.

D. E. Kooker and M. Costantino. "Mechanical Properties of Compacted Granular Material: A Workshop Summary," 1986 JANNAF Propulsion Systems Hazards Subcommittee Meeting, CPIA Publ. 446, Vol. 1, pp. 81-97, March 1986.

H. Krier and S. S. Gokhale. "Modeling of Convective Mode Combustion Through Granulated Propellant to Predict Detonation Transition," AIAA J., Vol. 16, pp. 177-183, February 1978.

H. Krier and H. A. Kezerle. "Modeling of Convective Mode Combustion Through Granulated Propellant to Predict Transition to Detonation," University of Illinois, Urbana, IL, Final Report, October 1976-September 1977, AFOSR-TR-78-007, October 1977.

H. Krier, S. Rajan, and W. F. Van Tassell. "Flame Spreading and Combustion in Packed Beds of Propellant Grains," AIAA J., Vol. 14, No. 3, pp. 301-309, 1976.

A. K. Kulkarni, M. Kumar, and K. K. Kuo. AIAA Journal, Vol. 20, pp. 243-244, 1982. (See also AIAA Paper 80-1210, 1980).

R. K. Kumar. Combustion Science and Technology, Vol. 30, pp. 273-288, 1983.

M. Kumar and K. K. Kuo. AIAA Journal, Vol. 18, pp. 825-833, 1980.

M. Kumar, J. E. Wills, A. K. Kulkarni, and K. K. Kuo. 19th Symposium (International) on Combustion, The Combustion Institute, pp. 757-767, 1982.

M. Kumar, J. E. Wills, A. K. Kulkarni, and K. K. Kuo. AIAA Journal, Vol. 22, pp. 526-534, 1984.

M. Kumar, J. E. Wills, AA. K. Kulkarni, and K. K. Kuo. AIAA Journal, Vol. 22, pp. 526-534, 1984.

K. K. Kuo. "Principles of Combustion," John Wiley and Sons, New York, 1986.

K. K. Kuo, and C. Nydegger. "Cold Flow Resistance Measurement and Correlation in a Packed Bed of WC 870 Spherical Propellants," Journal of Ballistics, Vol. 2, No. 1, pp. 1-25, 1978.

C. O. Leiber. AGARD Conference Proceedings No. 367, 1984.

G. Lengelle. AIAA Journal, Vol. 13, pp. 315-322, 1975.

A. H. Lepie and M. B. Moran. J. Applied Polymer Science, Vol. 30, pp. 3153-3161, 1985.

B. Lewis and G. von Elbe. "Combustion, Flames, and Explosions of Gases," Academic Press, New York, 1951.

T. P. Liddiard, Jr. "The Detonation of Burning in High Explosives by Shock Waves," 4th Symposium (International) on Detonation, Washington, DC, October 1965. (ACR-126-ONR).

A. Linan and F. A. Williams. Combustion Science and Technology, Vol. 3, pp. 587-603, 1971.

A. Linan and F. A. Williams. Siam Journal of Applied Mathematics, Vol. 36, pp. 91-98, 1979.

Local Report. Brandschutz, September 1949.

R. A. Lucht and L. W. Hantel. "Mk 82 Bomb Characterization for the Sympathetic Detonation Study," 23rd DOD Explosives Safety Seminar, August 9-11, 1988, Atlanta, Georgia.

A. V. Lykov. Theory of Thermal Conductivity, Moscow, 1967.

Ch. L. Mader. "Numerical Modeling of Detonations," University of California Press, Berkeley, Calif., 1978.

Ch. L. Mader. "Recent Advances in Numerical Modeling of Detonations," Propellants, Explosives, Pyrotechnics, Vol. 22, pp. 163-166, 1986.

C. L. Mader and G. H. Pimbley. "Jet Initiation and Penetration of Explosives," Journal of Energetic Material, Vol. 1, pp. 3-44, 1983.

L. M. McAfee. "Jet Initiation of PBX-9502," LA-UR-87-3169, 1987.

P. B. McQuaide. 17e DOD Seminar on Explosives Safety, Denver, CO, 1976.

R. R. McGuire and C. M. Tarver. 7th Symp. on Detonation, 550, Annapolis, 1981.

A. G. Merzhanov and V. G. Abramov. Prop. and Exp., 6, 130, 1981.

A. G. Merzhanov, V. G. Abramov, and V. T. Gontkovskaya. Dokl. Acad. Nauk SSSR, 148, 156, 1963.

A. G. Merzhanov and A. E. Averson. Combustion and Flame, Vol. 16, pp. 89-124, 1971.

A. G. Merzhanov, V. V. Barzykin, and V. T. Gontkovskaya. Dokl. Acad. Nauk SSSR, 148, 380, 1963.

A. G. Merzhanov. Comb. and Flame, 10, 341, 1966.

A. G. Merzhanov and Y. M. Grigoryev. Fiz. Gor. Vzryva, 3, 371, 1967.

P. v.d. Mey and A. H. Heemskerk. Symposium Paul Vieille, Le Bouchet, France, September 1984.

P. v.d. Mey and A. H. Heemskerk. "Stability of Nitrocellulose Propellants Assessed Via Thermal Decomposition and Alternation of the Stabilizer Composition," AGARD Symposium on Smokeless Propellants, Florence, Italy, September 1985.

V. D. Moore. "Dragon Missile Warhead Sympathetic Detonation Analysis and Test Results," 23rd DOD Explosives Safety Seminar, August 9-11, 1988, Atlanta, Georgia.

P. Mosely. Department of Defense Explosive Safety Board Meeting, DDESB, 1986.

H. Moulard. "Une Condition de Surfache Critique por l'Armorcage par Onde de Choc des Explosifs Solides," Propellants and Explosives, Vol. 6, pp. 63-66, 1981.

M. P. Mullins and S. S. Penner. "Explosions, Detonations, Flammability, and Ignition," Pergamon Press, New York, 1959.

NAVORD OD 44811, 160, 1972.

C. Munroe. "Modern Explosives," Scriber's Magazine, Vol. 3, pp. 563-576, 1888a.

C. Munroe. "Wave-Like Effects Produced by the Detonation of Guncotton," American Journal of Science (Silliman), Vol. 36 (Series 3), 48 pp., 1888b.

C. Munroe. "The Application of Explosives," Popular Science Monthly, . Vol. 56, pp. 444-455, February 1900.

NATO AC/258

NATO AC/310 Handbook, 1 October 1987, Issued by Material Management Systems Section, Defence Support Division, NATO Headquarters, 1110 Brussels, Belgium.

Naval Surface Weapons Center. "Notes from Lecturers on Detonation Physics" by Donna Price and Sigmund Jacobs; Frank Zerilli, transcriber and editor. Silver Spring, Maryland, NSWC, October 1981 (NSWC MP 81-399).

T. J. Ohlemiller, L. H. Caveny, L. DeLuca and M. Summerfield. "Dynamic Effects on Ignitability Limits of Solid Propellants Subjected to Radiative Heating," in Proc., 14th Symposium (International) on Combustion, The Combustion Institute, 20-25 August 1972.

J. Pakulak and S. Cragin. NWC TP 6414, July 1983.

T. P. Parr, T. L. Boggs, C. F. Price, and D. M. Parr. "Measurement of the Temperature Sensitivity of HMX Burning Rates," 19th JANNAF Combustion Meeting, Vol. I, pp. 281-288, October 1982.

G. Parsons, L. Pitts, P. Summers, and G. Glenn. "Suppression of Sympathetic Detonation in Stacks of 500 Pound Bombs," 23rd DOD Explosives Safety Seminar, August 9-11, 1988, Atlanta, Georgia.

D. T. Pilcher. "Modeling the DDT Process," ONR/AFOSR Workshop on DDT, CPIA Publ. 299, pp. 142-160, September 1978.

D. T. Pilcher, M. W. Beckstead, L. W. Christensen, and A. J. King. "A Comparison of Model Predictions and Experimental Results of DDT Tests," Sixth Symposium (International) on Detonation, pp. 258-266, 1976.

D. T. Pilcher, M. W. Beckstead, L. W. Christensen, and A. J. King. "A Comparison of Model Predictions and Experimental Results of Deflagration-to-Detonation Tests," AIAA/SAE 13th Joint Propulsion Conference, AIAA Paper 77-858.

C. F. Price and T. L. Boggs. "A Simultaneous Mathematical Treatment of Deflagration and Ignition Phenomena," 22nd JANNAF Combustion Meeting, October 1985. (CPIA Publication 432.)

C. F. Price and T. L. Boggs. "Modeling the Deflagration to Detonation Transition in Porous Beds of Propellant," The Eighth Symposium (International) on Detonation, Preprint 850706, Vol. 2, 1983.

C. F. Price, T. L. Boggs, R. A. Gould, J. L. Eisel, and D. E. Zurn. "The CBREDII Program as Used with Closed Bomb Testing of Damaged Propellant from LAM and Shotgun Tests," 15th JANNAF Combustion Meeting, CPIA Publ. 297, Vol. III, p. 149, February 1979.

D. Price and R. R. Bernecker. "Sensitivity of Porous Explosives to Transition from Deflagration to Detonation," Combust. Flame, 25:91-100 (1975).

E. W. Price, H. H. Bradley, Jr., G. L. Dehority, and M. M. Ibiricu. AIAA Journal, Vol. 4, pp. 1153-1180, 1966.

Prins Maurits Laboratory, Explosion Utrecht, Netherlands 1967, TNO No. TL 1968-09.

K. Pringle, et al. "The Reaction of Solid Propellant Motors to Fragment Impacts," JANNAF Propulsion System Hazards Meeting, Redstone Arsenal, Huntsville, Alabama, March-April 1987.

W. C. Prinse and M. W. Leeuw. Annual meeting ANNC, Oslo, 1986.

Proceedings of Workshop on Insensitive Munitions Information Exchange, Fleetbank House, London, England, 13 to 15 October 1986, NATO AC/310 CP-001, March 1987.

Public Attorney's Report on Train fire in Linden, Germany on June 22, 1969.

M. Rat and R. Kent. Proc. Int. Jahrestagung, Karlsruhe, 1981.

M. Rat and R. Kent. Proc. 13th Int. Jahrest. ICT., pp. 137, Karlsruhe, 1982.

Recommendations on the Transport of Dangerous Goods, Tests and Criteria, UN, Section 9, 41, New York, 1986.

H. P. Richter, A. H. Lepie, and A. Adicoff. "A New Shear Dilatometer for Characterization of Filled Polymers," CPIA Publication 331, pp. 107-116.

R. D. Richtmeyer and K. W. Morton. Difference Methods for Initial Value Problems, Wiley, New York, 1967.

E. K. Rideal and M. J. Robertson. Proc. Roy. Soc. London, Ser. A, 195, 135, 1948.

E. K. Rideal and A. J. B. Robinson. The Spontaneous Ignition of Nitrocellulose 3e Symposium on Combustion, 1948.

H. M. Roylance. "Quantity-Distance Protection," in Prevention of and Protection Against Accidental Explosion of Munitions, Fuels, and other Hazardous Mixtures, E. Cohen, editor, Annals of the New York Academy of Sciences, Vol. 152, Art. 1, pp. 10-17, 1968.

R. M. Roylance in Prevention of and Protection Against Accidental Explosion of Munitions, Fuels, and Other Hazardous materials, N. Y. Academy of Sciences, 1981.

H. W. Sandusky. "Compressive Ignition and Burning in Porous Beds of Energetic Materials," 1983 JANNAF Propulsion Systems Hazards Subcommittee Meeting, CPIA Publ. 381, Vol. I, pp. 249-257, September 1983.

H. W. Sandusky and R. R. Bernecker. "Compressive Reaction in Porous Beds of Energetic Materials," Eighth Symposium (International) on Detonation, Preprint Vol. 2, p. 631, July 1985 (Albuquerque, NM), and H. W. Sandusky and T. P. Liddiard. "Dynamic Compaction of Porous Beds," NSWC-TR-83-246, 26 December 1985 (to be printed).

H. W. Sandusky, W. L. Elban, K. Kim, R. R. Bernecker, S. B. Gross, and A. R. Clairmont, Jr. "Compaction of Porous Beds of Inert Materials," Seventh Symposium (International) on Detonation, Naval Surface Weapons Center, NSWC MP 82-334, 1982, pp. 843-856.

A. San Miguel. U.S. Patent 4, 041, 869 8/1977 102/56 R.

M. A. Schrader, M. W. Leeuw, and A. C. van der Steen. Proc. Int. Jahrestagung, 623, 1983.

M. A. Schrader, M. W. Leeuw, and A. C. van der Steen. Proc. Ninth Int. Pyr. Sem., 881, 1984.

M. A. Schrader, M. W. Leeuw, and A. C. van der Steen. Proceedings of AGARD Conference, AGARD-CP-367, 19-1, Lisse, 1984.

N. N. Semenov. Z. Phys., 42, 571, 1928.

R. G. S. Sewell. Personal communication, 1982.

Naval Weapons Center. "Fragment Initiation of Cased Explosives (U)," by R. G. S. Sewell and K. J. Graham. In Airborne Weaponry Technology Program for Strike Warfare Weaponry, January-March 1983. Volume 4, Warheads (U), by Airborne Weaponry Technology Program Office, China Lake, CA, NWC, April 1983. (NWC TP 6350-6, Vol. 4, publication CONFIDENTIAL.)

C. P. Smyth. International Chemical Series Dielectric Behavior and Structure," McGraw-Hill Co., Inc., New York, 1955.

STANAG 4117. On Stability Test Procedures and Requirements for Propellants Stabilized With Diphenylamine or Ethyl Centralite, NATO Document AC/225, Panel IV, D/18 (revised), 17u-6-1968.

J. J. Starkenberg, Y. K. Huang, and A. L. Arbuckle. "Numerical Modeling of Projectile Impact Shock Initiation of Bare and Covered Composition B," Technical Report ARBRL-TR-02576, 1984 and Journal of Energetic Materials, Vol. 2, pp. 1-42, 1984.

A. Stolovy and others. "Electron Beam Initiation of High Explosives," 7th Symposium (International) on Detonation, White Oak, MD, June 1981. (NSWC MP 82-834.)

L. G. Strakovskii. Combustion, Explosion and Shock Waves, Vol. 21, pp. 38-41, 1985.

E. Strømsøe, A. Oddan, and L. Omholt. Proc. AGARD Conf. 367, 6-1, Lisse, 1984.

D. Sutton and P. C. Wellings. Rocket Propulsion Establishment, Westcott Report 45 - 1964.

G. M. Swallow and J. E. Field. Proc. Roy Soc. Lond. A379, p. 389-408, 1982.

M. Swisdak, T. L. Boggs, P. M. Howe, and J. Foster. "Prevention of Sympathetic Detonation," in Workshop on Insensitive Munitions Information Exchange, NATO A/C 310 CP-001, March 1987.

C. M. Tarver, R. R. McGuire, E. L. Lee, E. W. Wrenn, and K. A. Brein. Proc. 17th Symp. (Int. on Combustion, 1407, Pittsburgh, 1978.

F. R. Thomanek. Die Entwicklung der Ausgekleideten Hohlladung," Explosivstoff, Vol. 8, pp. 177-179, 1960.

R. U. E. 't Lam and A. H. Heemskerk. 7th Symposium on Chemical Problems Connected With the Stability of Explosives, Smygehamn, Sweden, June 1985.

O. M. Todes. Zh. Fiz. Khim., 4, 71, 1933.

United Nations Recommendations for the Transport of Dangerous Goods (the Orange Book).

U.S. Mil-Std-1648(AS), 1974.

J. L. C. Van Geel. TL-1971-1, 7360-I, Rijswijk, The Netherlands.

R. F. Vetter. NWC TP 5921, China Lake, Calif., 1977.

M. G. Vigil. "Explosive Initiation by Very Small Conical Shaped Charge Jets," 8th Symposium (International) on Detonation, 1985 [Proc.], pp. 470-479, 1985.

M. von Förster. "Versuche Mit Komprimierter Schiebbaumwolle," Berlin, Mittler & Sohn, 1883.

M. W. Wagenhals. "FRAGMAP, presented to NATO Insensitive Munitions Information Center, Laurel, Maryland, January 1990.

F. E. Walker and R. J. Wasley. "Critical Energy for Shock Initiation of Heterogeneous Explosives," Explosivestoffe, Vol. 17, pp. 9-13, 1969.

C. Weickert. "Jet Initiation of Explosive/Metal Sandwiches," 10th International Symposium on Ballistics, 1987.

Weingart, et al. "Acceleration of Thin Flyers by Exploding Metal Foils: Application to Initiation Studies," 6th Symposium (International) on Detonation, pp. 653-663, 1976.

A. R. West. "Solid State Chemistry and its Applications," John Wiley and Sons, New York, 1984, pp. 534-540.

A. Weston and E. Lee. "Modeling 1-D Deflagration to Detonation Transition (DDT) in Porous Explosives," Eighth Symposium (International) on Detonation, Preprint Vol. 1, p. 258, 15-19 July 1985 (Albuquerque, NM).

F. A. Williams. "Asymptotic Methods in Ignition Theory," Memoria del VII Congreso de la Academia Nacional de Ingenierie, Oaxace, Mexico, pp. 224-2227, 1981.

F. A. Williams. "Combustion Theory," 2nd Ed., The Benjamin/Cunnings Publishing Company, Menlo Park, California, 1985.

S. Wise, J. J. Rocchio, and H. Reeves. "The Ignitability of Composite Nitramine Propellants," 17th JANNAF Combustion Meeting, Hampton, VA, November 1980. (CPIA Publication 6329.)

T. A. Zaher, Department of Defense Explosives Safety Board Meeting, DDESB, 1975.

L. Zernow, I. Liebermann, and S. Kronman. "An Exploratory Study of the Initiation of Steel-Shielded Composition B by Shaped Charge Jet," Ballistic Research Laboratories, BRL Memo Report 944, October 1955.

J. Zinn and C. L. Mader. J. Appl. Phys., 31, 323, 1960.

J. Zinn and R. M. Rogers. J. Chem. Phys., 66, 2626, 1962.

D. E. Zurn and A. I. Atwood. "Problems Encountered in the Installation of the NWC CO_2-Laser Ignition System," in Proc., 18th JANNAF Combustion Meeting, Vol. III, CPIA Pub. 347, October 1981.

ANNEX I

DIFFERENT WAYS OF SAFETY ASSESSMENT

There are different philosophies of safety assessment. According to the approach used, the meaning of the words <safe> and <safety> may differ:

A. In the terms of a deterministic approach there exists a safe system, if undesired events are to be completely excluded under given circumstances. The intended goal is to identify all possible risks in order to avoid them.

B. In the terms of a probabilistic assessment there exists a safe system, if specific undesired events under given circumstances are below a given and prescribed low probability of occurrence in order to get most favorable combination with reliability.

In the terms of a quantitative analysis a system is safe, if the risk in the terms of probability of accident x consequential loss is less than a prescribed value. Risks are ranked according to their severity of consequences in order to minimize the potential hazard i.e., to improve the countermeasures. It is to be remarked, that there exist an individual and a public risk which are different. While the individual risk near an explosion in a city remains the same, the public risk increases as density of population increases.

A. DETERMINISTIC METHODS

The methods of this class are mainly used in systems design. The principles of work are careful thought, and the use of formal aids and tables (check lists).

USE OF SAFETY MARGINS

Mainly for constructional purposes, like the strength of material, safety margins are a measure of the designed and required strength of a component. Also sometimes this principle is used in the case of sensitivity to onset of ignition or initiation of energetic materials. In this case irregulations occur if the response of the material does not follow the severity of the stimulus. Therefore this method is limited to classical systems, where the steps of development remain small. Safety margins must be adjusted following further mishaps and investigations.

SINGLE ERROR CONCEPT

Coming from the demand that a system must work even if a single independent error is present, which induces under adverse circumstances further ones, one comes to avoid this to a redundant system. Here the existence and not the severity of the error is of importance. This method is mainly in use for electronic firing systems.

The following methods can be used to analyze the behavior of a system.

RELATIONSHIP CHARTS:

Binary interdependences are sketched in a matrix, see Figure A.I.1.

Fields of problems are to be evaluated. The main advantage of this chart is, that no point may be forgotten. Each square corresponds to a principal possible binary interaction.

An example of this method is the study of chemical compatibility between a propellant and its contact materials.

FAILURE MODE AND EFFECTS ANALYSIS:

A failure of a single component and the effects of this are considered. Complete understanding of the system is essential, and knowledge of the interdependences with adjacent systems or the environment is essential. This may be done for each subsystem. Examples are given below.

FAILURE ANALYSIS OF SUBSYSTEMS:

At an early stage of development the effect of failure of a subsystem is evaluated with respect to the main systems response.

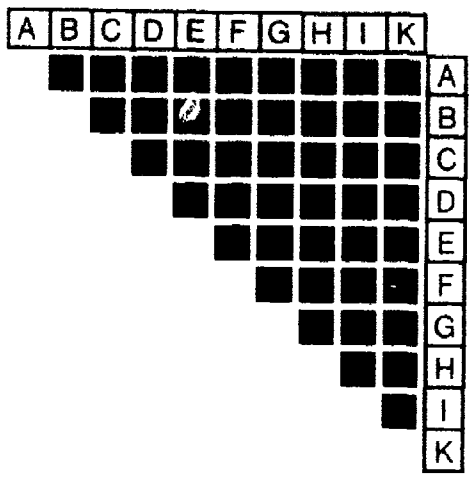

Figure A.I.1. Relationship Chart of Conceivable Binary Interactions.

PRELIMINARY HAZARD ANALYSIS:

By experience, checklists of intuitively dangerous elements by themselves or in conjunction with other elements are listed. Sources of possible hazards and their mitigation are evaluated. This is done at a very early stage of design.

HUMAN ACTION ERROR ANALYSIS:

This analysis evaluates the human reactions to a system, such as in maintenance, transport, storage, etc., also personal escape ways are considered. The results are part of the operational instructions.

All human actions on the system at any time are to be considered. Something may be done: (1) not at all, (2) not adequately, (3) too early, (4) too late, or (5) erroneously.

This analysis is complicated, and ergonomic experience is required.

INFORMATION DEFICIT AND EFFECTS ANALYSIS:

The procedure is similar to that above, and a sheet may be used. The goal is to identify all necessary information and prescriptions for safe use of the system.

Faults occur if information is: (1) wrong, (2) not relevant to the case considered, (3) not clear or misleading, (4) too general or incomplete, or (5) not present at the right placd when needed.

This analysis is adequate during the period of design. In combustion and detonation science these faults are very frequent.

HAZARD AND OPERABILITY STUDIES (HAZOP):

The goal is to predict and to find out the reasons of faults for estimating the consequences and finding out suitable ways to avoid them. Similar to the Failure Mode and Effects Analysis one follows the flow of action(s) using key words. [What happens if something: (1) not or no, (2) more or less, (3) as well as well, (4) partly, (5) the reverse or opposite, or (6) otherwise than occurs.] The reasons and effects are evaluated.

B. PROBABILISTIC METHODS

These are methods of reliability technology. It is interesting that about 1960 the fault tree analysis had been first introduced for predicting accidents in the military missile program.

FAULT TREE ANALYSIS:

In the fault tree analysis the undesired event, like fire or explosion, is given and one searches for all reasons leading to this. The single probabilities of the single events are evaluated for estimating the undesired events probability. Whereas this method leads to quantitative results in the case of

mechanistic models, where failure probabilities are (in principle) defined and declarable, in chemical processes and detonics only poor and qualitative results are obtained. The reason is, that chemical events on many factors depend gradually,which may develop gradually. Therefore probabilities are not adequate.

INCIDENT SEQUENCE ANALYSIS (CAUSE-CONSEQUENCE ANALYSIS):

Contrary to the fault tree analysis in the incident sequence, all undesired events are evaluated which result from a specified cause (trigger event). One may construct event trees or event networks (Figure A.I.2).

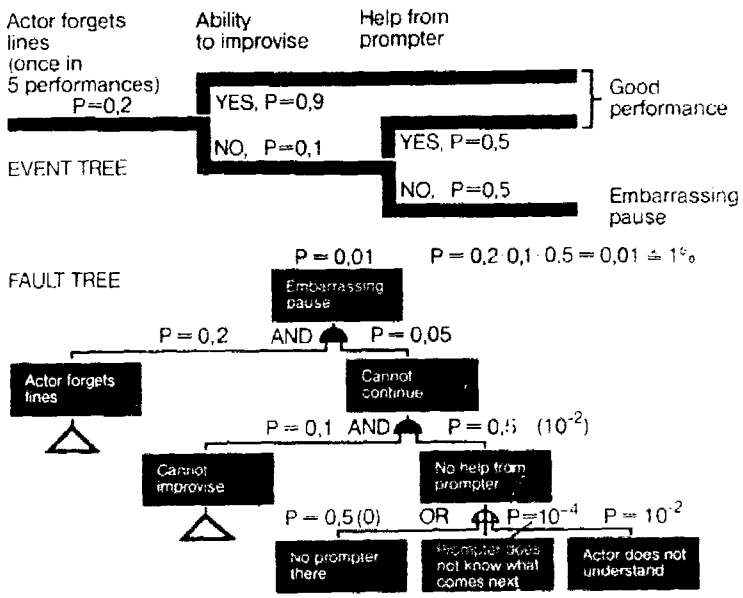

Figure A.I.2. Analysis of the Risk of an Actor Forgetting His Lines.

COMPARISON OF THESE METHODS:

It is evident that in the case of energetic materials at the best one comes to 3 or 4 levels of interpretation only. Due to the multiparametric behavior and the fact that the controlling parameters are within the substance, no prevention is possible besides the trivial case of cooling. In the majority of cases we cannot attribute failure probabilities to energetic materials.

While the arguments in the flow charts do hold in principle, the quantitative details may be obscure in the case under consideration. As a further example take the Analysis of Attack by a Shaped Charge Jet, Figure 3.5 in this Chapter 3 of the AGARDograph. In this event tree the deciding question on the critical diameter is settled. While this criterion is physically true, the numbered aspects remain obscure in the practical case. The reasons are that (1) the area of the shaped charge jet is not specified, (2) the critical diameter is not known for the appropriate overdriven state, and (3)the critical diameter of the possible damaged propellant at normal initiation.

So we have an accurate event tree of no value for direct safety estimates, but we get a feeling on the influencing parameters.

CONSEQUENCE ANALYSIS

Introduction

Consequence analysis is the part of risk analysis which considers the physical effects and the damage caused by these physical effects. It is done in order to form an opinion on potentially serious hazardous outcomes of accidents and their possible consequences.

Consequence analysis should be performed by professional technologists and chemists who are experienced in the actual problems of the technical system. The logic chain of consequence analysis in the process of decision making is given in Figure A.I.3.

The first step in the chain is a description of the technical system to be investigated. In order to identify the undesirable events one is forced to construct a scenario of possible incidents. It must be pointed out that the construction of a scenario is influenced by the subjective views of the investigator. The next step is to carry out model calculations in which damage level criteria are taken into account. Then, after discussion, conclusions can be drawn.

Feedback from model calculations to the scenario is included, since the linking of the outputs from the scenario to the outputs of models may cause difficulties. There is also another feedback, viz, from damage criteria to model calculations in case these criteria should be influenced by possible threshold values of the legislative authorities.

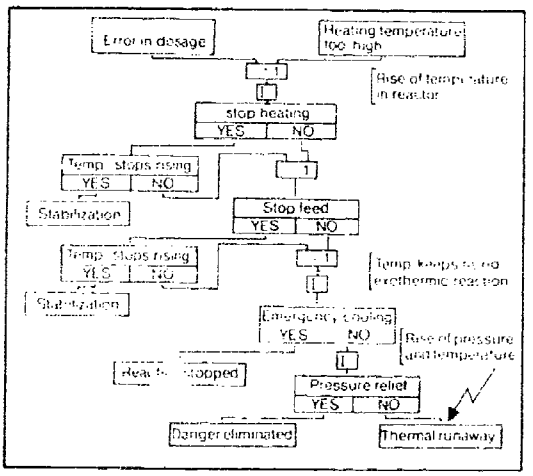

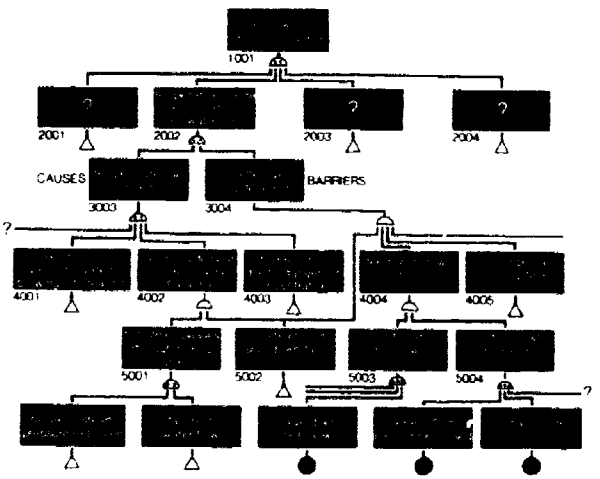

Figure A.I.3. Logic Chain of Consequence Analysis.

Effect/Output Model

Physical effects result from corresponding physical phenomena. The effects can be calculated by means of effect models in which the vulnerability of the environment is not taken into account. The most important effect models are: (1) electrical discharge, (2) discharge of liquids, gases, and vapor,

(3) discharge of two-phase flows, (4) evaporation of liquids on land and on water, (5) dispersion of neutral and heavy gases, (6) heat radiation of burning pools, flash fires, flames, and BLEVES, and (7) explosion of vapor clouds.

Hazard Result/Damage Models

In the preceding effect/output models, the damage to the environment was not taken into account. This damage can be assessed by means of models which are discussed in terms of explosion damage, fire damage, and toxic injury.

For the assessment of damage, the U.S. Coast Guard Vulnerability Model is frequently used. It is a deterministic non-stochastic model which predicts the catastrophic damage to people and property resulting from physical phenomena. In Table A.I.1. a survey is given of the model.

Table A.I.1. U.S. Coast Guard Vulnerability Model.

Damage causing event	Cause of injury or damage	Vulnerable resource	Type of injury or damage
TOXICITY	Toxic vapour: concentration or cumulative dose	People	Death Non-lethal injury Irritation
EXPLOSION	Direct blast Impact Flying fragments Two of more of the above	People	Death Non-lethal injury: Eardrum rupture, Bone fracture, Puncture wounds, Multiple injury
		Structures	Structural damage Glass breakage
POOL BURNING	Thermal radiation	People	Death First degree burn
		Structures	Ignition
FLASH FIRE	Thermal radiation	People	Death First degree burn
		Structures	Ignition

By using this vulnerability model the type of damage can mostly be calculated with so-called probit functions. A probit function is a measure of the percentage of the vulnerable resource that is affected. As compared to probabilistic models the vulnerability model estimates the maximum consequences of an incident. It is a drawback that in the hazard result/damage model most assessing methods are based on surface bursts of nuclear weapons and on thermal pulses from the same sources.

Accuracy in Models Mentioned

In general for most effect models the following limitations hold:

- Models are based on idealized systems.
- Models are only verified by small-scale experiments.
- In models influences of environment (obstacles, constructions, buildings, etc.) are neglected.

In view of the above limitations it is not surprising that physical models do not permit a high standard of precision.

Concerning the hazard result/damage models it can be stated that they are in an early stage of development and up to now sufficient validation has not been carried out. They have been developed for ease of use, computational economy and high problem transparency. They are by no means as precise or accurate a simulation as would be possible with current technology and it should be possible to imagine simulations of higher fidelity.

In conclusion the accuracy of consequence models can be summarized as follows: This analytical exercise might be considered to be objective. However, it must be realized that because of the large body of assumptions, estimates, judgments, and opinions involved much of the input information is often subjective. Because of this there is a tendency for the analyst to "err on the side of caution," thereby giving a deliberate bias to the assessment and overestimating the risk.

At present, considerable skill is needed to interpret the results produced by quantified risk analyses. In the present state of development these techniques should only be used by those who understand their limitations and then only with caution.

It is, of course, important to realize that there is no absolute standard of safety. One could have a requirement of safety in the sense of legal regulations, which in the view of a safety expert would still leave considerable risk in comparison with what is technically possible. Also, for large consequence, low frequency type of event such as a nuclear reactor incident a very sophisticated, scientific approach could be required.

ANNEX II

DETONATION PHENOMENA IN CHARGES WITH AN AXIAL HOLE

Introduction

Selle (1932) started the interest on the investigation of detonation phenomena of charges with an axial hole, or axially cavitated cylinders. Independently Ahrens (1938-1945) in Germany and Woodhead and Titman (1939-1945) in England conducted very detailed investigations without any theory or model as a guide.

The detonic behavior of cavitated charges, maybe internal as an axial hole, or external as an air gap, let say a gap between a cartridge and the bore hole, is considerably different from that of a homogeneous charge. Significant increases or decreases of "sensitivity" may be observed, and these alterations are not unidirectional. Since in the case of a detonating rocket motor both cases may become important, some experimental facts from small scale experiments on high and commercial explosives are sketched with the intent to illuminate the considerable gap of knowledge for judging these relevant safety problems in the real problems under consideration. Furthermore, critical diameter aspects of full cylindrical charges do not hold in this case (Mallory, 1987).

Experiments

Cylinders with an axial hole show an increased plate penetration compared with a full size cylinder. Accordingly, the brisance value according to Kast is increased, not constantly, but as a function of the sensitivity of the explosive, and the size of the hole, where also a decrease gets possible. The relative value is largest for an insensitive explosive like TNT and decreases as sensitivity increases in the order TNT - picric acid - tetryl - PETN with wax - RDX - PETN. Whereas, the crushing of the copper cylinders is about constant for different lengths of full charges, this value depends on the length of the charges with axial holes. Between 4 and 40 cm length of the charge there is a factor of 6.

The hole acts also ballistically. A steel ball of 5 mm diameter at the end of a 80 cm long charge of TNT of an outside diameter of 21 mm and hole diameter of 4 mm acquired a velocity between 4.200 nd 4.500 m/s. Leiber, 1968, had not been able to reproduce this effect with short charges.

The detonation velocity D_h had been determined optically from the reaction luminosity. Apparently this value is relatively independent from the density, is constant, but changes from experiment to experiment, see Table A.II.1. D_h increases as charge asymmetries increase. If the end of the charge is open, this velocity is lower than if closed. And another behavior in detonation velocity D_k is obtained for mixed charges (full cylinder and axial hole cylinders). These effects disappear, if the cavity is filled with water (Kirsch, Papineau-Couture, Winkler, 1948).

Table A.II.1. Detonation velocities of full cylinders, outside diameter 21 mm,and axial cavitated charges of 4 mm inside diameter, and mixed charges(axial cavitated cylinder/full cylinder) according to Ahrens, 1965.

	Density g/cm^3	Cylinder full D (m/s)	with axial hole D_h (m/s)	Mixed charge D_k (m/s)
TNT	1.44	6.490	7.000	
	1.50	6.690	6.920	7.160
	1.55	6.800	7.060	
PETN	1.40	7.100	8.450	9.480
	1.50	7.480	8.680	9.800
	1.55	7.630	8.720	9.860
	1.60	7.780	8.570	9.880
	1.66	7.960	8.580	10.210

Contrary to the homogeneous high explosives, where usually $D_h > D$, in the case of commercial explosives mostly the opposite behavior $D_h < D$ is observable.

The differences in crushing (Kast) do not correlate with the value $(D_h - D)/D$, where D is the detonation velocity of the full cylinder, whereas the detonation transit times behave additively. Not, however, if the charge is mixed with full cylinders and cylinders with a hole, see Table A.II.1. In this latter case detonation velocity depends on the density.

If in the case of PETN, density 1.5, the inside of the hole is lined with a lead foil, and the ends are open, the detonation velocity D_k lowers to 8320 m/s compared to D_h = 8680 m/s, whereas in the case of covering only the ends of the charge with lead the velocity rises to D_k = 9120 m/s.

If the hole is lined throughout with lead one gets D_h = 7650 m/s, compared to the value D = 7480 m/s for a full cylinder. If only three quarters of the circumference of the hole is covered, one gets on the uncovered side D_h = 8110 m/s, and on the covered side 7390 m/s.

If the charge is periodically interrupted with foils of inert materials, the detonation velocity D_h depends on the area density of this material. If this area density r < 0.005 g/cm^2 no influence is observed. If r > 0.008 g/cm^2, jump of D_h is obtained again. For the case r > 3 g/cm^2 the detonation velocity D of the full cylinder is obtained. This effect depends on the distances of the disks, and is greatest for 40 mm in the case investigated, above this value a decrease is obtained again.

Luminous Phenomena

At the end of a TNT-charge with an axial hole a first luminosity with a velocity of 9470 m/s had been emitted compared to the detonation velocity D_h = 7030 m/s. A bit later a further luminous component had been released with a longer range of distance appears. Both events depend on the charge length, sensibility, and brisance of the explosive. Sometimes even an advance initiation of detonation is induced.

Very large velocities are obtained in vacuum, see Table A.II.2, where the differences in time between the first and second flash go up to 50 µs.

Table A.II.2 Velocities of the luminous events leaving the cavitated charge in vacuum according to Ahrens (1965).

	Density g/cm^3	Hole Length/Diam. mm/mm	D_h m/s	First fast flash m/s	Slow second flash m/s
TNT	1.55	40/3		17.040-15.400	13.160 - 8.180
		200/3		17.080 - 14.980	12.480 - 5.060 18.380
PETN	1.50	800/0	7.760 8.600	--	13.900 - 6.300 15.700
		800/6	8.470	18.580	13.420 - 4.900 23.340

These luminous ejecta may correspond to Cooks heat pulse, responsible for initiation. For further, more extensive summary, with some attempts at explanations, see Johansson and Persson (1970).

REFERENCES

H. Ahrens. "Uber den Detonationsvorgang bei zylindrischen Sprengstoffladungen mit axialer Hohlung," Explosivstoffe 13 (1965)$_5$, p. 124/134; Explosivstoffe 13 (1965)$_6$, p. 155/164; Explosivstoffe 13 (1965)$_7$, p. 180/198.

H. Ahrens. Communication (commercial explosives). Explosivstoffe 13 (1965)$_{10}$, p. 267/276; Explosivstoffe 13 (1965)$_{11}$, p. 295/309.

C. H. Johannson and P. A. Persson. "Detonics of High Explosives," Academic Press, London, New York, 1970.

M. Kirsch, G. Papineau-Couture, C. A. Winkler. "The Detonation Velocity of Axially Cavitated Cylinders of Cast DINA," Can. J. Res. 26, Sec. B (1948)$_5$, p. 435/440.

D. W. Woodhead and H. Titman. "Detonation Phenomena in a Tubular Charge of Explosive," Explosivstoffe 13 (1965)$_5$, p. 113/123; Explosivstoffe 13 (1965)$_6$, p. 141/155.

ANNEX III

Background

It has been known and accepted for a long time (Bowden and Yoffe, 1958) that a weak stimulus initiation to detonation follows a path, sketched in Figure A.III.1. Whereas some of the mechanisms leading to a linear burning are resolved, still the phenomena of turbulent burning are less well understood. If the rate of chemical decomposition increases further, suddenly a regime is entered, where a pressure coupled chemical decomposition takes place, and it is not unusual, that even a steady state is possible under ideal circumstances. Such events are observable in liquids as well as in solids, and are characterized by a detonation pressure of the order 5 to 20 kbar, and velocities of low detonation ordering to 1000 up to 2500 m/s (Brown and Collins, 1967; Belyaev and others, 1975; and Leiber, 1982). Depending on the confinement and other factors, suddenly a transition from Low to High Velocity Detonation (HVD) can take place, where the pressures reach hundreds of kbar, and the velocities order to > 6000 m/s.

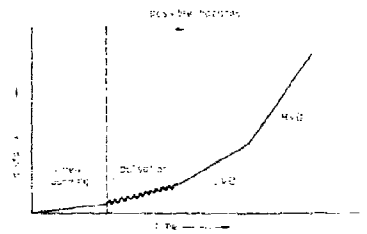

Figure A.III.1. Transition from Weak Stimuli Up to Detonation. The most weak stimulus which leads to an escalation, governs sensitivity. Therefore any event on the right-hand side of linear burning may lead to hazards.

Low Velocity Detonation (LVD) can under circumstances be more dangerous than the HVD. The reason is, that large low velocity debris can reach a larger width, up to 2000 m, than small high velocity debris, with a fragment distance of about 600 m.

Usually tests are done with relevance to ignition and HVD events only. Coming from Figure A.III.1 this is at least for HVD-tests not conclusive, since any escalating process cannot be judged from the final state of the HVD. If escalation is to be envisaged, the weakest stimulus is decisive for any safety consideration, and it is necessary to know mechanisms which lead to initiation of detonation. Furthermore classical models often imply, that sensitivity is a matter of the chemical composition, whereas LVD- or more general explosion-risks are controlled by the mechanical properties of the whole system. Therefore often even generic tests may fail to predict hazards.

To get ideas on hazards we have two options:

1. Safety tests, where the most severe problem is to find adequate tests focussing the real problems under consideration, which often are not specified. Even if this is realized, the test confidence of the go/no go type is poor. The reason is, that we should exclude undesired events with a high reliability. The consumer risk must be much lower than the producer risk. To realize this is practically impossible by go/no go tests. Leiber, 1986, gives more details.

CRITICISM OF 'SAFETY TEST' METHODS

For avoiding such disasters like that of the USS Forrestal, we are interested in the question, whether such tests are comprehensive. In other words, we face the question whether there are weak or strong correlations between safety tests and accidents.

Actually we have no chance to answer this question for the variety of rocket motor materials, since these are too sensitive to always allow the reasons of accidents to be evaluated. Requirements for a test substance to investigate this are:

- homogeneous material,
- material long in use, and much experience with it,
- material involved in the past in several accidents,
- material at the low end of the explosives sensitivity scale.

Examples of such candidate materials are calcium hypochlorite, alkaline chlorates and perchlorates, and ammonium nitrate. Whereas the above chlorates, perchlorates, and nitrates in accidents tend to explode, calcium hypochlorite tends to burn.

We have chosen alkaline chlorates due to the common but erroneous understanding that neat alkaline chlorates without combustibles would always fail to detonate. Furthermore, a great number of international test results exist, done over a long period of time, exceeding in number and type by far those on propellants, and we have 15 case histories.

Chlorate explosions mostly had been caused by external fire in storage, where catastrophic consecutive explosions occurred with cratering. Even mechanical stimulation is possible, so a drum falling from the table to the floor leads to cratering.

Tests, even on a whole drum failed to demonstrate explosiveness of sodium chlorate. Even boosting a 100 kg drum with a 10.6 kg charge of blasting gelative failed to detonate it as did burning tests with and without combustibles.

Positive tests had been a bon-fire test in the ton-scale with several consecutive explosions; in addition, a Low Velocity Detonation test (with boosters down to 10 gm TNT) of analytical grade sodium and potassium chlorate in heavy confinement produced rates between 1000 and 2000 m/s and very deep dents in lead plates.

Since all other tests failed except the above, the two positive tests are not to be linked with the apparent accident stimulations. We conclude that there is generally only a weak correlation between test results and real life accident causes. Possibly we are ignoring in the tests questions such as the critical diameter and very weak stimulations as the cause of accidents.

We do not know any reason why this situation should be more favorable in the case of more sensitive materials like rocket motors or even insensitive high explosives. The result is that we will possibly be able to develop insensitive explosives according to the current specification, but these do not address the prevention of accidents like those of the John Forrestal type.

2. To compensate the test reliability a little, we may use former experience, often absent in the case of new ventures, and/or theory or models. Unexpected hazards may indicate the poor state of the art. However, if we follow up the reasons of this error, we have the opportunity to improve our knowledge. We only learn from errors, not from the "truth."

PROBLEMS WITH THE THEORY

As outlined in Section 5.3 some ideas exist on the mechanism of burning. Paths of possible escalations are scarcely resolved. Insight in pulsating combustion is at its best crude. The well established steady state thermohydrodynamic laminar plane wave theory of HVD does not address these problems. Nevertheless it is an excellent engineering tool for estimations of steady state detonation. Unfortunately this tool is so excellent that many detonation researchers are not aware of its estimative character. This, however, becomes obvious in safety considerations. The reason of this is that thermodynamics is used, which quite naturally does not contain mechanisms which may be at work in the detonation zone. A characteristic shortcoming of this steady state model is that neither the transition from burning to detonation (DDT) nor the existence of an LVD is to be seen as a consequence of this classical theory. Therefore in the US such phenomena often are called pressure wave accompanied combustion or the like. Contrary to USA, in Russia on this matter considerable progress has been obtained (Belyaev and others, 1975). As a matter of fact appears the strong influence of the confinement, which controls the stability of LVD. Contrary to the usual US assumptions not the impedance, but the strength of the confinement is important for stability and also for obtaining LVD for dense solid energetic materials and final transition to HVD. Curiously enough, the detonation velocity appears to be a strong function of the wall thickness. Typically the initiating pressure is low, and no safe low end up to now is known. German experiments have shown that an explosive blow of the order of 8 bar may initiate warm nitromethane (Wild, 1982), whereas Russians seem to have found that an explosive of 4 bar may initiate solid TNT (Borisov, 1986). Usually the initiating pressures of HVD are assumed to be 10^4 times larger.

In BICT we didn't believe at first such risks on solid strand propellants; however, these had easily been detonated in a strong confinement (inside/outside diameter < 0.3), and the detonation velocity measured as 1500 to 2000 m/s.

ASSUMPTIONS OF THE CLASSICAL DETONATION MODEL

The microscopic ZND-profile of detonation shows the reaction zone as a black box, where energy release occurs. From the thermodynamic aspect, the events in this "black box" are squeezed into an appropriate Equation of State (EOS), where the underlying mechanisms are still a matter of discussion.

Possible Mechanisms in the Black Box of Reaction Zone

1. The classical assumed mechanism in this black box is a volume homogeneous shock heating process until onset of thermal chemical decomposition takes place, which drives the detonation wave. This concept has been suggested by Le Chatelier for gases at the beginning of this century, and is the basic approach of the present state of engineering calculations by detonation codes, even for condensed explosives.

Besides a far too optimistic view of initiation risks, experimental and theoretical reasons have been found that a volume homogeneous piston like decomposition mechanism never realizes a plane wave detonation.

2. Molecular dynamics, suggested by Karo, Hardy, and F. E. Walker (1978), and later Dremin (1981), finds the detonation mechanism in the molecular state, where shock rise occurs within one to three atomic distances, and bond scission and onset of reaction occurs. This concept provokes several questions:

Why usually is the detonation front not smooth, neither for liquid nor for solid crystalline explosives?

Why is the rise length of a shock in crystalline materials of the order of tens of microns, as has been shown by three independent experimental methods (Mogilewskij, 1973; Leiber, 1975; and Winkler, 1976)? Below it will be outlined why molecular dynamics is not opposing this said dimension of the shock rise.

Let us find another rationale for providing estimates of risks.

SKETCH OF THE IDEA

In a microscopic scale burning or chemical reaction occurs at discrete local points. Due to the reaction at these points a volume $\dot{V}$ increase with time occurs. According to the basic theories of pressure wave generation of Lord Rayleigh (1886) and Lighthill (1962) such a volume variation $\dot{V}$ with time in a medium of density ρ is one of several pressure generating mechanisms. The energy of reaction escapes from these reaction sites basically in two different ways: (1) by a dynamic without pressure wave, or (2) by a pressure wave emission leading to a dynamic compression (explosion).

In solid propellant rocket motors the first case is desirable, whereas the second one may lead to hazards. it is of importance therefore to find basic keys to guarantee in principle that the first path predominantly is used, and which factors may favor the second path.

MECHANISTICS UNDERSTANDING OF DDT

The classical approach is that in the plane wave piston model of detonation, the velocity piston, as a mass flow rate, drives the detonation wave where this piston is impermeable; whereas, in the case of combustion, this piston is completely permeable and no detonation is therefore possible. The key model of a plane wave DDT-process is that an initially permeable piston by different mechanisms and processes chokes more and more so that backventing does not occur. Basic ideas on such choking mechanisms follow.

Probably Kistiakowsky (1948) first suggested that "the formation of the detonation wave by a shock wave running ahead of the flame front. . ." may be responsible for initiation. With this idea a link is therefore possible between DDT and shock to detonation transition (SDT), where the "burning pressure" corresponds to the shock.

Such a "burning (gas) pressure" may be produced by an exceptional increase of reaction rate (Ubbelohde, 1948), which for porous systems by a convective burning may be realized. Pore collapse by compression, fusion of the particles, or hydrodynamic resistance or gas permeation and other mechanisms cited in the last paragraph may lead to an impermeable piston (see also Belyaev, Bobolev, et al, 1975).

We now assume that burning occurs at discrete pockets, and the reaction products expand the matrix like balloons. In this way they inject mass into the surrounding medium, and produce pressure generating elements. This chemically liberated energy,E, in a unit volume, V_o, of a material of density, ρ, may escape from the reaction sites solely by the kinetic energy flow.

$$E_{kin.} = \frac{1}{2} \rho V_o u^2 \qquad (1)$$

or as potential energy of compression:

$$E_{pot.} = -\int p\, dV = \frac{V_o}{2\rho c^2}\, p^2 \qquad (2)$$

where u is the velocity of plow, p the pressure, and c the sound velocity. Using for simplicity acoustic harmonic quantities we compare the following plane waves

$$\phi_{plane\ wave} = A\, e^{ikx} \qquad (3)$$

with harmonic (time-free) spherical waves, adequate for reaction centers.

$$\phi_{spherical\ wave} = A\frac{e^{ikr}}{r} \qquad (4)$$

where x is the linear, and r the radial distance. $k = 2\pi R/\lambda$ relates the dynamic quantity of a wave length to geometrical distances.

In Table III.1, the main differences between plane and spherically wave solutions are presented. Contrary to plane waves, which only show a far field (FF), the spherical waves show in addition a near field (NF) out of phase with pressure, which dominates near the sources of radius r = R. Therefore the ratio of potential and kinetic energy is not constant as in the case of a plane wave approach. This ratio depends on the dynamics, the reaction cluster size, and on the distance. We use for this ratio the quantity (Re Z)/ρc, which is the ratio of the real part of the spherical and the plane wave impedance, see Table A.III.1.

Table. A.III.1. Comparison of Plane and Spherical Waves.

Quantity		Plane Wave	Spherical Wave
pressure	$p =$	$-i k \rho c \phi$	
particle velocity	$u_r =$	$-i k \phi$	$-i k \phi - \phi/r$
far field term (FF)	=	$-i k \phi$	
near field term (NF)	=	0	$-\phi/r$
potential energy	=	$\frac{1}{2}\rho V_o k^2 \phi^2$	
kinetic energy (FF)	=	$\frac{1}{2}\rho V_o k^2 \phi^2$	
kinetic energy (NF)	=	0	$\frac{1}{2}\rho V_o \frac{\phi^2}{r^2}$
$E_{pot}/E_{kin.}$ (FF)	=	1	
$E_{pot}/E_{kin.}$ (NF)	=	∞	k^2r^2
$\frac{\text{potential energy}}{\text{total kinetic energy}}$	=	1	$\frac{k^2r^2}{1+k^2r^2} = \frac{\text{Re } Z}{\rho c}$
Impedance $Z = -p/u$	=	ρc	$\rho c\left[\frac{k^2r^2}{1+k^2r^2} + i\frac{kR}{1+k^2r^2}\right]$
Power of radiation per unit	$N =$	$\rho c \frac{u^2}{2}$	$\rho c \frac{k^2r^2}{1+k^2r^2}\frac{u^2}{2}$

This means that far from the sources ($r \Rightarrow \infty$) the plane wave approach is a good approximation, not, however, near the sources. If dynamics is low (wavelength $\lambda \Rightarrow \infty$) the power of radiation tends to zero; if high, the plane wave expectation is finally obtained, where half of the energy is in the flow, and the other part in compression. So DDT is resolved as a matter of energy partition. This is basically absent in each DDT-plane wave theory.

Since R^2u is proportional to $\dot{V}$, it is obvious that the dynamics of combustion is important, but not the exact shape of the reaction center. The value of Re Z/ρc of reaction cluster agglomerations is a function of the location of the sources and their strength, and no general asymptotic estimate near the

sources is possible. DDT may be triggered by external pressure waves, where the stimulating shock in its amplitude may be far below a SDT-initiation amplitude.

The above considerations indicate very little likelihood of a DDT arising in a cast and not damaged rocket propellant motor. In other words, mechanical stability of the matrix is a safety relevant parameter, see the comprehensive summary of Bernecker (1984).

We now have to evaluate mechanisms for producing a volume variation with time $\dot{V}$. Beside local combustion, also the occurrence of a crack in a solid, which opens (or closes) leads to a mass injection $\rho \dot{V}$ into the surrounding volume. Therefore, risks arise from fracture too. By using such an idea, we have to find out, in which way by a compression wave a crack may be opened.

In the following we discuss mechanisms in which pressure pulses directly or indirectly create cracks in homogeneous dense solids (double base propellant), and in inhomogeneous materials like composite propellants.

PRESSURE WAVES IN AN AELOTROPIC MEDIUM

Pressure waves of amplitude p in a homogeneous medium I are reflected at the side boundaries. Within an assumed plane wave-model in the case of normal incidence the relative impedances of the medias I $(\rho c)_I$, and II $(\rho c)_{II}$ decide the amplitude p_t, which is transmitted over the boundary or reflected p_r, and whether the reflected part is a pressure- or tension-pulse. c is the sound velocity or more precisely the shock velocity u_s. In perfect homogeneous solids - also in the microscale - therefore there is little risk to obtain tension pulses, if the impedance of the confinement is larger than that of the medium, whereas in the opposite case scabbing (spallation) may occur.

$$\frac{P_t}{P} = \frac{2\,(\rho c)_{II}}{(\rho c)_I + (\rho c)_{II}} \tag{5}$$

$$\frac{P_r}{P} = \frac{(\rho c)_{II} - (\rho c)_I}{(\rho c)_I + (\rho c)_{II}} \tag{6}$$

For the particle velocity u_p the following relations hold:

$$\frac{u_{p,t}}{u_p} = \frac{2\,(\rho c)_I}{(\rho c)_I + (\rho c)_{II}} \tag{7}$$

$$\frac{u_{p,r}}{u_p} = \frac{(\rho c)_I - (\rho c)_{II}}{(\rho c)_I + (\rho c)_{II}} \tag{8}$$

with the consequence that in free air with $(\rho c)_{II} \approx 0$ the free surface velocity $U_{fs} \approx 2U_p$ is obtained.

In the case of oblique incidence of pressure waves much more complications result, and even shear waves are obtained. For details see the monographs (Kolsky, 1963; Rinehart, 1975; and Wasley, 1973). Therefore edges, corners, and slots in the material are serious problems to be considered. As a rule of thumb one can state that, if according to statical views unlikely fracture occurs (not the thinnest, but the thickest part breaks, as example), dynamic stress waves are at work.

In the case of an aelotropic medium the sound velocity in single crystals is different in different directions. This is seen best by presenting the Youngs-modulus body for PETN (calculated from the single crystal elastic constants measured by Morris, 1976), as an example, where the Youngs-modulus E is shown as function of crystal-direction, see Figure A.III.2. Up to now only for PETN we know the complete set of single crystal elastic constants. Since $U_s = \sqrt{E/\rho}$, also the impedances depend on the direction of the crystal. The consequence is that in a polycrystalline material an assumed initially plane and smooth pressure front of infinite steepness broadens and roughens more and more, and pressure-, tensile-, and even shear pulses get possible. Further it gets possible, that the directions of energy propagation and wave propagation get different. By a pressure pulse p a

tensile pulse is obtained. This is also the case in double base propellants of zero porosity, since this exhibits in the microscale areas of different impedances.

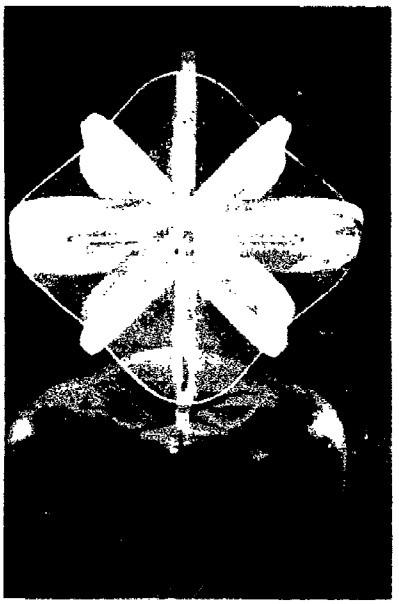

Figure A.III.2. To demonstrate the meaning of aelotropy, two single crystal Youngs-modulus bodies of PETN are shown, where E is a function of the crystallographic direction. In the lower half the c-axis shows to the top, and the c-axis of the glassy model shows to the viewer.
The polycrystalline material exhibits therefore different internal impedance areas, leading to reflections, and tensile pulses, and broadening of any initial steep pressure rise.
The mechanical properties reflect structural properties of chemistry: The NO_2-groups are situated in the corners of the lower part of the body.

PRESSURE WAVES IN AN INHOMOGENEOUS MEDIUM

Unfortunately the condition of identical compressibility of the media I and II is not sufficient for uniform behavior, since in addition the densities must be the same. Let us assume that there is a particle with density ρ' in a medium of density ρ_∞, and a pressure wave of finite shock rise stimulates this particle, then this may remain fixed by viscous forces on the spot. However, if the pressure pulse overcomes these forces, then this particle acquires a velocity u'_p with respect to that of the matrix $u_{p,\infty}$, which in addition depends on the relative size of the particle and the shock rise length. For a rigid point particle, not fixed by viscous forces, the expression (König, 1891 and Lamb, 1932)

$$\frac{u'_p}{u_{p,\infty}} = \frac{3}{2\,(\rho'/\rho_\infty) + 1} \qquad (9)$$

holds. Leiber (1976) derived the free particle mobility as a function of particle size for different density ratios according to Lamb (1932), see Figure A.III.3. Full solutions for a rigid particle, however, are given by Temkin and Leung (1981), and their treatment is applied by Leiber (1979) to further cases.

Experiments to demonstrate this behavior cannot be performed on explosive materials, since these materials decompose. For model experiments cast and spheroidal cast iron with the density ratio $\rho'/\rho_\infty \approx 0.25$ have been used. The amount of carbon has been kept constant, but the particle size and their distribution have been different. Figure A.III.4 shows shocked cast iron, where a graphite particle has driven a crack. Tiny particles destroy the matrix like moving wedges. That the above particle really has moved is demonstrated by the striation pattern on the surface of the iron, Figure A.III.5. This effect is absent if the sample is broken statically.

Figure A.III.3 Free particle velocities in a dynamic field as a function of particle size and density ratio. As to be seen, a dynamic homogeneous behavior is obtained for particle sizes corresponding to the condition Re $(u'_p/u_{p\infty}) = 1$. This may be used to estimate the shock rise length.

In the case of spheroidal cast iron, the spherites remain on the spot, move into or even contrary to the shock direction (Figure A.III.6), and dissipate the shock energy very rapidly (Figure A.III.7). The vibration of the spheres dissipates the energy. The vibration of the spherites are absent in the case of static fracture.

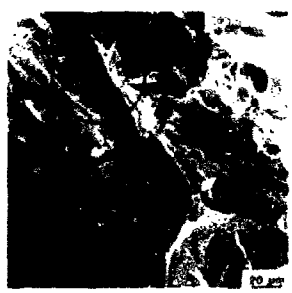

Figure A.III.4. Shocked cast iron, where the graphite particle (in the circle) drives the crack. That this particle really has moved is shown by Figure A.III.5, which is a micrograph of the new surface of the iron of the upper left (in the circle) near the graphite particle.

Figure A.III.5. The surface of the iron surface (Fe, dark in Figure A.III.4) shows vibration structures produced by the mobility of the graphite particle C. In statically broken cast iron this structure is completely absent. The arrow indicates the shock direction.

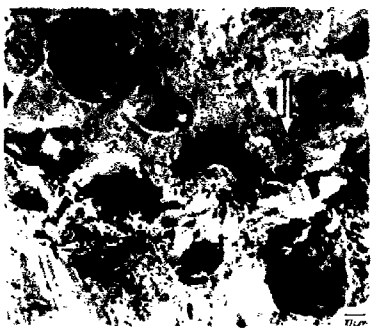

Figure A.III.6. Shocked spheroidal cast iron of same composition as the cast iron of Figure A.III.4. Upper left a larger spherite breaks up into a larger piece, moving contrary to shock direction (arrow), and the small one moves with the shock direction. The spherite in the center remains on the spot, but is deformed due to its pressure reflection properties corresponding to kR = 1.75.

Figure A.III.7. View into a broken graphite spherite, where the vibration patterns have absorbed the pressure energy. Statically loaded spherites do not exhibit this structure.

That even a void may act like a particle is shown in Figure A.III.8 where a void in molybdenum has driven this trail. This means, that even dynamic activated voids act like wedges, which drive the cracks.

Figure A.III.8. Dynamic trail of a void in molybdenum. The void did not close in spite of the high dynamic pressure of 375 kbar, whereas such a void completely disappears by hot forging.

Another dangerous situation occurs if dense particles acquire a relative velocity ($u'_p - u_{p,\infty}$) contrary to the shock direction: If this relative velocity is slow, the trail closes like in a laminar flow. If this velocity gets larger, a wake formation occurs and this wake will be driven like a void (Figure A.III.8) into shock direction. So one gets a hydrodynamic pair formation of wedges. This is demonstrated in Figure A.III.9, where a tungsten particle impacted the upstream side, and the resulting cavity the downstream side. The matrix was aluminum. That the downstream side hole has been really produced by a void has been established by the similarity of cavity impacts on metals

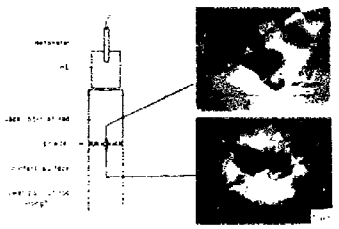

Figure A.III.9. 1 μm tungsten particles of density $\rho' \approx 19.3$ g/cm^3 in the boundary between the aluminum pieces of density $\rho_{oo} \approx 2.7$ g/cm^3 impacted the upstream part only. The downstream impacts produce cavitation damage.

These results indicate that the dynamic behavior of any solid material depends on the voids. In order to realize this, we gathered all available measurements on the Hugoniot Elastic Limits (HEL) of different ceramics, see Figure A.III.10. Under the assumption that the variance of these values is specific for a specified failure process, with a statistical significance of up to 99% the high density failure mechanism is different from that of larger porosities than 0.8%. A further result was that the HEL-determining mechanisms for single crystals are different from those of the polycrystalline materials.

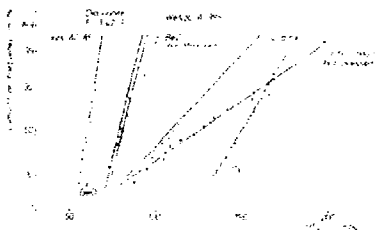

Figure A.III.10. Cumulative frequencies of the Hugoniot Elastic Limit for different types of brittle ceramics. With 99% significance the HEL-determining mechanism is different for the high density samples Lucalox and Carborundum hot pressed.

It is of interest to know whether such differences may be found by mechanical static experiments. As to be seen in Figure A.III.11 the failure mechanism of the bend strength of the polycrystalline material is independent from this porosity. For more details see Leiber (1974).

Figure A.III.11. Contrary to the above, the static bend strength mechanism is with a statistical significance of 99% the same for high density and porous materials.

The porosities are listed in the following. The dynamic strength behavior is different for the two columns, and the same within one column.

Material	Porosity in %	Material	Porosity in %
Coors AD 85	6.6	Carborundum	
Diamonite P-1342-1	5.5	hot pressed	0.8
Wesgo Al-995	4.0		
Boron carbide	2	Lucalox	0.2
Beryllium oxide	5.6		

We know from the case of TNT, that indeed the porosity strongly influences the initiation behavior. High density TNT ($\rho > 1.65$ - 1.66 g/cm^3) is not suitable for blasting purposes, but a density of ≈ 1.62 g/cm^3 corresponding to a porosity of about 2% is favorable. In the case of propellants, therefore, a larger porosity than 0.8% may lead to a significant increase of hazard. It is possible to induce such a porosity by rough handling, see below.

We learn from these facts, that the dynamic behavior of composite materials is very complex, and the behavior is not a unique function of the chemical composition. Even the dynamic behavior of relatively homogeneous materials, like double base propellants is not to be guaranteed under such circumstances. Therefore some aspects of material damage caused by mechanical or thermal (very) low level stimuli are discussed in the following.

STRUCTURAL INFLUENCES ON MECHANICAL STABILITY AND SENSITIVITY TO HAZARDS

If a subcritical mechanical or thermal stimulus acts on a rocket motor without destroying or cracking it, one is tempted to assume that it may still be in its physical status originally specified. In general there are reasons that this may be not true, particularly in the case of composite propellant transport. By nondestructive mechanical or thermal loads, maybe in storage or in operation, it is possible, that the rocket motor gets some porosity, originally absent. This induced porosity may alter the mechanical properties, mainly in the dynamic case, and the sensitivity hazards.

BEHAVIOR OF A DENSE HOMOGENEOUS ELASTIC AND THERMALLY ISOTROPIC MATERIAL

A dense homogeneous elastic and thermally isotropic material shows in arbitrary directions in the macroscopic and microscopic scale the same properties. By a mechanical uniaxial stress the sample elongates and contracts in the orthogonal directions, and neither torsion nor angle variations will be observed. If hydrostatic pressure is applied, each direction is compressed by the same amount. An analogous behavior is to be observed in the case of the variation of the temperature.

Inside the volume compression waves remain compression waves, and the same holds for shear waves, and no interconversion takes place (except at the boundaries in the case of oblique incidence).

BEHAVIOR OF A SINGLE CRYSTAL

The above described behavior is not observed in the case of a single crystal. The stress/strain relations differ in different crystal directions, as does the thermal expansion. The macroscopic Poisson ratio depends on e direction too and, in addition from the side considered, planes may get distorted and angle variations also take place.

Crystals of a lower class than cubic (like aluminum) in general exhibit different compressibilities in different directions, and curiosities may be observed. There exist materials, tullurium as an example, which elongate in one direction by application of a hydrostatic pressure (or low temperature), whereas the overall volume shrinks. This mechanical behavior is not always accompanied by corresponding thermal behavior; it is also possible that the thermal expansion or compressibility is only anomalous. In a polycrystalline material, such phenomena induce catastrophic effects by the volume incompatibilities arising.

The sound velocities vary with the crystallographic directions too, and interconversions between the modes are usual. This may be the reason for a spectacular effect, that the direction of wave propagation and direction of energy propagation are different. Only in specified crystal directions, transmission of pure modes gets possible.

Symmetry elements in the crystals reduce the anisotropic behavior as the regularity increases. The thermal expansion anisotropy is less sensitive to the crystal classes than the mechanical elastic constants, both depend on temperature of course.

POLYCRYSTALLINE MATERIALS

If we have a statistical agglomeration of many single crystallites of the same type within a volume, and the crystallites are fixed by cohesive forces, we may finally observe a macroscopic isotropic behavior, if no preference is given to certain crystal directions by the fabrication process or otherwise.

Space averages of the stiffnesses (elastic constants c_{ik}), as carried out by Voigt, assume uniform strains - and nonuniform stresses - throughout the statistical sample. Contrasting to this, Reuss (1929) assumes uniform stresses - and nonuniform strains - in the volume, which means, that he performs a space averaging of the elastic compliances s_{ik}. As often, the truth is between the extremes. Neerfeld and Hill indicated that the static macroscopic constants are best described by the arithmetic

mean of Voigt- and Reuss-averaging. It is interesting to note that in the bulk modulus and the Youngs-modulus some different single crystal elastic constants are present. We can estimate the isotropic polycrystalline constants and sound velocities with good accuracy from the single crystal data. (All references in Hearmon, 1961).

If we have, as in a composite propellant, a mixture of ammonium perchlorate, aluminum, and a binder, in principle we would be able to give estimates of the elastic constants. But quite another problem is much more important. We have macroscopic averages values of the thermal expansion, Youngs modulus, compressibility of the matrix, composed from the constituents. If a single grain shows larger or lower values than the average, stresses or strains arise which must be balanced by the materials cohesive strength. Asymptomatically these forces are related to the anisotropy, characterized by the ratio maximum/minimum value, and the strength decreases as this anisotropy increases. In practice this means that an originally non-voided rocket motor charge may acquire voids simply by mechanical "subcritical" loads or thermal cycles.

As an example an aluminum/perchlorate composite propellant is considered with an assumed binder polystyrene. In Figure A.III.12 the Youngs-moduli E of the single crystals of the components are shown in the same scale. In addition the crystals have different (anisotropic) thermal expansion coefficients α. The thermal stresses Δ_0 of temperature shocks ΔT must be balanced by the cohesive strength of the material. Whenever this is surpassed, debonding or dewetting of the grains in the matrix occurs, which results in local weakening of the material strength, and induces an additional porosity, which increases as the number of the cycles increases. A rough estimate of the order of internal stresses is obtained by:

$$\Delta_0 = \{(E\,\alpha)_{max.} - (E\,\alpha)_{min.}\}\,\Delta T \qquad (12)$$

With the maximum values for aluminum E = 756 kbar; $\alpha = 2.3\ 10^{-5}\ K^{-1}$ and the minimum for polystyrene E = 34.6 kbar; $\alpha = 7\ 10^{-5}\ K^{-1}$ we get as an order of the internal stress 15 bar/K or 1.5 N/mm^2K. Therefore high strength, high plastic toughness materials are preferable as binders, and not brittle ones. Since in double base propellants such Youngs modulus variations are absent, these are less sensitive to low level mechanical or thermal influences.

Similar estimates may be done for uniaxial mechanical loads or hydrostatic compression. Due to the anisotropy of compression for noncubic materials, see Figure A.III.13, a debonding gets possible by hydrostatic compression of the material.

For the following reasons these points are very serious. The physical properties of the components of the energetic material (aluminum, ammonium perchlorate, and binder) are not to be altered. Only the binders strength and, most important, toughness, may lead to some mitigations.

As a point of a possible improvement the replacement of the metallic aluminum may be seen, or very plastic binders.

Future needs are to give more attention to investigations and measurements of the anisotropic physical properties of the energetic material and its constituents.

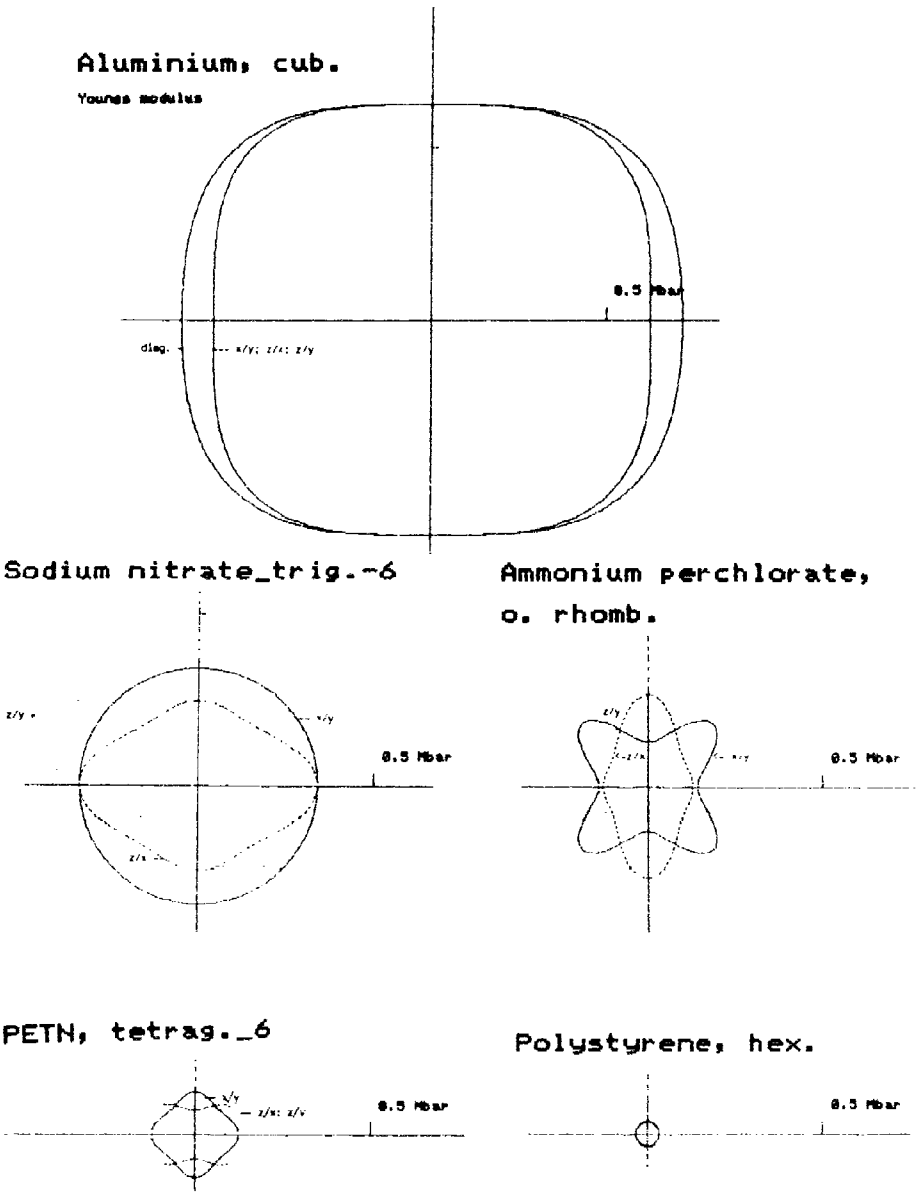

Figure A.III.12. Single Crystal Youngs Moduli of Some Propellant Components in the Same Scale in Orthogonal Crystal Planes.

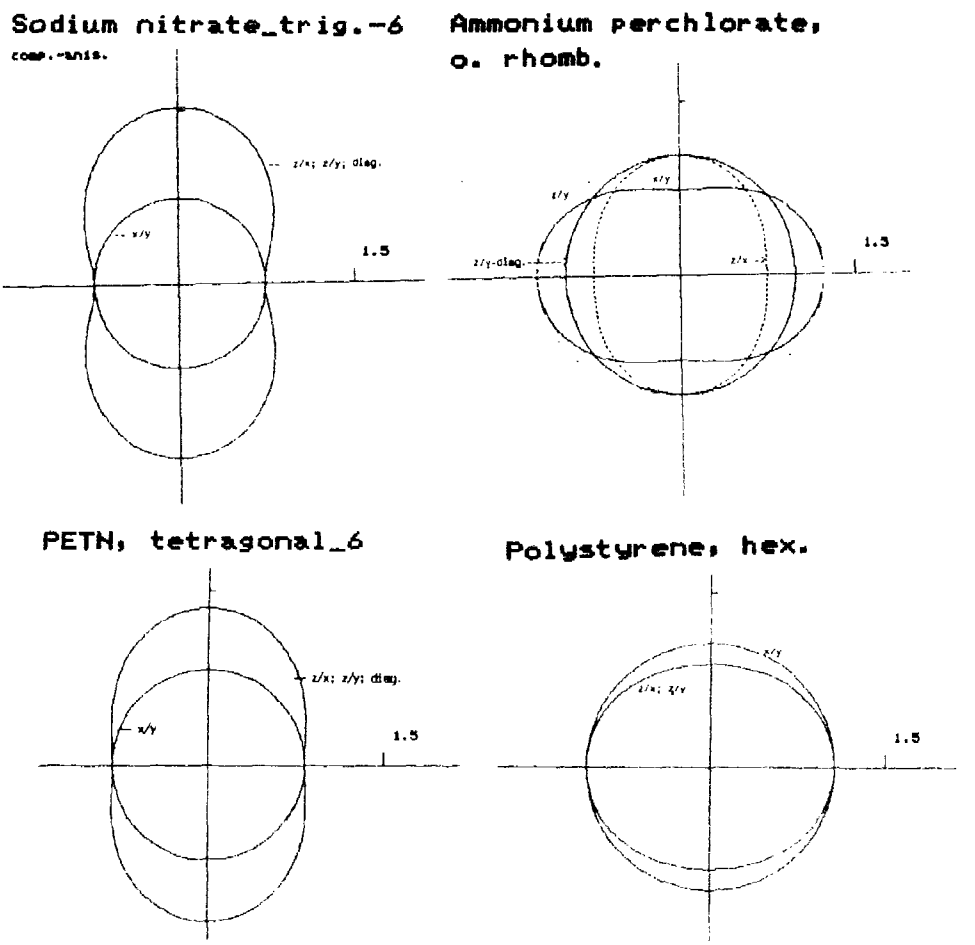

Figure A.III.13. Single Crystal Compressibility Ratios of Some Propellant Components. For cubic materials, like aluminum, this compressibility always is a sphere with radius 1. Plotted is the ratio of the uniaxial compressibility in the indicated crystal planes over 1/3 of the volume compressibility.

BASIC FRACTURE DYNAMICS

If tension pulses are present, we get the basis of fracture dynamics, which had been pioneered from first principles by Steverding and Lehnigk (Steverding and Lehnigk, 1970; Steverding and Lehnigk, 1971; Steverding and Lehnigk, 1970; Steverding, 1971; Steverding, 1971; and Steverding and Lehnigk, 1971). Their result was, that a volume or surface crack of the length c is opened by a tensile pulse (due to boundaries or the nature of the aelotropic polycrystalline material)

$$p \alpha \sqrt{\frac{\gamma E}{c}} \tag{13}$$

Here, and in the following, factors are omitted. Latter condition is similar to that of Griffiths (1920) static condition of maximal strength. However, in the case of dynamics in addition a critical pulse duration t is required for opening a crack of length c, which means, that the tensile pulse must pass the crack over the length c in order to open it.

$$t \alpha \frac{c}{u_s} \tag{14}$$

E is Young's modulus, γ is the surface energy, different for surface and volume cracks. For an order of magnitude estimate in brittle materials Cottrell, reference in Steverding and Lehnigk (1970) has given the expression

$$\gamma = \frac{E_b}{20} \tag{15}$$

where b is the interatomic distance. For a plastic fracture, however γ increases by orders of magnitude.

In order to examine whether fracture dynamics, besides theoretical reasons, may be at work in the black box of reaction zone, we make use not only on theoretical calculations, but also of excellent experimental results of many researchers on detonation, who have found laws and rules of initiation to detonation. Whenever such events should be caused by fracture, these rules and laws should be based on fracture dynamics.

APPLICATION TO INITIATION

Dependence of Sensitivity From the Grain Size

If we assume for a dense material without voids intercrystalline fracture at the grain boundaries, then c approximates to the grain size, and from Eq. (13), we obtain a Petch-type relation

$$p \alpha \sqrt{1/c} \tag{16}$$

and deviations may be caused by intercrystalline fracture of the grains.

LVD- Pressure

If it is assumed that the ultimate dynamic strength is obtained for the crack length of the interatomic distances c = b, then with Eqs. (13) and (15) the order

$$p \approx E/(4.5 \ldots 10) \tag{17}$$

corresponds to the LVD-pressure. This LVD-pressure corresponds to the maximum mechanical strength of the material, above which material is broken up into atomic debris.

For a material of density 1.5 g/cm^3 and sound velocity u_s = 2.500 m/s this pressure approximates 10 - 20 kbar. For HVD another additional effect comes into play, which is not considered here.

Walker-Wasleys Initiation Law

Combining Eqs. (13) and (14) one gets

$$\frac{p^2 t}{\rho u_s} \alpha \gamma \tag{18}$$

which is the well known Walker-Wasley result (1969), which does not hold for liquids (de Longueville et al, 1976).

Pop Plot (Dynamic Weibull) Relation

It is conceivable to assume that the pulse duration is proportional to the length L of a specified sample. Then as a scale of full fracture (initiation) one gets from Eqs. (13) and (14).

$$\log p \alpha - 0.5 \log L \tag{19}$$

and the dynamic Weibull term 0.5 is close to values of experimental pop plots, see for example Dobratz and Crawford (1985). In addition, static terms of material strength influence this exponent.

Held's Velocity-Diameter Scaling Law

If a bar of diameter Ø or cross-sectional area √F and velocity v hits the explosive material, tension

$$p \alpha v \rho u_s$$

results. Equating with Eq. (13) leads to

$$v \alpha \sqrt{\gamma/\rho c}$$

c is given from Eq. (14), where t is determined by the entrance of the "rarefaction" wave (Kharitons critical diameter principle)

$$t \alpha \frac{\varnothing}{2u_s} \alpha \frac{\sqrt{F}}{2u_s}$$

and one gets

$$v \alpha \sqrt{\frac{\gamma}{\rho\sqrt{F}}} \alpha \frac{1}{\sqrt[4]{F}} \alpha \frac{1}{\sqrt{\varnothing}} \qquad (20)$$

This is known as Held's (1984) initiation scaling law which is extensively confirmed by experiments.

These conclusions seem to be appropriate, but the question arises: What about the detonation chemistry, or in other words, is there a link between fracture and chemical decomposition?

FRACTURE AND CHEMICAL DECOMPOSITION

Why chemical decomposition and pressure waves are coupled in detonation processes is an old question in detonation physics since Becker's work. An approximate classical answer is that by the shock heating process, thermal chemical decomposition takes place (piston model), which in turn supports the pressure wave. According to this decoupling between shock and chemical decomposition should not occur; nevertheless, this is observable in experiments. Therefore another answer should be given.

Energy leading to fracture splits into several parts, such as into

a. elastic energy,
b. plastic deformation at the crack tip,
c. medium separation at the crack tip,
d. surface energy,
e. possibly release of chemical energy,
f. kinetic energy of the cracks, which produce a mass flow without compression into the surrounding medium by their volume increase.
g. Energy of compression leading to pressure waves. Due to the mass injection by the volume variation of the cracks, classical pressure generating mechanisms of Lord Rayleigh (1887) are activated, which lead to compression/tension waves.

All these processes are phase locked. Whereas the amounts of (a), (c), and (d) remain small, the others vary greatly with dynamics.

It is less known for inert solids that temperature increase and chemical decomposition are phenomena associated with fracture. So for PMMA Döll (1972) determined the heat evolution by fraction as a function of the crack propagation velocity between 200 and 750 m/s and the molecular weight of PMMA between 100,000 and 8,000,000. This heat evolution measured with thermocouples increased with the crack propagation velocity and had been largest for the largest molecular weight. Fuller, Fox, and Field (1975) monitored by a liquid weight PMMA (250,000) an increase in temperature of 500 K over the velocity range (200-650 m/s) studied. Former investigations of Regel, Muinov, and Pozdynakov (1966) demonstrated by mass spectroscopy that by fracturing PMMA, decomposition products appear like those from slow thermal decomposition.

This result on PMMA is important since it demonstrates that decomposition by fracture is a quite general event, and not restricted to energetic materials.

Fox and Soria-Ruiz (1970) found a fracture induced decomposition of β-lead azide, where about 10 atomic layers at the side walls of the crack decomposed to products similar to those of thermal decomposition. Chaudri (1972), however, failed to initiate β-lead azide with crack velocities below 600-800 m/s.

Ng, Field and Hauser (1986) summarize experiments done on PETN and address the questions on various mechanisms of decomposition. Since at the crack tip, a bond scission appears more likely than a thermal decomposition, these authors investigated the products of PETN of low and high energy fracture and laser-induced chemical decomposition. They found for low energy fracture as an initial break down step R-NO_2, similar to thermal decomposition, and for a high energy fracture R'-CH_2ONO_2, corresponding to a C-C scission. For a higher energy laser input R"-ONO_2 had been the first fission. Moreover former results of others show that in the case of slow cleavage, little or no emission occurs; in the case of slow compression, electron emissions take place; and n the case of impact loading, enhanced electron emission as well as photons and radiation are to be observed. According to this, electrons and photons are a result of structure, and probably do not directly induce a fracture. With respect to the electrostatic sensitivity, which depends on field break through, this conclusion desires a future reconsideration.

In the case of propellants and powders we, therefore, get a quite wide spread field of phenomena if these are brought to fracture by various stimuli. The damage varies from no effect to dewetting, bubble formation, microscopic and macroscopic cracks, burning, and explosion up to detonation. The critical impact velocity for explosion may be as low as 150 m/s, depending on type, shape, and size of the samples. A very comprehensive study and summary on this is given by Lee, James et al (1984).

The behavior of propellant cracking in the more benign ballistic range is studied principally by Kuo and coworkers.

We learn that onset of pressure wave propagation is controlled by the primary mechanical events, which induce a chemical decomposition and not the reverse. Therefore a decoupling between wave propagation and chemistry gets possible depending on the entering mechanical stimulus. A further conclusion is that tests which ignore the dynamics of the events to be simulated may give misleading results.

Since the rate of chemical decomposition is related with the crack velocity, and this crack velocity is not restricted to subsonic velocities. It is possible to relate the initiation of solid explosives to dynamic fracture. According to the required tension pulse, sensitivity should increase as the elastic anisotropy of the single crystallites in the polycrystalline material or the heterogeneity of the material increases. In terms of solid propellant rocket motors this means composites are more sensitive than double base motors.

It must be noted, however, that fracture dynamics is only an asymptotic rationale in the case of highly energetic dynamics, since in the falling weight test, for example, the plastic flow of PETN is decisive (Field et al, 1982), however, in each case initiation occurs directly or indirectly via a volume flow generation. Up to now no exception to this is known.

As known, there exists also a shear band model of initiation pioneered from Frey (1981), and we have the question, whether this will apply. In the following it will be outlined, why shear may be excluded and included into this frame.

Coming from the well established classical basic pressure generating mechanisms, a mass, and/or impulse, and/or curl-injection into the unit volume are essential. The effectiveness depends on the Mach-number of the flow in the detonation zone. For a low Mach-number, a mass injection is the most effective term. A mass injection can only be realized by volume variations $\dot{V}$ with time into the unit volume. This means that the pressure generating mechanisms require definitely a two-phase system. In the terms of fracture we need therefore volume variations by opening or closing of cracks, and in the case of liquids analogous opening or closing of reaction centers (bubbles). For demonstrating the applicability of this view we model qualitatively a very complicated detonation pattern of (liquid) diluted NM, which had been produced from Mallory and Greene (1969) by the impedance mirror technique. There are within the same detonation smooth and rough fronts separated by dark waves. Such a sequence had never been understood in classical engineering terms.

We simply model this behavior from the contributions of the single pressure sources, which had been assumed to be harmonical. Quite naturally we get a dark wave at those places, where the sources are absent, and the transition from smooth to rough depends on the concentration of the sources only, see Figure A.III.14.

Apparently this seems to be contrary to Frey's shear band model, but this is not the case.

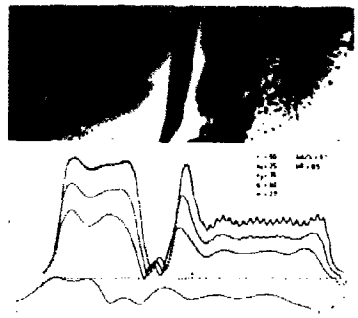

Figure A.III.14. Upper part is the detonation profile of diluted nitromethane from Mallory and Greene, which is modeled in the lower part. The dark wave is the result of the absence of pressure sources, a smooth front is obtained by small distances of the sources, which penetrate each other, and the rough profile is the result of the increased distances of the pressure sources (reaction centers). Source penetration is only possible in the case of HVD.

By shear a viscous heating may lead to chemical decomposition. In this moment, automatically we get a two-phase system, where the growth of the reaction products provide the mass injection into the surrounding unit volume. In the shear band concept we have therefore a two-step mechanism to realize pressure generation in classical terms.

HOW DOES THIS MODEL COMPARE WITH THE CLASSICAL THERMODYNAMIC VIEW OF DETONATION?

Leiber (1984) has shown that such a behavior may be pressed into a quasi-continuous laminar plane wave approach. For this simplification we have to pay with an appropriate Equation of State (EOS), where - contrary to the original sense of the EOS - time dependence and inertial effects are important. Within this frame therefore, any further attempts to find a correct and "true" EOS are meaningless, since our appropriate parameter-fitted EOS is nothing else than a correlation function of the real two-phase behavior in plane wave terms in the black box of detonation zone.

ESTIMATION OF THE IMPEDANCE OF A PENNY SHAPED CRACK

Equation (14) implies that a pressure pulse must pass the crack length in order to open it. In terms of harmonic waves this condition may be approximated by $\lambda \approx 2\ u_s t$, and one gets dimensionless acoustic crack diameter $kc = \pi c/u_s t$, which approximates to π. We have to evaluate the real part of the impedance of such a penny shaped crack. This may be done by calculating the impedance of a piston membrane, however, Skudrzyk (1971) has pointed out that there is also a good approximation to use the equivalent sphere surface of radius $R = c/2\sqrt{2}$, and one gets $kR = kc/2\sqrt{2} = \pi/2\sqrt{2} \approx 1.11$. So one gets, according to relations in Table A.III.1, $\mathrm{Re}\ Z/\rho c = (kR)^2/[1 + (kR)^2] \approx 0.55$ for one dynamic crack, which means that the ratio of pressure wave emission over energy of flow approximates to 0.55.

The question arises, what happens if we have more cracks. May the impedance increase or decrease?

COOPERATIVE EFFECTS

As usually known one crack does not produce an explosion or detonation. Many cracks in a unit volume may produce such an event. For demonstrating such a possibility, and the uncertainty to determine such risks we use a linear array of n = 20 (spherical) pressure sources, where the distances between the sources $\Delta d/\lambda$ may vary.

Since we are interested on the energy release by pressure wave emission, we have to calculate the relative impedance. This is done by taking the quotient of pressure and particle velocity in the direction of wave propagation at the point of observation. At this point all the contributions of the single sources are summed up using Huygens principle.

Considering the relative impedance in the center of this array as a function of the source distances, see Figure A.III.15, one notices, that under some circumstances pressure wave radiation dominates (large Re $Z/\rho c$, and relatively small Im $Z/\rho c$), and elsewhere pressureless flow (large Im $Z/\rho c$, and

small Re Z/ρc). It is not possible to produce such a diagram of general validity, since the functions depend on many factors. However it explains several points which are known by experience: It is not possible to estimate hazards on small scale samples, nor are there present scaling up rules from small to large samples. Further it may not be the most "severe" input in the sense of a high pressure amplitude which determines on safety but a certain critical, maybe soft, stimulation. Even the local distribution of all the pressure sources strongly influences the mixture of hazardous and benign behavior. This is finally the reason why the test results are not adequate to judge low stimulus impacts.

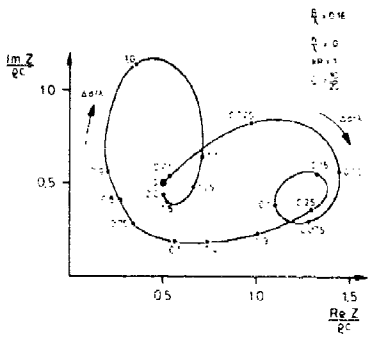

Figure A.III.15. Relative impedances of an array of n = 20 sources of size kR = 1 as function of the dynamic intersource distance Δd/λ in the center of the array. As may be seen, there exist benign and hazardous domains.

A direct demonstration of this gives Trimborn (1985) with the German spigot test, see Chapter 5. As the spigot penetrated the rocket propellant, very many reaction centers appeared over a period of up to some seconds. Finally these reaction flashes produced an explosion. This result is to be explained only by the cooperative effects just mentioned.

REFERENCES

A. F. Belyaev, V. K. Bobolev, A. I. Korotkov, A. A. Sulimov, and S. V. Chuiko. "Transition from Deflagration to Detonation in Condensed Phases," Moscow, 1973, English translation: Jerusalem 1975.

R. R. Bernecker. "The Deflagration-to-Detonation Transition Process for High-Energy Propellants - A Review," AIAA Journal, Vol. 24, pp. 82-91, 1986.

F. P. Bowden and A. D. Yoffe. "The Initiation and Growth of Explosion in Liquids and Solids," Cambridge Science Classics, Reprint 1985.

F. P. Bowden and A. D. Yoffe. "Fast Reactions in Solids," Butterworth Sci. Pub., London 1958.

P. B. Butler and H. Krier. "Analysis of Deflagration to Shock to Detonation Transition (DSDT) in Porous Energetic Solid Propellants Hazard Studies for Solid Propellant Rocket Motors," AGARD Conf Proc. No. 367, pp. 5-1/5-10, 1984.

J. A. Brown and M. Collins. "Explosion Phenomena Intermediate Between Deflagration and Detonation," Esso Res. Rept., Linden, NJ, 1967.

M. M. Chaudri. "Shock Initiation of Fast Decomposition in Crystalline Solids," Combustion and Flame, Vol. 19, pp. 419-425, 1972.

B. M. Dobratz and P. C. Crawford LLNL Explosives Handbook, UCRL-52997, Change 2, from January 31, 1985.

W. Döll. "Einfluß des Molekulargewictes aur die beim Bruch von PMMA freiwerdende Wärme, K

A. N. Dremin and V. Yu. Klimenko. "The Effect of the Shock-Wave Front on the Origin of Reaction" in J. R. Bowen, N. Manson, A. K. Oppenheim, and R. I. Soloukhin, "Gasdynamics of Detonations and Explosions," Vol. 75, American Inst. Aeronautics and Astronautics, pp. 253-268, 1981.

J. E. Field, G. M. Swallowe, and S. N. Heavens. "Ignition Mechanisms of Explosives During Mechanical Deformation," Proc. Roy. Soc., London A382, p. 231-244, 1982.

P. G. Fox and J. Soria-Ruiz. "Fracture-Induced Thermal Decomposition in Brittle Crystalline Solids," Proc. R. Soc., London, A317, pp. 79-90, 1970.

R. B. Frey. "The Initiation of Explosive Charges by Rapid Shear," 7th Symp. Int. Detonation, NSWC MP 82-334, p. 36-42, 1981.

K. N. G. Fuller, P. G. Fox, and J. E. Field. "The Temperature Rise at the Tip of Fast-Moving Cracks in Glassy Polymers," Proc. R. Soc., London A341, pp. pp. 537-557, 1975.

A. A. Griffith. "The Phenomena of Rupture and Flow in Solids," Phil. Trans. Roy. Soc. A221, pp. 163-198, 1920.

R. F. S. Hearmon. "An Introduction to Applied Anisotropic Elasticity," Oxford, 1961.

M. Held. "Critical Area for the Initiation of High Explosive Charges" in J. R. Asay, R. A. Graham, and G. K. Straub, "Shock Waves in Condensed Matter," Elsevier Pub., pp. 555-557, 1984.

A. M. Karo, J. R. Hardy, and F. E. Walker. "Theoretical Studies of Shock-Initiated Detonations," Acta Astronautica 5, pp. 1041-1050, 1978.

G. B. Kistiakowsky. "Initiation of Detonation of Explosives," 3rd Symp. Combustion and Flame and Explosion Phenomena, Williams & Wilkins, Baltimore, Maryland, U.S., pp.

W. König. "Hydrodynamisch-akustische Untersuchungen," Ann. Physik und Chemie NF 42, p. 353-370, (1891).

H. Kolsky. "Stress Waves in Solids," Dover Pub. New York, 1963.

H. Lamb. Hydrodynamics, 6th edition, Cambridge University Press, §298, 1932.

E. L. Lee, E. James, L. Green, W. von Holle, C. Tarver, D. Curran, W. Murri, and D. Seaman. "Response of Propellants to High Dynamic Stresses. The Uses of Gun Launch Techniques," AGARD Conf. Proc. No. 367, Hazard Studies for Solid Propellant Rocket Motors, pp. 10-1 - 10-32.

C. O. Leiber. Vergleich der Stoßbruchmechanismen bei dichter und poroser Keramik sowie bei Einkristallen, Planseeber. Pulvermetallurgie 22, pp. 41-47, 1974.

C. O. Leiber. "A Simple Model for the Initiation of Chemical Systems," Proc. Int. Conf. Res. Primary Explosives, Waltham Abbey, Vol. I, pp. 3/1-3/17, 1975.

C. O. Leiber. "Dynamic particle Motion in Materials as a Consequence of the Finite Shock Rise," 5th Int. Conf. High Energy Rate Fabricaton, Denver, Colorado, U.S., pp. 1.5.1-1.5.16, 1975.

C. O. Leiber. "Shock Augmentation by Bubble Flow," J. Appl. Phys. 47, pp. 3971-3978, 1976.

C. O. Leiber. "Zur Ahrens' Selektivitat, Ansatz zu einer Theorie gewerblicher Sprengstoffe," Nobel-Hefte 45, pp. 65-76, and p. 167, 1979.

C. O. Leiber. "Phänomene der Langsamen Detonation bei festen Explosivstoffen," BICT-Rept. 2.1-3/5737/82 A, J. Ind. Expl. Soc., Japan, 1982 and J. Ind. Expl. Soc, Japan, 48,, pp. 258-271, 1987.

C. O. Leiber. "Ballistic/Detonic Transition of Propellants," AGARD Conf. Proc. No. 367, Hazard Studies for Solid Propellant Rocket Motors, pp. 17/1-17/14, 1984. Approximative Quantitative Aspects of Synchronously Stimulated Hot-Spots, BICT-Rept. 2.1/7067/36.

C. O. Leiber. "Approximative Quantitative Aspects of a Hot Spot II: Initiation, Factors of Safe Handling, Reliability, and Effects of Hydrostatic Pressure on Initiation," J. Haz. Mat., Vol. 13, pp. 311-328, 1986.

M. J. Lighthill. The Bakerian Lecture 1961: Sound Generated Aerodynamically, Proc. Roy. Soc., London A 267, pp. 147-182, 1962.

Y. de Longueville, C. Fauquignon, and H. Moulard. "Initiation of Several Condensed Explosives by a Given Duration Shock Wave," 7th Symp. (Int.) Detonation, ACR-221, pp. 105-114, Office of Naval Research, 1976.

H. D. Mallory and G. A. Greene. "Luminosity and Pressure Aberrations in Detonating Nitromethane Solutions," J. Appl. Phys. 40, pp. 4933-4938, 1969.

M. A. Mogilewskij. Fizika gor. vzryva 9, p. 905-909, 1973.

C. E. Morris. "Adiabatic Elastic Moduli of Single Crystal Pentaerythritol Tetranitrate (PETN)," 6th Int. Symp. Detonation, ACR-221, pp. 396-402, 1976.

W. L. Ng, J. E. Field, and H. M. Hauser. "Thermal, Fracture, and Laser-Induced Decomposition of Pentaerythritol Tetranitrate," J. Appl. Phys., Vol. 59, pp. 3945-3952, 1986.

J. W. S. Rayleigh. The Theory of Sound, Vol. II, Dover Pub., New York, reprint 1945.

V. R. Regel, T. M. Muinov, and O. F. Pozdnyakov. "A Mass Spectrometric Study of Volatile Products Evolving in Degradation of Solids," Oxford Conf. on Physical Basis of Yield and Fracture, London Inst. Phys., Phys. Soc. pp. 194-199, 1966.

J. S. Rinehart. "Stress Transients in Solids," Hyperdynamics, Santa Fe, New Mexico, U.S., 1975.

E. Skudrzyk. "The Foundations of Acoustics," Springer, Wien, New York, 1971.

B. Steverding and S. H. Lehnigk. "Response of Cracks to Impact," J. Appl. Phys., Vol. 41, pp. 2096-2099, 1970.

B. Steverding and S. H. Lehnigk. "Impact and Fracture," Am. Cer. Soc. Bull., Vol. 49, pp. 1057-1061, 1970.

B. Steverding and S. H. Lehnigk. "Collision of Stress Pulses With Obstacles" and "Dynamics of Fracture," J. Appl. Phys., Vol. 42, pp. 3231-3238, 1971.

B. Steverding. "Size Effect for Dynamic Fracture," Mater. Sci. Eng., Vol. 7, pp. 342-347, 1971.

B. Steverding and S. H. Lehnigk. "Die Physik des Brechens," Physikalische Blatter, Vol. 27, pp. 351-356 and 452-456, 1971.

S. Temkin. Elements of Acoustics, John Wiley, New York, 1981.

A. R. Ubbelohde. "Transition from Deflagration to Detonation: The physico-chemical aspects of stable detonation," 3rd Symposium Combustion and Flame and Explosion Phenomena, Williams and Wilkins, Baltimore, Maryland, U.S., pp. 566-571, 1949.

V. Voigt. "Lehrbuck der Kristalliophysik," Teubner Leipzig, 1910.

F. E. Walker and R. J. Wasley. "Critical Energy for Shock Initiation of Heterogeneous Explosives," Explosivstoffe 17, pp. 9-13, 1969.

R. J. Wasley. "Stress Wave Propagation in Solids," Marcel Dekker, New York, 1973.

R. Wild and J. Müller. "Verhalten von Nitromethan bei Beaufschlagung mit einer Gasexplosion, BICT Rept. 2.3-2/57989/82, 1982.

S. Winkler, D. A. Shockey, and D. R. Curran. "Crack Propagation at Supersonic Velocities I, Int. J. Fracture Mech., Vol. 6, pp. 151-158, 1970.

S. Winkler, D. A. Shockey, and D. R. Curran. "Crack Propagation at Supersonic Velocities II: Theoretical Model, Int. J. Fracture Mech., Vol. 6, pp. 271-278, 1970.

S. Winkler. Messung von Profilen schwacher Stoßwellen, Verhandl. DPG (VI) Vol. 11, pp. 136-137, 1976.

ANNEX IV

BASICS OF SOLID ROCKET MOTOR PROPULSION

The following brief notes are intended to present the basic aspects of solid rocket motor propulsion theory. For consideration of the more advanced aspects, such as propellant erosive combustion, structural design considerations and nozzle and blast-pipe design, a text book on rocketry should be consulted.

The propulsion of a rocket motor is achieved by applying a force to accelerate it, or to maintain a constant velocity against a resisting force. The propulsive force is obtained by ejecting hot combustion gases at high velocity through a nozzle from a combustion chamber containing burning propellant.

A useful parameter for performance evaluation is the specific impulse I_{sp}, which is defined as the thrust obtained when the propellant mass flow rate m is unity:

$$I_{sp} = \frac{F}{\dot{m}} = C \qquad (IV.1)$$

The total impulse, I, is the integral of thrust, F, over the burning time, t. It can also be defined as a function of specific impulse.

$$I = \int_o^t F dt = \int_o^t I_{sp} \dot{m} dt \qquad (IV.2)$$

For constant thrust or constant specific impulse the relationships can be simplified to

$$I = Ft \qquad (IV.3)$$

In applying the principle of momentum to a rocket motor in which a pressurized gas is expanded through a nozzle into a lower ambient pressure, the resultant thrust is the sum of the momentum thrust and the pressure thrust:

$$F = \dot{m}c + (P_e - P_o) Ac \qquad (IV.4)$$

The momentum thrust results from the increase in momentum of the exhaust gases during expansion through the throat and is primarily determined by the propellant composition. This element is the principal component of the total thrust, thus it is clear that a high exhaust velocity is always required if maximum thrust is to be produced with a given mass flow of propellant. The pressure thrust, $(P_e - P_o)A_e$, results from the summation of pressure forces acting at the nozzle exit plane (subscript e) and is determined by the nozzle design. At high altitudes this pressure thrust term increases as the ambient pressure, P_o, decreases, so that the maximum value is reached in a vacuum.

When the exhaust pressure, Pc_o, is equal to the ambient pressure, P_o, the thrust, F, is given by equation (IV.1).

This condition gives maximum thrust for a given propellant and chamber pressure. The nozzle design which permits the expansion of the propellant products to the pressure that is exactly equal to the ambient pressure, is referred to as the rocket nozzle with optimum expansion ratio.

In nozzle design many parameters must be considered including chamber and atmospheric pressure, γ, (the ratio of specific heat at constant pressure to that at constant volume) and the nozzle expansion ratio. In practice these are combined into one simple basic equation called the ideal thrust equation:

$$F = C_f P_c A_t \qquad (IV.5)$$

where C_f is called the thrust efficient, P_c the chamber pressure, and A_t the throat area. Because C_f is a function of chamber pressure, the thrust is not quite proportional to P_c. However it is directly proportional to the throat area. The thrust coefficient determines the amplification of thrust due to the gas expansion in the rocket nozzle as compared to the thrust that would be exerted if the chamber pressure acted over the throat area only.

By combining equations (IV.1) and (IV.5) we get

$$\dot{m}c = C_f P_c A_t \tag{IV.6}$$

and thus it can be seen that increasing C_f amplifies not only the thrust (Equation (IV.5)) but also gas velocity (Equation (IV.6)).

The characteristic exhaust velocity C* has frequently been used in rocket literature. It is defined as

$$C^* = C/C_f \tag{IV.7}$$

and can be expressed as a function of the gas properties in the combustion chamber. Using equations (IV.7), (IV.1), and (IV.5)

$$C^* = \frac{C}{C_f} = \frac{F}{\dot{m}C_f} \tag{IV.8}$$

or

$$C^* = \frac{P_c A_t}{\dot{m}} \tag{IV.9}$$

C* is a figure of merit of the propellant combination and combustion chamber design and is essentially independent of nozzle characteristics. It can be considered as a gas generation parameter for a given motor configuration.

In a rocket motor the chamber pressure and burning rate have definite steady-state values. This arises because there are two independent relationships between chamber pressure and burning rate

One is characteristic of the propellant only and can sometimes be expressed by a simple power law such as $R_B = ap_c^n$ where n is known as the pressure exponent (Figure IV.4 Curve A). With other propellants a more complex function is found, exhibiting a plateau in the burning rate versus pressure curve.

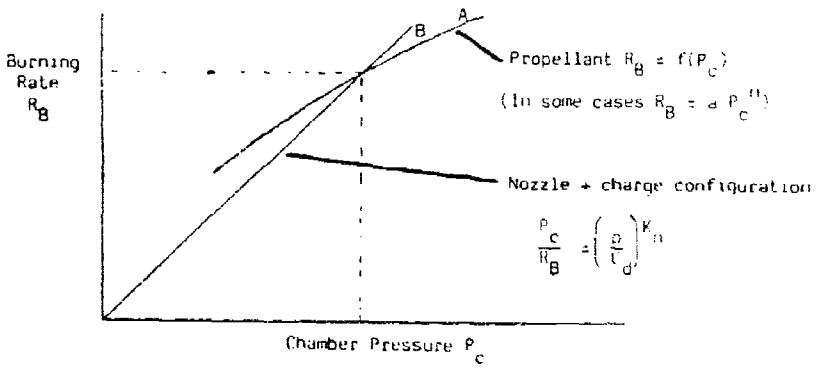

Figure IV.4.

The mass rate of gas generation is given by

$$\dot{m} = R_B S \rho \tag{IV.10}$$

where R_B is the linear burning rate, S the burning surface area, and ρ the density.

The mass flow rate of gas from the nozzle is given by

$$\dot{m} = P_c A_t C_c \tag{IV.11}$$

(where C_d is the discharge coefficient). At equilibrium the mass rate of gas production and discharge are equal and this gives the chamber pressure/burning rate relationship as determined by the nozzle and charge configurations:

$$R_B S r = P_c A_t C_d \qquad \text{(IV.12)}$$

i.e.

$$\frac{P_c}{R_B} = \frac{Sr}{A_t C_d}$$

from which it is evident that chamber pressure is influenced by both geometric properties (S and A_t) and propellant characteristics (R_B and ρ). Because of the critical importance of burning surface and nozzle throat area, frequent use is made of their ratio defined as the restriction ratio K_n given by

$$K_n = \frac{S}{A_t} \qquad \text{(IV.13)}$$

Thus equation (IV.12) becomes

$$\frac{P_c}{R_b} = K_n \frac{\rho}{C_d}$$

This relates the chamber pressure to burning rate as a function of nozzle and charge configuration and is represented by the straight line, B on Figure 2.1. The intersection of lines A and B gives the steady-state values for chamber pressure and burning rate.

The symbols used are listed below:

A_e	Nozzle exit area	L^2
A_t	Nozzle throat area	L^2
C	Effective exhaust velocity	LT^{-1}
C*	Characteristic exhaust velocity	LT^{-1}
C_d	Discharge coefficient	$L^{-1}T$
C_f	Thrust coefficient	Dimensionless
F	Thrust force	MLT^{-2}
I	Impulse	MLT^{-1}
I_{sp}	Specific Impulse	MLT^{-2}
K_n	Restriction ratio	Dimensionless
m	Mass flow rate	MT^{-1}
P_c	Chamber pressure	$ML^{-1}T^{-2}$
P_e	Gas pressure at nozzle exit	$ML^{-1}T^{-2}$
P_o	Ambient pressure	$ML^{-1}T^{-2}$
R_B	Burning rate of propellant	LT^{-1}
S	Burning surface area of charge	L^2
t	Burning time	T
γ	Ratio of specific heat at constant pressure to specific heat at constant volume	Dimensionless
ρ	Propellant density	ML^{-3}

REPORT DOCUMENTATION PAGE

1. Recipient's Reference	2. Originator's Reference	3. Further Reference	4. Security Classification of Document
	AGARD-AG-310	ISBN 92-835-0581-6	UNCLASSIFIED

5. Originator Advisory Group for Aerospace Research and Development
North Atlantic Treaty Organization
7 rue Ancelle, 92200 Neuilly sur Seine, France

6. Title HAZARD STUDIES FOR SOLID PROPELLANT ROCKET MOTORS

7. Presented at

8. Author(s)/Editor(s) Edited by Thomas L.Boggs and Ronald L.Derr

9. Date September 1990

10. Author's/Editor's Address Various

11. Pages 202

12. Distribution Statement This document is distributed in accordance with AGARD policies and regulations, which are outlined on the Outside Back Covers of all AGARD publications.

13. Keywords/Descriptors

Detonation	Munition design
Energetic munitions	Munition safety
Explosion	Rocket motors
Handling of explosives	Safety hazards
Hazard analysis	Solid propellants
Ignition of explosives	Threats to energetic material

14. Abstract

This AGARDograph summarizes hazard studies for solid propellant rocket motors over the period 1984 to 1989. The AGARDograph presents concepts and methods for evaluating hazard risks associated with solid propellant rocket motors and the technology for minimizing potential damage due to these hazards.

This AGARDograph was prepared at the request of the Propulsion and Energetics Panel of AGARD.